Geophysical Investigation of the Geothermal System in Pagosa Springs, CO

COLORADOSCHOOLOFMINES
EARTH • ENERGY • ENVIRONMENT

2016 Geophysics Field Camp

June 2016

Abstract

This report describes the acquisition, processing, and results of the Colorado School of Mines Department of Geophysics 2016 Summer Field Camp. From May 15th through May 27th, a team of undergraduate students from the Colorado School of Mines, along with faculty, TAs, and industry aides, conducted a series of geophysical surveys at both a main line site and a student designed site in the town of Pagosa Springs, Archuleta County, Colorado. The main site of investigation occurred along County Road 302, otherwise known as Mill Creek Road. The main survey line began at the road's intersection with Highway 84 on the western end and continued for 11 kilometers down the road to the east. Deep seismic, gravity, magnetics, differential GPS (DGPS), and self potential surveys occurred along the entire main line with additional results contributed from hammer seismic, DC resistivity, magnetotellurics, and time domain electromagnetics (TDEM). While the main line was predetermined by School of Mines faculty, the student participants also permitted, designed, and conducted surveys at the student site, located on County Road 200 and the surrounding pastures. In this area, gravity and magnetics surveys occurred along the entire line while partial results were provided by hammer seismic, DC resistivity, TDEM, frequency domain electromagnetics, DGPS, and total station. Following the collection of data in Pagosa Springs, participants returned to the Colorado School of Mines in Golden, Colorado to process and interpret the results of the field surveys.

The main objective of surveying in Pagosa Springs was to find and characterize the mechanisms of geothermal fluid flow feeding the Mother Spring in downtown Pagosa. For the past four field camps and again this year, the Geophysics Department at the Colorado School of Mines has pursued this main objective, along with secondary goals of characterizing stratigraphy and structural geology in the area. The results of this year's main line reveal regional dip to the east on the east side of Pagosa Springs. A dike along the line as well as some faulting in the subsurface reveal the structural composition of the area and could potentially explain the mechanisms of fluid flow in this area. For the student site, surveying demonstrated a similar regional dip and revealed a potential normal fault. The final integrated results for both sites contribute to the general geologic understanding of the Pagosa Springs area and, although these results might not necessarily characterize the nature of fluid flow to the Mother Spring, they do provide interesting hypotheses on regional fluid movement.

Disclaimer

This report and its contents are derived from a summer field camp for undergraduate students in the Department of Geophysical Engineering at the Colorado School of Mines. The primary objective of this field camp is education, focusing on the instruction of applied field geophysics. All data contained in this report was acquired, processed, and interpreted primarily by students from the Colorado School of Mines. Therefore, all results and conclusions should be regarded appropriately. The Colorado School of Mines and its Geophysics Department do not guarantee the validity of the information or results contained in the remainder of this report.

Acknowledgments

The 2016 Colorado School of Mines Geophysical Engineering Field Camp would not have been possible without the generous financial contributions and support from a number of organizations and individuals. The students who attended Field Camp this year are immensely appreciative of everyone involved in making this experience a reality.

We are grateful for the generous financial contributions provided by:

- College of Earth and Resource Sciences & Engineering (CERSE), Colorado School of Mines (CSM)
- Department of Geophysics, CSM
- Department of Environmental Health & Safety, CSM
- Society of Exploration Geophysicists (SEG) Foundation
- Anadarko Petroleum Corporation
- Apache Corporation
- Chevron
- ConocoPhillips
- Haliburton
- Shell

The students of the 2016 Field Camp are thankful for being provided with valuable knowledge, pertinent equipment, and industry-quality software by:

- Aahrus GeoSoftware
  - Bjarke Roth
- Dawson Geophysical
  - Stuart Wright
  - Steve Kite
  - Dustin Kite
- Sercel
  - Alba Guerrero
- US Army Corps of Engineers
  - Ryan North
- Reservoir Characterization Project (RCP), CSM
  - Bob Benson
  - Tom Davis
- United States Geological Survey (USGS)
  - Ben Bloss
  - Seth Haines
- Pagosa Verde
  - Paul Foley
  - Kirsten Skeehan
- Center for Gravity, Electrical & Magnetics Studies, CSM
- Colorado School of Mines
  - Ben Bloss
  - Michael Sleevi

Additionally, the students of the 2016 Field Camp extend special recognition to Bob Basker and Marvin Johnson for their personal expertise during seismic data acquisition and processing.

Critical resources and support were provided by:

- Terry Schaaf, CSU/Archuleta County Extension Office
- Becky Jacobson, CSU/Archuleta County Extension Office, 4H
- Laura Rand and Leticia Gallegos, Archuleta County Schools
- J.D. Kurz, Pagosa Springs High School
- Kristen Hentschel and Linda Reed, Pagosa Springs Middle School
- Kathy Keyes, Pagosa Springs Baking Company and Geothermal Greenhouse Partnership
- Laura Elguezabal and Staff, San Juan Motel
- Town of Pagosa Springs

We are thankful that the following Pagosa Springs community members allowed us to perform our geophysical investigations on their roads and private property:

- Archuleta County
- Bob DeWees
- District Ranger Kevin Khung, U.S. Forest Service
- Charlotte and Steven Williams
- Diane Burnett
- J. Robert (Bob) Formwalt
- James Morehouse, Morehouse Family Partnership
- Jamie Sharp
- Raymond Lattine
- Robyn Bennett
- Timothy and Elizabeth Vail
- Tony and Dawn Overman

The donation of valuable knowledge, assistance, and time were a crucial part of making this experience a resounding success. We would like to extend our appreciation to the following faculty and staff:

- Field Camp Director
  - Dr. Andrei Swidinsky
- Professors
  - Dr. Bob Raynolds
  - Dr. Ed Nissen
  - Dr. Paul Sava
  - Dr. Rich Krahenbuhl
  - Dr. Yaoguo Li
- Adjunct Faculty
  - Dr. Cici Martinez
  - Hugo Garcia
  - Matt Wisneiwski
- Terry Young
- Teaching Assistants
  - Liz Maag
  - Andy McAliley
  - Colton Kohnke
  - Joe Capriotti
  - Stephen Cuttler
  - Thomas Rapstine
- Equipment Manager
  - Brian Passerella
- Program Assistants
  - Dawn Umpleby
  - Michelle Szobody

Colorado School of Mines Geophysics Field Camp 2016 Student Participants:

- Project Manager
  - Aspen Anderson
- Assistant Project Manager
  - Samuel Courville
- Geology/GPS
  - Teresa Pilato (Group Leader)
  - Jill Remmers
  - Whitney Schultz
- Well Logging
  - Donald Arthur
  - Jared Stultz
- DC Resistivity and Self Potential
  - Ashton Kranjnovich (Group Leader)
  - Brennah McVey
  - Juliann Coffey
  - Logan Copass
  - Max Mifkovič
  - Mitchell Paradis
- Hammer Seismic
  - Adren Rigdon (Group Leader)
  - Chivithaya Xiong
  - Diana Tamayo
  - Patrick Corwin
  - Will Boni
- Gravity and Magnetics
  - Hanna Flamme (Group Leader)
  - Glenna Crookston
  - John Hinton
  - Michael Fryman
  - Tasha Markley
- Electromagnetics
  - Hubbell Rowe (Group Leader)
  - Edwin Mendoza
  - Eric Bunzli
  - Morgan Sander-Olhoeft
- Magnetotellurics
  - Luke Brown (Group Leader)
  - Hannah Peterson
  - James Hogan
  - Lorena Tello
  - Taylor Mackay
- Deep Seismic
  - Micaela Pedrazas (Co-Group Leader)
  - Michelle Pedrazas (Co-Group Leader)
  - Ammar Mohammed Anuar
  - Brandon Clayton
  - Hayden Powers
  - Katherine Biegel
  - Iker Madera
  - Thanyanat Akarapatima

Unless otherwise noted, photography provided by the following participants of Field Camp:

- Ashton Krajnovich
- Aspen Anderson
- Brandon Clayton
- Brennah McVey
- Colton Kohnke
- Dawn Umpleby
- Donald Arthur
- Glenna Crookston
- Hannah Peterson
- Iker Madera
- Jared Stultz
- Jill Remmers
- John Hinton
- Michelle Szobody
- Seth Haines
- Seth Haines
- Stephen Cuttler
- Tasha Markley
- Whitney Schultz

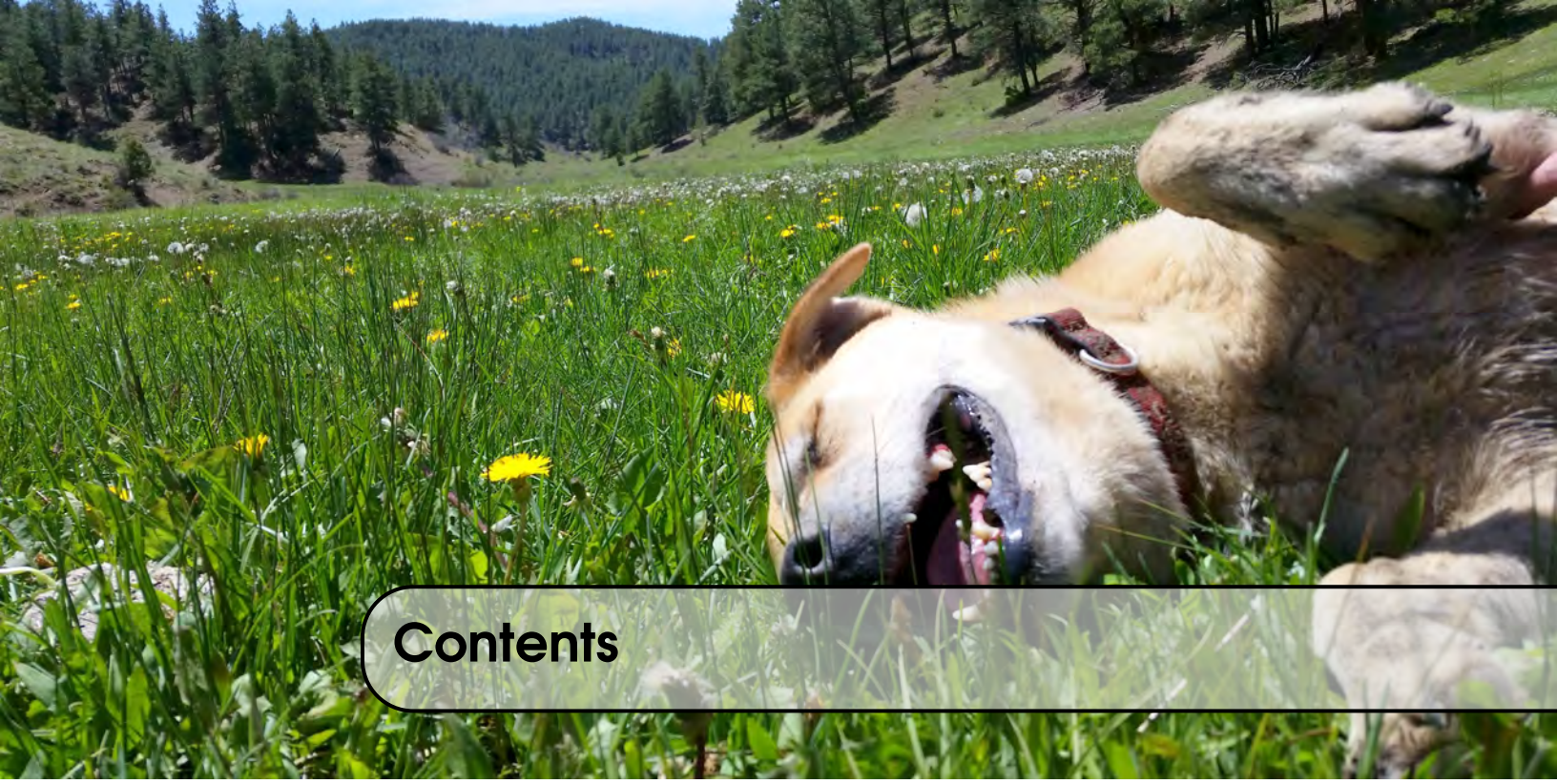

Contents

List of Figures

List of Tables

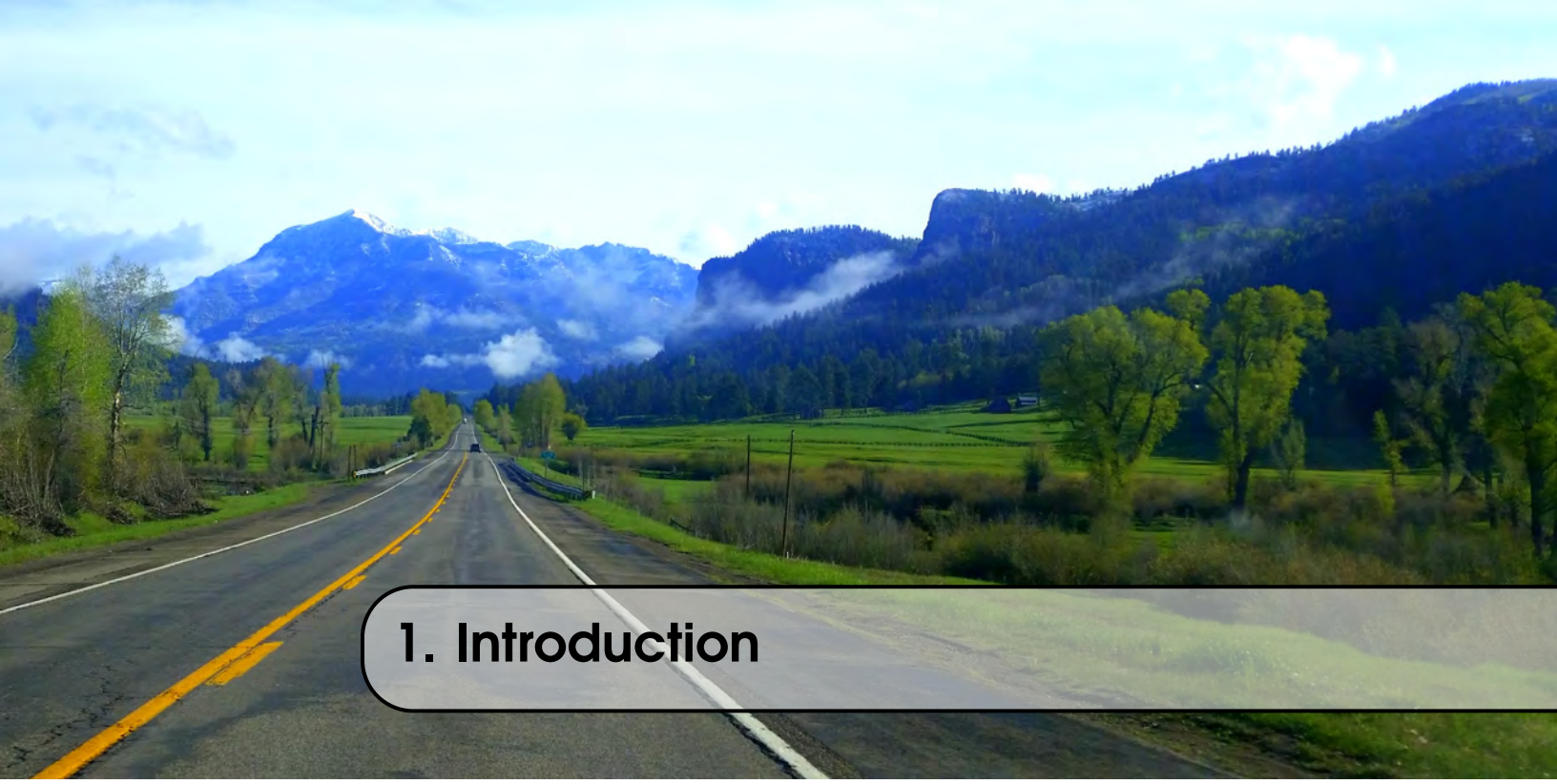

1. Introduction

Contents

1.1 Geophysics Field Camp Background

The Colorado School of Mines geophysics field camp is a required portion of the undergraduate curriculum which provides students with hands-on experience using a variety of geophysical methods, and complements the theory learned over the previous several semesters. With the assistance of industry and academic experts, the students conduct surveys over a specific location with the goal of imaging subsurface geologic features. Along with conducting surveys, the students create an extensive report of their findings. This report is a collective summary of the activities and results of the 2016 field session and is made freely available to the public. Accompanying this report is a presentation given to the public on June 10th, 2016 at the Colorado School of Mines.

The Colorado School of Mines held its 2016 field camp near Pagosa Springs in Archuleta County, Colorado. Geologic and geophysical surveys were conducted from May 15th to May 26th, 2016. The field camp has been held in or near Pagosa Springs in the past, in turn the surveys were designed to build off of information learned in previous years.

1.2 Objective

The foremost objective of the Colorado School of Mines 2016 Geophysics Field Camp was to be an academic exercise for the 41 undergraduate students enrolled in the program. The two weeks spent conducting surveys provided the students with valuable hands on experience applying the theory learned in class lectures from the semesters beforehand. During field camp, the students participated in the entire process of data collection and processing, concluding in a formal presentation and written report. Thus, the Field Camp provides students with the chance to conduct a complete geophysical survey from start to finish with a tangible result upon completion.

Although the primary goal of Field Camp is to be educational, the final report and findings are made available to the public. The students approached the creation of this report with the goal of characterizing the subsurface geothermal system that gives life to the "Mother Spring" within the Pagosa Hot Springs. Building upon information learned from previous field camps in Pagosa Springs, this report will add additional details to help develop an understanding of the Pagosa Hot Springs.

1.3 Location: Pagosa Springs

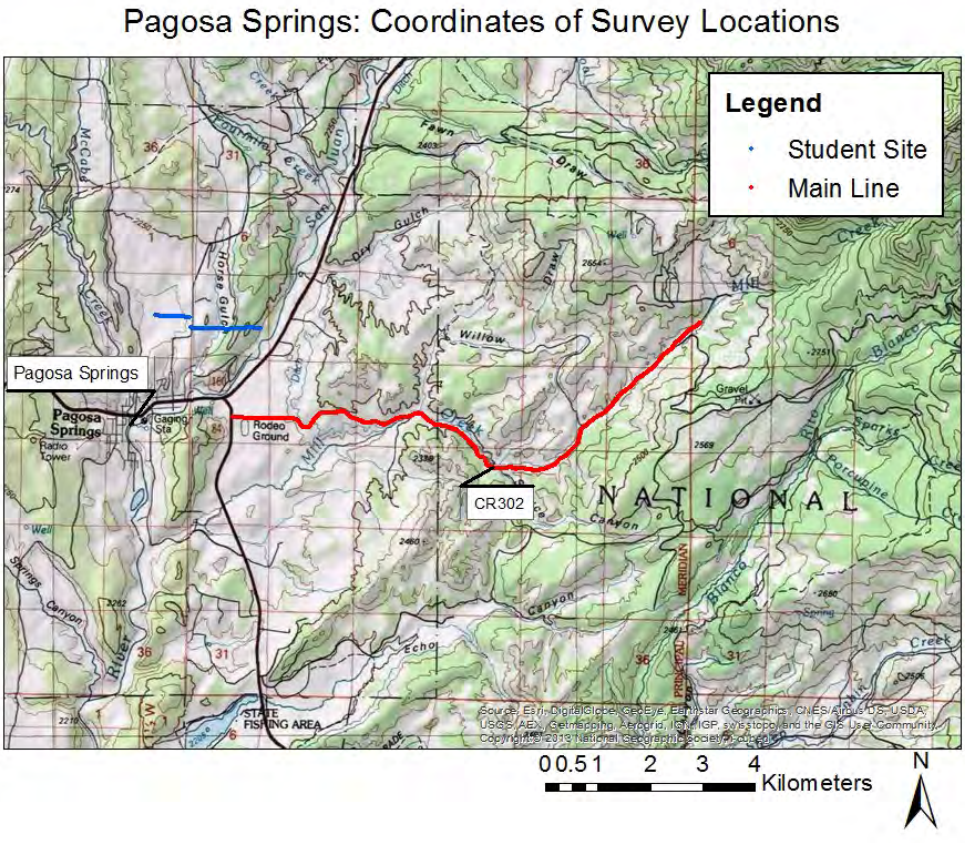

Figure 1.1: *Colorado School of Mines Geophysics Field Camp's 2016 survey sites. The main survey line is shown in red whereas the student site is shown in blue. The sites were chosen with the hope of imaging fluid flow to the hot springs in Pagosa Springs.*

1.3.1 Pagosa Springs History

Long before the town of Pagosa Springs was founded, the Ute People discovered hot springs in the area which they named "Pah Gosa." Loosely, this translates to water with a bad smell. The Utes believed the springs had healing powers; a legend that spread and became the source of travel and tourism to the area [4]. In more recent times, use of the hot springs has expanded. Along with fueling several hot spring resorts, a geothermal heating system transfers the heat from the hot spring water to clean water which is pumped throughout the town of Pagosa Springs. The town primarily draws its geothermal energy from the Mother Spring in downtown Pagosa Springs. This spring holds the Guinness World Record for being the deepest hot spring in the world with a measured depth of 1002 feet [2]. This provides the town with a sustainable hot water source.

Although Pagosa Springs is a small town of only about 2,000 residents, strong interest exists in continuing to use the hot spring water as a sustainable resource. For example, the Geothermal Greenhouse Partnership, a public green initiative, is currently building a series of geothermally heated greenhouses near the center of the town. Despite the interest and continued use of the hot springs, the source of the hot water itself remains in question. The drilling of wells near Pagosa Springs in search of hot water has achieved various levels of success [3]; although, none of the drilling attempts have yielded a well suitable for producing geothermal energy. Wells drilled in and around Pagosa Springs have unpredictable water temperatures. In order to properly use the geothermal resources in the area, a better understanding of the subsurface features is needed.

1.3.2 Mainline Survey Site

The town of Pagosa Springs, along with the Mother Spring, is situated along a bend in the San Juan River. The river crosses a ridge, known as Reservoir Hill, in the location of this bend. The 2012 geophysics field camp successfully identified a fault (The Victoire Fault, [1]) running along Reservoir Hill, and the 2013 field camp provided further characterization. The main line for the 2016 field camp, chosen by course instructors, runs to the East from the aforementioned ridge along CR302 (See figure 1.1). The line totals 11 km in length. It was chosen with the hope of imaging subsurface fluid flow from the San Juan Mountains toward the area of the hot springs, as well as characterizing the structural geology and stratigraphy of the Pagosa Springs region.

1.3.3 Student Survey Site

In addition to the mainline survey site, the students decided on another location for study. The site was located to the northeast of Pagosa Springs near CR200 (See figure 1.1). The students picked the site with the goal of imaging a continuation of the Victoire Fault. The student site survey tracked East-West, similar to the mainline, and was oriented perpendicular to the ridge located in the area.

1.4 A Hitchhiker's Guide to this Report

Within this report, you will find sections focusing on each geophysical method used during the 2016 geophysics field camp. Bring along a towel for the read through.

We begin this report by discussing the geologic setting of Pagosa Springs. This provides basic information for interpreting geophysical methods later in the report. Next we explain how the survey sites were spatially recorded. The GPS section describes the various methods of determining the survey site locations. This section outlines all survey locations as well. Following the GPS section, we present a chapter for each geophysical method used during the 2016 Field Camp. Within each method chapter is a discussion of the theory behind the method, the location and parameters of the data acquisition, an explanation of how the data was processed, and finally a discussion of the results from the method. After the individual method chapters, we compile a joint interpretation of the collective results. We use this joint interpretation to develop our final conclusion. Finally, we provide recommendations for future geophysics field camps and their surveying of Pagosa Springs.

1.4.1 The Geophysical Process

Geophysics measures physical properties on Earth's surface to determine material properties of the subsurface. Inverse modeling is used to link the physical properties measured by geophysical equipment to their corresponding material properties. For example, inverse modeling allows acoustic impedance to be determined from measurements of displacement of the ground over time. Geophysics also exploits the use of forward modeling: modeling a material property before a survey in order to determine what the measured response should be. It is important to note that inverse modeling is subject to the non- uniqueness theorem; a model created might fit the data that was acquired, but theoretically there are an infinite amount of solutions that will fit the data set. During the course of this paper many methods will be explored and different material properties will be integrated in order to create a final geologic model of the subsurface.

References

[1] S. C. A. Revil, J. Z. M. Karaoulis, and M. B. B. Raynolds, "The plumbing system of the Pagosa thermal Springs, Colorado: Application of image-guided geophysical inversion and data fusion", English, *Journal of Volcanology and Geothermal Research*, volume 299, pages 1–18, Jun. 2015. DOI: 10.1016/j.jvolgeores.2015.04.005. [Online]. Available: http://dx.doi.org/10.1016/j.jvolgeores.2015.04.005 (cited on pages 3, 111, 112).

[2] *Pagosa Geothermal Hot Springs Makes Guinness Book of World Records*. [Online]. Available: http://www.waterinfo.org/node/5467 (cited on page 3).

[3] "Recovery Act: Direct Confirmation of Commercial Geothermal Resources in Colorado Using Remote Sensing and On-Site Exploration, Testing and Analysis", Pagosa Verde LLC, Tech. Rep. DE-EE0002828, 2015 (cited on page 3).

[4] T. S. R.
bibinitperiod Spa, *History of Pagosa Hot Springs*. [Online]. Available: http://www.pagosahotsprings.com/#!history/c1rvd (cited on page 3).

2. Geology

Contents

2.1 Introduction

Pagosa Springs is located roughly 300 miles southwest of Denver on the Western slope of the Continental Divide in Archuleta County, Colorado. Geologically, Pagosa Springs is located in the northeast corner of the San Juan Basin on the Archuleta Anticlinorium. Understanding the regional and local geology of this area was a key component for this study. Geology guided the processing of different geophysical data sets and also guided our final interpretations. Having a clear understanding of the geology ultimately helped to draw more accurate conclusions about the geothermal system of Pagosa Springs.

2.2 Regional Geology

2.2.1 History & Timeline

In the Paleozoic Era, Colorado was a low relief area with an ocean, during which passive sedimentary layers were deposited. This is often referred to as the Paleozoic succession. The first relevant major geologic event was the Ancestral Rocky Orogeny, which occurred 300 million years ago. This included a succession of uplifts and downdrops in the same region as the current Rocky Mountains. Pagosa Springs was an Ancestral Rocky Mountain high during this time, and therefore high levels of erosion characterizes this period. As the Ancestral Rocky Mountain Orogeny concluded, the ground stabilized and there was a period of equilibrium. During the Triassic and Jurassic periods the landscape healed; high points eroded and low points and valleys were filled in, creating a new period of shallow relief topography. The Entrada, Wanakah, and Morrison Formations formed during this time.

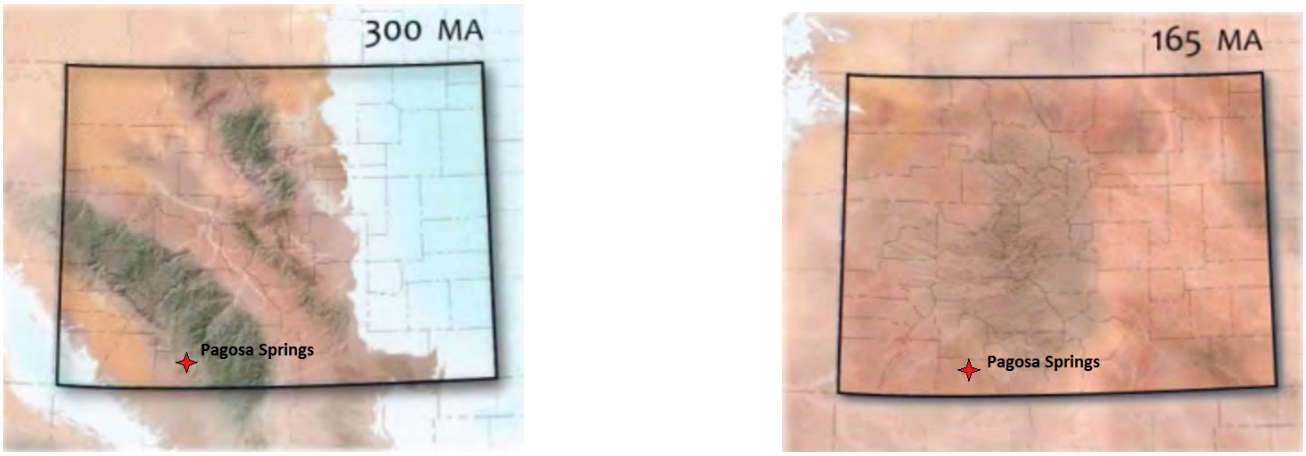

(a) *Ancestral Rocky Mountains*

(b) *Triassic and Jurassic Period Flatlands*

Figure 2.1: *(a) This is an illustration of what the Ancestral Rocky mountains might have looked like across Colorado at the beginning of the Permian Period. The Pagosa Springs area was a topographic high and experienced a period of erosion. (b) This is the period of low relief topography after the erosion of the Ancestral Rocky Mountains near the end of the Jurassic Period [16].*

The Cretaceous Interior Seaway marked the beginning of the next major change in depositional environments. Transgression of the seaway brought the deposition of sandstones as the environment of deposition changed to reflect a beachfront. This base sandstone is known as the Dakota Sandstone, and will be further discussed in the stratigraphy section. The Cretaceous Interior Seaway covered much of the interior of the continent for roughly 30 million years, accumulating shales in this low energy environment. The Mancos Shale was deposited during this time, as well as its subdivided groups relevant to the Pagosa Springs area: the Mesa Verde Group and Colorado Group. Regression of the Cretaceous Interior Seaway was marked by accumulation of sandstone known as the Picture Cliffs Sandstone.

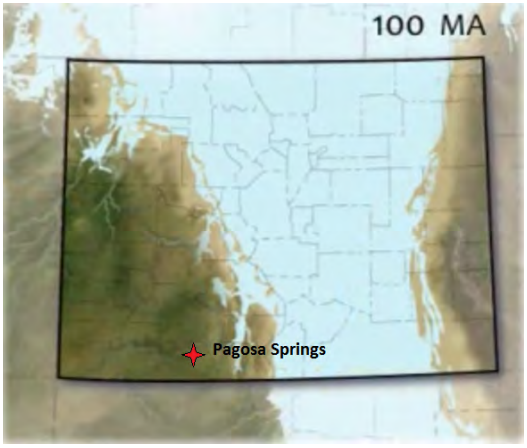

(a) Early Cretaceous Interior Seaway

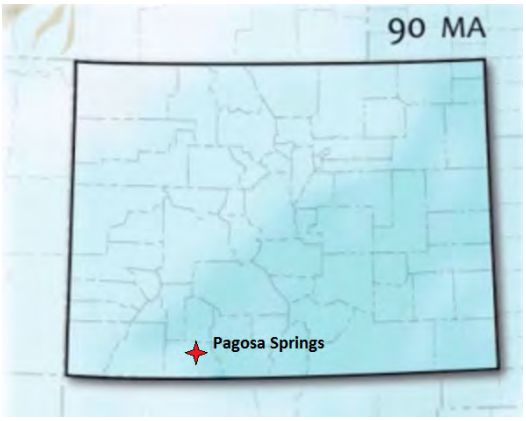

(b) Middle Cretaceous Interior Seaway

Figure 2.2: *(a) During the Cretaceous Interior Seaway transgression, the Pagosa Springs area was one of the last areas in Colorado to become submerged. As the seaway encroached on the Pagosa Springs area, it became a beachfront and then a shallow marine environment. During this time the Dakota Sandstone was deposited. (b) At the height of the Cretaceous Interior Seaway, the entirety of Colorado was submerged. This is when the Mancos Shale and its subgroups (Mesaverde Group and Greenhorn Limestone) were deposited [16].*

The late Cretaceous was marked by the Laramide Orogeny 70 million years ago, during which massive uplift created the current Rocky Mountain range, and in the Pagosa Springs area, the Archuleta Anticlinorium formed. 28-30 million years ago, near the end of the Laramide Orogeny, the Pagosa Springs area was a volcanic province. The volcanic terrain and areas with high relief allowed for high energy deposition and the flat areas in between volcanoes allowed for low energy deposition. This resulted in a variety of facies of rock during this time period, and explains the shales, sandstones, and felsic igneous conglomerates with angular feldspars that are observed above the Pictured Cliffs Formation.

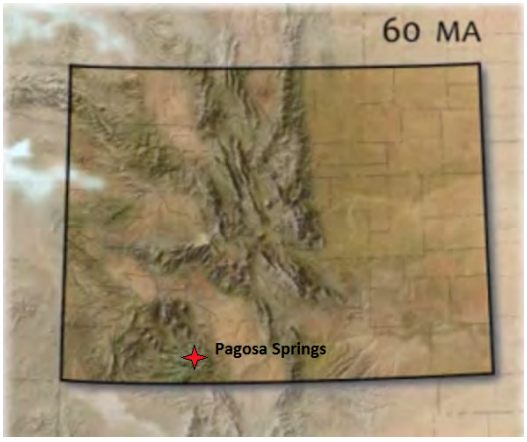

(a) During Laramide Orogeny

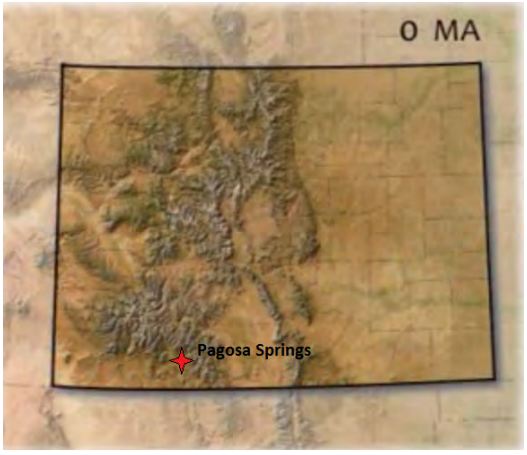

(b) Present Day Topography

Figure 2.3: *(a) Illustration of the current Rocky Mountains during the Laramide Orogeny. The Archuleta Anticlinorium formed near the end of the Laramide Orogeny; then, the Pagosa Springs area was a volcanic province and various layers of extrusive volcanic rocks were deposited. (b) Current topographic profile of Colorado. Further erosion and infill of basins has occurred since the Laramide Orogeny and volcanic period [16].*

The most recent geologic events in the area are two glaciation events during the Pliestocene that covered the San Juan Mountains and further shaped them to their current form. The combination of glaciations and uplift has transformed the region into an area of erosion. Many sedimentary rocks in the area have been completely removed or truncated [17]. Recently, the San Juan River and its tributaries have been the primary geomorphological driver in the region. They have carved small floodplains and deposited alluvial sands and gravels.

2.2.2 Structure

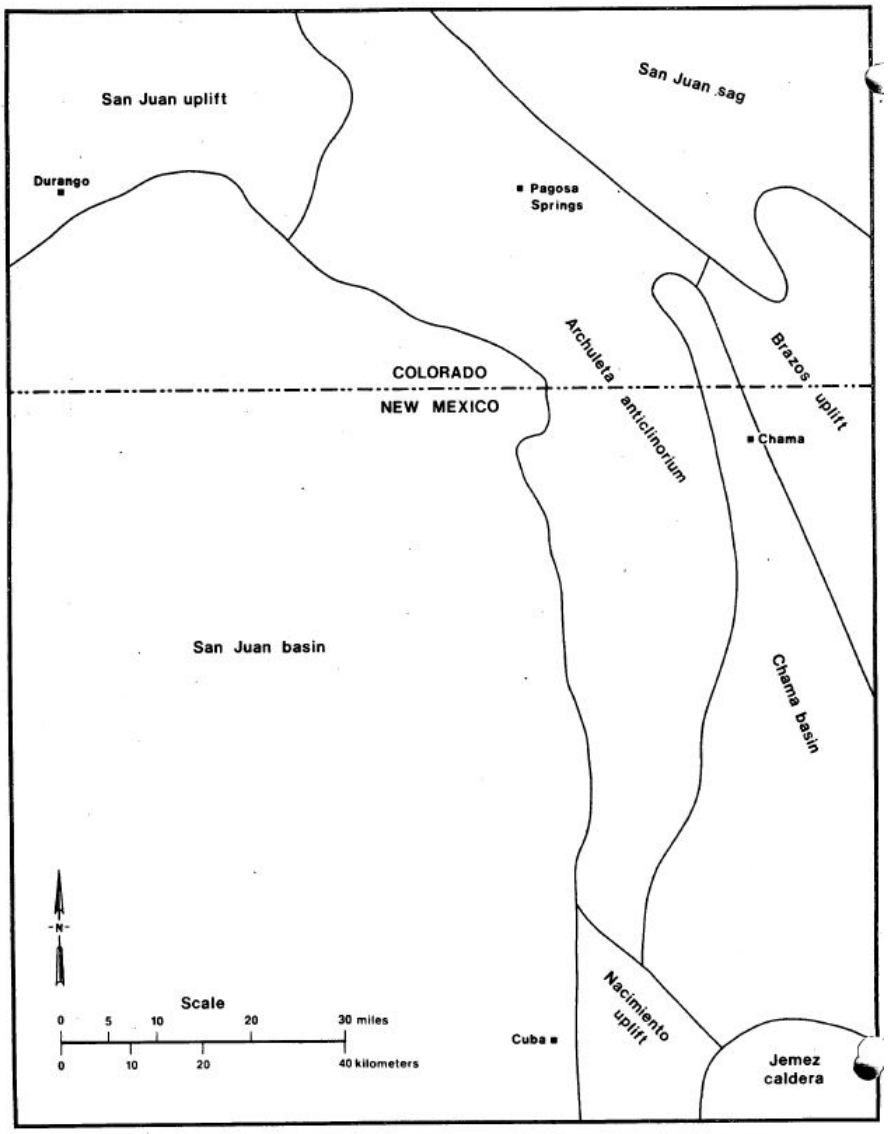

Figure 2 – Regional Structure of the Pagosa Springs Area, Colorado

Figure 2.4: *Map of the structural geology surrounding Pagosa Springs, specifically showing the San Juan Basin, Archuleta Anticlinorium, San Juan Sag, and Chama Basin [10].*

Understanding the regional structural geology and tectonics of the area is key to guiding our interpretations regarding the hydrothermal system of Pagosa Springs. Pagosa Springs is located northeast of the San Juan Basin, a large basin that developed during the Late Cretaceous in Southwestern Colorado and extending into Northwestern

New Mexico, Southeast Utah, and Northeast Arizona. As seen in Figure 2.4, Pagosa Springs sits on the top of the east flank of the Archuleta Anticlinorium, a feature that separates the San Juan Basin from the Chama Basin. The Archuleta Anticlinorium is a completely folded and faulted, northwest trending arch that developed during middle of the Eocene. This arch developed as the main stress distributions and structural styles of the region changed. These fundamental changes are characterized by two major events: loading and subsidence in the San Juan Basin and regional stress and compression due to the Laramide Orogeny [6].

Figure 2.5 shows a general cross section of the Archuleta Anticlinorium, extending roughly 90 miles from the San Juan Basin to the San Juan Sag. Faults associated with the anticline occurred due to extensional stresses, resulting in a system of normal faults. As shown in Figure 2.6, one system of faults in this area run northwest-southeast, and the second system are oriented in the northeast-southwest direction [17]. One of the major faults mapped in the area is the Eight-Mile Mesa Fault, a northwest trending, nearly vertical normal fault with roughly 100 meters of vertical displacement and a nearly vertical dip [10]. This is located southwest of Pagosa Springs, and was mapped in further detail by the 2013 Field Camp. Faults from the late Eocene displace the dikes, while faults that formed during the late Miocene generally do not displace them [10].

At the end of the Laramide Orogeny, the area became a volcanic province that deposited thousands of feet of extrusive volcanic rocks. These resistive rocks make up the San Juan Mountains. The volcanism also created many Northeast trending dikes as seen in Figure 2.6. A couple of these dikes cross the main line near the center, and we expect to see them in many of the geophysical surveys later in the report.

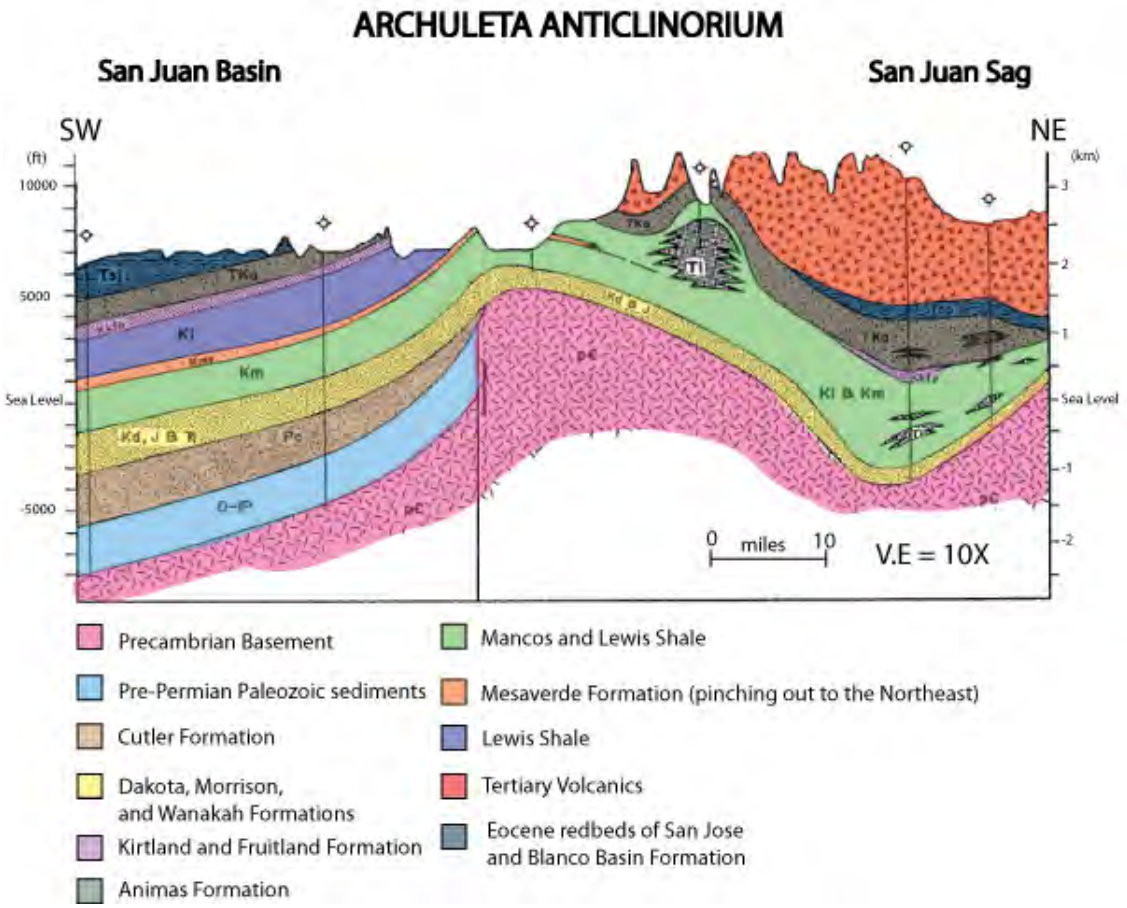

Figure 2.5: *Cross section of the Archuleta Anticlinorium, extending from the San Juan Basin to the San Juan Sag. This cross section extends roughly 90 miles and uses a vertical exaggeration of 10 times. Adapted from [6].*

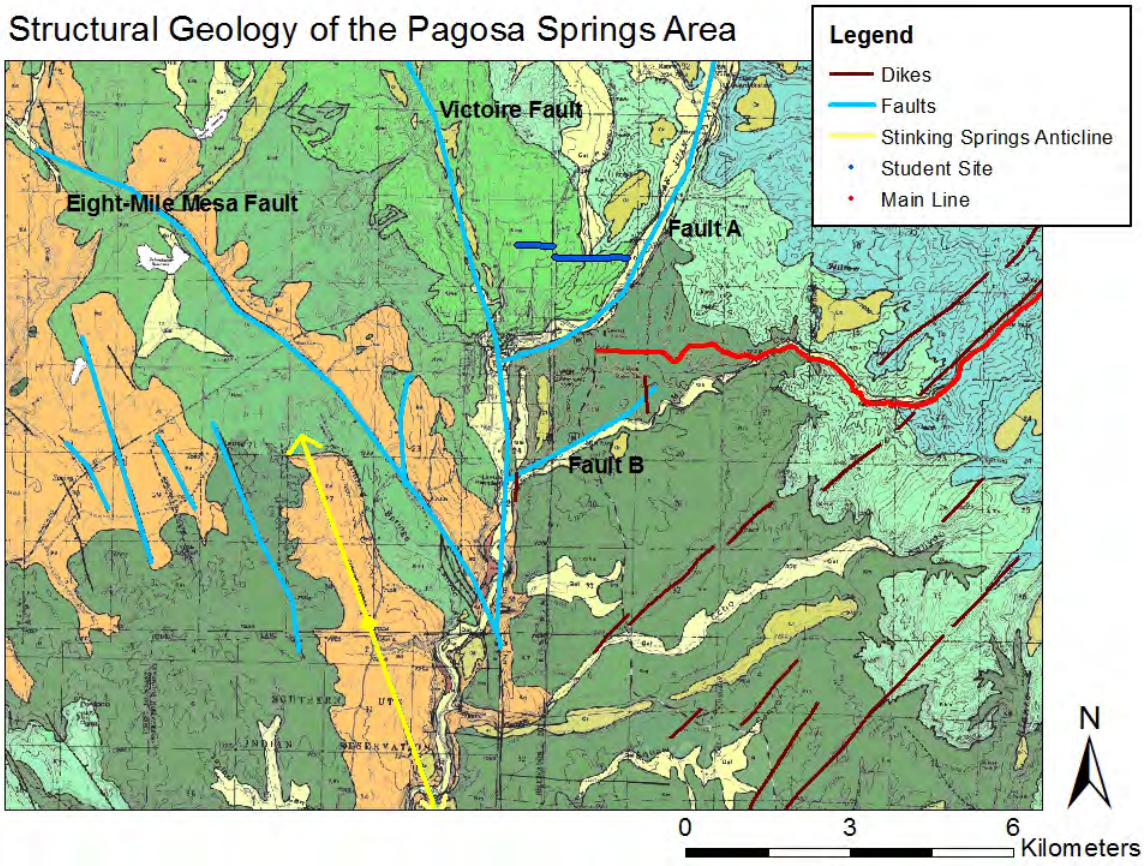

Figure 2.6: *Overview of faults and dikes in the Pagosa Springs area. The mainline and student site are shown by red and blue lines, respectively. Adapted from [10] and [17].*

Precambrian Basement

The oldest rocks in this area are metamorphic and igneous crystalline rocks from the Precambrian era and are 1.1 billion years old. They are comprised of 45% granite, 30% schist and gneiss, 15% quartzite and phyllite, and 10% greenstone [13]. The metamorphic rocks vary throughout the San Juan Basin, though they are the most diverse and well known on the north side near Pagosa Springs. The schist and gneiss are metamorphosed and probably include rocks of varying ages. Intrusive and extrusive rocks, and some originally clastic rocks, are also present in this area [13].

Entrada Formation

The Entrada Formation sits on top of the Precambrian basement, indicating a major nonconformity between the Precambrian and Jurassic periods [11]. This formation extends from Colorado into Arizona, New Mexico, Utah, and Wyoming [8]. It is comprised of fine to medium grained quartz, was deposited in a marginal marine environment, and is about 190 to 360 feet thick [11].

Wanakah Formation

The Wanakah formation was deposited after the Entrada Formation in the middle Jurassic period [18]. It is a Lacustrine deposit with a similar regional extent as the Entrada Formation, but it does not extend into Wyoming.

It contains white crystalline anhydrite with medium to dark gray fine crystalline limestone [17]. It is about 100 feet thick [11].

Morrison Formation

The Jurassic Morrison overlies the Wanakah formation and is indicative of an alluvial plain depositional environment [11]. The Morrison formation was deposited during the Jurassic time period, marking the transgression of the Western Interior Seaway. Mudstones, sandstones, and claystones make up the roughly 700 foot thick layer of sediment accumulation, and in general, the unit is more coarsely grained, crossbedded, and lenticular in comparison to the overlying Dakota Sandstone [7].

Dakota Sandstone

The Dakota Sandstone is dark-gray to black carbonaceous shale and silt stone. It overlies the Morrison formation but is separated by a 50 million year old disconformity [10]. The Dakota Sandstone varies in thickness, ranging from 110 to 270 feet. It is crossbedded, massive, and fine to coarse grained, indicating the environment of deposition was similar to a beachfront and also occurred during the transgression of the Cretaceous Interior Seaway. The upper members of the formation intertongue with the Mancos Shale.

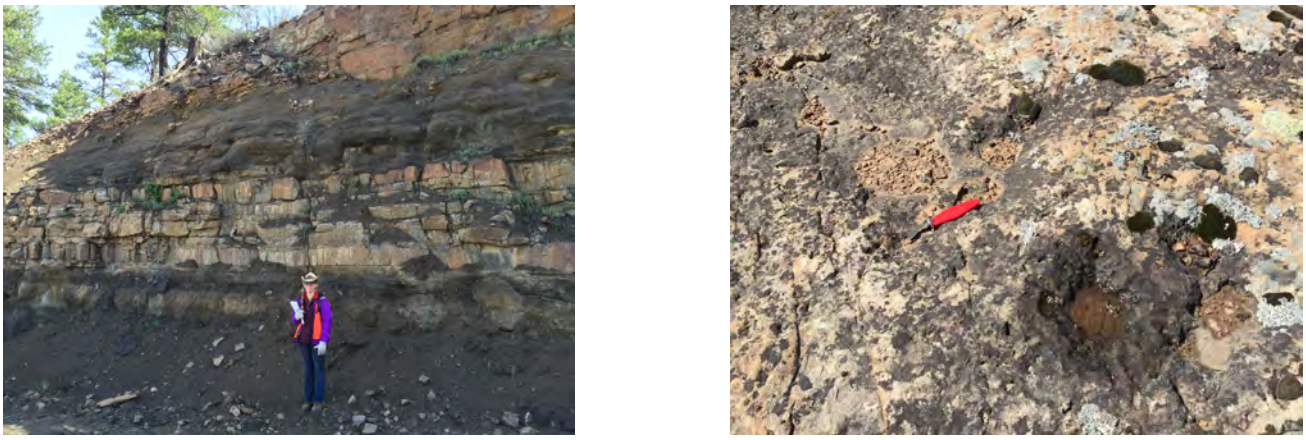

(a) *(b)*

Figure 2.7: *(a) Outcrop of Dakota Sandstone near Eight Mile Fault. (b) Dipslope outcrop of Dakota Sandstone.*

Mancos Shale

Overlying the Dakota Sandstone is the Mancos Shale, which was deposited during the Upper Cretaceous in a deep sea environment. The Mancos Shale varies in thickness from 2100 to 2370 feet, and is roughly 1800 feet thick on the east side Pagosa Springs. This geologic unit is comprised of carbonaceous shales that are dark-gray to black and interbedded with sandstones and limestones, appearing massive to fissile [10].

Colorado Group

The Colorado Group is part of the Mancos Shale and includes the Greenhorn Limestone, Carlile Shale, Graneros Formation, and Niobrara Formation. The Greenhorn Limestone is about 40 to 60 feet thick. It is comprised of alternating beds of dense gray limestone and darker gray calcareous shale. It is generally more resistive than the Mancos shale that surrounds it and forms ridges [7]. The Carlile Shale and Graneros Formation are not encountered in this region of Colorado. The Niobrara Formation lies on top of the Greenhorn Limestone in Pagosa Springs. It is a dark-gray fissile marine shale that is about 500 feet thick [19].

Mesaverde Group

The Mesaverde group is characterized by interbedded sandstones and shales. The environment of deposition is predominately coastal plain and occurred during a regression of the Cretaceous Interior Seaway. The water was shallow enough for the waves to sort and distribute the sand and mud [15]. Near Pagosa Springs it is hard to differentiate from the overlying and underlying shales. There are various members of this group including the Cliff House Sandstone, Point Lookout Sandstone, and the Menefee Formation [14].

Lewis Shale

The Lewis Shale overlies and intertongues the Mesaverde group. It is characterized by light to dark gray shale with sandy beds at the base and top [10].

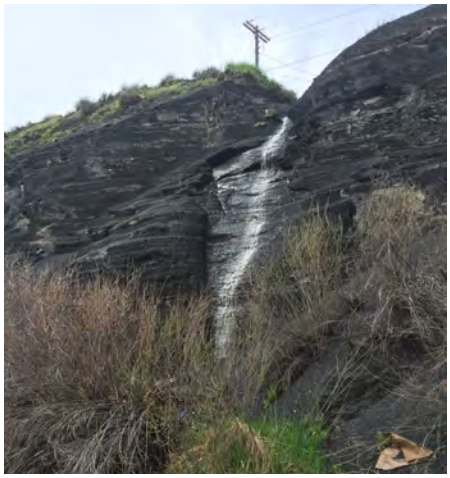

Figure 2.8: *An outcrop of Mancos Shale near the Mother Spring.*

Pictured Cliffs Sandstone

This formation was deposited on the shoreline during the final regression of the Cretaceous Intercontinental Seaway [9]. It is not seen in our cross sections or surveys because of erosion in the area, but it is an interesting formation. It marks the end of the Cretaceous Intercontinental Seaway.

Other Formations

Formations such as the Fruitland, Kirtland, and Nacimiento appear after the Pictured Cliffs in many locations across Colorado, however, they do not appear in Pagosa Springs due to erosion.

Figure 2.9: *An outcrop of the Mesaverde Group along the Piedra River on CR166.*

Volcanics

The San Juan Mountains in the region are composed mostly of extrusive volcanic rocks of intermediate composition. The ranges up to 5050 feet of eruptive volcanics and volcaniclastics [19]. There are also sets of intrusive rocks. The Archuleta dike swarm in the area includes dikes up to 12 feet wide and 8.5 miles long with baked zones up to 5 feet. The baked zones are prominent in the Mancos and Lewis shales, and there is no evidence of hydrothermal alteration associated with the dikes. North of Pagosa Springs, drill holes have encountered Cretaceous age intrusive rocks that may be part of a subvolcanic batholith [10].

Figure 2.10: *An outcrop of the volcanic welded tuff by Wolf Creek Pass.*

Alluvial deposits

There are many alluvial deposits throughout the Pagosa Springs area deposited by the San Juan River and its tributaries. These are recent deposits and include many of the rock types that are higher in the stratographic column than Pagosa Springs. Some examples include Volcanic tuff, Fruitland, and Pictured Cliffs.

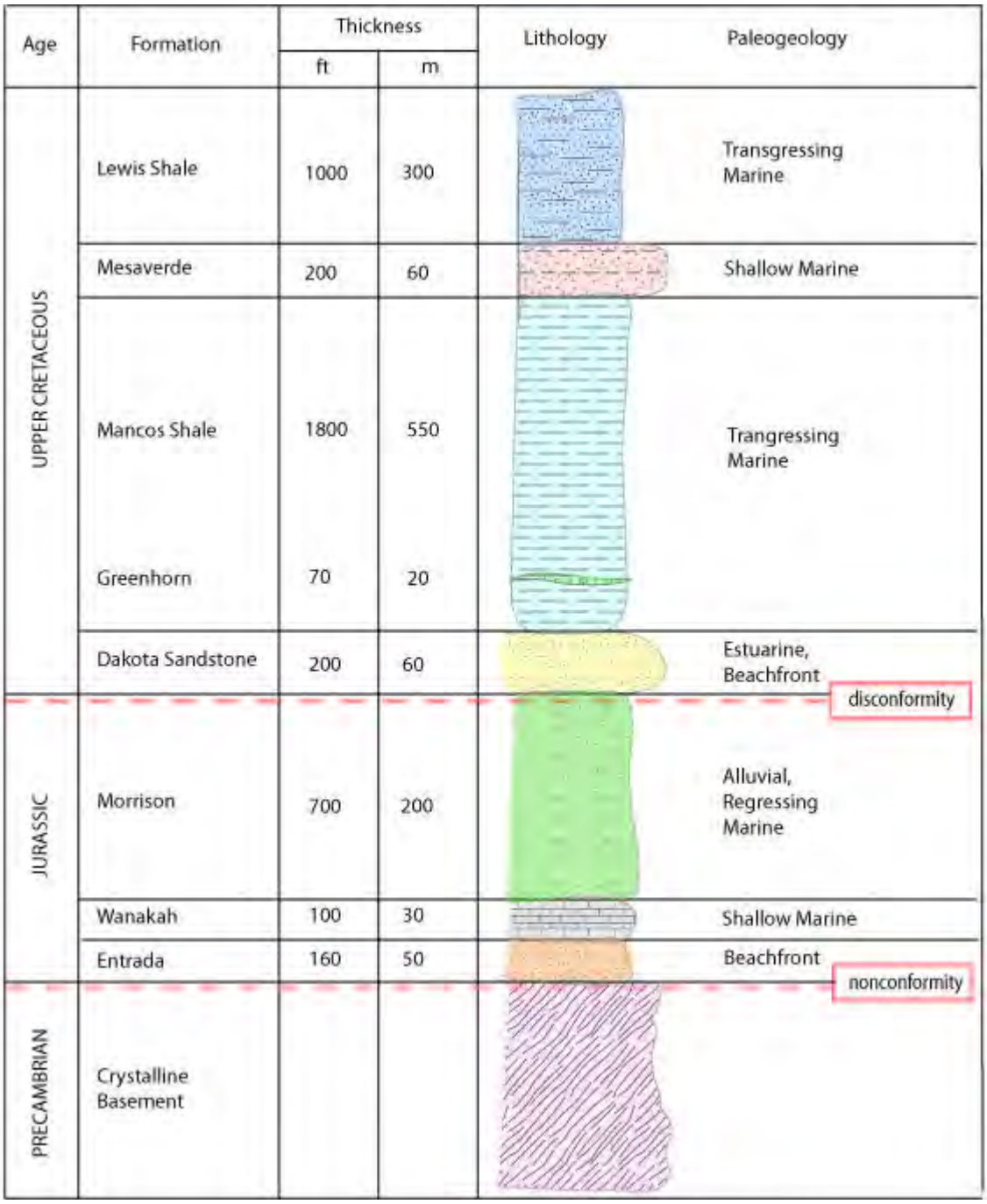

Figure 2.11: *Stratigraphic column correlating to the East end of the main line. [10].*

2.2.3 Rock Properties

This section summarizes rock properties such as bulk density, velocity, resistivity, and porosity. These rock properties will provide restraints and guide inversions for different geophysical methods. Table 2.1 shows the average rock properties calculated from the Brown Federal #1-17 Well Logs, and Table 2.2 shows the average rock property values calculated from the Pagosa Verde PVTG1 Well Logs.

Brown Federal #1-17 Well Rock Properties			
	Bulk Density g/cc	Sonic (velocity) m/s	Resistivity Ohm-m
Lewis	2.42	3086.47	9.71
Mesaverde	2.53	3503.45	10.66
Mancos	2.56	3575.62	12.89
Niobrara	2.57	3810	21
Greenhorn	2.35	4064	14
Dakota	2.45	3761.94	20.55
Morrison	2.60	4261.68	21.83

Table 2.1: *Rock properties of the geologic formations, taken from the Brown Federal Well logs.*

Pagosa Verde PVTG1 Well Rock Properties				
	Bulk Density g/cc	Porosity %	Sonic (velocity) m/s	Resistivity Ohm-m
Mancos	2.6297	5.233	3310.9	30.2120
Dakota	2.6284	5.3028	4249.2	109.5012
Morrison	2.6304	5.1111	4302.5	64.9515
Wanaka	2.680	1.2752	6975.1	1768.4

Table 2.2: *Rock properties of the geologic formations, taken from the Pagosa Springs PVTG1 Well logs.*

2.3 Geothermal System

2.3.1 Heat Sources

Since there has been volcanic activity in the past, a batholith would be a reasonable heat source. However, there is no current geologic information indicating a heat source from an intrusive structure, therefore it is likely that the heat is provided by an enhanced regional thermal gradient [10]. Figure 2.12 shows the geothermal heat flow in the area. Pagosa Springs is located right in the center of the increased heat flow area with decreased heat flow to the northeast. Based on the water temperature and a twice normal geothermal gradient, water would have to circulate down 1 to 2 kilometers. This suggests that the basement rock is the primary geothermal reservoir [10]. The age of the thermal system is unknown due to the erosion of large sections of rock.

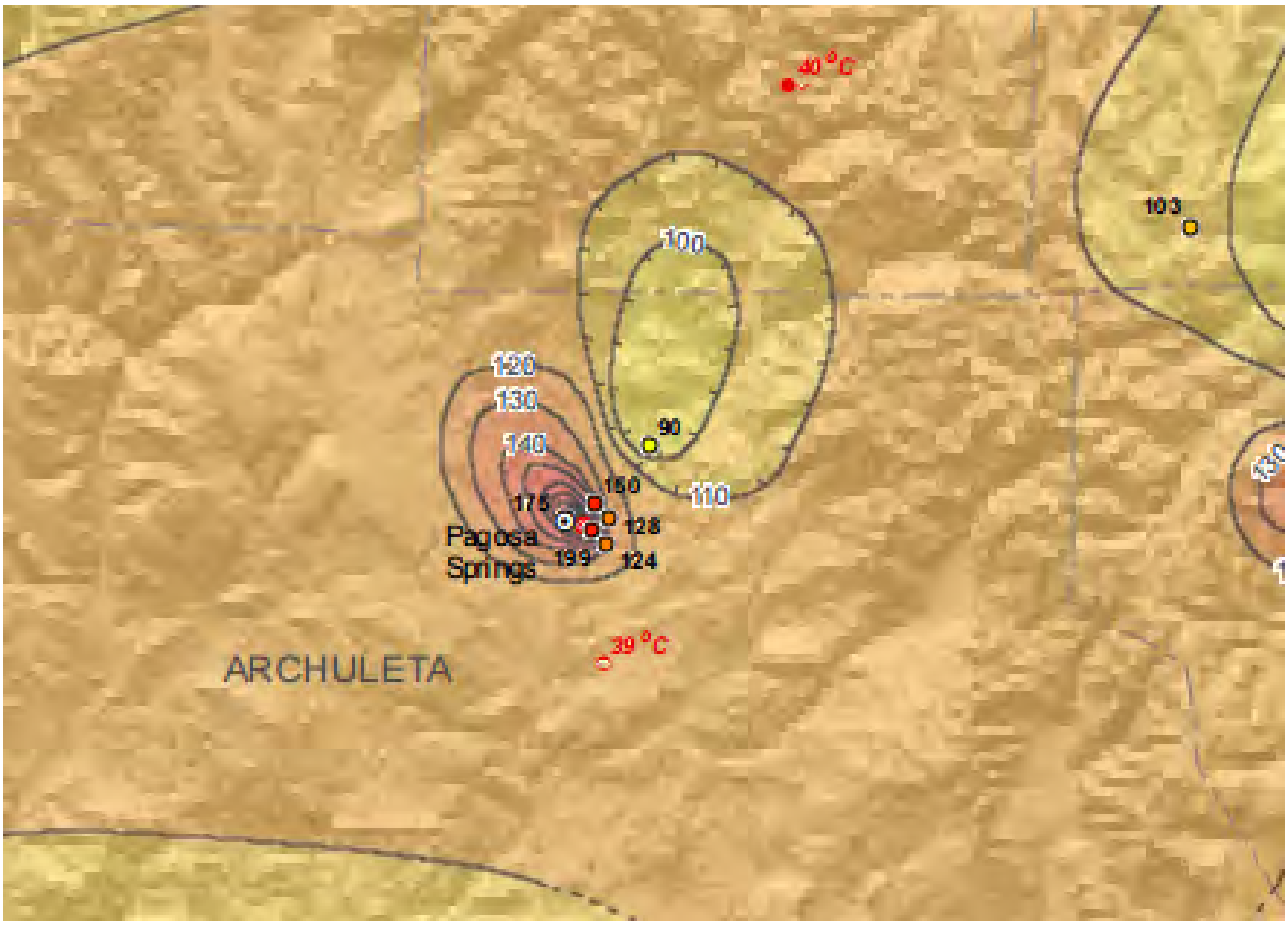

Figure 2.12: *This image shows the large scale geothermal heat flow of the Pagosa Springs area. There is increased heat flow directly under Pagosa Springs and a region of lower heat flow to the northeast. Photo courtesy of the Colorado Geological Survey [5].*

2.3.2 Hydrology

There are two main aquifers in the Pagosa Springs area; one is held in the Mancos Shale, and the other is in the Dakota Sandstone. Water flow in the Mancos shale is a result of fractures and intergranular porosity. The groundwater quality from this aquifer is generally poor [10]. Groundwater flow in the Dakota sandstone is confined and results from fracture porosity. It is possible that this formation holds two semi-independent aquifer (fracture) systems that are separated by black shale sequences [10]. Water quality from this aquifer is similar to that of the Mancos shale.

The water from the hot springs carries calcium carbonate which precipitates out at surface temperature and pressure conditions [12]. This creates the travertine deposits seen at the Mother Spring. Geochemical analysis of the water has shown that it is meteoric in origin. The chemistry also indicates a high degree of inter-connectivity between the rock units.

One of the main questions this paper is trying to address, is how the water is flowing to the Mother Spring. The water could be flowing laterally through the Dakota sandstone or fed vertically to the Dakota by some permeable feature. The fault system in the area contains many nearly vertical faults that could potentially provide a flow path for the hot water. One argument for a system controlled by a vertical feature is the high groundwater flow present in the Dakota Sandstone [10]. Vertical faults could be conduits for water flow from the basement.

2.4 Mainline Geology

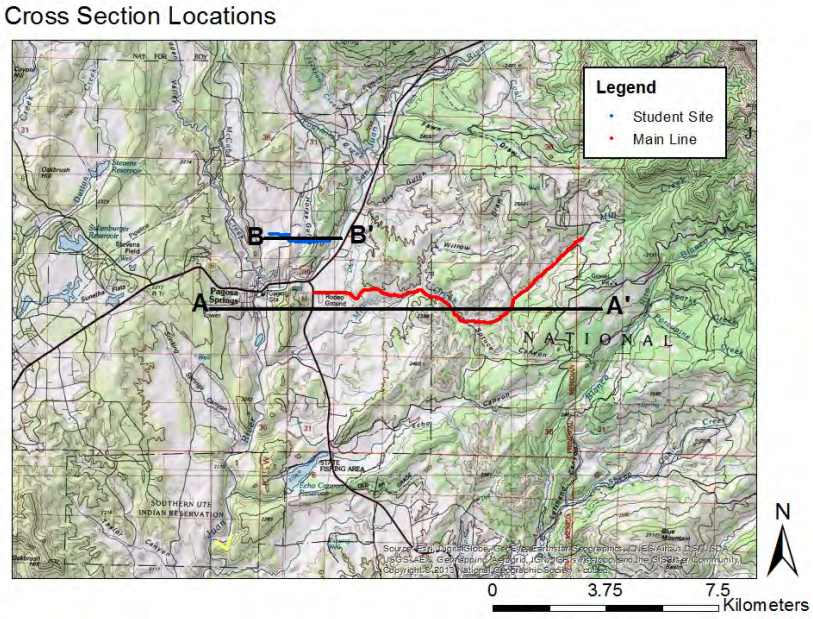

Figure 2.13: *Map showing the location of the cross sections. A-A' is the cross section for the mainline. B-B' is the cross section for the student site. The red line is the actual location of the mainline, and the blue line is the actual location of the student site.*

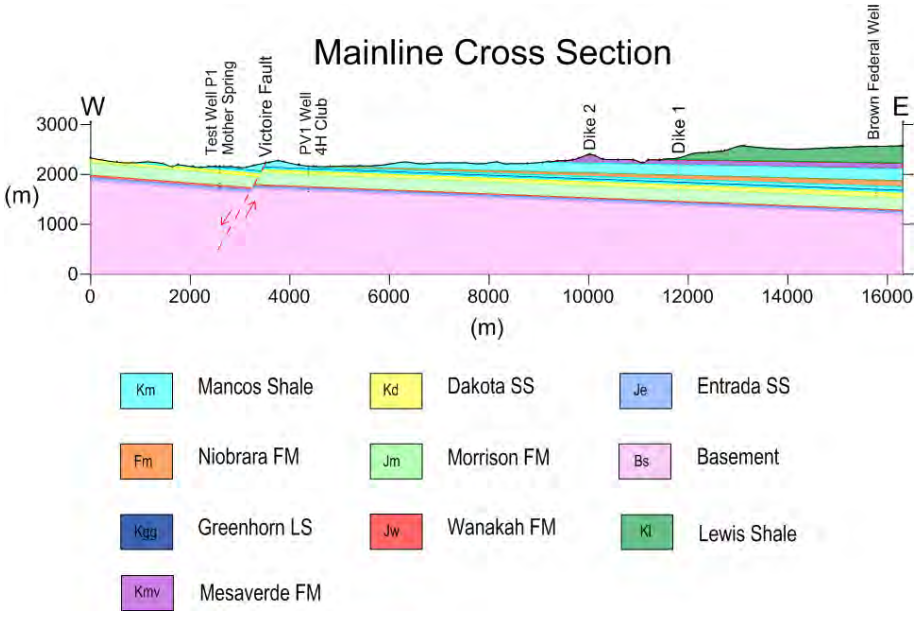

Figure 2.14: *Main Line cross section from A - A' shown on Figure 2.13.*

2.5 Student Site Geology

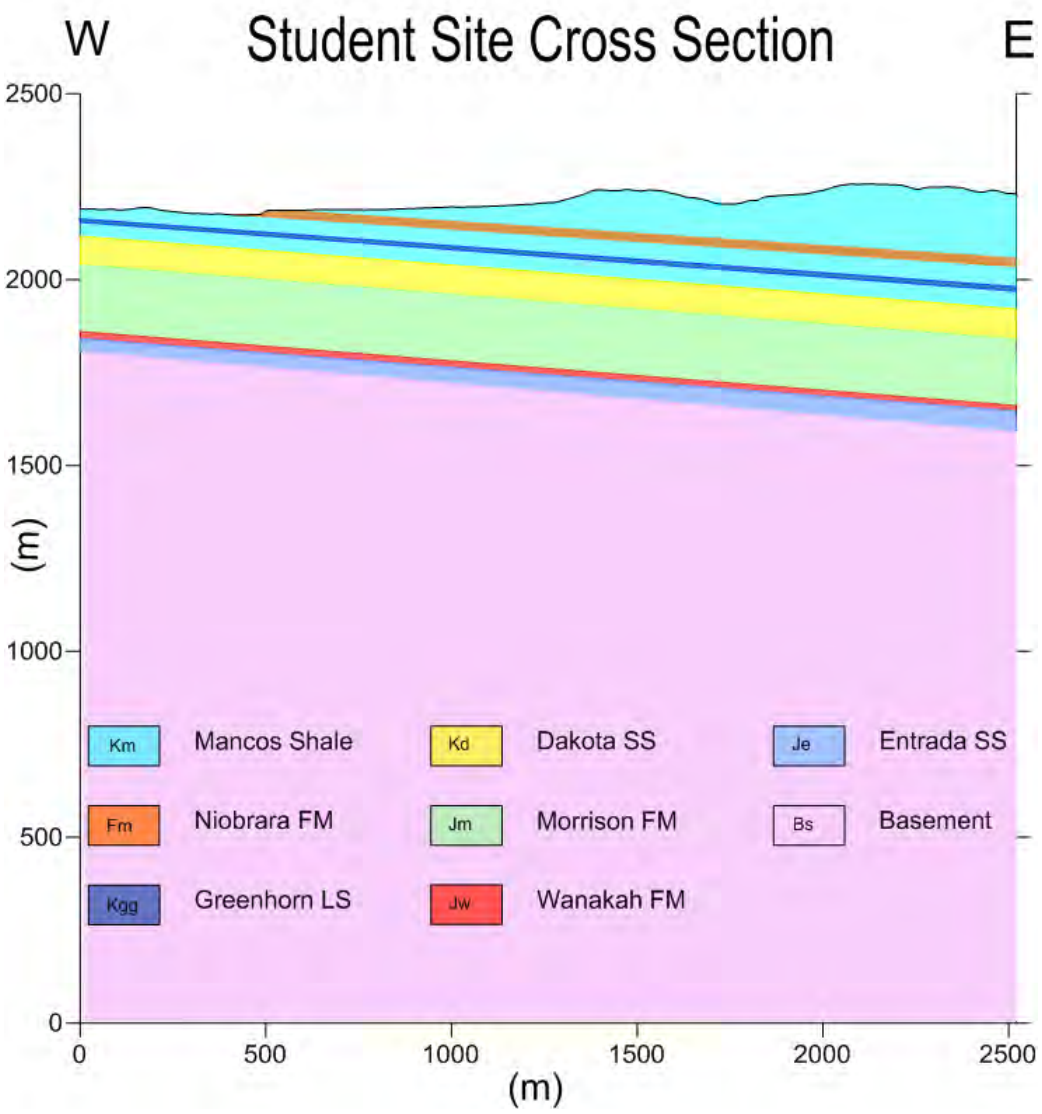

Figure 2.15: *Student Site cross section from B - B' shown on Figure 2.13.*

2.6 Recommendations

During the data processing portion of the field camp, it would have been helpful to have had a small separate group focused on researching past geophysical studies in the area. One of their tasks could be to look at the various wells in the region and make a resistivity profile of the geologic layers, specifically the Dakota Sandstone, since it is an important reservoir layer in the region.

2.7 Conclusion

Millions of years of erosion and deposition has transformed the landscape of Pagosa Springs into what it is today. The most important features of the area relating to the hot springs are the Archuleta Anticlinorium, the

various faults, the dikes, and the various sedimentary layers, through which, the groundwater is flowing. These structures could be important factors controlling ground water flow. Based on the chemical composition and temperature of the water, it is meteoric in origin and it most likely flows into the basement rock before going back up to the surface. Faults and dikes could be important conduits directing the flow of the hot water. Geophysical methods may be able to give further insight into additional geologic structures in the area and how the water is flowing along the main line and student survey lines.

References

[5] F. E. Berkman and C. J. Carroll, *Interpretive Geothermal Gradient of Colorado*, Geothermal Heat Flow Map, Oct. 2007. [Online]. Available: http://coloradogeologicalsurvey.org/wp-content/uploads/2013/08/LoRes_Plate1_Interpretitive_Geothermal_Heat_Flow_Map.pdf (cited on pages 15, 190).

[6] B. S. Brister and C. E. Chapin, "Sedimentation and Tectonics of the Laramide San Juan Sag, Southwestern Colorado", English, Rocky Mountain Association of Geologists, Tech. Rep., Jan. 1994 (cited on page 9).

[7] D. Carle, "The Dakota Sandstone and Mancos Shale of the Eastern Side of San Juan Basin, New Mexico", Washington, D.C: U.S Geological Survey, 1960, pages 63–74 (cited on page 11).

[8] *Entrada Sandstone*, English, Jan. 2015. [Online]. Available: http://3dparks.wr.usgs.gov/coloradoplateau/lexicon/entrada.htm (cited on page 10).

[9] J. E. Fassett, "Geology and Coal Resources of the Upper Cretaceous Fruitland Formaion, San Juan Basin, New Mexico and Colorado", English, U.S. Geological Survey, Tech. Rep. 1625-B. [Online]. Available: http://pubs.usgs.gov/pp/p1625b/Reports/Chapters/Chapter_Q.pdf (cited on page 12).

[10] M. J. Galloway, "Hydrogeologic and Geothermal Investigation of Pagosa Springs, Colorado", English, Colorado Geological Survey Department of Natural Resources, Denver, CO, Tech. Rep., 1980 (cited on pages 8–15).

[11] "Geophysical Investigation of the Geothermal System within the Chromo Anticline", English, Colorado School of Mines, Upper San Juan Basin, Archuleta County, CO, Tech. Rep., Jun. 2015. [Online]. Available: http://inside.mines.edu/UserFiles/File/geophysics/fieldcamp/GPGN468_FinalReport.pdf (cited on pages 10, 11).

[12] "Geophysical Investigation of the Pagosa Springs Geothermal System", English, Colorado School of Mines, Upper San Juan Basin, Archuleta County, Colorado, Tech. Rep., Jun. 2013. [Online]. Available: http://inside.mines.edu/UserFiles/File/geophysics/fieldcamp/2013Report_Final.pdf (cited on page 15).

[13] V. C. Kelley, "Pre Cambrian rocks of the San Juan Basin", English, volume 1, New Mexico Geological Society, 1950, pages 53–55. [Online]. Available: https://nmgs.nmt.edu/publications/guidebooks/downloads/1/1_p0053_p0055.pdf (cited on page 10).

[14] *Mesaverde Formation*, English, Jan. 2015. [Online]. Available: http://3dparks.wr.usgs.gov/coloradoplateau/lexicon/mesaverde.htm (cited on page 12).

[15] "Mesaverde Formation at Chromo Anticline, Archuleta County, Colorado", *The Mountain Geologist*, volume 1, number 1, pages 15–24, 1964 (cited on page 12).

[16] D. B. Raynolds and K. Johnson, *Ancient Paintings*, English, Jan. 2016. [Online]. Available: http://coloradostratigraphy.com/videos.html (cited on pages 6, 7).

[17] D. A. Revil, "Resistivity Investigation of Northeastern Pagosa Springs, Archuleta County, CO", English, Colorado School of Mines, Pagosa Springs, Tech. Rep., May 2013 (cited on pages 8–11).

[18] *Wanakah Formation*, Jan. 2015. [Online]. Available: http://3dparks.wr.usgs.gov/coloradoplateau/lexicon/wanakah.htm (cited on page 10).

[19] W. J. Warren Jr., "A Geothermal Exploration Project in Pagosa Springs Colorado", English, Master of Science Thesis, Colorado School of Mines, Golden, CO, May 1986. [Online]. Available: https://dspace.library.colostate.edu/handle/11124/78485 (cited on pages 11, 12).

3. GPS

Contents

3.1 Introduction

Many survey methods record and utilize geospatial data sets. These data sets depend on knowledge of their exact positioning in both easting and northing as well as in elevation relative to sea level. Further processing of the geospatial data sets also requires the data locations for various correction processes, such as elevation or terrain corrections. Techniques that can collect spatially accurate data include Global Positioning Systems (GPS) and remote sensing. The spatial techniques utilized in Pagosa Springs include hand-held GPS, differential GPS, total distance measurement (TDM), and digital elevation models (DEM).

3.1.1 Background

A digital elevation model (DEM) for the Pagosa Springs area served as a basis for the GPS surveys. The GPS elevations collected were compared to the DEM's in order to make a more accurate elevation model along the survey lines. DEMs are digital surfaces made up of x, y, and z coordinates; where x is easting, y is northing, and z is elevation. DEMs are obtained using various remote sensing methods such as LIDAR. The DEM for Pagosa Springs has a 30 m resolution. The DEM that contains Pagosa Springs is a part of the National Elevation Dataset (NED) [25].

3.1.2 Theory

Hand-held GPS

The hand-held GPS is a small hand-held unit that utilizes a network of satellites meant for spatial positioning points on the surface of the earth. In order to determine a latitude, longitude, and elevation for a location, at least 4 satellites must be visible to the hand-held unit. The satellites send signals with position and time information, and the difference between signal sent and received allows the distance from the satellite to be determined. By using the distance from each satellite and trilateration, the hand-held GPS is able to determine its location. The accuracy for hand-held GPS ranges from 3 meters to 10 meters [21]. Elevation values are less accurate than easting and northing values with this device, so methods that need accurate elevation do not use the hand-held GPS. Accuracy of this device is decreased by the following factors [20]:

- Ionosphere and troposphere delays: signals slow as they pass through the atmosphere
- Signal multipath: errors in the travel time due to the signal reflecting off objects
- Receiver clock errors: timing errors due to the fact that the receiver's clock is not as accurate as the satellite's
- Orbital/Ephemeris errors: reported location of the satellite is inaccurate
- Number of visible satellites: the fewer the satellites, the less accurate the position

Differential GPS

Differential GPS, or DGPS, is a GPS system that uses a base station and rover to triangulate GPS coordinates at a higher precision and accuracy then the hand-held GPS. DGPS uses a stationary base to eliminate common errors in the data that may result from travel time or timing errors. The base station requires a signal or connection to four different satellites before it takes a measurement. The DGPS uses these satellites to triangulate the location of the base station and the rover at the same time. The base station serves as a known reference station with regards to the rover. The roving receiver is able to obtain more precise spatial coordinates due to the corrections provided by the base station. Therefore the DGPS method accounts for most errors except for signal multipath and receiver errors, which are general errors only associated with the roving receiver or the stationary base [24].

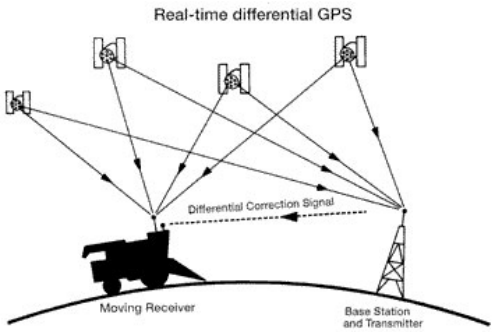

Figure 3.1: *Satellite configuration for DGPS. The DPGS system utilizes two receivers that connect to the same satellites in order to get GPS coordinates. Due to the simultaneous connection to the satellites, timing errors can be eliminated from the GPS data, resulting in better GPS accuracy [23].*

For the DPGS method to work with precision and accuracy, it is necessary that the base station has a clear view of four or more satellites as well as a connection to the rover. Any obstruction of these views between the satellites or rover due to trees or clouds hinders the accuracy and precision of the data obtained. In ideal conditions, the DGPS produces data with a maximum error of 1m [21]. The survey size and topography of the area dictate the ease of mobility for the DGPS. In areas of higher topographic variation, the base station may need to be moved multiple times. Additionally, a roaming antenna may be necessary in larger survey areas to extend the range of the DGPS.

Total Distance Measurement

Total distance measurement (TDM) is a method for determining exact coordinate positions that uses a total station theodolite in conjunction with a roving mirror. Through optics, the total station theodolite, survey instrument which measures angles, with an electronic distance meter, is able to locate a roving mirror with reference to its own location and orientation. The roving mirror is moved in sight of the base station. The base station theodolite is able to calculate the mirror's relation to the base station by shooting a laser at the roving mirror which reflects the laser back at the theodolite. Based on the travel time and phase of the laser, the total station theodolite measures and records the azimuth, slope distance, and zenith angle of each position of the mirror, as seen in Figure 3.2.

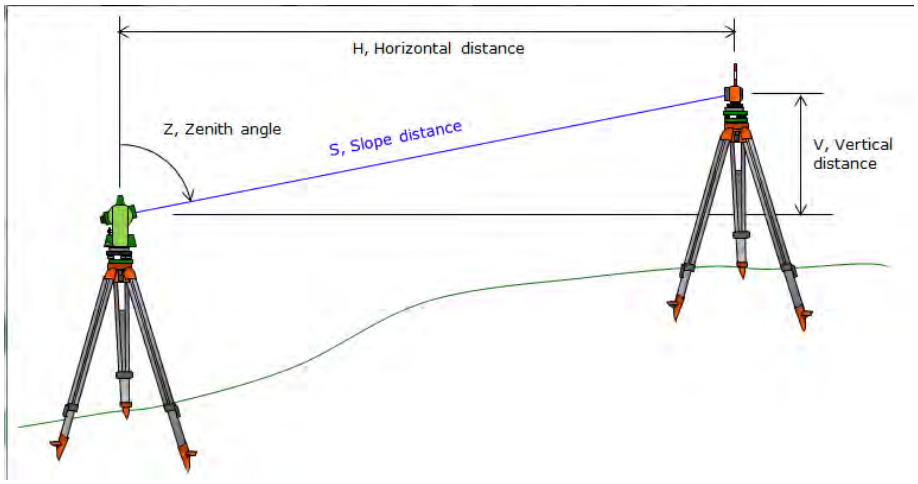

Figure 3.2: *Illustration of the geometry of TDM. By using trigonometry, the horizontal and vertical distance between the theodolite and the mirror can be determined. Further incorporating the azimuth allows for the determination of location of the roving mirror in x, y, and z [22].*

From these values, along with the known GPS location of the total station theodolite and instrument dimensions of the theodolite and the roving mirror, the survey coordinates of the roving mirror are calculated. These resulting coordinates are only relative to the total station theodolite location. The location of the theodolite must be anchored to some known coordinate in order to determine easting and northing [22].

The precision and accuracy of the total station theodolite depends on the precision and accuracy of the known location of the base station. If there are any errors within the total station theodolite receiver, then the errors are carried to all of the other survey coordinates obtained with this total station. For the optics to work, the total station must have a clear view of the mirror at all times.

3.2 Objectives

1. Obtain spatial coordinates at all survey locations: mainline, student site, DC extension of the student site, hammer seismic line parallel to student site, MT sites, TEM sites, and borehole sites.

2. Process and combine all obtained spatial coordinates into a usable format: easting, northing, and elevation.

3. Further process the data to compare the measured GPS elevations to the known DEM model in order for the gravity method to make accurate elevation corrections to their data.

3.3 Methods

3.3.1 Survey Location

GPS coordinates were collected along all survey locations. DGPS was used along the entirety of the main line and for most of the student site. Trees covered part of the East side of the student site, so the DGPS base station could not find a signal and the total station was used instead. Hand-held GPS was utilized at the survey sites of electromagnetics and magnetotellurics because GPS accuracy, specifically elevation, is not as important with these methods. Internal GPS was also used with magnetotellurics for timing purposes, and the hand-held GPS was used for location. The DC resistivity survey extended beyond the west side of the student line and hand-held GPS was used to collect the coordinates of this extension. Additionally, hammer seismic collected data on a line parallel to the student site. Only a couple of hand-held GPS points were taken on this seismic line. All of the GPS locations can be seen in Figure 9.1.

3.3.2 Flagging

Flags were laid out along both the main line and the student site. The main line flags were placed with 10m spacing and labeled 1000 to 2100 from west to east. The student site had 20m flag spacing and had irregular flag numbers because the flags had been labeled prior to the field camp and were not sorted before they were placed. Although the flag numbers are irregular, the majority of the surveys done on the student site ran from west to east.

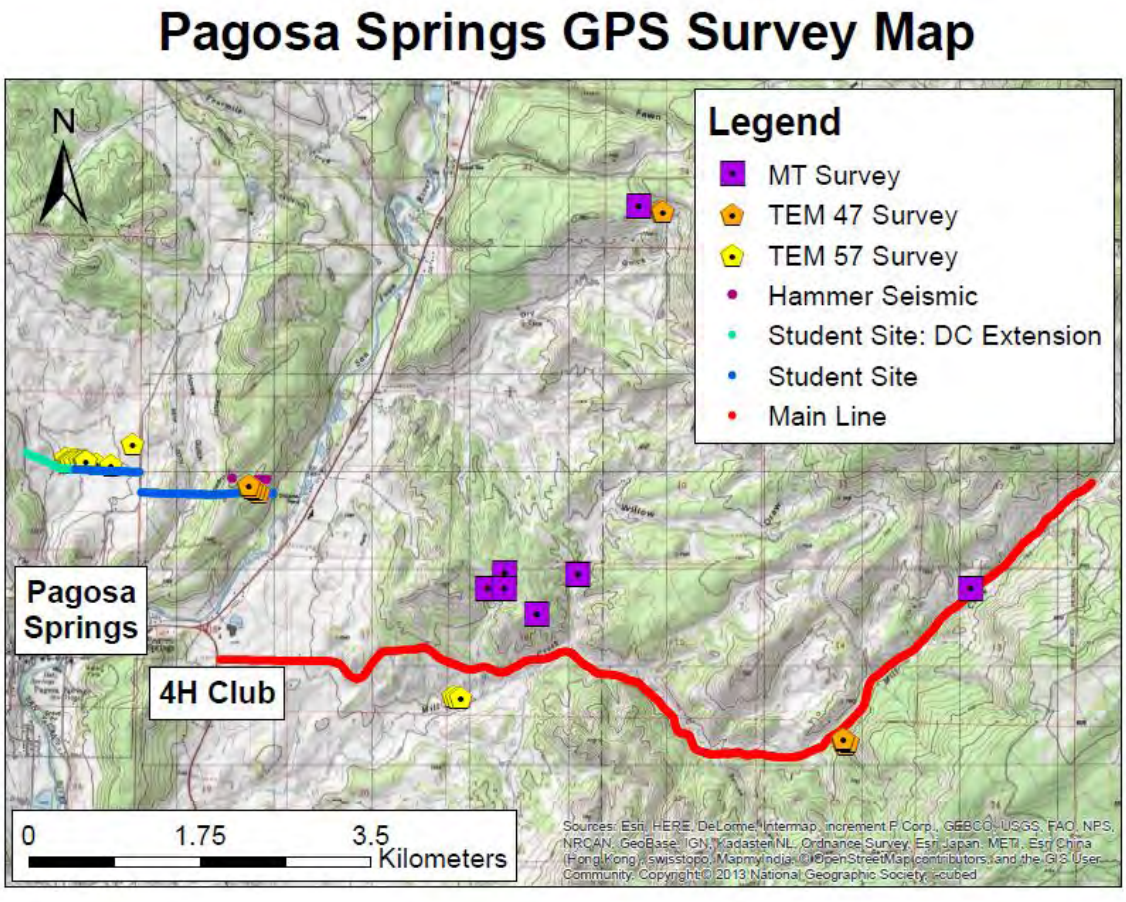

Figure 3.3: *Detailed map with all GPS coordinates of survey locations. An extension to the west of the student site line was obtained for DC resistivity. Hammer seismic shot a line parallel to the student site line. Overlap seen in the image is due to the concentration of surveys in some areas.*

Method	DGPS	Total Station	Handheld GPS	Internal GPS
Deep Seismic	x			
Hammer Seismic	x		x	
DC Resistivity	x	x	x	
Self Potential	x			
Magnetics	x	x		
Gravity	x	x		
Electromagnetics	x	x	x	
Magnetotellurics			x	x

Table 3.1: *GPS type used for each geophysical method.*

3.3.3 Equipment List

The following equipment was used in the collection of the GPS data:

- Trimble DGPS system, including rover, base station, and roaming antenna
- Garmin hand-held GPS unit
- Pentax R-323 NX Total Station
- Distance reflection lens, OMNI Prism

3.3.4 Data Acquisition

Students collected DGPS data along the mainline from May 19^{th} to May 22^{nd} with the Trimble DGPS rover and base station. The DGPS system was set up with two antennas. One antenna was installed at a high elevation and connected to the Trimble base station. The other antenna, the roaming antenna, was attached to the rover, or mobile unit, which extended the range of the rover. Students collected DGPS data until the rover was no longer within range of the base station. The base station was relocated at several locations in order for the rover to be within proximity.

Figure 3.4: *Student surveyors using the roving DGPS and antenna on the mainline.*

GPS data collection on the student site started on May 22^{nd}. Students collected DGPS data along the west side of the student site and sporadic points along the east side that day. Due to tree cover on the east side, students could not take regular DGPS readings at each flag, resulting in sporadically spaced GPS points in the clearings. To fill in the missing data on the east end of the line, students used TDM with the total station. GPS data collection from the total station began on May 23^{rd} and was completed on the 24^{th}. The total station was set up within view of two to three previous DGPS coordinates. This provided enough spatial information for calculating the GPS coordinates of the base station. Once the total station was leveled and aligned with north, the roving mirror or prism was moved to the location of the flags along the student line, and a distance measurement was taken. Students repeated this process for every flag location that the DGPS was not able to record, and the total station was moved as needed when the prism was no longer visible from the total station.

Throughout the data acquisition process, less accurate position coordinates were taken at all the TEM and MT sites with the hand-held GPS. Additionally, students took hand-held GPS coordinates at the DC resistivity extension of the west end of the student site as well as the on the hammer seismic line parallel to the student site.

Figure 3.5: *Picture of student surveyor and mentors using the total station to take points at the student site.*

3.3.5 Processing

DGPS data for the mainline was compiled into one master file. Additional processing was required for the data to be incorporated into gravity corrections. This additional processing only applied to gravity. Other methods require stand-alone elevations, which did not factor in elevations from a DEM model. For gravity, the differences between the DEM elevations and DGPS elevations were determined, and the DGPS data was shifted to match the DEM elevations.

The final student site data was compiled from the DGPS and total station data. The total station data had to first be converted into easting and northing. The data then had to be corrected to true north, due to incorrect alignment of the theodolite during data collection. The total station data was then combined with the DGPS data to produce a master file for the student site. Due to the nonlinear numbering system of the student site flags as well as missing flags or incorrect flag numbers, compiling all of the GPS data into one file was problematic. However, the final GPS data was compiled into a master file. Again, the final student site data was shifted to fit the DEM model for further use in gravity processing.

All final GPS data corresponds to the projected coordinate system of WGS 84/UTM zone 13N. Additionally, all of the GPS data was compiled into ArcMap for further use and interpretation.

3.4 Discussion

3.4.1 Errors and Uncertainty

There are both human and instrument errors associated with each GPS method. Hand-held GPS is only accurate within 3-10 meters, and the accuracy of the point taken is dependent upon the visibility of satellites. The visibility of the satellites also affects the accuracy of the data obtained with the DGPS. To produce the most accurate data with the DGPS, the rover must be held level while obtaining a GPS location. If the total station is not leveled correctly or set to true north, errors occur when calculating the x, y and z components for the UTM coordinates. Additionally, the resulting UTM coordinates need to be anchored by a known accurate total station location for the total station accuracy to carry through. Similarly, the total station base station needs to be leveled as well as possible in order to improve accuracy of the data points taken.

Human errors could have easily been made on the student site, as flags were numbered non-linearly. This could have resulted in labeling data points with the wrong flag number and placing the flags incorrectly in space. Further more, vegetation and tree cover on the east side student site was extensive, reducing the accuracy of the DGPS and hand-held GPS and making it difficult to find a clear line of view for the total station. Instrument errors on the mainline could have occurred when the DGPS rover was at the furthest range of the base station. Another possible source of error could be due to the DPGS rover not being level while recording.

3.5 Conclusion

GPS data was collected at all survey locations using a variety of different techniques. Problems were encountered when attempting to compile the data for the student site because of the combination of different techniques. Despite difficulties, complete datasets were compiled for the main line, student site, and surveys that were not located directly on the lines. For future surveys, flags should be numbered in a linear and logical order for simpler processing of the data.

References

[20] Garmin Ltd., *GPS Accuracy*, English, 2016. [Online]. Available: http://www8.garmin.com/aboutGPS/ (cited on page 21).

[21] GNSS Committee, *USGS Global Positioning Application and Practice*, English, Feb. 2016. [Online]. Available: http://water.usgs.gov/osw/gps/ (cited on page 21).

[22] J. Mahun, *Edm: Operating Principles*, English, Aug. 2013. [Online]. Available: http://jerrymahun.com/library/Distance/a.htm (cited on page 22).

[23] D. Pfost, W. Casady, and K. Shannon, *Precision Agriculture: Global Positioning System (GPS)*, English, Nov. 1998. [Online]. Available: http://extension.missouri.edu/p/WQ452 (cited on page 21).

[24] Trimble Ltd., *Trimble GPS Tutorial - How Differential GPS works*, English, 2016. [Online]. Available: http://www.trimble.com/gps_tutorial/dgps-how.aspx (cited on page 21).

[25] USGS, *National Elevation Dataset (NED)*, English, database, Jun. 2016. [Online]. Available: https://www.sciencebase.gov/catalog/item/4f70a58ce4b058caae3f8ddb (cited on page 21).

4. Well Logging

Contents

4.1 Introduction

Borehole investigation is a powerful reference for geologists and geophysicists alike. The advantage of drilling a well is to allow scientists to understand the subsurface of the earth at a given point. Whether through passive or active tools, the logging of a well returns a great deal of indirect measurements open for analysis and interpretation. Other Geophysical methods such as DC, SP, Seismic and EM can work in conjunction with well bore analysis to further enhance interpretation and gain a deeper knowledge of what is below the surface of the earth. Traditionally, the primary interest is the characterization of lithologies with special interest in reservoir fluids, movement, and migration tendencies. For the well logging portion of this article, we have attempted to interpret the information at hand from local boreholes to aid in the development and understanding of the geothermal system in the Pagosa Springs area.

4.1.1 Background

While the scope of formation evaluation in the region may be extensive, its use as an informative investigative tool depends on proximity to other geophysical methods performed. Ideally, ground geophysics is performed, then the resulting data is interpreted and an educated choice of a well location for drilling is chosen. At this point, core samples are extracted or well logging tools are deployed, or both. This information may corroborate with geophysical measurements taken at the surface along a site(s). The 2016 Geophysics Field Camp was fortunate to be able to interpret well log data in the area of the main line, and investigate a near surface well in the student site area.

Borehole analysis utilizes variety of geophysical methods, all of which are measuring tools; lowered down a hole drilled into the subsurface of the earth. Generally, the tools are attached to a wireline and lowered down the borehole after drilling the well. However, some measurements may be taken during drilling, or logging while drilling (LWD). Figure 4.2, an example piece of equipment may take multiple and various measurements of data. These may also be stacked on top one another. This increases efficiency and reduces costs of gathering data. The general theory of methods utilized for analysis within this report are included below.

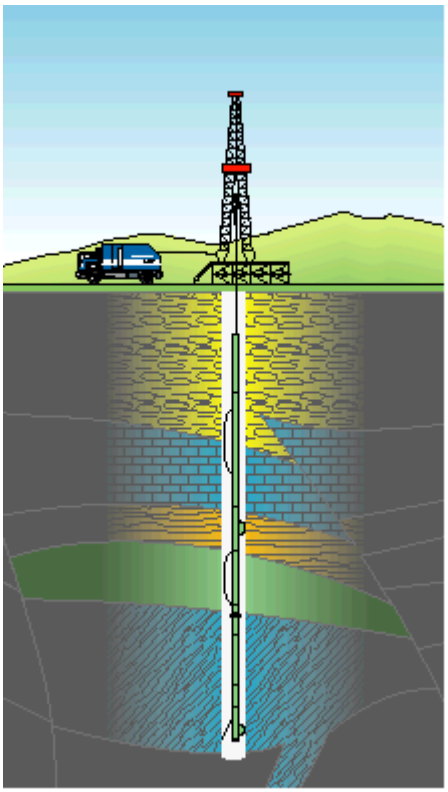

Figure 4.1: *To understand lithological layers within the subsurface, borehole drillers may use logging methods to quantify rock properties as seen in this cartoon [29].*

- Sonic log - Provides a formation interval transit time. In other words, it provides data as to how fast (velocities) a wave can propagate through a subsurface formation. Formation types have different speeds at which a wave may propagate through the material matrix, which also will depend upon any fluids present. This tool may be used to interpret formation velocities.

- Gamma ray (GR) logging - Measures naturally occurring gamma radiation within a formation. This information is useful in formation evaluation to characterize the rock or sediment in a borehole. Different types of rock emit different amounts and different spectra of natural gamma radiation. Additionally, the gamma radiation may be dependent on the amount of water, gas, oil or organic material contained within the rock. In particular, shales will usually emit more gamma rays verses other sedimentary rocks because radioactive potassium (K) and the cation exchange capacity of clay causes them to absorb uranium (U) and thorium (Th). Sandstones, gypsums, salts, coal, dolomites, and limestones will normally have lower amounts of natural gamma ray amounts. These properties allow for the gamma ray tool to distinguish between shales and non-shales.

- Deep Resistivity or Deep Induction Log (ILD) - The ILD is used to determine what the resistivity and conductivity properties are within the lithologies. The ILD log is also useful in characterizing the sediment in the borehole and may also identify any fluids which may be present. Different rocks and fluids will give off different resistivity values which helps geophysicists to categorize the formations and to identify any water, gas, or oil zones.

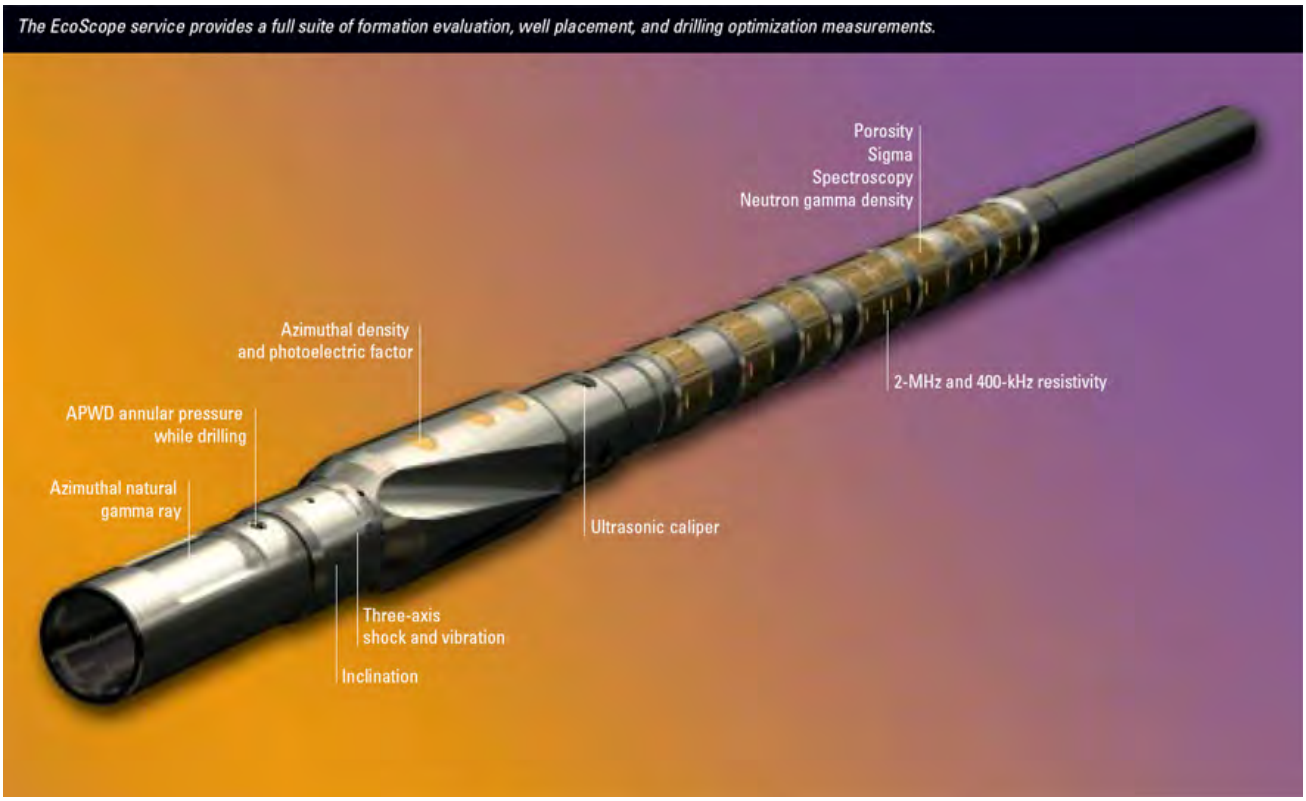

Figure 4.2: *A single sonde may utilize multiple geophysical methods during an investigation of a borehole. This specific tool is designed to measure while drilling [26].*

- Density log (ρ_b) or RHOB - Gives bulk density readings of formations. Bulk density is a function of a rock's mineral composition and fluid saturation. The density logger works by emitting gamma rays which penetrate the formation and bounce back to the tool. [27]. The number of gamma scatters to reach the tools detector reads the formations electron density. The distance between the receiver and transmitter is known in order for conversion to bulk density, the following equation illustrates this.

$$\rho_b = \frac{2Z}{\rho_e A} \tag{4.1}$$

  where Z is the atomic number, ρ_e is the electron density reading, and A is the molecular weight of the material. Normal readings from this log would be from 2.0 to 3.0 g/c^3 with a clean sandstone reading of 2.65 g/c^3 and a limestone reading of 2.71 g/c^3.

- Acoustic Impedance (AI) - AI is calculated using the product of density and velocity. This impedance will vary among different sedimentary and rock formations. The difference in acoustic impedance between formations affects the reflection coefficient. In this report, sonic and density logs are used to calibrate acoustic impedance sections. Equation 4.2 describes acoustic impedance, where ρ_b is bulk density of the formations.

$$AI = \rho_b * velocity \tag{4.2}$$

- Reflection Coefficient - The reflection coefficient is a ratio of the incident wave and the reflected wave which is an indication of how much energy is reflected. Equation 4.3 describes the reflection coefficient R, where ρ is the bulk density and V is the velocity. The reflection coefficient is unit-less because it is a ratio.

$$R = \frac{(\rho_2 * V_2) - (\rho_1 * V_1)}{(\rho_2 * V_2) + (\rho_1 * V_1)} \tag{4.3}$$

- Self Potential or Spontaneous Potential (SP) - A passive method to differentiate between shales and sandstones via potential (voltage) differences of non-permeable and permeable formations. This method is dependent on charges and current flow.

4.2 Objectives

The objective of borehole analysis or well logging is to substantiate alternate ground geophysical methods. This may be done using a variety of the tools discussed, passive and active. Understanding the subsurface characteristics may help to identify fluid flow, faulting, and geologic anomalies specifically related to recognizing how the natural Pagosa Springs geothermal system operates. It is the hope that the study of geophysical well methods will contribute to the overall understanding of this system by the students of the 2016 Field Camp.

4.3 Methods

4.3.1 Survey Location

The wells of interest were chosen by proximity to the main survey line or student site. The wells were targeted for pertinent and specific information, as seen in Figure 4.4. The proximity of these wells to the main line and student site are used to bound the other methods used during Field Camp when interpreting stratigraphy more comprehensively.

4.3.2 Data Acquisition

The Colorado Oil & Gas Conservation Commission (COGCC) has collected borehole data within the area of interest in Pagosa Springs, CO. Sonic, density, gamma ray, neutron porosity and resistivity logs were acquired from the Brown Federal well, Figure 4.4. Additionally, sonic, density, gamma ray, self potential and resistivity logs were acquired from the TG1 well, courtesy of Pagosa Verde, a community based organization interested in local geothermal energy resource allocation and management. The student site data, collected from the Local Well, consisted of a group of students setting up a small scale borehole survey down an abandoned private water well using a sonic, resistivity, gamma ray, temperature, and an optical televiewer tool. Figure 4.3 shows students at this site with an overturned well house, a winch lowering a tool, and a computer to gather data.

Figure 4.3: *Students conducting a borehole survey.*

Equipment List

Well logging equipment essentially consists of a winch and cable system to lower a variety of cylindrical tools into a borehole. The size of the borehole depends on the well, but usually has a diameter of ± 8 inches with

a typical tool diameter of ± 5 inches. Coincident with the tools, the attached cable transmits information to a recording and interpretation device (computer).

The student site equipment specifically consisted of these tools:

- Matrix Geophysical Logging System
- QL40-FTC Fluid Conductivity and Temperature Probe
- OB140 Optical Televiewer
- 2SAA-1000-F Full Waveform Sonic Probe
- 2PGA-1000 Gamma Probe
- 200 m mini winch
- Laptop with Matrix Logger Suite software

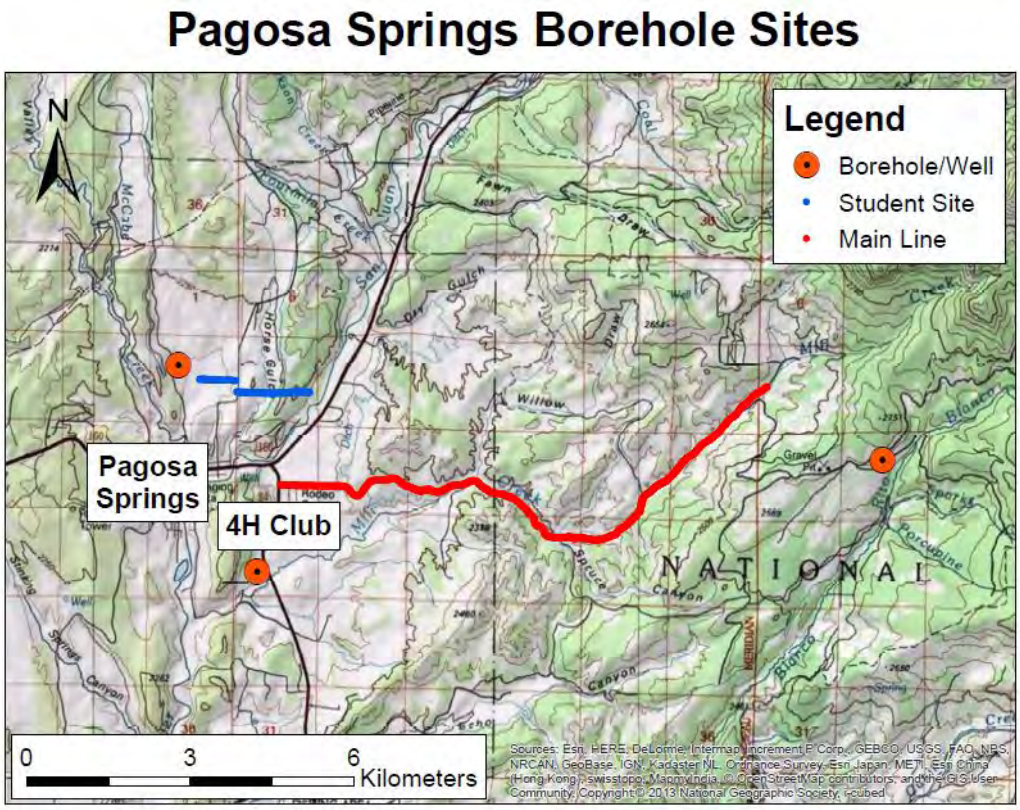

Figure 4.4: *The wells under review (denoted by red placemarkers), for calibrating a local cross section and other geophysical methods, are the Local Well, TG1, and the Brown Federal #1-17. The Brown Federal site is at the end of the main line while TG1 is closer to the beginning of the line, near the 4-H building.*

4.3.3 Borehole Analysis and Processing

For interpretation purposes and comparisons with other geophysical methods concerning lithology, multiple logs were reviewed. Beginning with the compensated sonic log from Samedan Oil Corporation (well Brown Federal #1-17), manual interpretation was performed on non-digitized slowness vs depth logs. Of interest were changes or trends within the log measurements. These were noted and recorded in an Excel spreadsheet as average slowness values per interpreted section along with the corresponding depth. The goal of this collection was to arrive at a column of acoustic impedance (AI) values. The AI values could then be used to assist the interpretation of seismic data by correlating velocities with lithologies.

Using the gamma ray density log and working in Microsoft Excel, we correlated slowness (sonic log)

according to presumed changes in lithology. Correlation of slowness boundaries were altered to coincide with observed changes in bulk density. Referring to Equation 4.1 as the base calculation, reflection coefficients were calculated using Formula 4.3.

After completion of these calculations, comparisons may be made to the formation depths supplied by the on site geology (mud log) from the Brown Federal well logging report. In a similar process, data was interpreted via core samples from the Pagosa Verde well. Once correlations have been completed, we provided the findings of the well log data to other geophysical methods. For example, gravity was interested in the matrix density of the Wanakah formation for building a cross section. Since the data was imported into MATLAB from the Pagosa Verde data, we were able to isolate the formation density values and take the mean value. Ultimately, the end goal here is to come up with a better understanding of how the subsurface is laid out throughout the region.

4.4 Discussion

4.4.1 Borehole Interpretation

Various lithologies are noted at certain depths on the Brown Federal reports. However, there is some doubt in the accuracy of the noted formation top depths. Students in the field viewed an outcrop in Pagosa Springs of the Greenhorn limestone. The limestone in the outcrop was about 30 feet thick, cutting through a lower portion of the Mancos shale formation. Approximately 140 ft (45m) of Mancos shale proved to be below the Greenhorn limestone before the Dakota sandstone formation began. Taking this into consideration, and comparing velocity and bulk density readings from actual log data, the Greenhorn top would start at 3925 ft and end at 3949 ft. Furthermore, the Mancos would return at 3950 ft and continue down 142 ft where the Dakota formation top start at 4112 ft. This would also indicate that the Niobrara would end at 3689 ft and Mancos shale would again dominate the next 235 ft until reaching the Greenhorn limestone. Results of the provided table may be seen in Figure 4.6, within the results section of this article. Currently, no core samples of this site have surfaced. Yet if such samples exist and are collected in the future, further studies of true formation tops and bottoms for lithology may be clearly identified.

Brown Federal Well #1-17 Measured Depths (ft)

Formation	Log Top
MESAVERDE	2176
MANCOS	2534
NIOBRARA	3214
GREENHORN	3940
DAKOTA	4112
MORRISON	4412

Figure 4.5: *Brown Federal measured depths of the formation on the East end of the Student Main Line. These measurements were based upon the interpretation of an on-site geologist during drilling.*

As previously mentioned, Figure 4.6 shows results of our joint interpretation, combining proposed well data with actual log data. Note the Greenhorn limestone and the Niobrara has been drastically “shrunk” in thickness based upon the velocity model, bulk density, and resistivity logs. These findings are substantiated in Figure 4.7, which is based upon calculations derived from the sonic log.

Continuing with the Pagaso Verde PG1 data, we were able to import data (.las files) into MATLAB. Method information was chosen based upon usefulness for corroboration and interest of lithological interpretation.

Concerning the student site well data, the 68 feet of data collected requires a computer software program WellCAD. The data was opened with this program and the conclusion suggests indiscernible amounts of shale (Mancos) with no identification of alternate markers. At this point, it may be safely assumed the Student Site valley consists of alluvial deposits lain atop shale.

4.4.2 Results

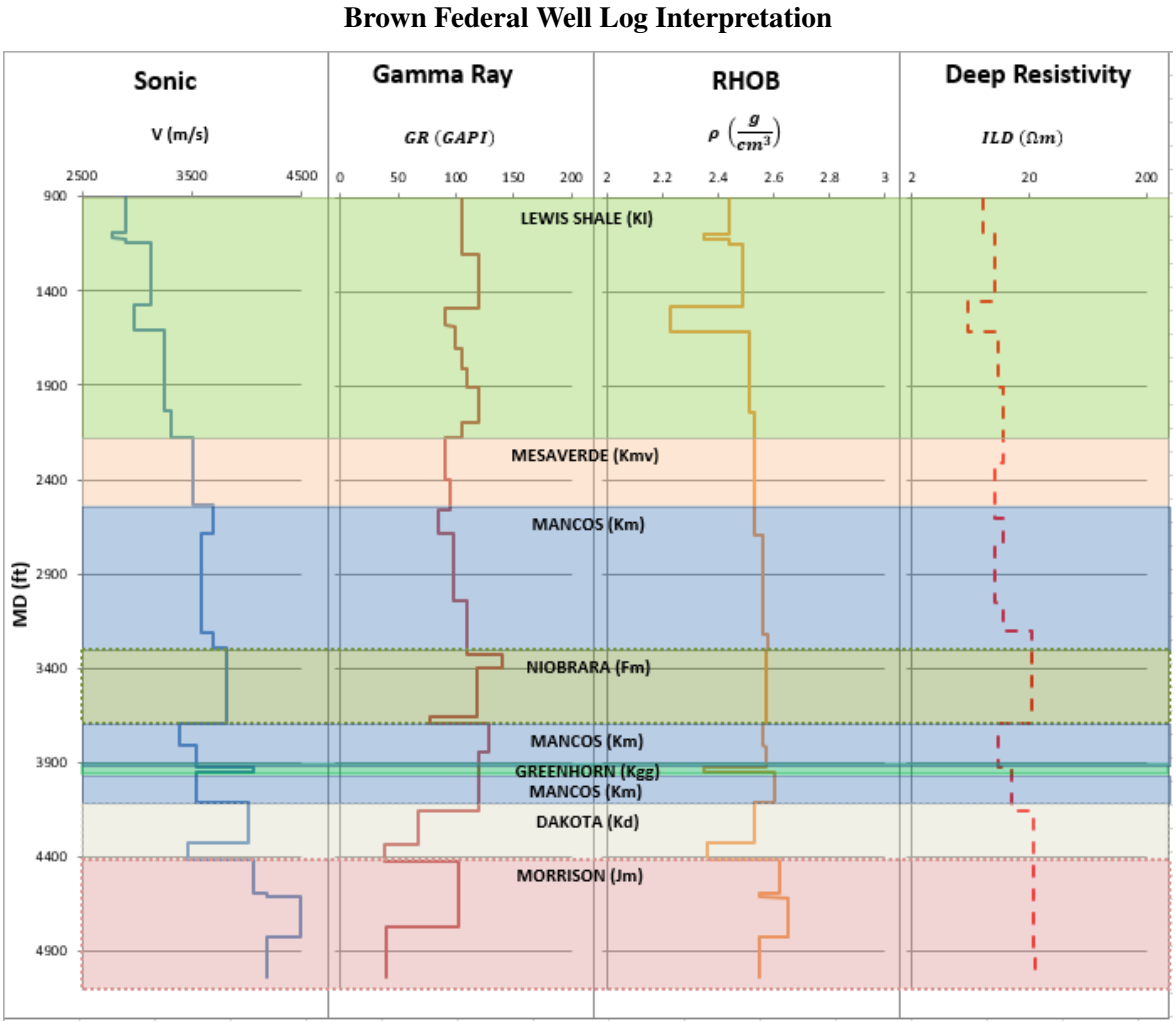

Figure 4.6: *Logs of sonic/velocity, gamma ray, bulk density and deep resistivity from well log data taken from the Brown Federal borehole. Due to lack of having digitized log data, this analysis was performed visually by inspection on an average basis at varying depth intervals. The shaded areas depict the separate lithology layers at depth, as indicated from the borehole log interpretations. It is worthwhile to note, not all changes within a specific layer are accounted for. A record may host many micro changes, or contrast, within a same "type" of formation. Water, salinity - pore space fluid - and variances in rock composition will shows differences of effects. In depth analysis should dominate over a short term prognoses of lithology.*

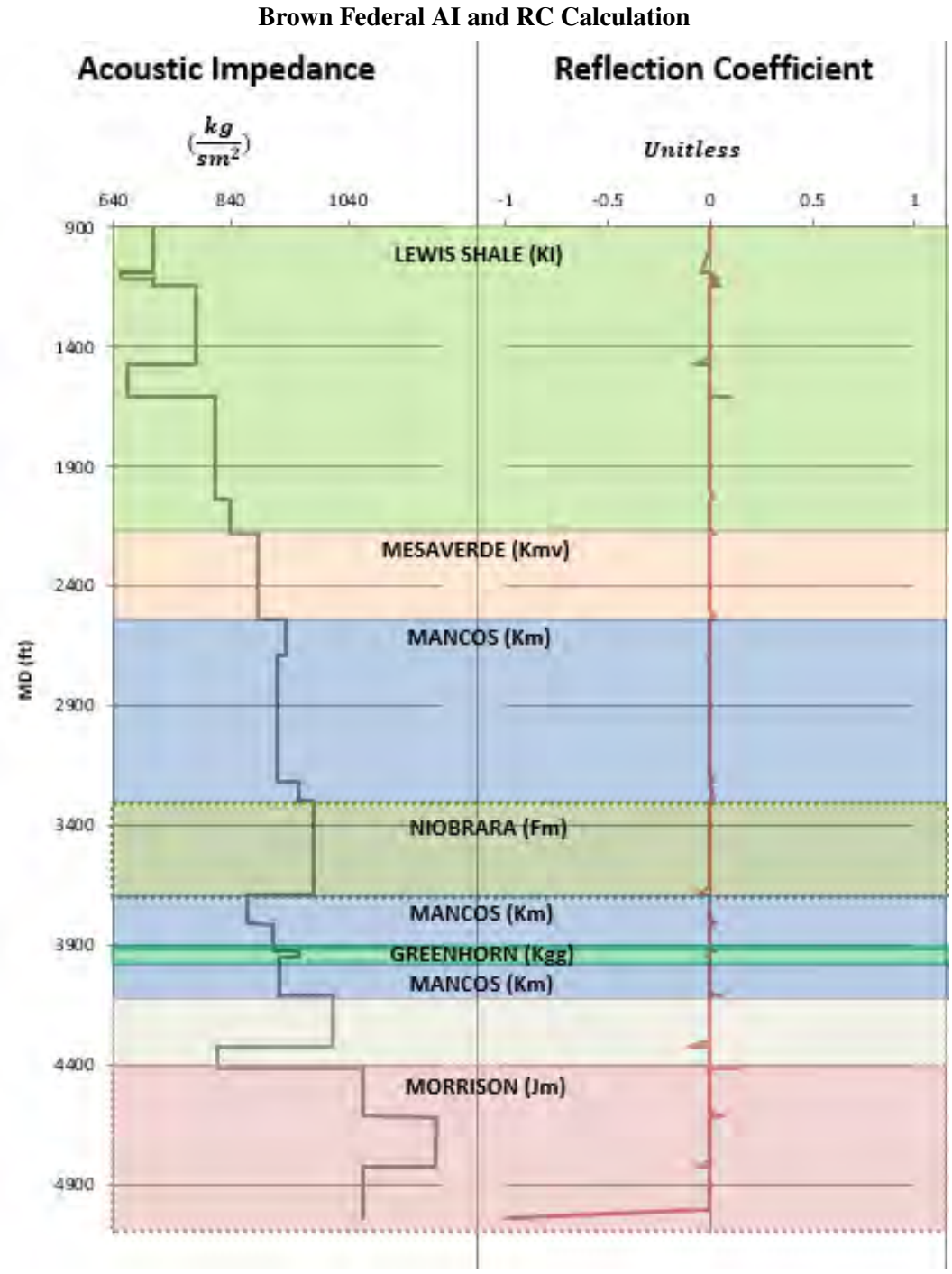

Figure 4.7: *The product of velocity and bulk density gives an acoustic impedance. The reflection coefficient is gathered by way of Equations 4.2 and 4.3. The shaded areas depict the separate geologic layers found at the depth indicated within the borehole. From these calculations, there are trends where lithologies migrate through physical property changes. Also looking at the reflection data, there are reflectors in the main subsurface layers which indicate possible environmental (depositional) changes in layers. This may hold true at the Morrison formation where several different events contained within may be seen by looking at the reflection coefficient spikes in the formation plot.*

Pagosa Verde Well Information

Core Library Number T414

Township:	35N	**Range:**	1W	**Section:**	19
Quarter:	NESW	**County:**	ARCHULETA	**State:**	CO
API Number:		**Operator:**	PAGOSA VERDE	**Well Name:**	PVTG1-2014
Latitude:	37.2519	**Longitude:**	-106.9962	**Coordinate Source:**	PROVIDED BY DONOR
Security Flag:	NO SPECIAL RESTRICTIONS				

5 Intervals

Min Depth	Max Depth	Age	Formation
226	356	CRETACEOUS	MANCOS
356	566	CRETACEOUS	DAKOTA
566	1352	JURASSIC	MORRISON
1352	1448	JURASSIC	WANAKAH
1448	1458	JURASSIC	ENTRADA

Table 4.1: *The United States Geological Survey (USGS) has hosted well information provided by Pagosa Verde. Pertinent information within the header shows this is a well of particular interest, since the latitude and longitude are within proximity to the Student Site. This well, for spatial reference, may be viewed in Figure 4.4. Core analysis may be the most complete record, since it is a direct physical recording of rock material and properties. This valuable information has been, with deductions of lithology, noted under the "5 intervals" section, with corresponding depths of the formations and geologic ages [28].*

Well information of the PG1 borehole, Figure 4.1, has provided us with a base guideline to create a solid picture of the various lithologies at this particular spatial point (latitude and longitude) in Pagosa Springs. The information is derived from a core sample, which has been delimited on other methods of well logs, shown in Figures 4.8 and 4.9. While the sonic and resistivity logs of Figure 4.9 clearly define reflectors or boundaries. It is interesting to compare the densities (g/cm^3) and porosity estimates of Figure 4.8. Note the Mancos density plot is bound together tightly, with a small leniency towards a lower bulk density, where as the sandstones, Dakota and Morrison, are more loosely parameterized, and offer a near opposite reflection of available pore space for fluids. Also as might be expected from empirical studies conducted on sandstones, the density values are within the 2.65 g/cm^3 range. Likewise, the Wanakah formation is approximately 2.7 g/cm^3 which is the expected range of a limestone formation. These results are encouraging, and lead us to believe we have been within reason in our interpretations.

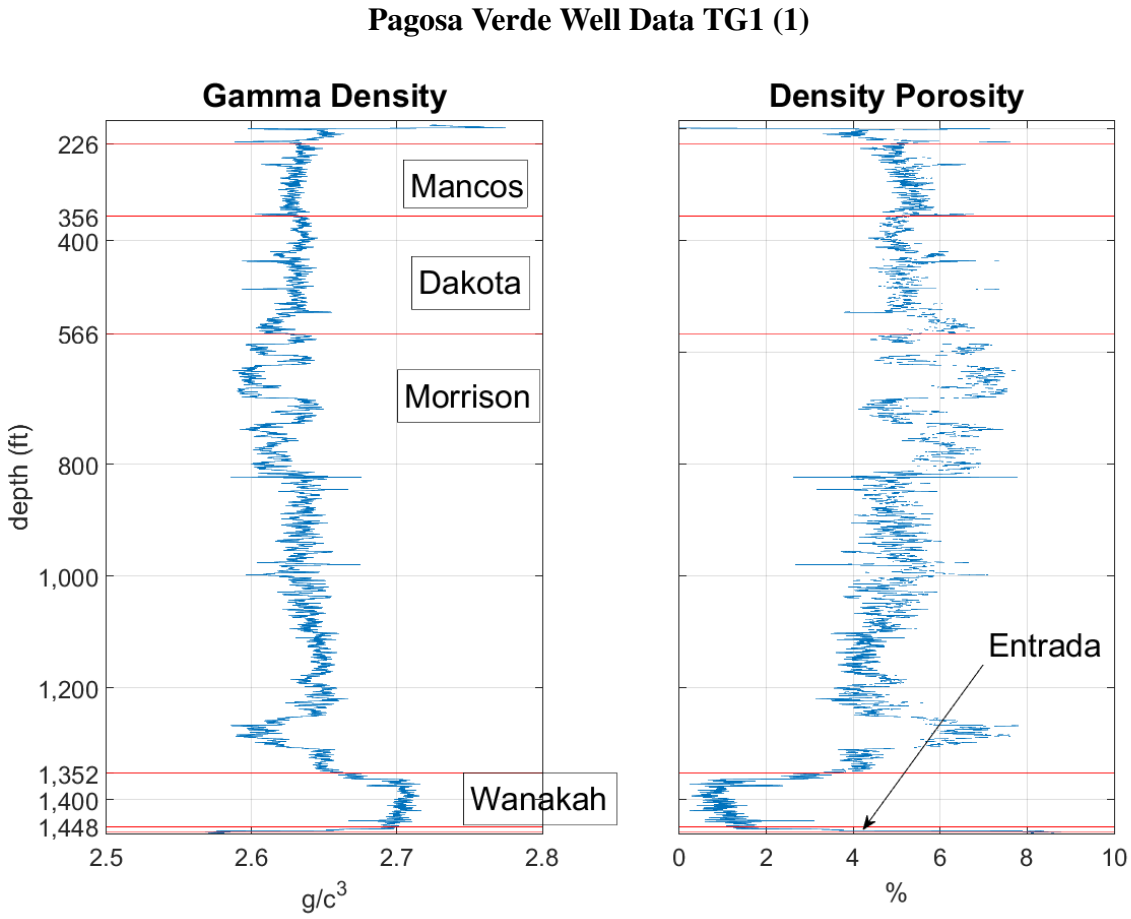

Figure 4.8: *TG1 Well Data. This data (.las file) was transferred into MATLAB for inspection. The red lines drawn on the figure represent lithological layering at the depths provided in Figure 4.1. Within this physical area in Pagosa Springs, rock layers exhibit unique signatures, as denoted by the Gamma Density Log. Corresponding porosity estimates, in percentages, of the formations are shown in the graph to the right. Readings of this data were recorded every 0.1 feet. Courtesy of Paul Foley, representing Pagosa Verde.*

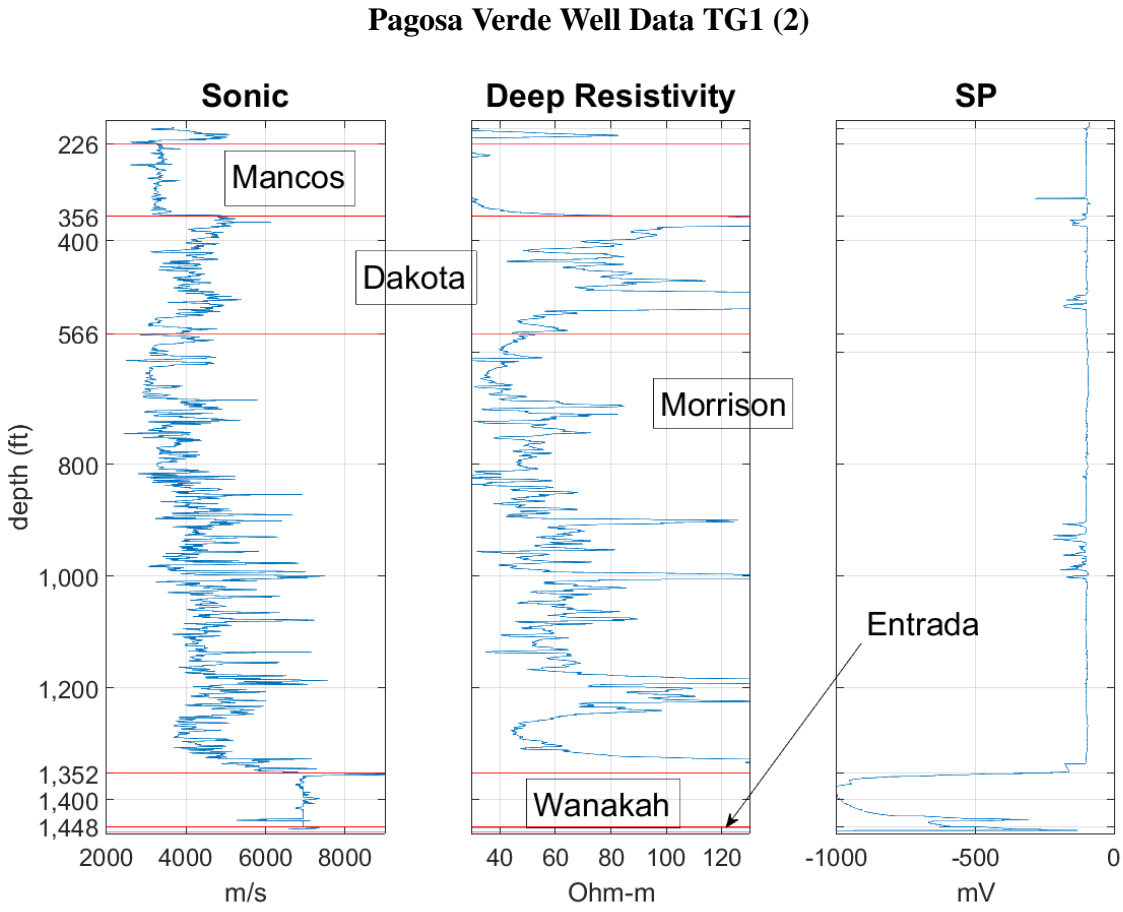

Figure 4.9: *As noted in Figure 4.8, this data was provided by Pagosa Verde. The Sonic Log data has been converted from slowness to velocity. The center plot, Deep Resistivity, measures the formation resistivity values in Ohm meters, which is believed to be a close approximation to the actual formation resistivity, beyond influences of the actual well. Self Potential (SP) logging data does denote some variances within the formation, where differences in potential voltage occur. Readings of this data were recorded every 0.1 feet.*

4.4.3 Errors and Uncertainty

The art of well log interpretation requires individual identification of boundaries and rock properties. However scientific findings often over rule arbitrary analysis, or mis-analysis, of certain lithological features. In essence, we are reducing the complexity of the subsurface using various tools so we may understand the general trends of rock properties, matrices, porosity, permeability and further more.

Errors and uncertainties may always exist in the collection of the data which was processed. The Brown Federal Well data was collected in 1988. Since then, many improvements to well logging data collection have been made to help minimize uncertainties. In 1988, it was common for a geologist to sift through the shavings of the well bore remnants as the mud circulated from depth to the surface. While such observations may certainly be valid, they are not necessarily attached to proper depths.

The wells were analyzed using the actual analog paper prints, not the raw data itself. Averaging trends of this data will lead to some discrepancy with actual recordings. Without the actual digital logs and physical core samples for this well, there is a margin of human error which may take place when interpreting the information.

With the Pagosa Verde well analysis, the errors discussed above have been reduced altogether. The logs were in a digital format and a core sample clearly defined the geologic layers. While confidence of this information is high, it should be noted that there may always be a human error factor anywhere along the processing line, including the inputting of files into MATLAB for computational purposes.

4.5 Conclusion

Generally, our borehole analysis team feels strongly about the validity of the interpreted subsurface layering models given the information at hand. With the help of Dr. Bob (geologist), COGCC, Pagosa Verde and the USGS, our interpretation on a preliminary order is fairly accurate. There have been multiple stages of interpretation and the models have changed from the original interpretations based upon logical thinking and reflection incorporating geophysics and geology. Clarification will remain an ongoing endeavor. Collaboration with students researching alternate methods will remain critical for advanced geological interpretations. Borehole data is highly beneficial to geophysical surveys and provides tangible subsurface data which can help to explain how and where the subsurface changes at measured depths.

4.5.1 Recommendations

The borehole team would recommend further research at any drilled well in the area where data may be obtained. The benefits of geophysical methods and core samples are numerous. Any situation where students are invited to participate in raw data collection, or rig drilling, should be seized with enthusiasm. Simply having the team present at any time of the surveys would be helpful in the processing of the data and recognition of where errors may occur and how significant they may be.

References

[26] *International Ocean Discovery Program*, English, Well Logging Industry, 2014. [Online]. Available: `http://iodp.ldeo.columbia.edu/TOOLS_LABS/LWD/lwd_ecoscope.html` (cited on page 29).

[27] S. of Petroleum Engineers, *Density Logging*, Industry, Oil & Gas, Sep. 2010. [Online]. Available: `http://petrowiki.org/Density_logging` (cited on page 29).

[28] USGS, *Central Region Core Research Center Administration*, English, Government, Jul. 2013. [Online]. Available: `https://my.usgs.gov/crcwc/core/report/78058` (cited on page 35).

[29] *Well Logging*, English, Informative, 2016. [Online]. Available: `http://seabed.software.slb.com/well_log/WebHelp/well_logging.htm` (cited on page 28).

5. Deep Seismic

Contents

5.1 Introduction

As one of the most widely applied geophysical methods, seismic surveys can describe both the stratigraphic column of the subsurface as well as regional structural geology. Geologic features such as folds, faults, and large changes in acoustic velocity can be identified on seismic images. These surveys account for the biggest portion of data acquisition in industries that utilize exploration geophysical methods, such as oil, gas, or mining exploration.

Seismic surveys are collected using a source-receiver method. The source induces an acoustic seismic wave which travels through different medias in the subsurface until it returns to the ground surface and is recorded at receiver stations by geophones. Sources include explosives, hammers, or vibrator trucks in land surveys, or acoustic air guns in marine surveys. The chosen source depends on the desired depth of investigation and accessibility. Usually, a small energy source, such as hammer seismic, will characterize the near surface whereas a large energy source, such as a vibrator truck, will be able to see several kilometers in depth. This survey in particular uses a vibrator truck as its source. To send acoustic waves into the ground, the vibrator truck lowers a platform, raises its weight off the ground, and shakes through a predetermined range of frequencies known as a sweep. The receivers, in this case a group of six geophones per receiver point, record the signal as the acoustic waves return to the surface.

The main goal of surveying the 2016 Main Line is to characterize fluid flow through subsurface layers. Ideally, the results of the deep seismic survey would identify flow pathways for geothermal heating to the Mother Spring. Additionally, the deep seismic data could identify new structural features (such as faults and folds) which have not been seen before and most likely contribute to the flow of water below the surface.

5.1.1 Background

Field surveys from past field camps near the Pagosa Springs area have mainly focused on the west side of downtown Pagosa Springs including carrying a main field survey at Pagosa Springs Airport and DC, Gravity, EM and SP surveys at the Mother Spring. Other years continued down toward the town of Chromo located 25 miles South of Pagosa Springs near the border with New Mexico. Although the surveys done near the Mother Spring did not include a deep seismic survey and the surveys in Chromo occurred in a different region of structural geology, the reports from the last several years still contain pertinent information applicable to this year's survey objectives.

The work done during the previous years aimed at understanding the existing boundaries between lithology and imaging the existing Chromo anticline in the Mesa Verde Sandstone, as well as faulting structures in the area. The 2014 Field Camp integration conclusions report hypothesized two models of fluid flow [30]. Both models originated at the San Juan mountains region. One model followed a path to the northwest of the Pagosa Springs region, transporting through fractures in the basement into the Chromo region, a Southeast direction of travel from Pagosa Springs. The second model followed a path flowing directly South toward the Chromo region. The 2015 Field Camp continued surveying the west side of Pagosa Springs (from Highway 84) [31]. This year's survey mainline marks the first time the Colorado School of Mines focused on the East side of Pagosa Springs and will perhaps encounter data that might support the second model made by the 2014 team.

Based upon the expected cross section done this year, seen in Figure 5.16, the major trend shows consistent dipping stratigraphic layers towards the East. Some faults might express on the East side of the line. The thickness of the Mancos Shale increases as the survey moves East. In fact, going East along the main line shifts up the stratigraphic column from surface expression of the Mancos Shale on the western end to Mesa Verde formation and then Lewis Shale on the Eastern end of the line. Surface expression of a dike at approximately Flag 1700 leads to a conclusion of intrusive igneous rocks or possible structural changes at this point in the subsurface. These anomalies will hopefully present themselves on the final seismic image. Lastly, the basement rock manifests at approximately 1500 feet below the surface on the western end of the line and approximately 5500 feet below the surface on the eastern end of the line. The basement reflector should be one of the stronger reflectors in the seismic image. With these concepts in mind, processing of the main line seismic data could begin.

5.1.2 Theory

In deep seismic acquisition, seismic waves propagate into the subsurface from a source at or near the surface. The source wave travels into the subsurface and then returns back to the surface after being reflected off of layer horizons. Once the wave returns to the surface, geophones, which operate on a system of magnets, record the data. The source type depends on the survey setting and desired acquisition location (i.e. whether on land or in marine

environment).

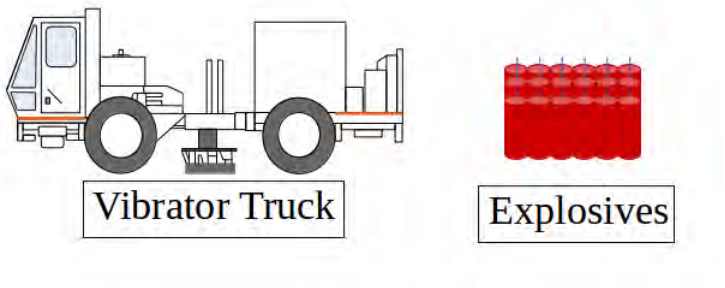

Figure 5.1: *Two commonly used conventional land-based seismic sources. A vibrator truck, is often used in large industry surveys. Explosives are an older more rudimentary source used in rougher terrain.*

As displayed in Figure 5.1, land surveys sources come in several different types. Usually, explosives work best in areas inaccessible to vibrator trucks due to heavy vegetation, steep slopes, or rugged terrain. Explosives such as dynamite cost less and can be safe when handled correctly, but also inefficiently transfer energy and cannot be repeated for poor shot records. Vibrator trucks allow for better control of frequencies at each shot, better repeatability, and more efficient transfer of energy.

Since the survey occurred along Mill Creek County Road, the vibrator truck could easily access the survey line and would allow for the most efficient survey. During our 2D land survey, a vibrator truck, provided by Dawson Geophysical, introduced seismic waves by vibrating the ground over a specific range of frequencies. The seismic waves that propagate into the subsurface start as P-waves or compressional waves as seen in Figure 5.2. As the wave hits an interface (a change in lithology that includes a density and wave velocity difference), the P-wave can transform into polarized S-waves, or shear waves that include SH (horizontally polarized) and SV-waves (vertically polarized). Additionally as the propagating wave hits an interface, reflections and refractions occur which can change the direction of propagation of the wave. The waves redirected back to the surface and recorded by the geophones may now include not only P-waves, but SH and SV-waves. As seismic waves physically displace the ground, the geophones will record how much the ground is displaced from the reflected and refracted waves. Although some geophones can measure displacement in all directions, the geophones that were used in our acquisition only measure vertical displacement (the compressional waves).

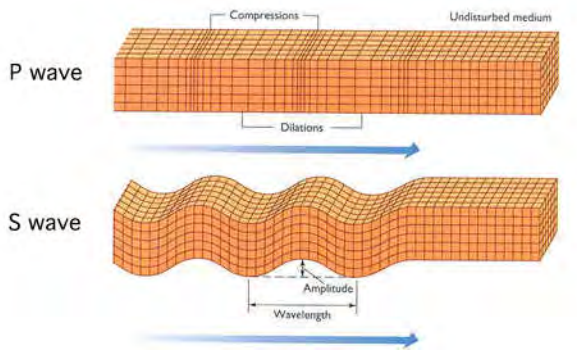

Figure 5.2: *Illustrations of both P (compressional) and S (shear) waves. The P waves work laterally through the earth, creating the compressional look. The S wave's propagation is much more vertical [33].*

The fundamental result of seismic imaging is the depiction of interfaces. As previously stated, these interfaces

correspond to lithological boundaries between rocks of different density and seismic velocity. Specifically, each lithological layer has its own acoustic impedance, a measure of resistance, defined as:

$$Z = V_p \cdot \rho \ , \tag{5.1}$$

where V_p is the P-wave velocity of the layer, ρ is the density of the layer, and Z is the resultant acoustic impedance.

Reflections and refractions can only occur when there is a difference in acoustic impedance between layers. Reflection wavefronts change direction after contacting an interface. The incoming wave or incident wave hits the interface at a certain incidence angle where as the reflected wavefront leaves the interface with a certain angle of reflection. According to the law of reflection, the angle of reflection equals the angle of incidence. Not all energy will be reflected when the wave hits an interface although the amount of energy reflected is determined by the reflection coefficient. Equation 5.2 shows the calculation for the reflection coefficient in terms of the acoustic impedance of two media.

$$R_c = \frac{\rho_2 V_2 - \rho_1 V_1}{\rho_2 V_2 + \rho_1 V_1} = \frac{Z_2 - Z_1}{Z_2 + Z_1} \ , \tag{5.2}$$

In Equation 5.2, Z_1 indicates the corresponding acoustic impedance of the first or top layer, Z_2 marks the corresponding impedance of the second or bottom layer, and R_c stands for the resultant reflection coefficient. The reflection coefficient, R_c, ranges from ± 1 and describes how much energy is reflected and consequently how much energy is transmitted through to the next layer. Depending if the value is positive or negative, the geophone records the reflected energy as either a peak or a trough. Because the geophones are laid out spatially from the source, the reflected wave reaches different geophones at different times. The time at which geophones along the line record a reflected wave can ideally be represented by a hyperbola:

$$T_x^2 = T_0^2 + \left(\frac{x}{V}\right)^2 \ , \tag{5.3}$$

where T_0 is the time at zero offset, T_x is the time at some offset x, and V is the velocity of the medium.

Similar to reflections, waves that are transmitted through an interface also propagate in a specific direction. Snell's Law, seen in Equation 5.4, describes the relation between the angle of the incident wave and the angle of the transmitted wave:

$$\frac{\sin(\theta_i)}{V_i} = \frac{\sin(\theta_t)}{V_t} \ , \tag{5.4}$$

where θ_i and θ_t is the angle of incidence and angle of transmittance, respectively, and V_i and V_t is velocity of the incidence and transmittance layer, respectively.

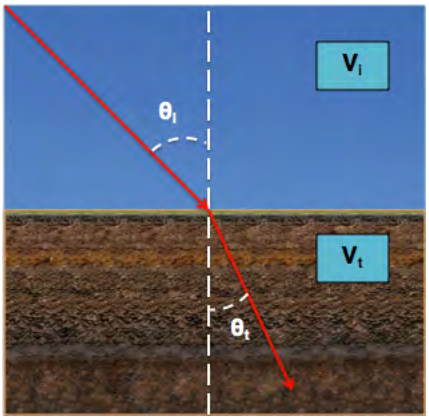

Figure 5.3: *An illustration of transmission across an interface, a visual representation of Snell's Law (Equation 5.4). Snell's law is the idea behind how changing velocities between interfaces relates to a change of angle of the direction of the wave within the new material.*

Refractions occur as a mathematical consequence of a special case of Snell's law, Equation 5.4. In this case, the angle of transmittance equals 90°. A 90° transmittance angle will occur when the incident wave arrives at the interface at the critical angle, θ_c. This angle is derived by setting θ_t to 90° in Equation 5.4, which results in :

$$\theta_c = \sin^{-1}\left(\frac{V_i}{V_t}\right) \tag{5.5}$$

When a ray path hits an interface with the critical angle, or larger, the transmitted wave's ray path travels parallel along the interface boundary (at the velocity of the lower layer). At some time the transmitted wave traveling along the boundary will change direction and travel upward toward the receivers. In accordance to the law of reflection, the angle of the refraction is equal to the angle of the incident wave. As a consequence of Equation 5.5, the velocity of the transmittance layer has to be greater than the incidence velocity because $\sin(\theta)$ cannot be greater than one. Thus if refractions exist, we can determine that a higher velocity layer exists beneath an interface.

Figure 5.4 presents a simplistic subsurface example of a source and multiple receivers, highlighting the difference between a reflection and refraction. In this example, the velocities increase with depth as shown by the ray path slope decreasing as the ray path travels into the subsurface. The reflected wave propagates toward the first interface, and because the next layer contains a greater velocity than the one above, the ray path will bend up toward the receivers upon transmission. As the wave propagates to the next interface the wave will simply reflect off that interface instead of refract because the ray path is not at the critical angle. The refraction propagates at a slightly greater angle which is equal to the critical angle when it hits the second interface. It will travel along the interface with the velocity of the lower layer and then change direction and go toward the receiver at the same angle of incidence.

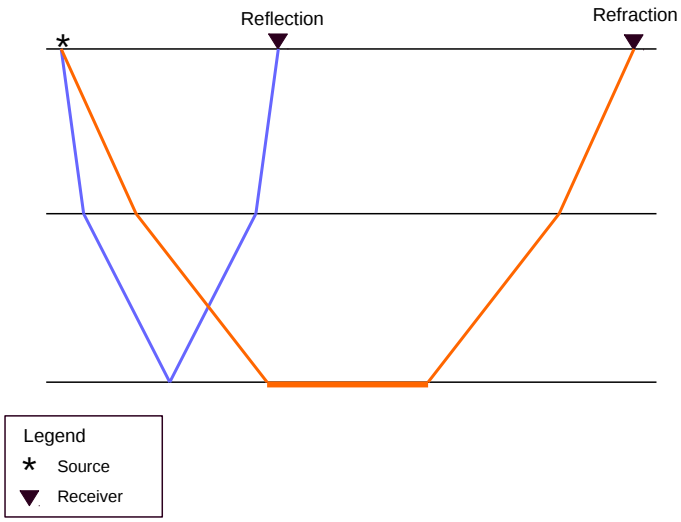

Figure 5.4: *Simplistic subsurface model highlighting the difference between a reflection (blue) and a refraction (orange). Reflection occurs when a wave hits an interface and returns to the surface while refraction occurs when a wave hits the interface at the critical angle which can then cause the wave to travel along the interface before returning to the surface.*

In data acquisition, a vibrator truck vibrates its pad according to a predictable signal, called a sweep. The vibrator produces a sweep signal, a sinusoidal wave signal of varying frequencies, from the ground motion.

Before the survey is conducted, multiple tests with varying sweep parameters are done to find the best sweep parameters that would optimize the data quality. The sweep parameters include type of sweep, frequency ranges, sweep length, and number of sweeps. The types of sweeps consist of upsweeps and downsweeps as well as linear and non-linear sweeps. Upsweep indicates frequency change from low to high while downsweep describes the changes in frequency amplitude from high to low. Linear sweeps describe linear changes in frequency with time, and non linear sweeps do the opposite. Throughout the survey, multiple sweeps are recorded at every shot location to increase the signal acquired and reduce the noise. The redundancy of measurements is exploited using the concept of common-midpoint (CMP) gathers. A simple example can be seen in Figure 5.5 To apply a CMP gather, three main assumptions of the subsurface need to be considered where the earth is flat, homogeneous, and isotropic. These assumptions allow both common midpoint and common depth gathers to take place. Thus, the alternate naming of CMP gather is Common-Depth (CDP) gather. CMP/CDP gathers sum all traces sampled at the same depth of reflector in the subsurface.

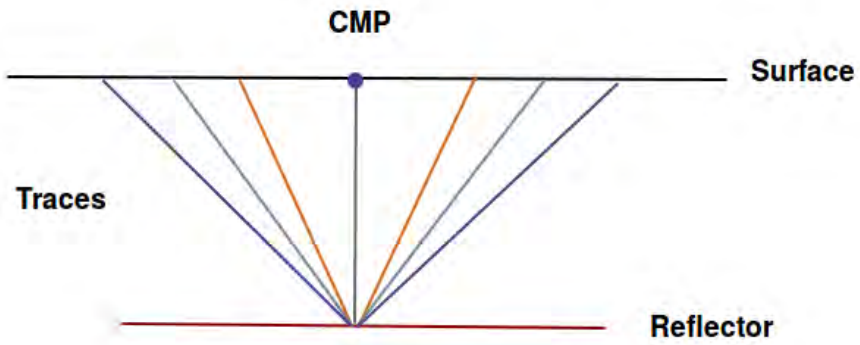

Figure 5.5: *Common midpoint gather geometry which highlights repeated measurements of the same location in the subsurface. The lines are colored specifically in order to track the initial shot position, the subsurface reflector, and where the receiver is recording the wave on the surface. All four of the lines shown have the same midpoint, labeled as CMP.*

The quantity used to evaluate the number of repeated measurements in the subsurface is described as a fold. By evaluating the number of folds, the coherent signal is amplified when folds are at a maximum and the incoherent noises is attenuated. Equation 5.6 models the relation between maximum number of folds and signal to noise ratio:

$$\frac{Signal}{Noise} = \sqrt{Number\ of\ Folds} \tag{5.6}$$

This relation shows that the signal to noise ratio increases proportionally with the square root of the number of measurements (fold). Therefore with a larger number of geophones laid out and connected, or live channels, the number of measurements increase which in turn increases the signal and decreases the noise. By taking more measurements, the survey becomes redundant and the random noise that does not repeat from one shot to the next can be filtered out whereas the signal that does repeat for all shots, is made stronger.

5.2 Objectives

The deep seismic survey took place along the main survey line and has a large depth of investigation compared to the other methods. Deep seismic outputs the highest resolution data of any of the other surveys done along the main line. Using these advantages, the main objective is to create a map of the acoustic impedance in the subsurface to locate any geologic features that may be present. The data will be uploaded and processed through SeisSpace while a baseline stratigraphic column incorporated into the seismic image will lead to better understanding of the final seismic image. The results will be cross analyzed with the other methods to gain a sense of confirmation of the layering seen in the final stacked section.

The objectives for processing of the seismic data include:

1. Using SeisSpace for data cleanup, corrections, and production of a final image that includes elements of stratigraphy and structure that can be interpreted in conjunction with other methods.
2. Working with other methods to compare final data sets and create integrated method images.
3. Interpreting data to understand the geologic features along the seismic line and possibly offering an explanation of fluid flow in this section of Pagosa Springs.
    - Ideally, determining the path of geothermal water upflow feeding the Mother Spring and mapping fluid flow of the eastern edge of Pagosa Springs.
    - Identifying potential faults, folds, and other geologic structures that either impede or contribute to fluid flow.
    - Concluding which geologic layers are identifiable using deep seismic.
4. Working with the geology crew to produce a final cross-section of the main survey line which has been updated to more closely match seismic results and the results of other section.

Overall, the objective of the deep seismic survey along the mainline is to characterize the geology of the subsurface, particularly to understand the stratigraphic layering while identifying subsurface structures. The end result of the survey will be a geologic cross-section of the Pagosa Springs region created by modeling subsurface acoustic velocity contrasts.

5.3 Methods

5.3.1 Survey Location

The deep seismic line is situated on Mill Creek Road, west of the main 4H Club building. This main line runs approximately East to West and is 11 kilometers long. The location for the seismic line was determined based on ease of accessibility for the vibrator truck and therefore occurred directly along Mill Creek Road and followed the entire 11 kilometers of the main line. Figure 5.6 highlights the acquisition line in Pagosa Springs, CO.

5.3.2 Data Acquisition

Before a deep seismic survey can take place, optimization of the production rate must occur in order to ensure completion of the survey in the given time frame. This process includes understanding and taking into consideration many different parameters. Topography is one of the major considerations. The deep seismic survey took place along Mill Creek Road. To optimize the data quality, a deep seismic survey should be done in a straight line, reducing the midpoint offset. Mill Creek Road is not perfectly straight and therefore requires an additional quality check in the form of a crooked line geometry correction. The elevation also increases as the line extends east. This elevation change needs to be recorded using accurate GPS so that elevation corrections can be applied to the data. Other considerations include safety factors, noise that comes from vehicles on the road, and also skipped stations due to houses, driveways, and culverts in close proximity to the road.

The seismic source used for the survey was a vibration source from a vibrator truck. The vibrator sends energy into the ground by allowing low and high frequencies to pulse through the metal plate which is lowered from the truck. The propagated energy reflects back to the geophones which are placed along the survey line. Therefore,

the sweep parameters for the vibrator need to be designed so that the data can be optimized and a high resolution image of the subsurface can be made.

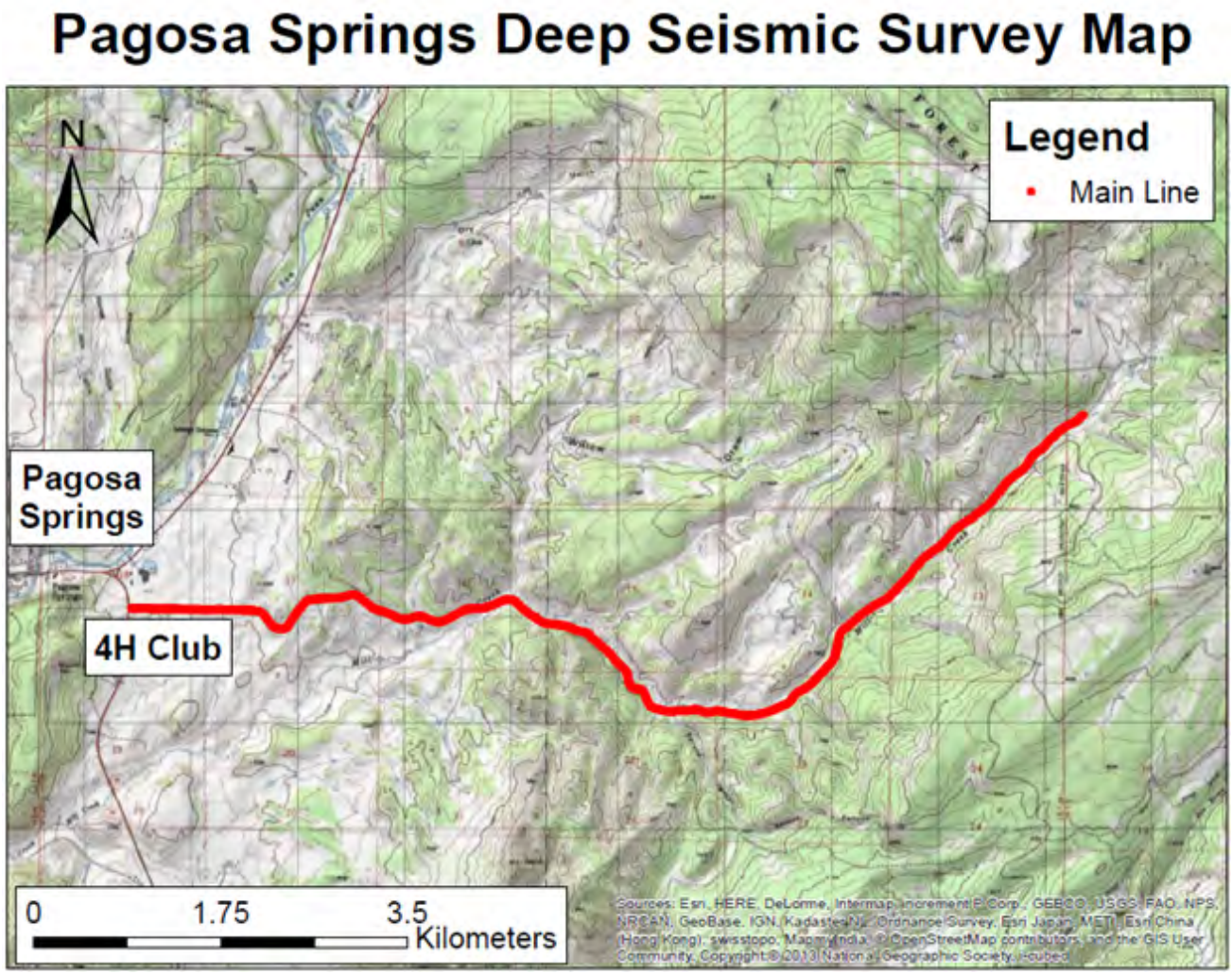

Figure 5.6: *Survey Map. Red line indicates the 11km long mainline. The deep seismic survey only took place along the mainline, and did not occur over the student site. The entire mainline is located East of Pagosa Springs, starting at the 4H club (where CR-302 and Highway 84 intersect.*

Sweep Parameters

Sweep parameters describe the energy generated by shaking created by the vibrator truck. These parameters include the frequency ranges, the type of sweeps, the time of vibration or sweep time, and the number of repeated sweeps. The frequency range must be able to image the subsurface by showing clear reflections of the interfaces. The frequencies ranged from 4 Hz on the lower end to 128 Hz for the highest frequencies. These frequencies will be generated by the metal plate starting from the low frequencies and moving up until the highest frequency in what is known as a non-linear upsweep. Sweep time, the time for the vibrator truck to send the frequency range into the ground, was 10 seconds. After the sweep was done, the geophones will listen to the returning motion for a 3 seconds listening time to record the signals.

The recording time for one sweep, the summation of recording time and listening time, is 13 seconds. In order to maximize the signal to noise ratio, 6 sweeps occurred at every station, which means the process of vibrating the ground was repeated 6 times at every source. For a portion of the line ranging from Flag 1698 to Flag 1910, only

4 sweeps occurred instead of 6 sweeps due to time constraints. The equation used to calculate the total recording time states:

$$Num.\,of\,Sweep * (Sweep\,Length + Listening\,Time) + Move\,Up\,Time = Time\,to\,Record\ , \tag{5.7}$$

where move up time is the interval time between each sweep. Using all the finalized parameters, shown in Table 5.1, it would take approximately 30 hours of working at full pace to complete the survey.

Source	Vibrator Truck
Sweep type	Non-linear Upsweep
Survey line length	11 kilometers
Orientation	78.5 ° East of North
Station spacing	10 meters
Sweep length	10 seconds
Record length	3 seconds
Shot spacing	10 meters
Fold	120 (nominal)
Minimum frequency	4 Hz
Maximum frequency	128 Hz
Number of sweeps	6 sweeps for stations 1200- 1698, and 1910 - 2100 4 sweeps for stations 1698 to 1910

Table 5.1: *2D Seismic survey parameters used on 2016 Main Line. These parameters were determined by the second day seismic crew after tests of different parameters were completed. The variation in the number of sweeps was done to conserve time.*

Survey Parameters

With a shot spacing of 10 meters, the survey began at the first flag and the vibrator truck moved from one flag to the next toward the east. Unless otherwise noted due to road proximity to structures, the survey recorded sweeps at every flag with a separation of 10 meters each. For every shot taken, there were 120 active channels on either side of the vibrator truck. Receiver spacing had the same spacing as the sources at a constant 10 meters. The spacing between each geophone was 2 meters with 3 geophones placed on the east and west sides of the flag at an offset of 1 meter from the flag. A depiction of this setup is shown in Figure 5.7.

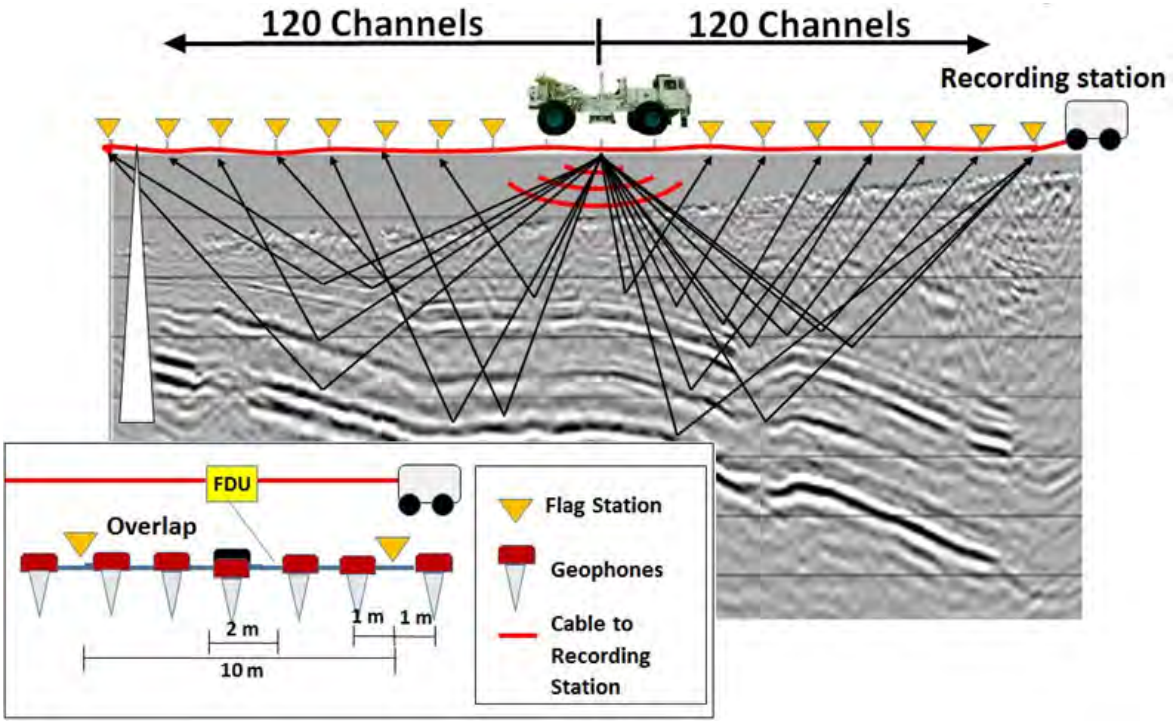

Figure 5.7: *Diagram of geophone placement relative to the flags and other geophones centered on a source point at the location of the vibrator truck. The background image is one of the brute stacks done in the early stages of analysis used only to illustrate an example of subsurface reflectors [36].*

(a) ***(b)***

Figure 5.8: *Geophone and geophone receiver set: a) Long pin geophone. These were used during field seismic data acquisition[34]. b) Single receiver, made up of six geophones, which get summed into one signal. It is this single signal that the doghouse reads from the receiver[32].*

Equipment List

Seismic surveys run on a collection of both complex equipment and simple collections of cable and geophones. The equipment used to create the line of receivers and to measure the seismic energy as it returns to the surface includes:

1. Sercel G-10 Geophones
   Geophones act as receivers for the survey. SG-10 geophones produce low distortion images and can operate to a temperature of -40°C to +70°C. There are two main types of geophones: long pin geophones and short pin geophones. The main difference being the location of the FDU cable connection which is either in the middle of the geophones or at the end.
2. Field Digitize Unit (FDU)
   This unit converts analog signals received from the SG-10 geophones and converts them to digital signals to be processed in the doghouse.

3. Land Acquisition Unit Land (LAUL) cables
   The LAUL cables connect receivers (geophones) together by FDU connection in order to create a single receiver line.

4. Land Acquisition Unit Cross (LAUX)
   These cables connect Land Acquisition Unit Land (LAUL) cables which transmit digital signal from FDU box to doghouse to be processed.

5. Wire protector
   These road guards protect geophone cables from damage caused by vehicles driving over them (mostly used at the entrance to driveways or gates).

6. Batteries
   Batteries give power to the geophones and geophone cables and aid in moving data to the doghouse.

The rest of the equipment used on the seismic line either generated the signals or controlled the survey as it was being run. This equipment includes:

5. Vibrator truck
   The vibrator truck used to provide energy into the ground was a model AHV-IV Commander INOVA provided and run by Dawson Geophysical, Inc. The energy transmits to the ground by shaking through a certain series of sweep parameters. The control of the sweep parameters and the shaking process occurs at the doghouse. A GPS receiver on the vibrator truck keeps the coordinate locations of each shot which are then used in the processing.

6. Dog house and power generator
   The dog house operates as the headquarters for checking survey lines and troubleshooting survey errors. The generator gives power to the computers in the dog house and allows the survey to run.
7. Sercel software in a dog house
   An operator in a dog house uses Sercel software in order to detect and troubleshoot errors during the survey and also to initiate sweeps at each source location.
8. SeisSpace software for processing
   Taking the data from the field and changing it into the final readable product requires processing it through different stages of noise correction and migrations using SeisSpace software.

(a) *(b)*

Figure 5.9: *Seismic data acquisition equipment: a) The vibrator truck is the source used across the survey line. The truck is capable of vibrating at a large range of frequencies [35]. b) The doghouse (recording station) is the main location for field data collection. The doghouse is capable of keeping track of the vibrator truck's position and finding dead or crooked geophones along the current line.*

5.3.3 Processing

The processing of the data was conducted using SeisSpace ProMAX, a Halliburton Landmark software specifically designed for land and marine deep seismic acquisition processing. There are a multiplicity of considerations when processing seismic data including the geometry of the acquisition line, the topography, noise including cultural and environmental noises, and the background geology of the line. Figure 5.10 presents a general flowchart of the processing steps used to transform the raw data obtained in Pagosa Springs, CO to a final interpretable subsurface image.

Crooked Geometry:

The first step when processing seismic data includes understanding the geometry of the survey line. The GPS survey data containing the X and Y position coordinates and elevation coordinates was imported into the database. The midpoint for each shot and receiver pair was calculated and used to generate a spatial distribution as can be seen in Figure 5.11. The white smear shows the midpoint distributions. A curve of greater than 10 degrees in a seismic line means that the line is considered crooked and needs to go through a crooked geometry correction. The line this year clearly falls into the crooked line category based on the overhead views of the road as seen in Figure 5.6.

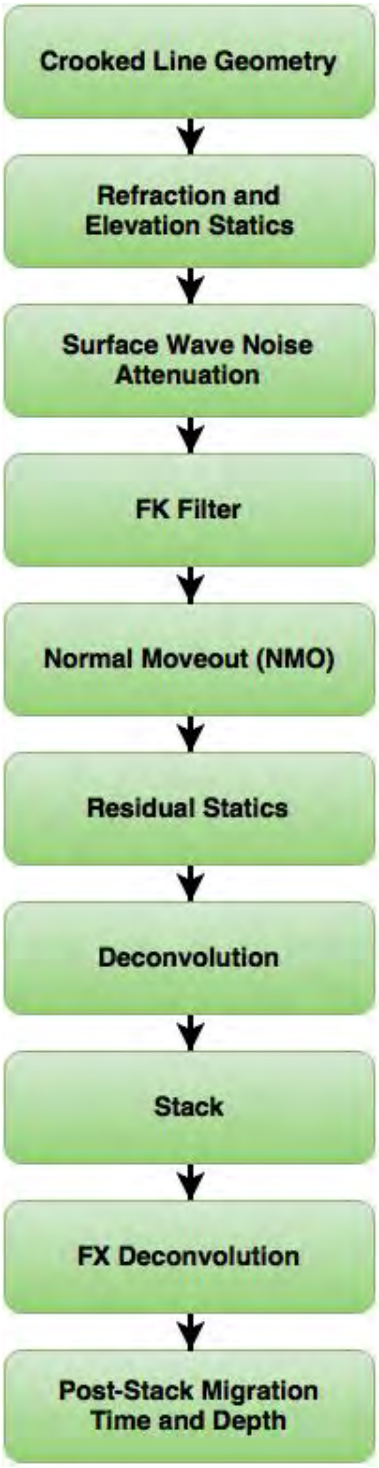

Figure 5.10: *Flowchart of steps taken in the processing of the seismic data. Each step has its own purpose removing noise and refining the data. Various stack images were made along the way to reference if the corrections being made were beneficial or not.*

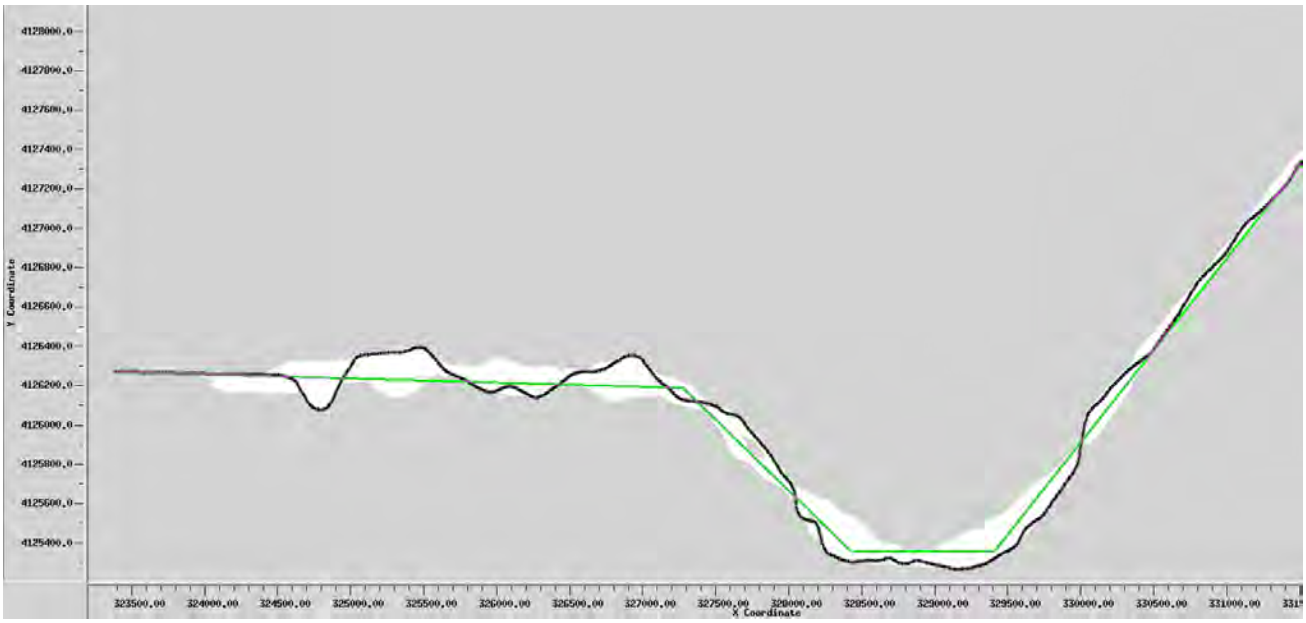

Figure 5.11: *Visible midpoints (in white) and their position along the main line (black). The crooked geometry correction follows the green path. There could only be a limited number of fixed lines for the correction as the total fold decreases each time there is a bend in the line.*

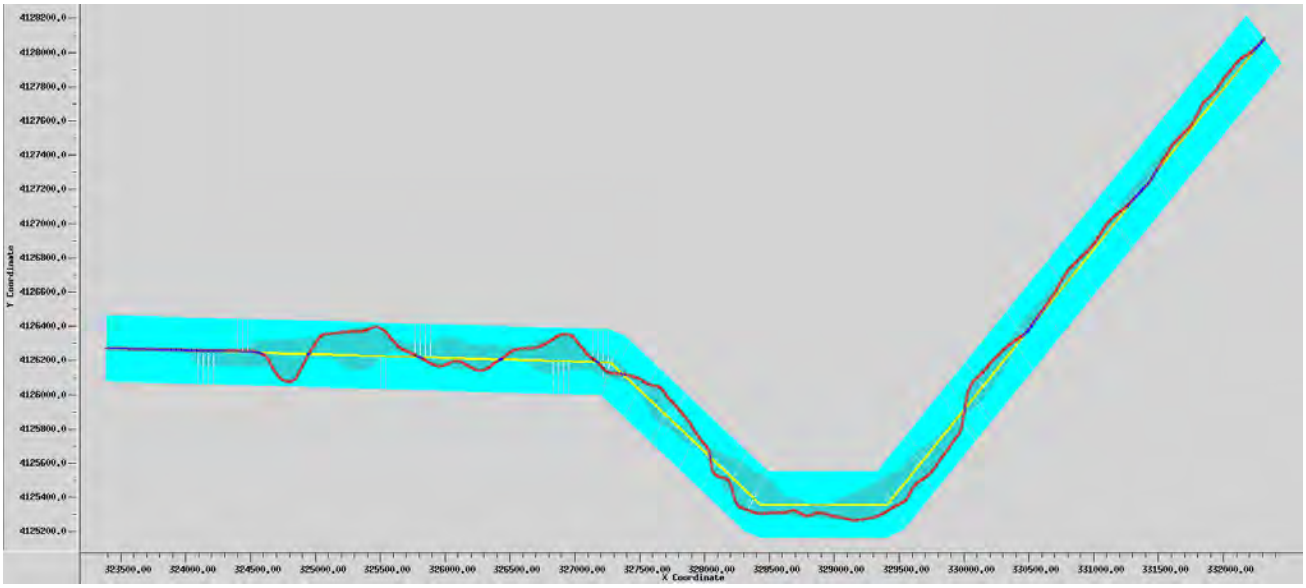

Figure 5.12: *Binning process outlined in blue. Individual bins were set to be 5m in width and span 200m on each side of the line. These bins grab all of the midpoints within them and summarize them to a given point along the line. The blue overlay shows the total area all bins cover.*

With this idea in mind, the crooked line fix was applied to the main line of seismic data. This process includes generating straight segments, a common midpoint (CMPs) track, and creating associated bins that sort midpoints at the center of the line. This process allows the data from the survey to be stacked and analyzed with accuracy, but is also an important step to keep in mind during the interpretation of the data as the results will be skewed slightly. A simple version of the binning process can be seen in Figures 5.11 and 5.12.

Refraction Statics Correction:

Running a refraction statics correction removes static time shifts introduced into shot traces by topography and near surface velocity anomalies that distort the normal moveout of reflections. These come in the form of:

- Weathering correction: This correction compensates for a layer of low seismic velocity material near the surface of the Earth that delays travel times and causes reflections to have high and low frequency undulations.
- Topography correction: This correction compensates for differences in topography and elevations between source and receiver pairs. Essentially, applying this correction brings measurements to a common datum point. For example: An undulating topography can produce moveout delays that can be interpreted as false structures in the reflector even if the reflector is flat. Therefore, this process removes the undulating topography.

With static corrections, the data appears to have been collected on a flat datum plane with no low velocity layer (LVL) at the surface of the Earth.

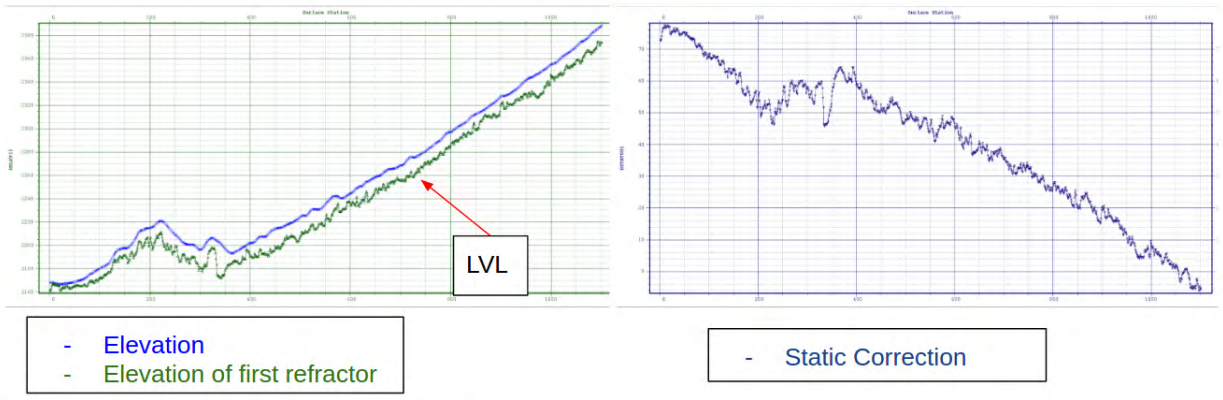

Figure 5.13: *Elevation and low velocity layer (LVL) correction. These are done by picking the headwaves. The elevations of the first refractors are then differentiated from the elevation to create a total static correction for data. This is also the process for the low velocity layer, but both are implemented at identical times.*

Surface Wave Noise Attenuation (SWNA):

This tool removes ground-roll or surface waves from data. It essentially applies a dip filter that only removes specific frequency and velocity ranges associated with surface waves.

FK Filtering:

FK filtering removes residual linear noise (ground roll) with a slow moveout velocity on shot records. Since the velocity is separated from the apparent velocity of reflections, this tool filters these velocities in the frequency domain, essentially muting one dip range from another based on the different slope velocities.

NMO Analysis:

Normal moveout (NMO) analysis on CDP gathers of seismic data allows for selection of stacking velocities which are applied to correct for normal moveout of reflectors.

Residual statics:

Applying residual statics corrects remaining shots and receiver high frequency statics and is applied to prestack gathers. Overall, this correction improves the alignment of reflections within a common depth point (CDP) gather allowing for a more coherent stack by correcting for one trace to move up or down a maximum of 20 ms for five iterations. Each iteration will allow more static correction such that the gather can be improved in small increments.

Deconvolution:

Deconvolution compresses wavelets to allow for sharper definition of events and is a smart filter that compares traces. Similarities become enhanced while differences become less visible.

Automatic Gain Control:

The Automatic Gain Control tool normalizes amplitudes values for all the points over a discretized window.

Stack:

Traces with a common reflection point, CMP data, stack to form a single trace which attenuates noise and enhances the signal. Signal will be repeatable across traces within a CDP gather, but noise will not and thus cancels out of the image. The number of traces added together during stacking is called a fold.

FX Deconvolution:

A post stack enhancement attenuates random noise and works in the FX (frequency-space) domain.

Migration:

Using the smoothed stacking velocities, the FK post stack time migration and the FD post stack depth migration move reflections in the seismic data to their correct locations in time and depth respectively. This process also collapses diffractions.

FK Filter:

This final step removes steep migration wavefront artifacts.

Overall Processing

To illuminate the differences created by the processing steps, Figures 5.14 and 5.15 show a comparison of the pre-processed and processed data. Both images represent the subsurface in time and contain no time migration. Figure 5.14 highlights the subsurface reflectors with only crooked line geometry applied. In comparison, Figure 5.15 highlights the processed subsurface reflectors containing elevation and refraction statics, surface wave noise attenuation, FK filter, NMO, residual statics, deconvolution, and FX deconvolution. Comparing the two images demonstrates that the overall resolution increases as the reflectors are defined better and more continuous in Figure 5.15.

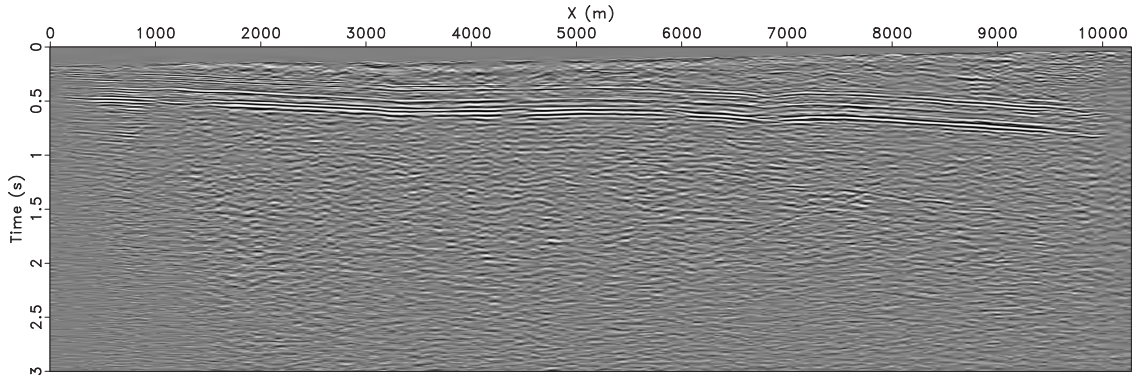

Figure 5.14: *Non-processed subsurface reflectors in time of the main acquisition line. Image contains crooked line geometry correction but no time migration. Image has true aspect ratio.*

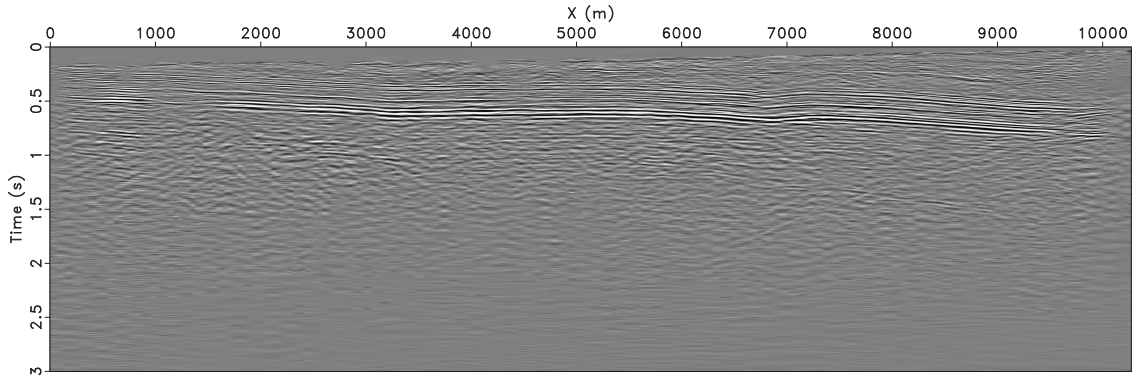

Figure 5.15: *Processed subsurface reflectors in time. Image processed using elevation and refraction statics, surface wave noise attenuation, FK filter, NMO, residual statics, deconvolution, and FX deconvolution. Image has true aspect ratio.*

5.4 Discussion

5.4.1 Expectations

The geological study provides valuable information of the subsurface underneath the seismic line which is expected to be observed in the results. The subsurface contains beds dipping approximately 5° toward the east side, as well as a Lewis Shale top bed that thickens toward the east. There are few structural features expected to appear in the seismic stack section. These include a dike intrusion around flag number 1700, and possible faulting along the main line. The general geological cross section of Pagosa Springs in Figure 5.16.

The different layers of rock formation underneath the main seismic line will produce strong interface reflections for seismic waves. Impedance in Equation 5.1 is defined as the product of P-wave velocity and density of rock layers. Every rock formation underneath the seismic line has different density values. Table 5.2 outlines the bulk density values of each rock formation obtained from well log information located on the east and west sides of the mainline.

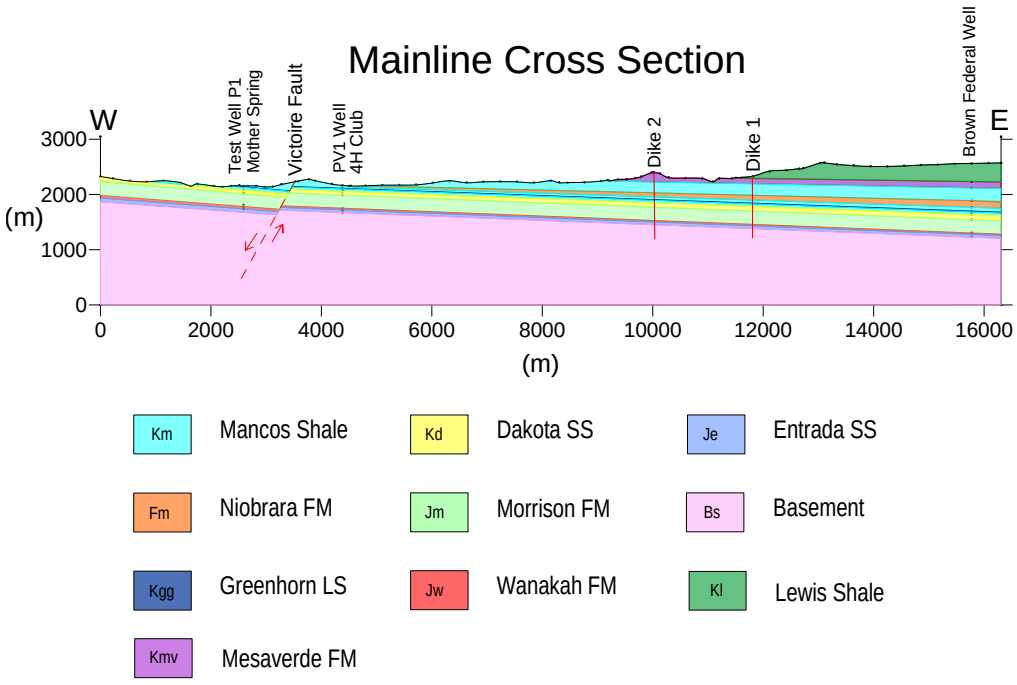

Figure 5.16: *Digitized West-East Cross Section of the main seismic line along Mill Creek Road. There are a total of ten distinct layers labeled on the diagram. All of them generally dip towards the East.*

	Pagosa Verde **PVTG1**	**Brown Federal** #1 – 17
	Bulk Density (g/cc)	
Mancos	2.6297	2.56
Lewis	-	2.42
Dakota	2.6284	2.45
Greenhorn	-	2.35
Mesa Verde	-	2.53
Morrison	2.6304	2.6
Wanakah	2.68	-
Niobrara	-	2.57

Table 5.2: *Density values for different geologic layers. These are important to know as the varying density values can create acoustic impedance.*

The density differences between each rock layer will give variations in acoustic impedance with respect to each lithological boundary which will then reflect the energy back to the surface. The degree of reflected energy at the interface is defined by the reflection coefficient in Equation 5.2. Thus, these reflections at the interfaces are assumed to appear in the seismic stack section with 5° dipping to the east. One geological feature which is expected to be visible in seismic stacking sections is the dike intrusion which was found extending from southeast to northwest across the mainline near Flag 1700. The dike will appear as high impedance contrast in seismic experiments due to density differences between the dike and the host rock surrounding it. A clear reflection of the dike is assumed to appear in the seismic stacking section and is expected to extend down to the Precambrian basement rock. Minor faulting, or perhaps one or two major faulting features, are also expected to be seen in the seismic reflections. During survey acquisition, there were no clear topographical signs indicating major faulting along the seismic survey line. However from the geologic cross section in Figure 5.16 and the general topography of the survey line, there could be some fault events that may be attributed to elevation changes toward the East. The formation of the dike near flag number 1700 could lead to some fault formation near it. Faults are expected to cause reflections in seismic stacking sections to be discontinuous.

5.4.2 Results

After all of the processing was finished, the results ended with two distinct images, Figures 5.17 and 5.18, with the coloring scheme being the main difference between the images. The first of the two shows the depth migrated image in grayscale while the other image is in "color", showing the reflectors in red and blue. The images show high resolution detail about the subsurface and both have a 1:1 aspect ratio for scaling to make them easier to interpret.

Dipping beds mark the major structural feature in these images. The beds appear to be dipping shallowly to the East, with a flatter area in the middle. The dip continues around 5100m on the horizontal axis. The part where the data breaks up (at approximately 7000 m) can be attributed to faulting in the area and presents in more or less the same spot as the surface expression of the dike. However due to the midpoint summing during the crooked line geometry correction, some of these aspects could be skewed from their original locations. The change in the dip of the beds most likely comes from the binning process and how the image was produced. The main seismic line was broken into four pieces during geometry correction which align approximately with the locations of the changes in dip.

Finally, the far East end of the line provides some interesting data. The geology appears to break off almost like a fault and then bend up slightly. The data at the far end of the line, being lower in quality than the rest of the line due to open channels, should not be trusted to the same extent. As the vibrator truck reached the end of the line, there were less and less geophones in front of the truck and more behind it until the final shot had 240 geophones just to the West. This survey set-up could cause problems in the data, so the odd geology seen is most likely not a real feature. The beds do appear to become flatter again, which could mean a slight change in the dip at the far end of the line.

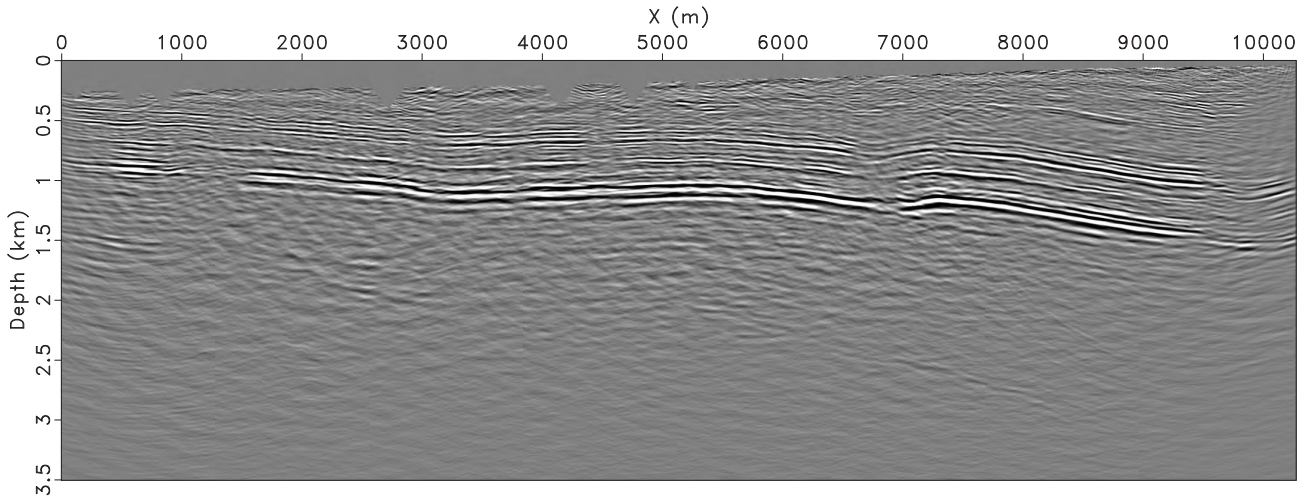

Figure 5.17: *Final grayscale depth migration at true aspect ratio, from West to East. This image was migrated from time to be shown in depth.*

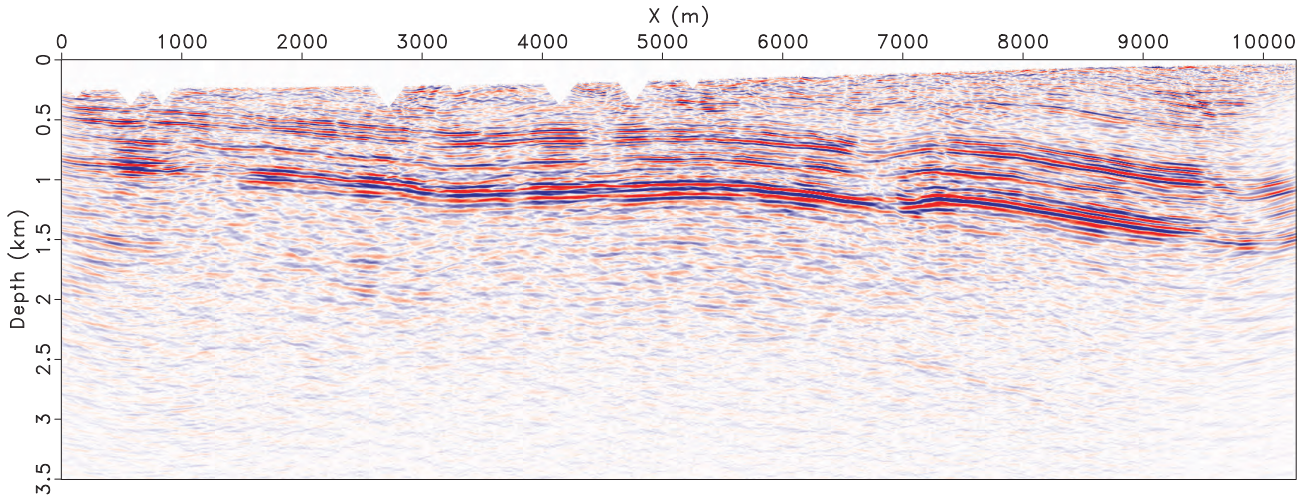

Figure 5.18: *Final depth migration in red-blue color at true aspect ratio, from West to East. This style allows the stronger reflectors to be seen with more ease, but does decrease the presence of some of the finer details in the image.*

5.4.3 Interpretation

Combining the final depth migrated images along with knowledge about the geology of the area, Figure 5.19 illustrates the final interpretation of the geology of the main line as provided by the seismic survey. The different colors trace the different stratigraphic layers and the reflectors that likely outline these layers. The black lines outline areas of faulting along with the motion of the fault as indicated by the arrows.

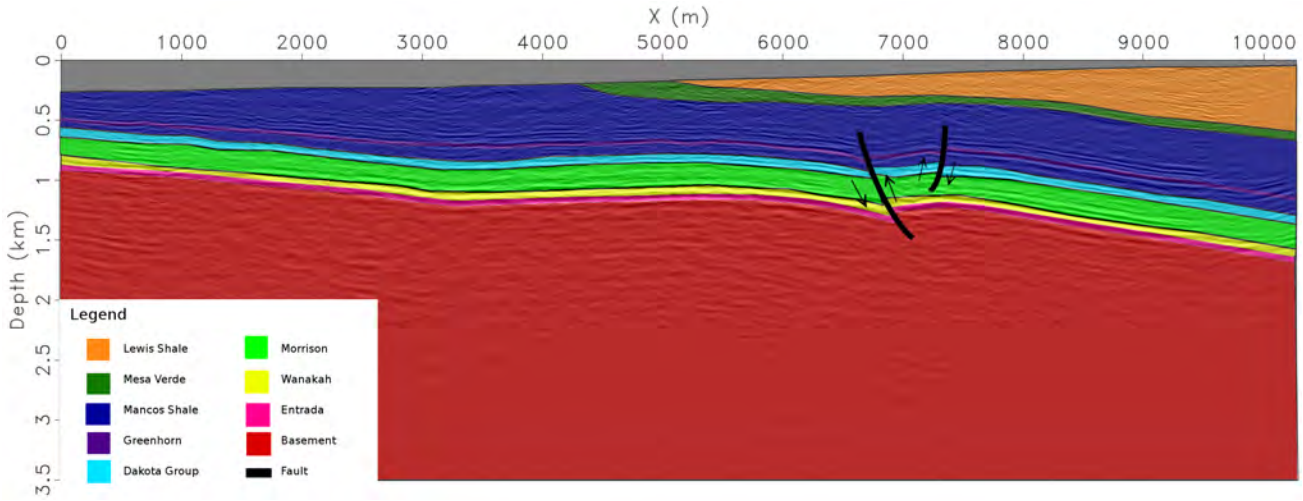

Figure 5.19: *Seismic final depth migration with colored geological interpretation at true aspect ratio, from West to East along the mainline. The stratigraphic layers dip toward the East while there is also a section of faulting located at approximately Flag 1700, in the same area as surface expression of the dike.*

The geological cross section in Figure 5.16 provides similar information that corroborates Figure 5.19 in terms of rock formation sequences and the dipping angles of the beds. In general, Figure 5.16 provided an estimate that the beds were dipping 5° and that the layers thicken toward the East side of the line. However, the dipping bed in Figure 5.19 does not dip in a straight line and decreases in slope from 5° to less steep slope near 3,000 meter and to a steeper slope near 6,500 meter. The changes in dipping slope are primarily the result of the crooked geometry correction for the seismic line which makes the beds have an apparent dip instead of a true dip.

The type of rock at the shallowest depth near the surface is Lewis Shale. Lewis Shale thickens toward the East at a constant rate until the line reaches 8,000 meters where it drastically thickens along the bottom edge of the layer. This pattern of thickening overlays the Mesa Verde Formation which thickens toward the surface as the cross section expected. Below the Mesa Verde Formation, Mancos Shale has an approximately constant thickness of 0.5 kilometers from the start to the end of the line. The pattern of the dipping bed echoes in other rock formations including the Dakota, Morrison, Entrada, and Greenhorn Limestone although the layers vary in thickness. There is a relatively consistent reflector located in the basement rock which could be the result of two different interpretation scenarios. First and most likely, this reflector might be a multiple given that it roughly follows in parallel to the Mancos Shale boundary. On the other hand, the basement might be interpreted as exhibiting two different layers categorized into intra-basement and basement and separated by this reflector. This scenario is less likely than the first scenario.

There are two faults found along the seismic section. The faults altered the dipping geometry of the beds, but only to a small degree. The faults do not extend to the surface or to basement and do not contribute to topographical expression on the surface. In terms of the fluid flow, these faults could contribute to geothermal flow, but definitely contribute to general fluid flow in the water table.

Seismic data alone does not provide enough information to interpret the mechanical aspects of fluid flow without information from other geophysical methods. In general, the geological interpretation of the final seismic section confirms the geological information from the cross-section. A few geological features particularly faults could be further examined using other methods. Gathering information from other geophysical methods helps in exploring the cause of fluid flow that might come from these geological features.

5.4.4 Errors and Uncertainty

1. **Culture Noises** comprise human activity that may cause noise during data acquisition such as passing vehicles, power lines, operational activities from nearby factories or farms, or even from the seismic crew. Several sources of culture noise include:
   (a) Asphalt factory
      - Located near the beginning of the line, the daily operations of this factory created consistent noise which appeared in the data particularly in the first 50 shot gathers.

   (b) Power lines
      - Power lines operate at 60Hz continuously which adds noise to the seismic shot record, which in turn has to be filtered out during data processing.

   (c) Passing vehicles
      - Passing vehicles create vibrations that are picked up by the geophones adding noise to the seismic shot record.

   (d) Other survey crews
      - Nearby surveys can create vibrations seen on the shot records while other electrical methods operate as various frequencies.

   (e) Wind and/or inclement weather
      - Geophones are very sensitive to changes in weather patterns. Rain can add noise as raindrops hit geophones. Wind gusts create vibrations that can be picked up during data acquisition. Additionally, rain water, mud, or dirt could get in the plugging ends of geophones or FDU cable which could decrease the quality of recorded seismic data.

2. **Field Operation Errors** include sources of noise that are inherent in the survey design and the equipment itself, as well as the crew's operation of the equipment.
   (a) Geophones were not spaced exactly 2m apart, but are summarized as a single unit for data processing. Therefore error in geophone placement can largely be ignored in processing since the errors are not significant enough to worry about.
   (b) Placing the geophones perfectly vertical is near impossible, which creates error. The doghouse can detect if one geophone is off more than 5° from the vertical so this often does not cause large errors in the data collection.

3. **Gaps in Data Acquisition** occur due to nearby infrastructure or inaccessible terrain and can be seen in Figure 5.21. These areas included driveways, gates, and parking lots along the line as well as any shots that were deemed to close to structures. The gaps in acquisition can be seen in white while the shots that did occur are in black in Figure 5.21.

4. **Processing and Interpretation Errors** occur during certain sections of processing (like first break picking) where the processor has freedom to choose their own corrections. This type of error led to every person of the processing team having a slightly different final processed image.
   (a) Each processor picks their own first break picks and velocities for stacking from de-noise processing in order to decrease ground roll attenuation.
   (b) Interpretation error is subjective to the interpreter and greatly depends on the parameters chosen by the processor.
   (c) Ground roll covers up a large portion of the data and its removal can mean the loss of good data if filters are too strong.

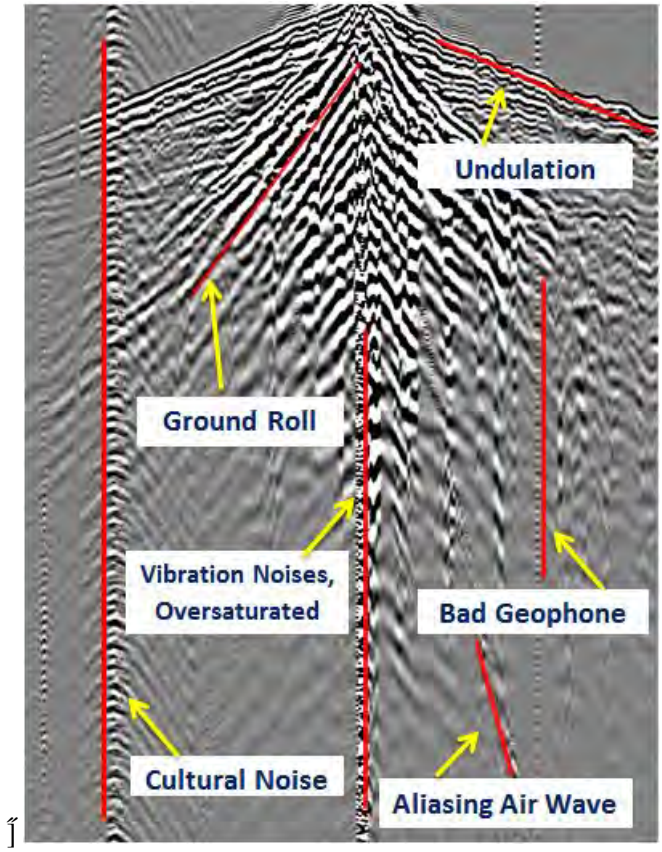

Figure 5.20: *Shot gather image with various types of observed noise. Undulations, ground roll, over-saturated vibrations, cultural noise, bad geophones, and aliasing air wave. All of these types of noise should not be seen when all of the processing steps have been completed.*

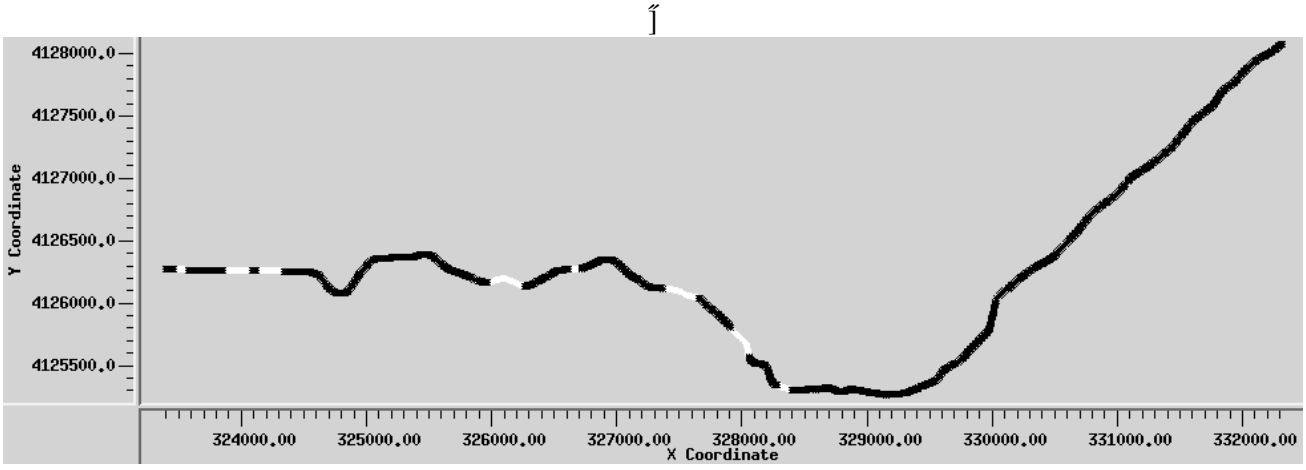

Figure 5.21: *Receiver locations are shown in white, and are overlapped by black shot points. All parts of the line seen in white are gaps where the vibrator truck did not operate.*

5.5 Conclusion

The seismic acquisition survey, being the largest survey at field camp, required by far the most man-hours and equipment. The line was 11km long and shots occurred every 10m along that line. The total number of shots would have been 1100 if not for some minor issues with location of the survey in relation to homes and other roads. The line crews composed mainly of students with minimal prior experience working with the seismic line equipment but still maintained a speed of over 2 km per day. Industry professionals managed the vibrator truck and the doghouse in turn guaranteeing a higher level of accuracy in the data acquisition and a smoother work flow. Initial processing in the field determined the data to be of good enough quality to produce a strong analysis in the lab back in Golden. Overall the field portion of the seismic survey went smoothly and all of the data was successfully transferred back to the processing team in Golden.

The next main portion of the work for the seismic survey took place in a computer lab. There were a few industry professionals who led the way in using SeisSpace as none of the students assigned to seismic data processing and interpretation had any prior experience with the program. SeisSpace contained all of the necessary functions and programs to clean up and de-noise the entire data set. The large amount of processing ended up producing a high quality set of data, which was then run through Madagascar to produce a final clean image.

The final image interpretation proved to be a complex process in itself. The crooked line geometry fix in SeisSpace changes the apparent dips seen in the Figure 5.17. The prediction of the beds dipping towards the East was accurate as the main reflectors are seen deeper down with no new major reflectors above them. There were also two faults found in the seismic image close to each other on the eastern edge of the line. Figure 5.19 outlines these faults in terms of their geologic context. These faults potentially provide one explanation for fluid flow as fluid can travel vertically through faults much easier than it can through the shale beds present. The discovery of the deeper reflector within the basement also interestingly might indicate a change in the beds at depth. Overall, the seismic results show promising information to characterize fluid flow and possibly finding other structures along the main line.

5.5.1 Integration with Previous Field Session Data

When looking at seismic data from previous years, it was observed that the 2013 Field Camp Line and this year's Main Line (2016 Field Camp) could be correlated due to minimal offset. The end of the 2013 Field Camp Line was located less than one kilometer South of the start of this year's Main Line as shown in Figure 5.23.

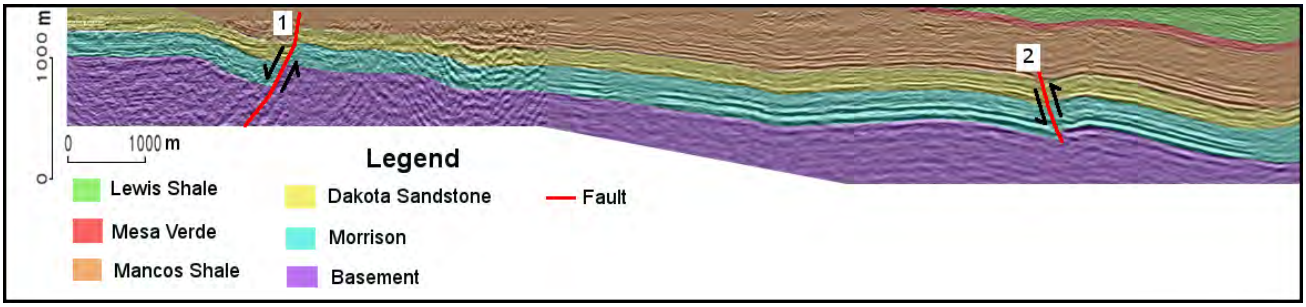

Figure 5.22: *By making the scales of the 2013 and 2016 seismic sections equal, the two sections could be stitched together. The western portion is the 2013 data, while the eastern side is the 2016 data. The overall section is oriented from West to East. The final product is a combined seismic section that is 17 km long. A geologic interpretation is overlaid on top of the seismic section. On this interpretation, the Mesa Verde, Morrison, Dakota Sandstone, Lewis Shale, Mancos Shale, and basement are shown. It was also determined that there are two faults. The westernmost one, is a normal fault commonly known as the 8 Mile fault, and has a large offset in it. The other fault is the one interpreted from the seismic section this year, and it is a reverse fault.*

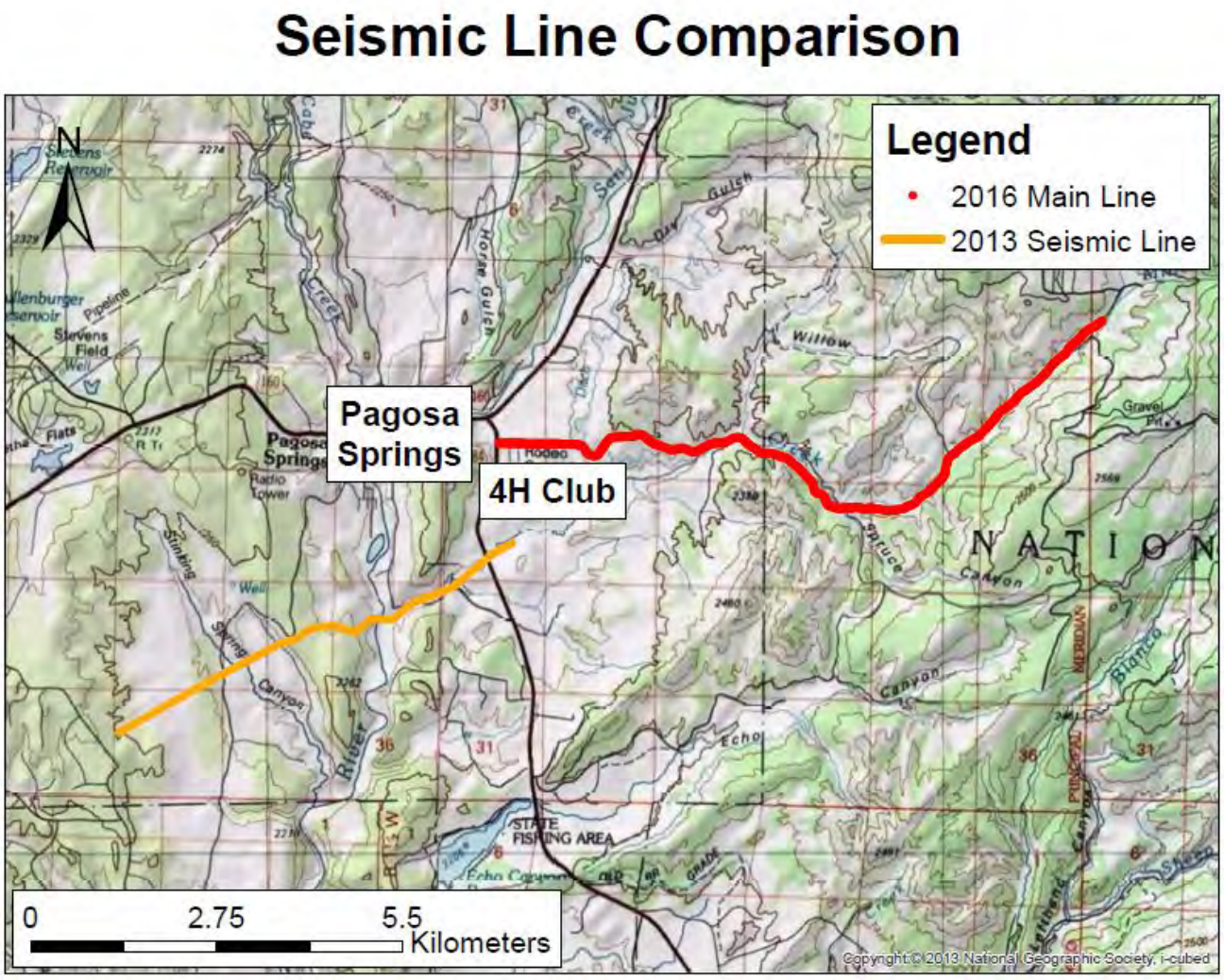

Figure 5.23: *Map of 2013 and 2016 seismic lines. The end of the 2013 line was located less than one km South of the start of this year's 2016 Main Line. Without this offset, the two lines would overlap. Thus, we can correlate the data from both lines.*

On this interpretation, the Mesa Verde, Morrison, Dakota Sandstone, Lewis Shale, Mancos Shale, and basement are shown. Some of the beds, like the Entrada and Wanakah, have been summarized into others as the western portion of the data was substantially worse than the eastern. On the left is the 8-Mile Fault and on the right is a fault found by this year's seismic crew. This interpretation was built using a combination of the 2013 seismic interpretation, this year's seismic interpretation, and this year's geologic cross sections.

There are some errors associated in stitching together two seismic sections that are separated by offset. The 2013 cross section follows a significantly different strike than this year's. Fortunately, the beds in the area dip gently, so the change in apparent dip is small and therefore, the errors associated with processing steps are also small. More error resulted from the poor quality of the seismic data from the 2013 field camp. This made following the reflectors a difficult task. The 2013 Field Camp group reported a total of four faults within their section, but upon further analysis, three of those can be attributed to scarce noise removal data processing. A comparison can be made between the basements of both sections. 2016's model seems to have a relatively low amount of noise in the basement, while the model from 2013 contains many apparent reflectors. The removal of ground roll by applying FK-filtering, is a fundamental step in seismic data processing; however, it appears that the

2013 Field Camp group did not utilize this tool.

In summation, the two seismic sections do have matching reflectors within the overlapping portion. It is possible to come up with a reasonable interpretation based on the two images stitched together. However, the 2013 seismic model is heavy with noise, so it is recommended for it to be reprocessed in order to yield more accurate results. Due to time constraints, the data could not be reprocessed this year.

5.5.2 Recommendations

Doing the field work and processing all of the data showed that there were several areas where things could be been more efficient and effective. To start, the frequencies chosen for the sweep ranged from 4-128 Hz. For these parameters, questions arose about whether or not it was necessary to run the sweep all the way up to 128Hz. Figure 5.24 shows the energy collected from certain frequency ranges in the data. The last couple portions of the figures (on the right) depict the energy seen above 100Hz. The figure shows an apparent decrease in data quality as the frequency increases. In turn, the vibe truck did not necessarily need to shake all the way up to those higher frequencies, and could have spent more time at the lower ones or even shortened the overall length of the sweep itself to save more time. Recommendations for future years include understanding that not a lot of the data will come from those high frequencies which mainly show data in the very near surface.

The second recommendation comes from some interesting things noticed on the right side of Figure 5.18. The beds appear to quickly change dip and are possibly offset from the rest of the bedding. However, this shift could be due a lack of good data at the end of the line due to restrictions in the number of geophones in front of the vibe truck. It would be interesting to continue the seismic line further up the road to the East and see if those beds could be better mapped in the subsurface which might unveil new faulting structures further to the East.

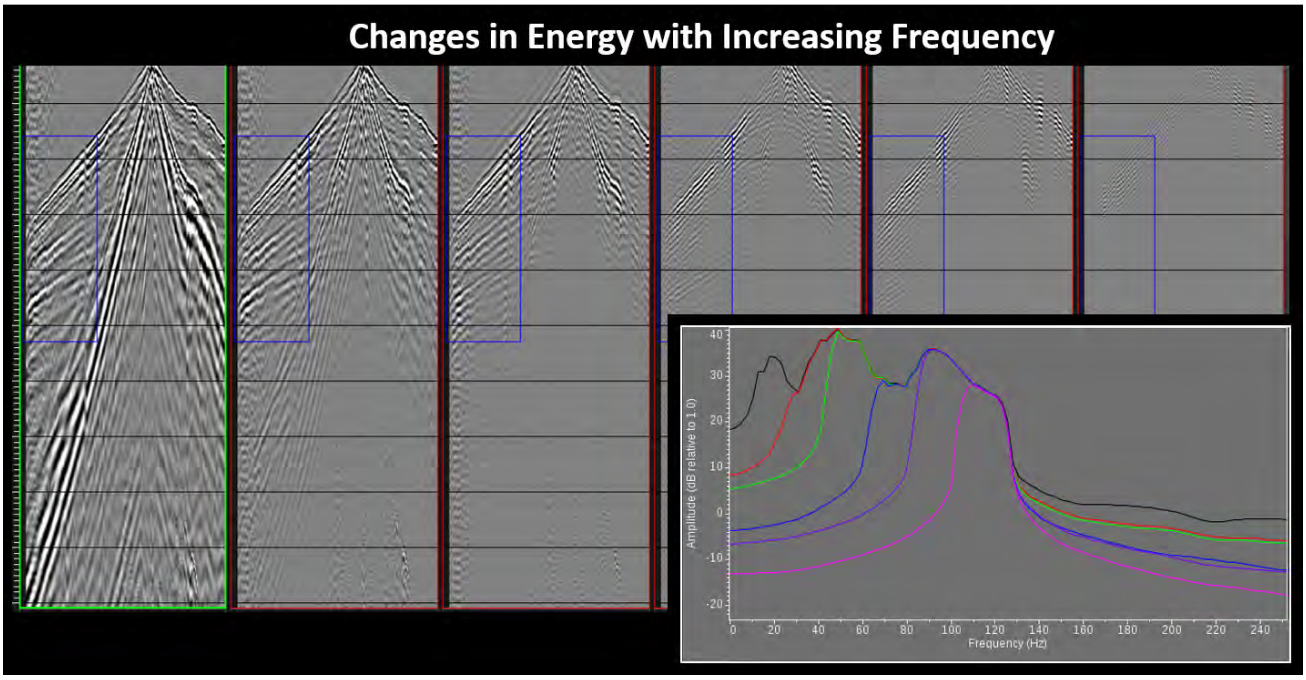

Figure 5.24: *Frequency spectra covering a full shot depicting varying levels of data seen from different frequencies. It is quite clear to see the decrease in energy as the frequency is increased.*

References

[30] "Geophysical Investigation of the Chromo Geothermal System", English, Colorado School of Mines, Upper San Juan Basin, Archuleta County, CO, Tech. Rep., 2014. [Online]. Available: `http://inside.`

mines.edu/UserFiles/File/geophysics/fieldcamp/2014_Geophysics_Field_Camp_Report_revised.pdf (cited on page 40).

[31] "Geophysical Investigation of the Geothermal System within the Chromo Anticline", English, Colorado School of Mines, Upper San Juan Basin, Archuleta County, CO, Tech. Rep., Jun. 2015. [Online]. Available: http://inside.mines.edu/UserFiles/File/geophysics/fieldcamp/GPGN468_FinalReport.pdf (cited on pages 40, 89).

[32] Longet, *Seismic Geophone String-LGT2100*, English, R&D and manufacture of seismic equipments, Jun. 2016. [Online]. Available: http://www.longetequ.com/Seismic%20Geophone%20String/231.htm (cited on page 48).

[33] T. Science, *Earthquake Warning*, 2015. [Online]. Available: https://www.seismicwarning.com/sws-science.html (cited on page 41).

[34] SERCEL, *JF-20dx Conventional Geophone*, English, Jun. 2016. [Online]. Available: http://www.sercel.com/products/Pages/jf-20dx.aspx (cited on page 48).

[35] D. Umpleby, *Driving Seismic Truck*, May 2016. [Online]. Available: https://drive.google.com/drive/folders/0B74qxSO_eo7kNVlMSlBGUXZXUWM (cited on page 50).

[36] USGS, *Seismic Data Processing & Interpretation*, Jun. 2015 (cited on page 48).

6. Hammer Seismic

Contents

6.1 Introduction

Hammer seismic is an active geophysical method in which a seismic source is created by hitting an aluminum plate with a sledgehammer. The seismic waves generated by the hammer propagate into the subsurface and are reflected, refracted, and/or diffracted based on the structure of the subsurface. These subsurface reactions travel back to the surface and are recorded by geophones. The behavior of the wave is influenced by material properties such as density, elasticity, and fluid content. These properties influence velocities, which we can measure. Hammer seismic is a near surface method and the depth of investigation depends on material properties

and the force created by the hammer swing. Hammer seismic has a shallow depth of investigation, optimally about 1/5 the length of the receiver line, but it allows us to focus on a smaller area [37].

The utility of the hammer seismic method stems from its simplicity - hammer seismic survey lines can be established off-road and in remote locations where conventional deep seismic crews would not be able to access. Following this principle, students chose three different lines around Pagosa Springs to perform hammer seismic. Two of these survey lines are located to the North of the Mother Spring in Pagosa Springs, along the East and West ends of the student site line (see Figure 9.1). These lines have the potential to reveal geologic features of interest (ie. an extension of the Victoire Fault), but the primary directive for performing hammer seismic at the student site is to bolster the general understanding of the near surface geologic environment in the area. The third hammer seismic line, located over a portion of the main line near the dike outcropping as seen in Figure 9.1, has a different objective. Because the deep seismic line covered this location, the purpose of hammer seismic here is not to evaluate the general geologic environment, but to act as an in-depth survey of the area over and around the dike outcropping. Students chose this third site after preliminary results from the deep seismic data suggested that the dike would not be sufficiently resolved in the deep seismic data.

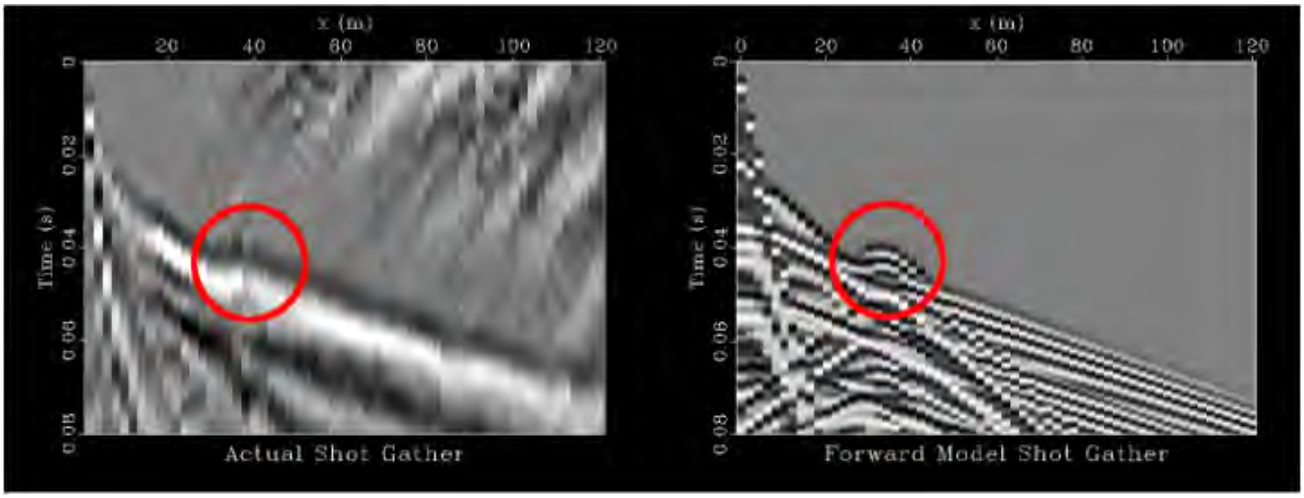

Figure 6.1: *Image from 2015 Geophysics Field Camp Report showing recorded data over a potential dike and a forward model of a dike [38]. The forward model of a shot gather for a vertical dike is shown on the right and a recorded shot gather with a potential dike in the same location is shown on the left. The forward model appears to match the recorded data which suggests that a vertical dike is present in the subsurface. This bump is the result of a seismic wave traveling through faster material and reaching receivers at an earlier time.*

6.1.1 Background

In previous years, students used hammer seismic to image the shallow subsurface in an attempt to find geologic structures, such as faults and dikes, that are linked to the geothermal system in Pagosa Springs. At the previous year's reconnaissance site, the students did not find evidence of any faults in the area but did successfully image a dike using refraction analysis and surface wave analysis as shown in Figure 6.1. They created a forward model with two layers and a vertical dike which was compared to their recorded data [38]. The comparison shows that a dike was likely observed in their data. By using the same types of analysis, an interpretation of near-surface geology at this year's student site can be built. Similar to last year's reconnaissance site, dikes can be identified by comparing this year's data to last year's forward model. This comparison will act as a first order interpretation. Since many types of surveys were conducted at this year's student site, the hammer seismic data can be compared to the data from the other surveys in order to refine the geologic interpretation of the site. The interpretation will help determine if there are potentially interesting geologic features relating to the geothermal system in Pagosa

Springs. If the data provides intriguing information, this area could be a potential location for the 2017 Field Camp main line.

6.1.2 Theory

Principles of Subsurface Wave Propagation

Seismic waves propagating in the subsurface are subject to the same rules of wave propagation as light waves. Through a uniform media, waves will travel radially outward from an impulse source [40]. There are two main types of waves, P waves and S waves. The velocity of the waves are dependent on physical properties of the subsurface such as porosity, pore pressure, effective pressure, and fluid content [38]. The P-waves are the primary waves that propagate faster into the subsurface while the S-waves are shear waves that are slower. The equation to describe a P-wave is:

$$\alpha = \sqrt{\frac{\lambda + 2\mu}{\rho}} \tag{6.1}$$

while the equation to describe a S-wave is:

$$\beta = \sqrt{\frac{\mu}{\rho}} \tag{6.2}$$

Lame's parameters μ and λ represent the shear modulus and the dynamic viscosity of a material, respectively. These parameters determine the behavior of the seismic waves. When interfaces of changing physical properties are present, these waves will be reflected, refracted, or diffracted (See Figure 6.2). When a wave encounters a sharp and continuous interface, a portion of the incident wave will be reflected and a portion will be transmitted. The degree to which the incident wave is reflected or transmitted is controlled by the velocity contrast across the interface, as well as the angle of incidence with the interface. When the angle of incidence reaches the critical angle, the transmitted wave will travel along the interface as seen in Figure 6.2.

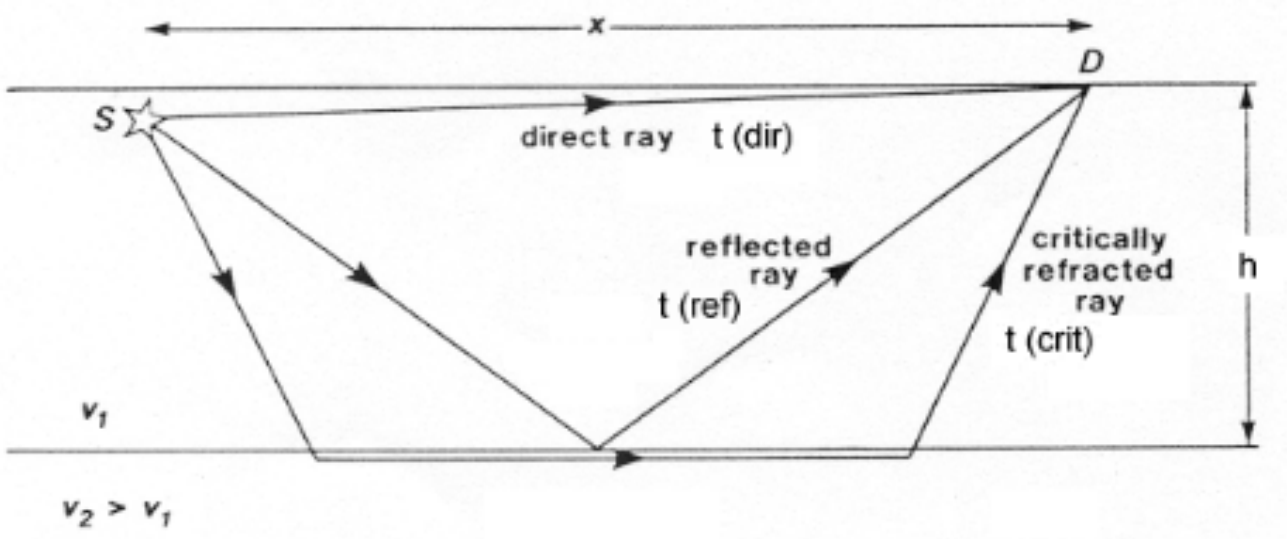

Figure 6.2: *Depiction of different wavefront interactions at a subsurface interface. Observe how the direct wave travels solely through the velocity above the interface, while the critically refracted wave travels through the velocity below the interface. Note that according to Snell's Law, in order for critically refracted waves to occur, the velocity below the interface must be greater than the velocity above the interface [40]. Image from F. Jones, UBC Earth and Ocean Sciences.*

According to Huygen's construction principle, the refracted wave traveling along the interface will generate wavefronts propagating radially outwards; these wavefronts arrive at the surface with the velocity of the refracted wave traveling along the interface; termed head waves (See Figure 6.5). The final interaction that can occur at an interface is a diffraction. Diffractions occur when there is a sharp and non-continuous interface, such as a corner. The resultant wave from a diffraction propagates radially outward from the diffraction point, acting similarly to an impulse source in the subsurface.

Identifying direct, reflected, and refracted wave arrivals in seismic data is required in order to draw conclusions on subsurface velocities. Differentiating refracted wave arrivals from direct and reflected wave arrivals involves knowing that the refracted wave will arrive at a later time, but with a greater velocity (refraction at the critical angle can only occur when the velocity below the interface is greater than the velocity above the interface). Furthermore, while direct and refracted waves appear with a linear moveout in seismic data, reflections will appear with a hyperbolic moveout, allowing for differentiation of reflected wave arrivals from the rest of the data [39], as seen in Figure 6.3.

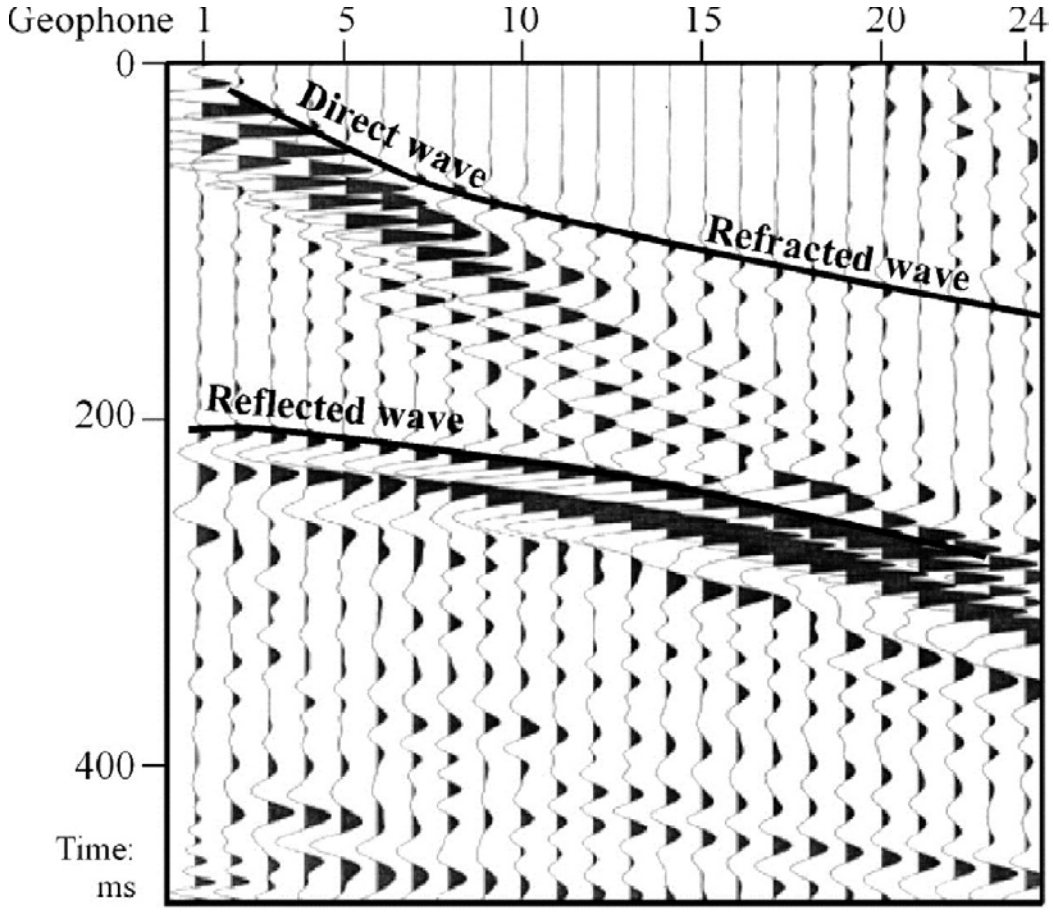

Figure 6.3: *A seismic shot gather showing a labeled direct wave, refracted wave and reflected wave. This illustrates the different moveouts of each wave type. Source: Woolery et al. Environmental and Engineering Geoscience, 2008.*

Reflection and refraction analysis are essential to establishing velocities and thicknesses to create a subsurface velocity model, while diffraction analysis is used to evaluate the efficacy of the chosen velocity model through the principle of diffraction focusing [43].

Travel Time and Slopes in Relation to Velocity

To calculate the velocity of a layer, look at the travel time curve associated with the layer. In general, the z-axis and the x-axis are in time and distance, respectively. By using the equation below, the inverse slope of a line is equivalent to velocity.

$$v = \frac{\Delta distance}{\Delta time} \tag{6.3}$$

In Figure 6.4, an example travel time curve is shown. As stated above, the velocity of the direct wave can be calculated by taking the inverse of the slope.

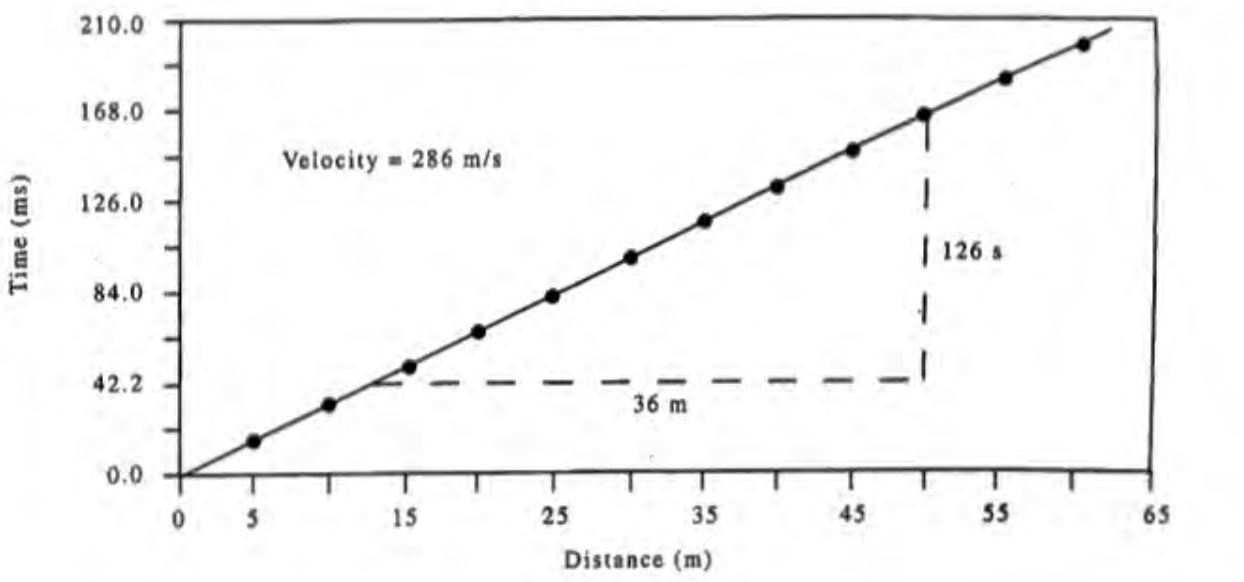

Figure 6.4: *Diagram of a travel time curve showing only the direct arrival. Source: Burger et al. Applied Geophysics, 2006.*

The example above is for a homogeneous subsurface. However, this is usually not the case. Thus, there are several geologic cases that can appear in the data. The first case is a 2D layered Earth with a horizontal interface. From a single shot gather, the velocity is calculated for the layer above and below the first interface.The slope of the direct wave represents the velocity of the layer above the interface V_1, and the slope of the head wave represents the velocity of the layer below the interface V_2. By tracing the head wave back in time to where it intersects the source location, the intercept time, t_i can be found. The intercept time has no physical meaning because the head wave does not exist at this time. A diagram showing this relationship is shown in Figure 6.5.

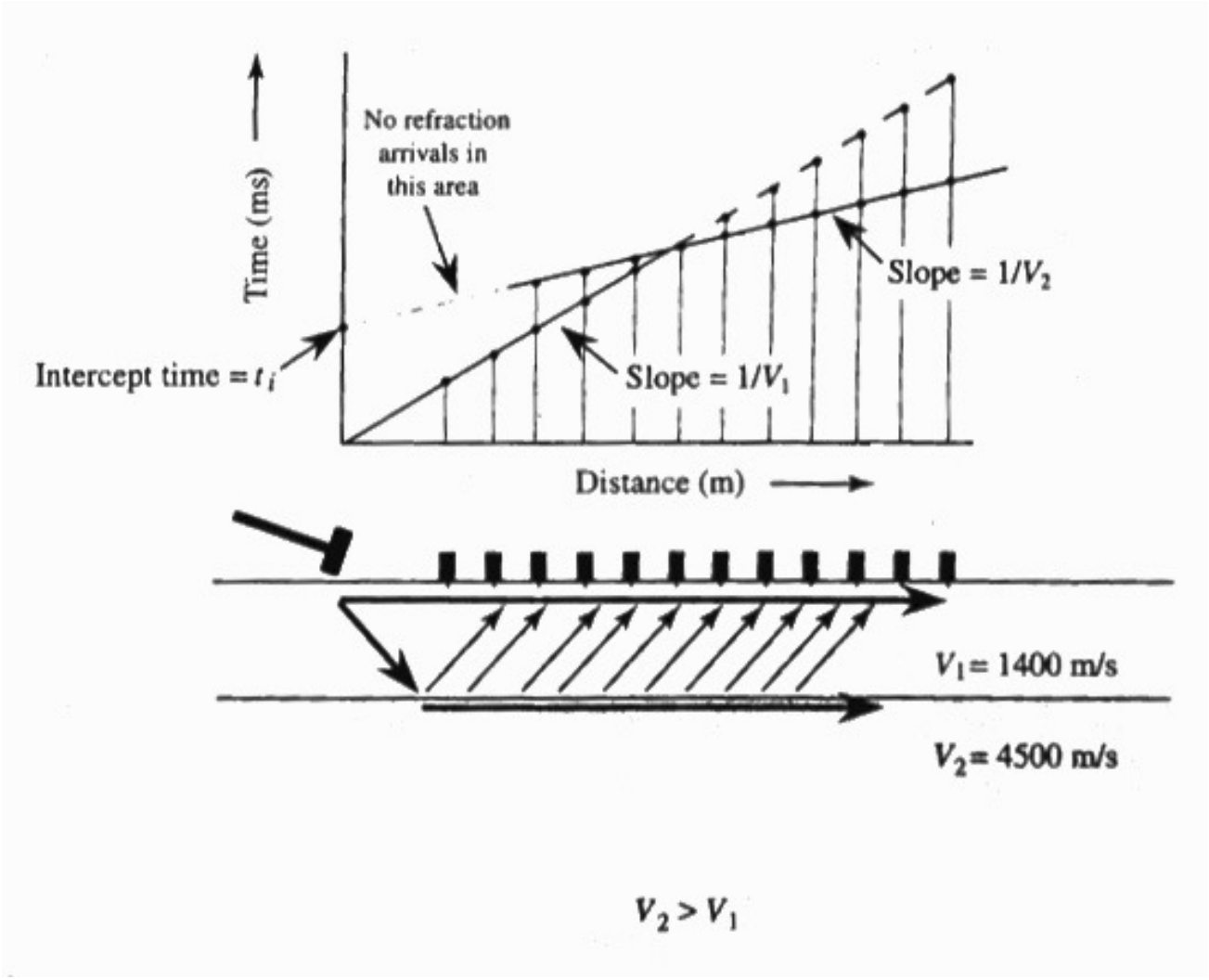

Figure 6.5: *Diagram showing ray paths in a subsurface with one horizontal interface. The relationship between the slope of the direct wave and V_1 and the refracted wave and V_2 is shown. Source: Burger et al. Applied Geophysics, 2006.*

Once V_1, V_2, and t_i are known, the distance between the surface and the interface h, can be calculated. The equation for h is given by the equation below, where V_1 is the velocity of the layer above the interface and V_2 is the velocity of the layer below the interface. This equation was derived from the travel time equation.

$$h = \frac{t}{2} \frac{(V_1 V_2)}{(V_2^2 - V_1^2)^{\frac{1}{2}}} \tag{6.4}$$

Another common case is a 2D Earth with a dipping interface. When there is a dipping interface, the velocities will be asymmetrical. The velocity up-dip will be faster than the velocity down-dip. When the dip angle is less than 10 degrees, the average of these two apparent velocities will be relatively equal to the true velocity [37]. A diagram demonstrating this case is shown in Figure 6.6.

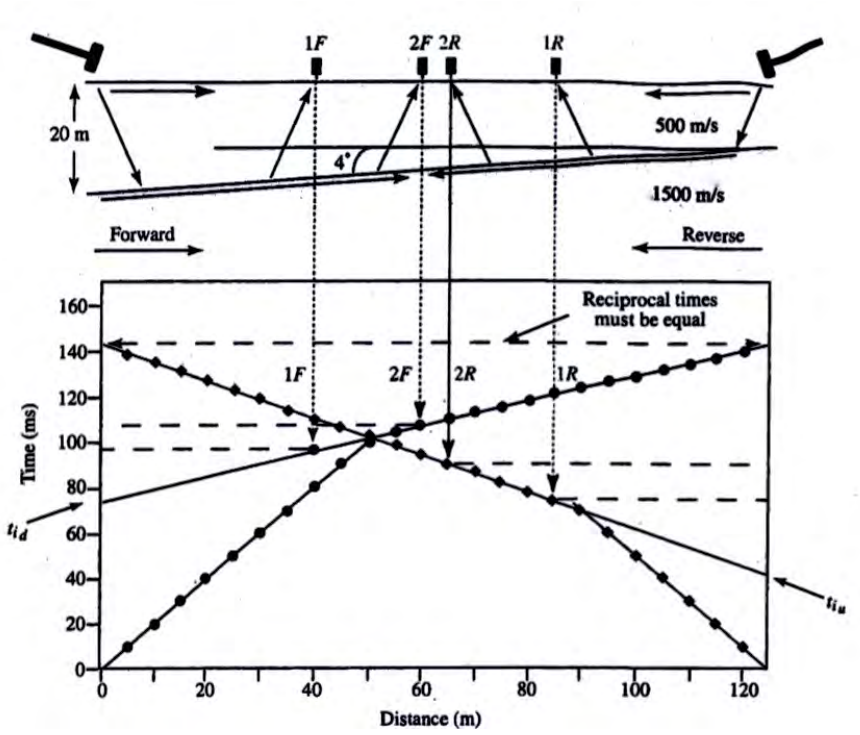

Figure 6.6: *Depiction of forward and reverse traverses over a dipping bed. By utilizing a spread of geophones, redundant forward and reverse traverses can be collected across any geologic features of interest. Source: Burger et al. Applied Geophysics, 2006.*

Noise Reduction

To improve the signal to noise ratio, we rely on the principle that signals due to real geologic features will appear consistently when viewed at different times from different orientations, while noise will appear inconsistently. By recording multiple shots at every trace and using a spread of geophones, the data captures consistent features, allowing for stacking to get rid of inconsistent noise and amplify signals by averaging out noise and stacking real geologic features. Shooting from several different locations provides a better signal to noise ratio, as it allows for the data to "illuminate" geologic features from different angles. This is helpful in processing and interpretation as it allows us to compare forward and reverse traverses of the same area. This comparison allows us to make inferences on the geometry of the geologic features as seen in Figure 6.6.

6.2 Objectives

1. Use hammer seismic to increase understanding of the near surface geology at the student site
2. Create near-surface velocity models of the earth under the hammer seismic lines
3. Use reflections on the west side of the student to determine depth and dip of deeper reflectors
4. Determine whether or not the student site has geology that is significant in terms of the Pagosa Springs geothermal system
5. Better image the dike located on the main line and pinpoint its location using refraction analysis

6.3 Methods

6.3.1 Survey Location

Hammer seismic groups surveyed the line along the west end of the student site as well as at a site near the east side of the student line. While these surveys are not along the main line, they will aid in determining the geology surrounding Pagosa Springs. Another survey line over the location of the dike along the main line will aid in imaging the dike. The dike location will be combined with other methods to create a better map of the subsurface and the dike itself.

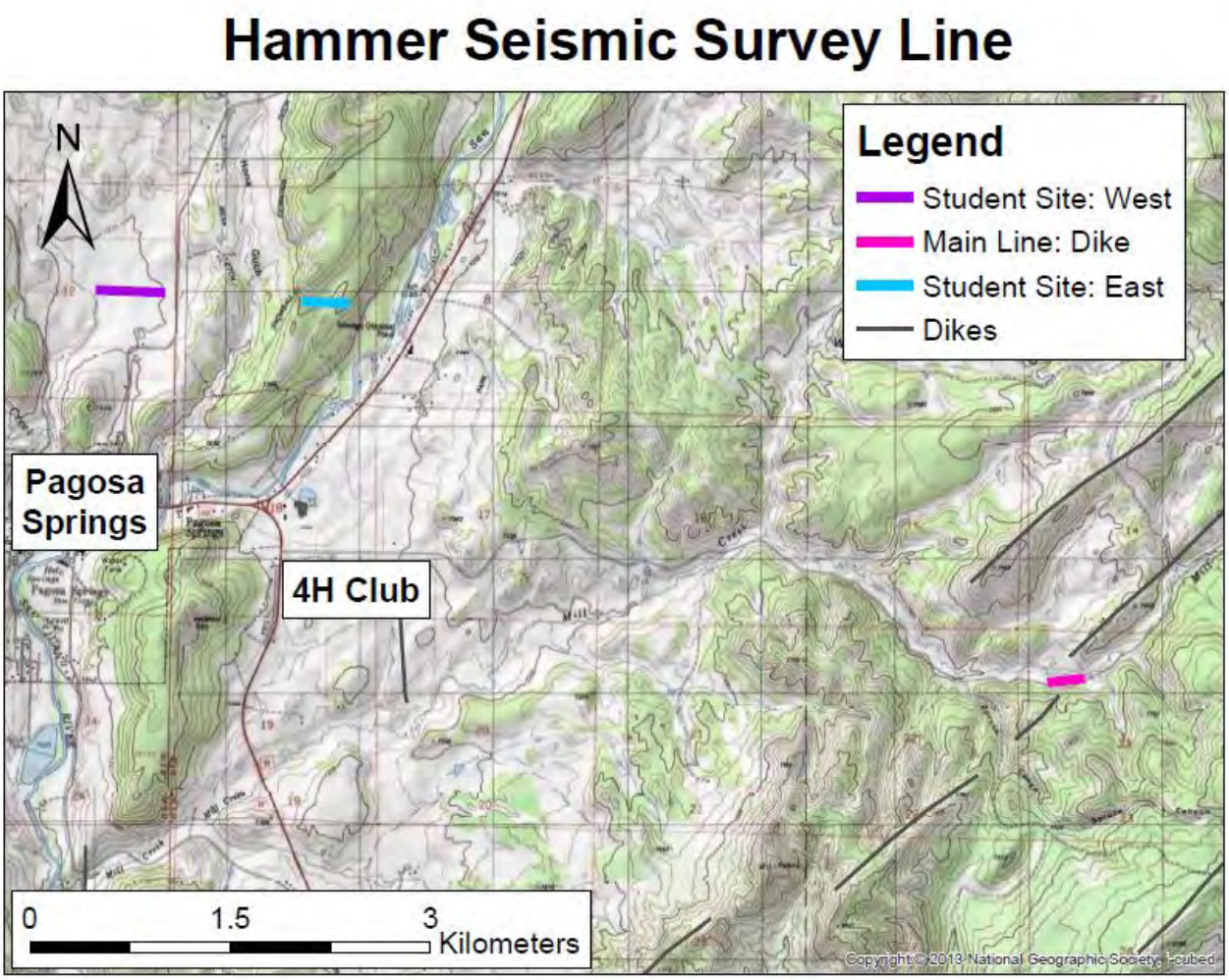

Figure 6.7: *Map of the three hammer seismic lines. The North West light purple line is the west end of the student line where as the darker purple line next to it is the east side of the student line. The east side of the line is located slightly to the North of the actual student line due to ease of access for the equipment.*

6.3.2 Data Acquisition

Survey Setup

At the student site 72 geophones were laid out using a 3m spacing, and on the main line 48 geophones were laid out with a 2m spacing. The tight spacing at the main line allows for a higher resolution, which is important when imaging something as thin as the dike which is only 1m thick at its outcrop on the nearby hill. To put a geophone into the ground, the geophone is placed in the correct location and then stomped into the ground while

ensuring it is oriented nearly vertical. When the ground moves under a geophone, it will move the geophone, which will create an analog electric signal that is recorded by the Geode seismograph and transmitted to the computer as a digital signal once every .5ms. A 3m spacing was chosen for the student site so that a larger area could be surveyed while maintaining small enough spacing that the entire waveform can be observed. For the main line, a tighter spacing and shorter line was used because the dike was a specific target and its location was fairly well known. These spacings follow from the Nyquist sampling theorem which states that sampling frequency must be at least twice the frequency of the signal being measured so that the signal can be fully reconstructed. Unlike deep seismic in which 6 geophones on a string are averaged into one channel representing an average over 10m of the line, in hammer seismic each phone is on its own channel as shown in Figure 6.8 with the multi-channel seismograph. This gives a higher resolution and more sensitivity to surface waves, which are more desirable in hammer seismic [37].

At each shot point at the student site, a sledgehammer is used to strike a metal plate for 5 strikes with 3 to 4 seconds between strikes to allow for the computer to listen for one second and reset. At the dike, the plate was only struck three times at each shot point, but this is compensated for by smaller shot and geophone spacing than the other surveys. The multiple strikes are used to increase the signal to noise ratio. Noise will change between the strikes, but the signal from reflections due to geology will not change. This allows for the noise to be filtered out once the shots are stacked. An aluminum plate is used to transmit energy from the hammer into the ground. Since seismic methods require a clear signal, the metal plate prevents material deformation from the hammer impacting the ground in order to cleanly translate energy into a non-distorted waveform. Different materials will also create a different source signal waveform so a consistent signal and therefore a consistent striking material is needed for a survey.

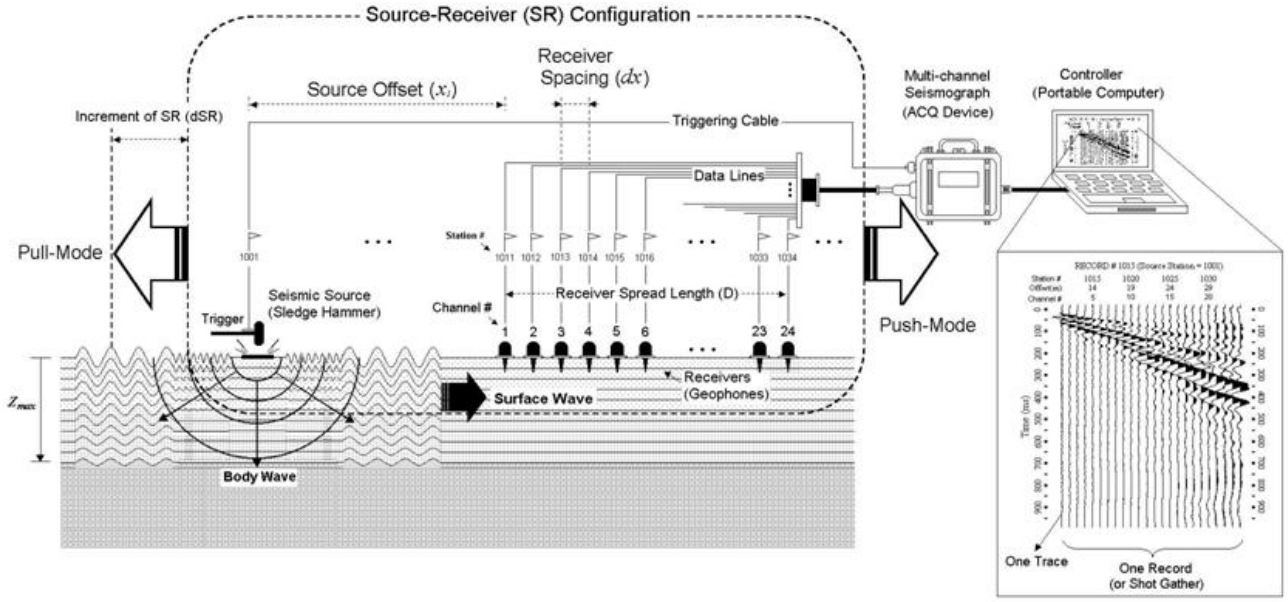

Figure 6.8: *The equipment for a hammer seismic survey is shown. The diagram shows how a source from the sledgehammer is converted to a shot gather on the laptop [42]. Image from Park Seismic LLC.*

Figure 6.9: *Photograph of hammer seismic survey being conducted over the east end of the student site. Pictured are crew members responsible for hammer swings and communicating between the recorder and swinger, as well as geophone and trigger cables.*

Figure 6.10: *Image of the Geode seismograph used for collecting hammer seismic data. Photo courtesy of Geomatrix Earth Science LTD [41].*

Equipment List

1. Sledgehammer with trigger sensor
2. Metal plate
3. Geophones
4. Battery
5. Cable
6. Geode seismograph (see Figure 6.10)
7. Laptop (record/review data)

6.3.3 Processing

The Madagascar and Software Construction (Scons) software suites for Linux computing systems allow the students to import, process, and visualize seismic data acquired from the hammer seismic surveys. Madagascar is an open-source software package widely used for seismic data processing. The numerous freely-available resources make Madagascar an ideal environment for the students to process the field data. Two different avenues of analysis are available when processing seismic data - reflection and refraction analyses. While reflection analysis allows for information regarding reflectors deeper in the subsurface, refraction analysis allows for information on the velocities in the shallow subsurface. By comparing two way travel times and slopes from reflected and refracted arrivals, students can create a rudimentary subsurface velocity model. By applying automatic gain control (AGC normalizes amplitude of input signals [ie. hammer strikes] to create a consistent output), bandpass filtering, and static corrections to the data, it is possible to isolate different arrivals in the data and make stronger inferences on the subsurface velocities and geometry that created the recorded waveform as seen in Figure 6.11.

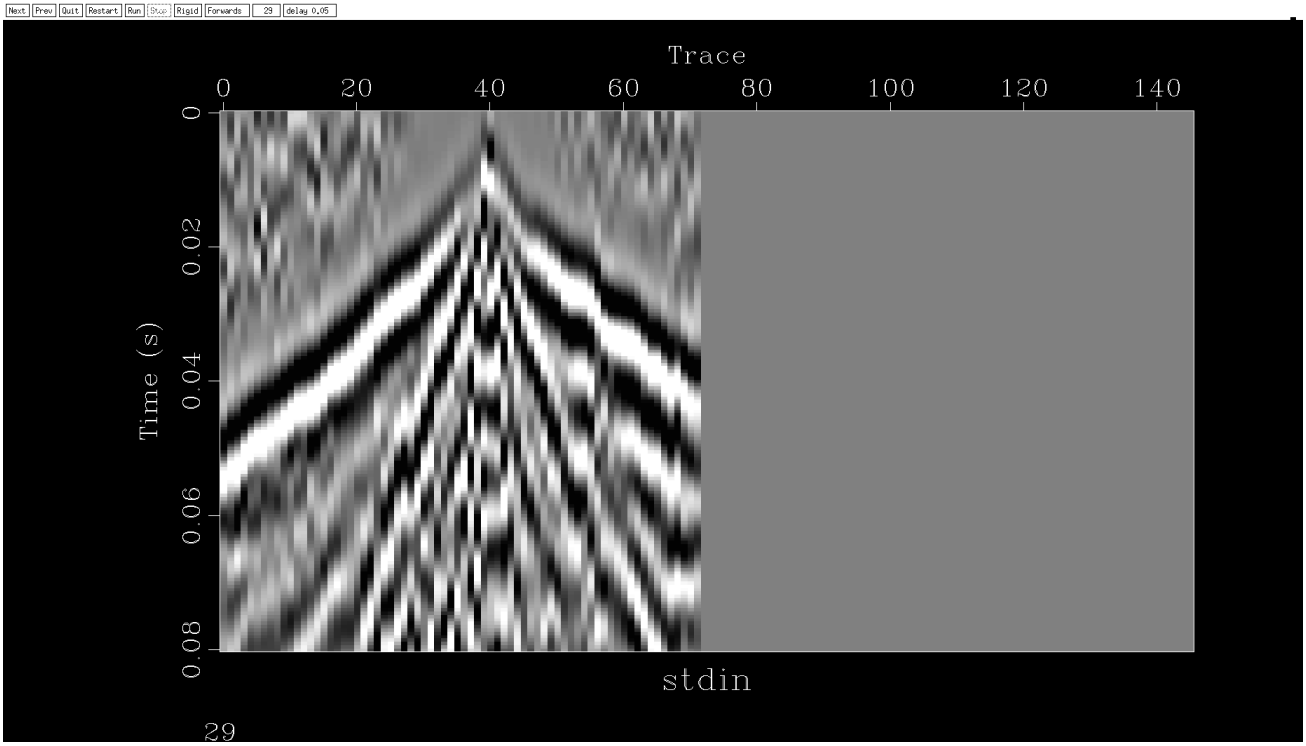

Figure 6.11: *A processed image of Shot 29 from the west side of the student site line. A bandpass filter has been applied and the image is ready for velocity picking and reflection analysis.*

A notable roadblock encountered during processing of the hammer seismic data involved stitching together

data files corresponding to consecutive sections of geophone rollovers. The hammer seismic recording software does not account for rollovers, meaning that files corresponding to consecutive spreads need be manually stitched together. This concatenation of rollovers is essential when creating common gathers of the data, which involves stacking of data from various shot and receiver offsets/locations in order to "illuminate" the subsurface from different orientations. The guiding principle behind stacking data is that signals due to real geologic features will appear consistently from different viewing orientations, while noise will appear inconsistently. Therefore, when data is stacked, inconsistent signals from noise will attenuate while consistent signals from real features will be amplified.

Reflection Analysis

The primary purpose of reflection analysis is to determine the depth to the first subsurface interface. To do this, the first reflection arrival must be isolated from the data by muting the effects of direct and surface wave arrivals in the data. This is typically done in a common offset gather, from which the direct waves (which arrive sooner than the first reflection) and surface waves (which arrive later than the first reflection) can be easily identified allowing for the first reflection arrival to be isolated.

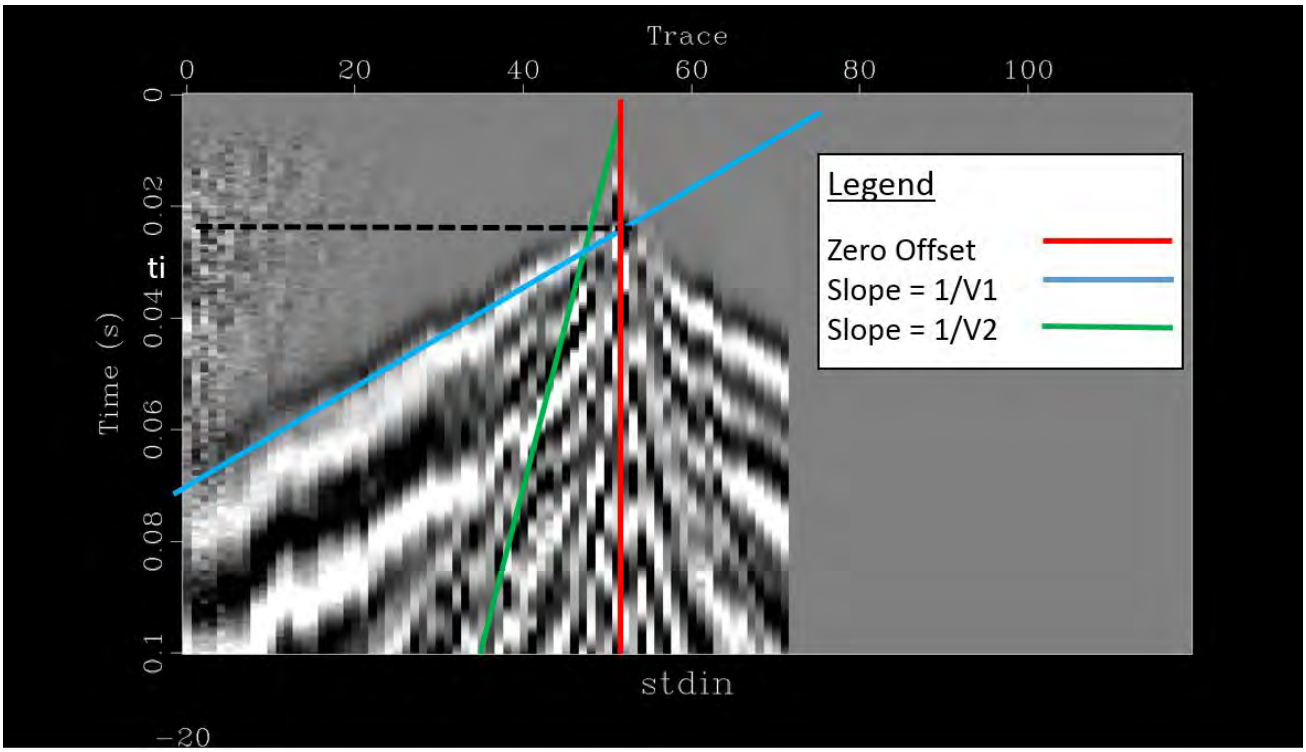

Figure 6.12: *Refraction analysis of Shot 50 on the east end of the student site. This region has two clear layers. The direct arrival is shown in blue and the head wave is shown in green. By taking the inverse slopes of each, we can calculate a velocities for the layer above the interface and below the interface.*

Refraction Analysis

Refraction analysis consists primarily of qualitative interpretations of the travel times and slopes of the direct and head wave arrivals. Because the direct wave travels along the surface, its travel time and slope are directly related to the velocity above the subsurface interface. Likewise, because the head wave travels along the subsurface interface, its travel time and slope are directly related to the velocity below the interface. Additional information on the geometry of the subsurface interface can be inferred by comparing forward and reverse traverses of the refracted waves using the delay-time method [37]. An example of refraction analysis is shown in Figure 6.12.

As shown, refraction analysis can be performed one shot at a time, giving us a series of 1D subsurface models. By stitching these 1D models together, a 2D interpretation of the subsurface is created. A Linear Moveout correction (LMO) takes a linear event and changes the slope of the line. The slope of a line on a seismic trace with time on one axis and distance on the other axis would be equivalent to velocity (distance over time). LMO is used to pick velocities for the dike site by changing the slope until the line is horizontal. The velocity for a head wave from a shot on the west end of the dike line was found using LMO and is shown in Figure 6.13.

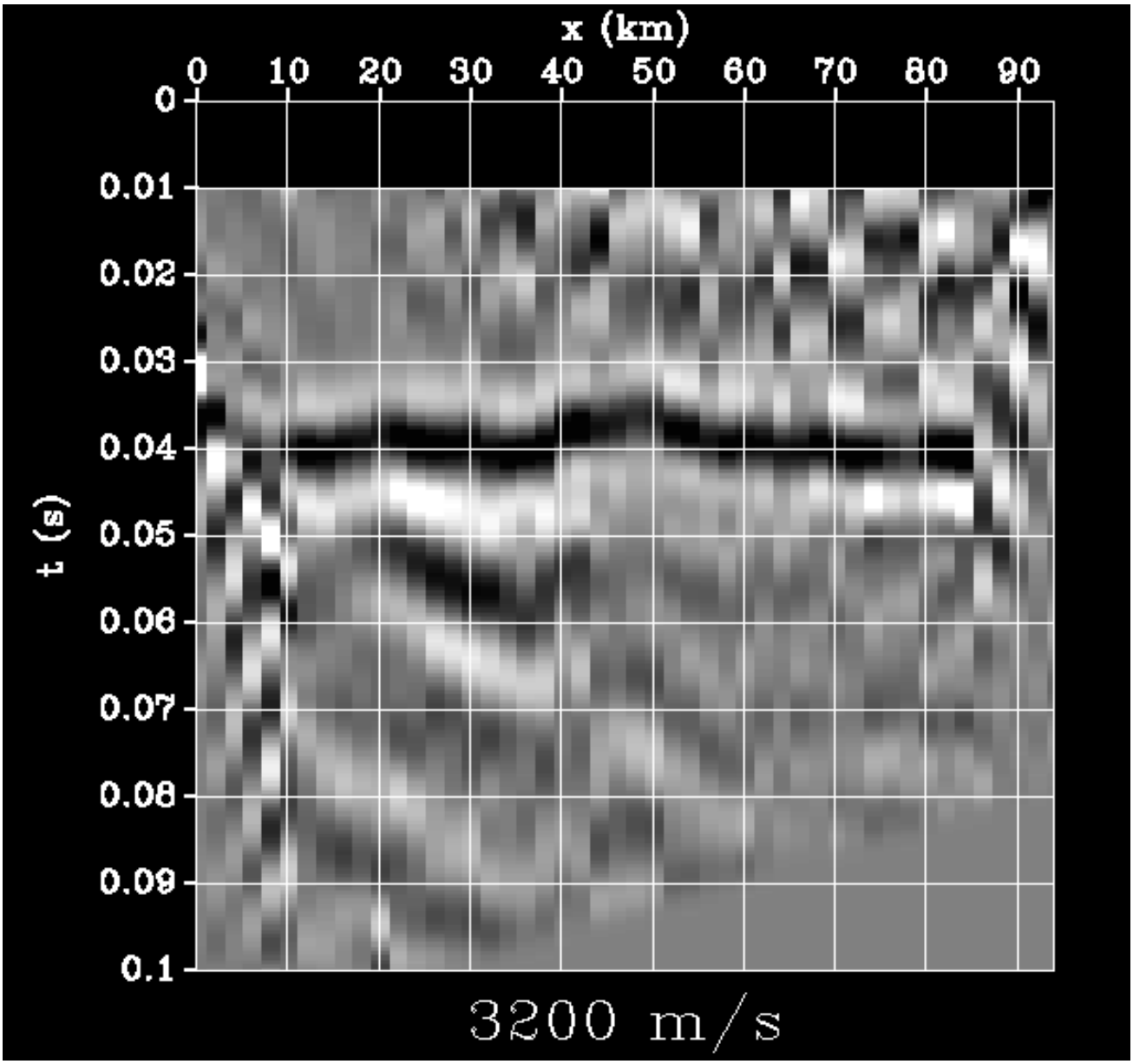

Figure 6.13: *An LMO corrected image from the dike line. This image shows how an LMO can be used to flatten out refractions and estimate velocities.*

6.4 Discussion

6.4.1 Expectations

A forward model was not created for any of the sites, but there is a general idea of what should be seen at each location. The West end of the student line lies in a valley that overlies the Mancos Shale, and is shown as a purple line on Figure 9.1. Shale is expected on the West end and maybe a reflection from the Dakota sandstone underneath the shale. The reflection from the sandstone will show up after the direct and head waves but will have more of a hyperbolic shape. The East end of the student line at the horse meadow contains a small hill and a flat plateau. The purpose of the survey was to find out why the hill is there and whether a fault or differing rock types created the topographic change. Under the loose dirt either the Mesa Verde or Mancos is expected, but refraction velocity analysis will not be able to tell the difference between these units.

For the main line a dike that appears near the surface is expected, based on nearby outcrops. Instead of creating a new forward model, the model of a shallowly buried dike from 2015 Field Camp data since aided in locating the dike. Additionally, the 2015 Field Camp students created a forward model to compare their data. The dike site should show a short spike in the seismic data that is representative of a faster igneous body then the background sedimentary rocks.

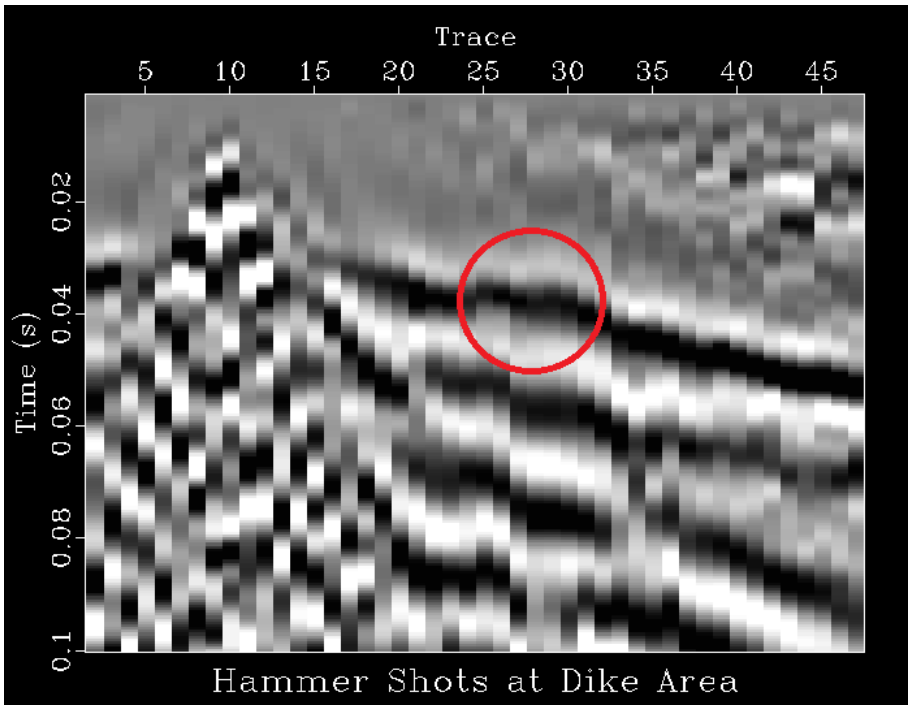

Figure 6.14: *Trace from a shot on the dike line. The left side of the figure is the west end of the line. Here the dike can be seen centered at about trace 28. This is just a few meters West of station 1673*

6.4.2 Results

As expected, a spike in the data was found, which is likely the dike. The dike is seen about 3 meters west of station 1673 at an approximate depth of 2-3 meters. This can be seen in Figure 6.14. The West side of this line started at 1667 and ended 100m East at station 1677. On the West end of the line, an interface is seen at a depth of 3m. The depth of the interface decreases towards the East end, with a depth of 2.5 meters towards the center of the line and a depth of 2.308 meters at the West end. The layer above the West-dipping interface has a constant velocity of 200 meters per second and the layer beneath the interface started at about 3200 meters per second on the East end and decreased to 2400 meters per second on the east end of the line shown in Table 6.1. The lower

layer is believed be Lewis Shale.

On the west side of the student line there is a good reflector that is located at a depth of approximately 100 meters, see Figures 6.15 and 6.16. This is deep for hammer seismic and the dip of the reflector is highly variable on static corrections from near surface velocities. This reflector could be a possible fault that has a true dip of about 60 degrees. Since the fault is not perpendicular to the seismic line, the dip seen in the stacks are apparent dip. The apparent dip was calculated to be 51 degrees shown in figure 6.16.

The West side of the student site was also subjected to refraction analysis, and a simple two layer velocity model of the subsurface was created in Surfer, Figure 6.20. There appears to be a layer of relatively slow material with a velocity of approximately 360m/s over most of the line that is from 1m to 1.5m thick, with the exception of a section from 50-100m in which the slow layer is not detectable. Under this low-velocity layer the underlying rock has a velocity of 1500-3500m/s, in the range of Mancos shale shown in Table 6.2. Velocity models were also created for the Horse Meadow as well as the dike site on the main line in Table 6.3. The Horse Meadow showed some of the thickest loose dirt, up to 6m in some places which shows in Figure 6.21. The main line dike site appears to have a relatively thick layer of slow material, ranging from 2.3m to 3m in Figure 6.18.

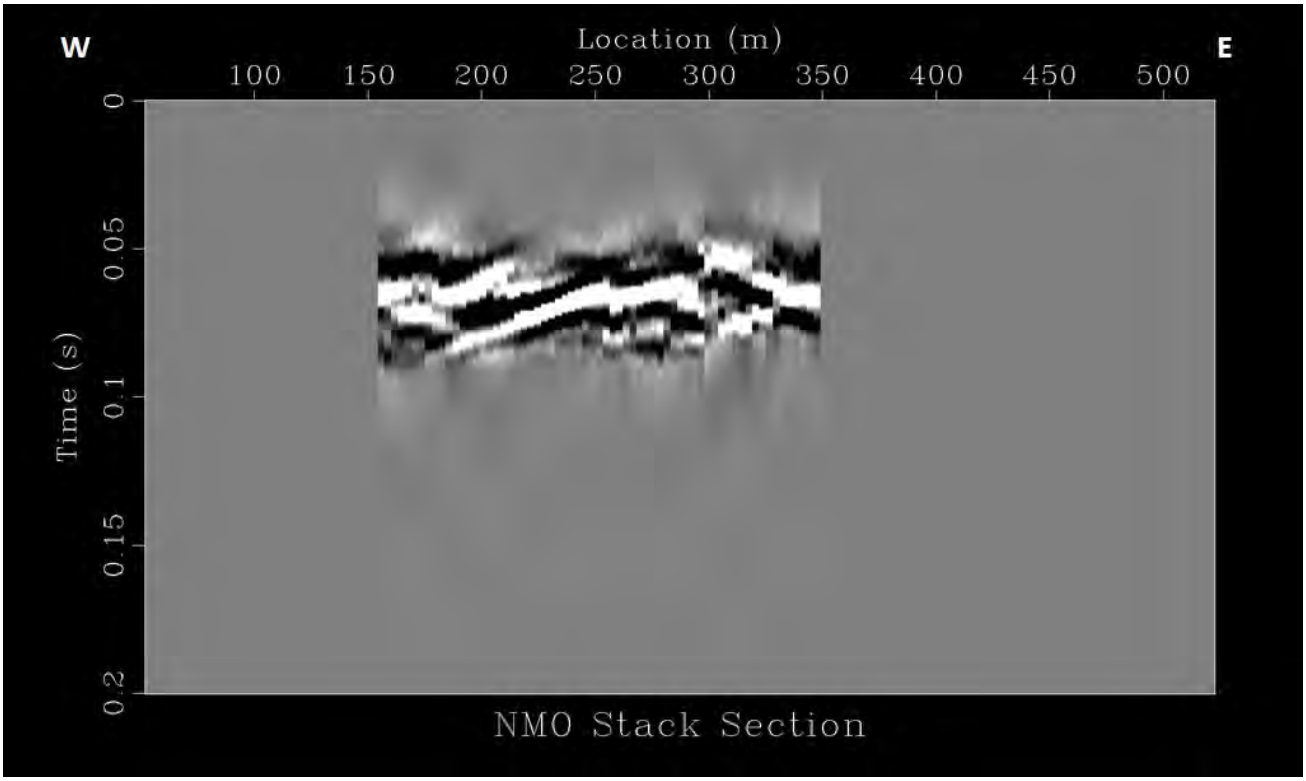

Figure 6.15: *The figure shows a windowed section of a normal moveout corrected stack section. The windowing is to highlight the reflector that is being seen which starts around .075 seconds and travels up to .06 seconds from 190 to 260 meters.*

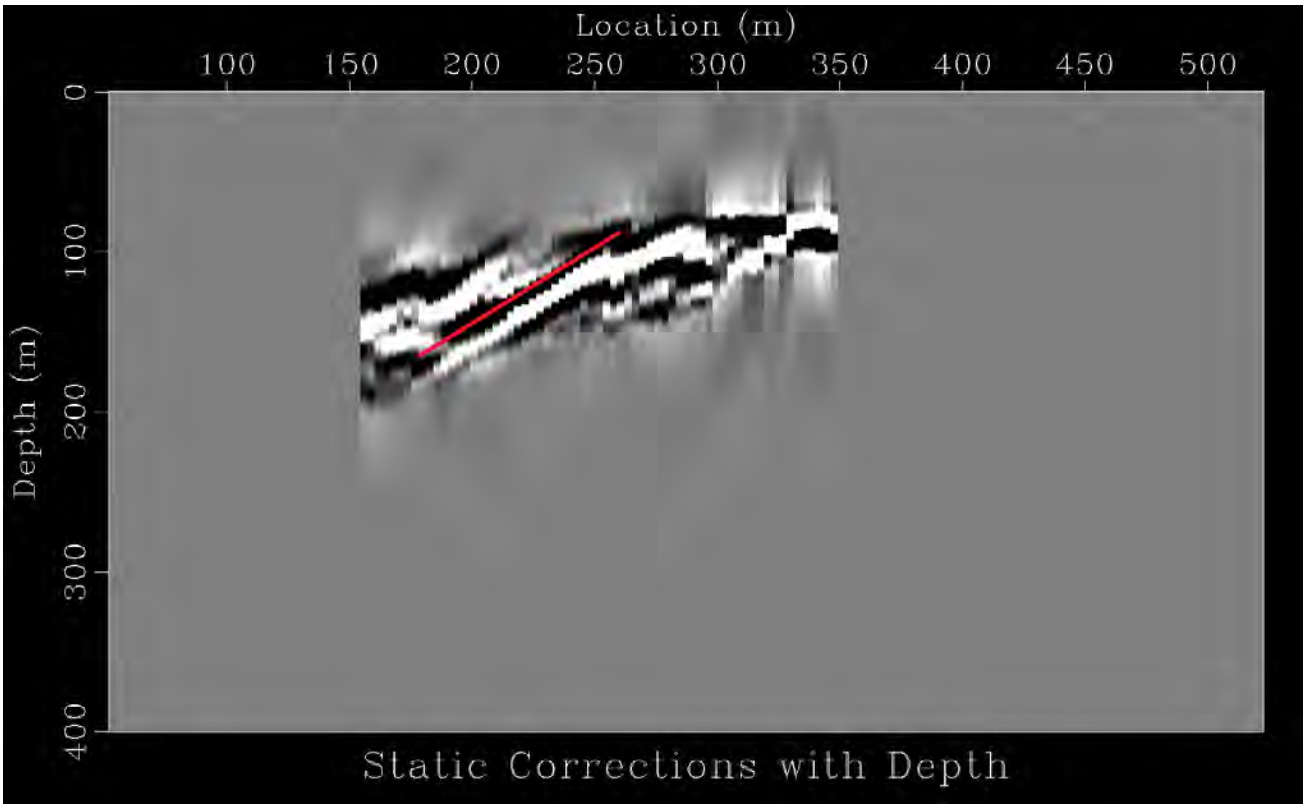

Figure 6.16: *A statics correction is applied to the stack section from Figure 6.15 as well as a time to depth conversion. The reflection has an apparent dip of about 51 degrees and is emphasized by the red line.*

Shot	1	8	15	15	26
Orientation	East	West	West	East	West
ti (s)	0.030	0.029	0.029	0.025	0.023
v1 (m/s)	200	200	220	180	190
v2 (m/s)	3240	2950	2850	2700	2540
h (m)	3.01	2.9	2.90	2.5	2.30

Table 6.1: *Results from the velocity analysis of the main line. V_1 is the velocity of the first layer, V_2 is the velocity of the second layer, t_i is where the slope of the head wave intercepts at zero offset, and h is thickness of the top layer. For each shot location, velocities were evaluated by measuring the slope of the direct wave and head wave. By using these velocities and t_i, the thickness of the the top layer can be calculated.*

Shot	10	29	29	79	79	118	118	130	130	141
Orientation	East	West	East	West	East	West	East	West	East	West
ti (s)	0.007	0.00	0.005	0.006	0.007	0.007	0.007	0.005	0.005	0.005
v1 (m/s)	272	188	400	281	476	474	315	429	315	315
v2 (m/s)	2220	1800	1500	2710	2440	2460	2870	3440	3290	3510
h (m)	1.28	0.00	0.09	1.09	1.09	1.28	1.27	0.90	0.90	0.90

Table 6.2: *Results from the velocity analysis of the west side of the student line. V_1 is the velocity of the first layer, V_2 is the velocity of the second layer, t_i is where the slope of the head wave intercepts at zero offset, and h is thickness of the top layer. For each shot location, velocities were evaluated by measuring the slope of the direct wave and head wave. By using these velocities and t_i, the thickness of the the top layer can be calculated.*

Shot	110	70	70	50	50	40	40	30	30
Orientation	West	West	East	West	East	West	East	West	East
ti (s)	0.040	0.030	0.031	0.020	0.020	0.017	0.018	0.010	0.012
v1 (m/s)	300	300	300	390	420	330	360	300	360
v2 (m/s)	4200	3000	4533	2833	3230	2400	3600	2727	3375
h (m)	6.02	4.50	4.66	4.00	4.24	2.83	3.26	1.51	2.17

Table 6.3: *Results from the velocity analysis of the east side of the student line. V_1 is the velocity of the first layer, V_2 is the velocity of the second layer, t_i is where the slope of the head wave intercepts at zero offset, and h is thickness of the top layer. For each shot location, velocities were evaluated by measuring the slope of the direct wave and head wave. By using these velocities and t_i, the thickness of the the top layer can be calculated.*

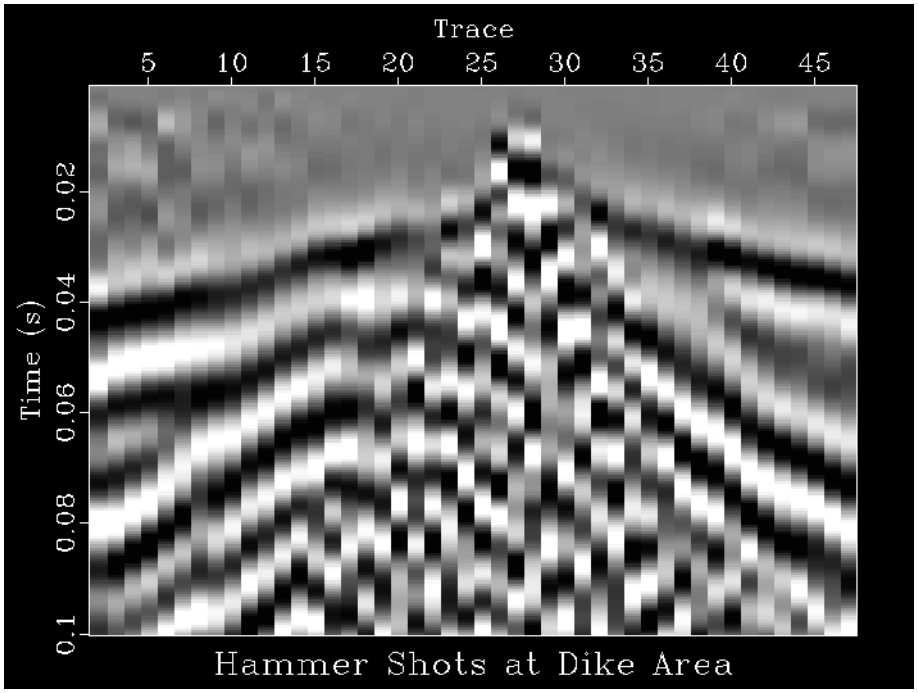

Figure 6.17: *Trace right above the proposed dike location.*

6.4.3 Interpretation

Main Line

The refraction analysis of the main line dike site located the dike with an uncertainty of approximately a meter, far beyond the resolution of deep seismic. Refraction analysis also shows that the dike is buried under at least a couple of meters of loose material. It is hard to estimate the depth to the top of the dike because it produces diffractions that show up as noise, making velocity analysis of the direct wave very difficult. The depth is at least a couple meters beneath loose dirt because in the image from the shot directly above the dike (Figure 6.17), the 200m/s wave was observed.

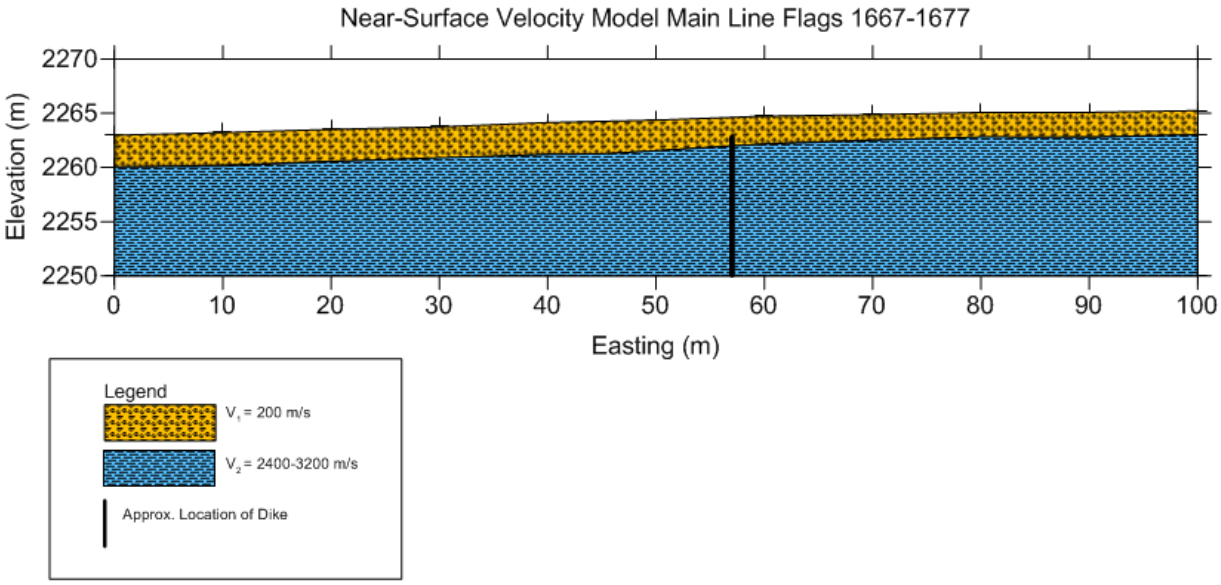

Figure 6.18: *Near surface velocity model of the main line created using refraction analysis. Using this velocity model, the location of the dike can be approximated.*

Student Site

Based on reflection analysis done on the West side of the student line, a reflector dipping gently to the West is located about 100-150 meters deep in Figure 6.16. The reflection is notable from 190 meters to 260 meters from the start of the line on the West side. The reflector is interpreted as a fault surface because there are no West dipping layers with an interface at about 100 meters deep. Assuming a true dip of 60 degrees and knowing apparent dip, the strike of the fault surface is 45 degrees Northeast as shown on Figure 6.19. The fault could be following a similar path as fault splays from the Victoire fault farther South. The fault on the student line could be curving North, but without more data the fault can not be accurately extended.

Refraction analysis provides subsurface velocity information which is used to calculate the thickness of the uppermost layer. In all the refraction analyses, there is top layer with a velocity in the range of 200-360m/s, considered to be V_1 in the models. The lower velocity represents dry, unconsolidated material. If this loose material were saturated with water, a higher velocity is expected. At both the West and East ends of the student site the slow layer is on top of material with much higher seismic velocity, considered to be V_2 in the two layer model. These high velocities found on the East end range from 2500-4500m/s and on the West end the high velocities range from 1500-3500 m/s, indicating bedrock instead of loose dirt. The values of 1500 and 1800m/s are centered over the portion where bedrock comes up to the surface, see Table 6.2, and these velocities slower because the bedrock is weathered in the first couple meters. For the West end of the student site the fast material

is likely Mancos Shale, based on area reconnaissance and cross sections. For the East end of the student site, the lithology beneath the loose material is harder to pin down. It is possible that the Mesa Verde formation underlies this area based on current geologic knowledge, but the Mesa Verde and Mancos do not have enough of a velocity contrast to be differentiated with refraction analysis due to the high margin of error.

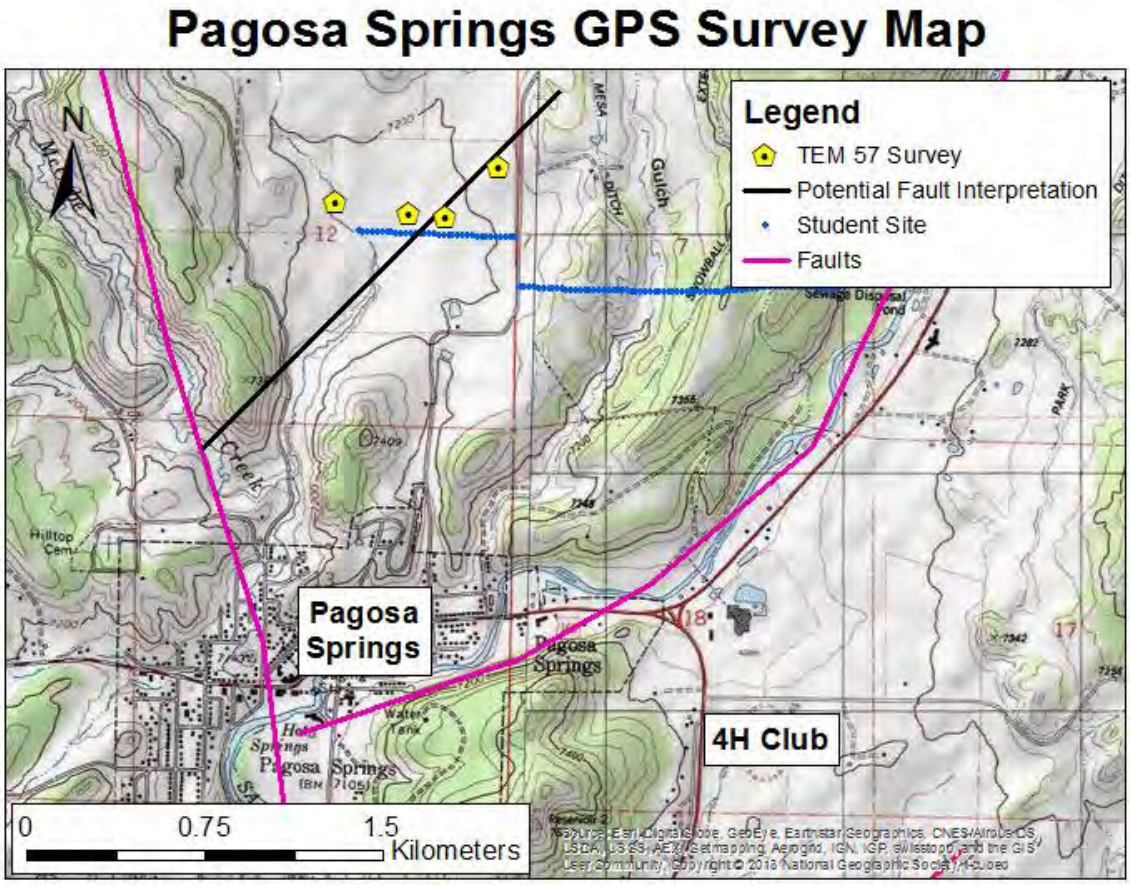

Figure 6.19: *Fault interpretation. The strike of the fault is found using the apparent and true dip. The fault was extended in a straight line but could be curved similar to the fault located just south of Pagosa Springs and moving North East.*

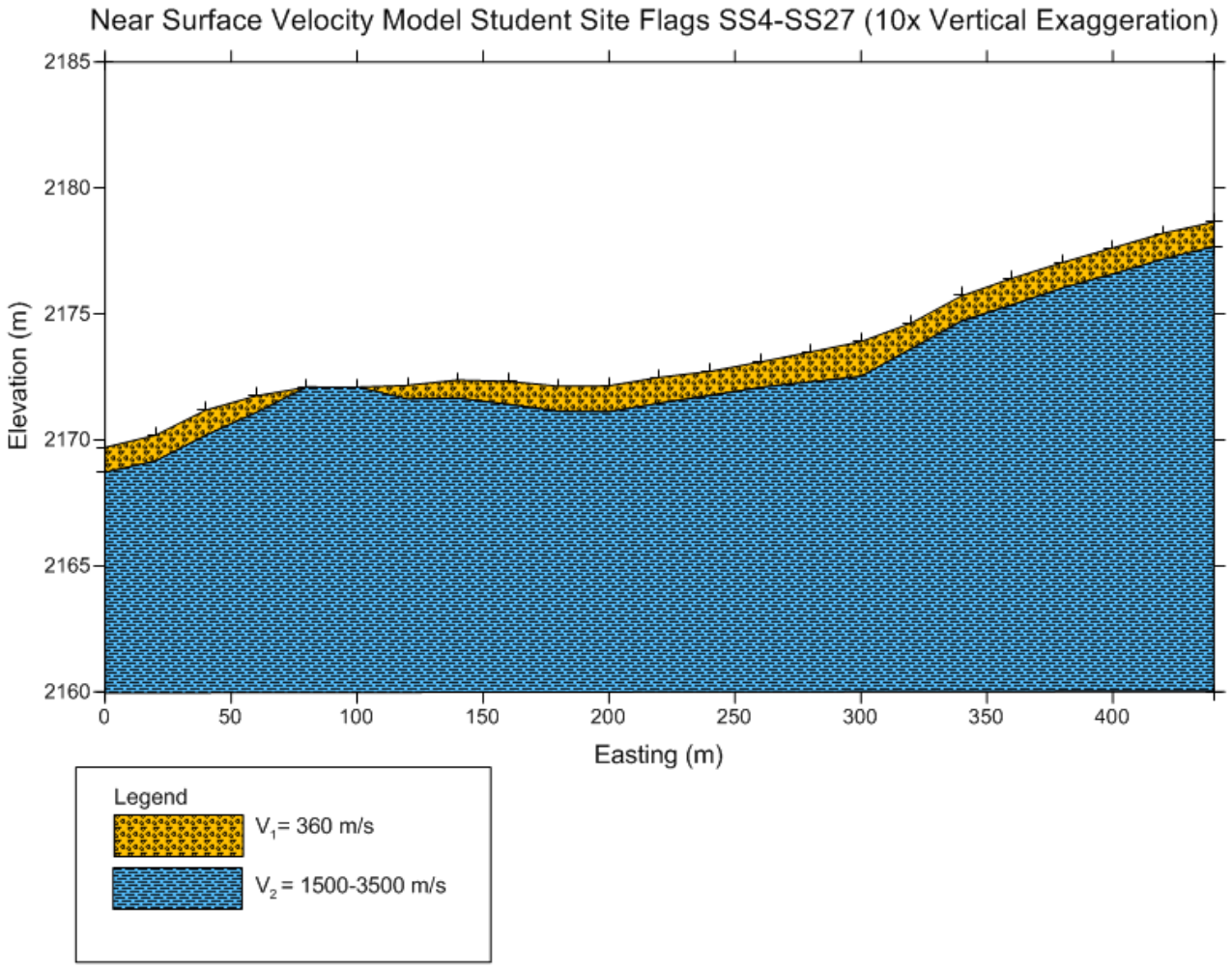

Figure 6.20: *Near surface velocity model of the West end of the student line created using refraction analysis.*

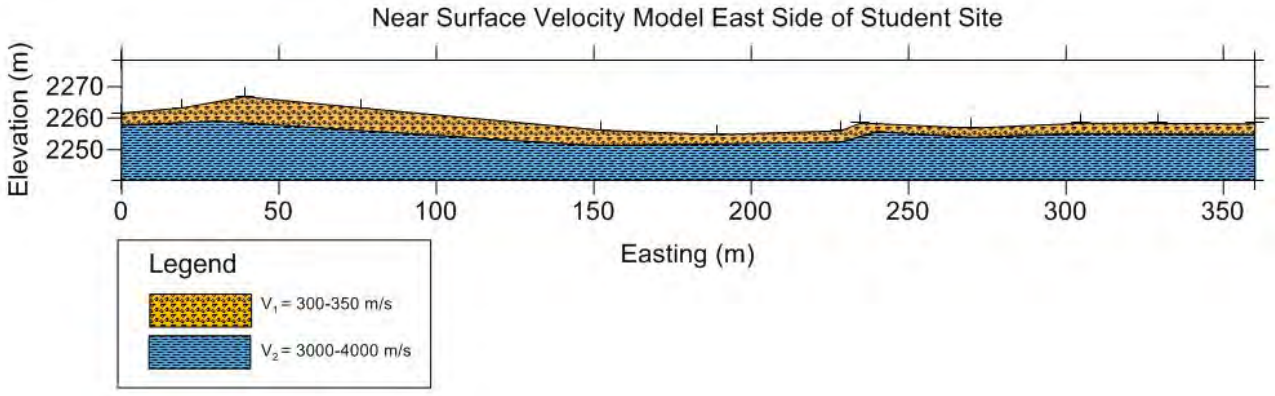

Figure 6.21: *Near surface velocity model of the east end of the student line created using refraction analysis. By taking into account velocities and topography, it appears that the top layer, V_1 is approximately flat.*

6.4.4 Errors and Uncertainty

Errors and Uncertainty in the Field

Hammer seismic contains lots of uncertainty in comparison to deep seismic. First, the source is not consistent because the person swinging the hammer can not apply the same force on every swing and different people are swinging the hammer between shots (See Figure 6.9). Furthermore, sledge hammers are a weak active seismic source the geophones are much more sensitive to small sources of noise, like footsteps and wind. Another contribution to the noise is the fact that the fold is not nearly as high as deep seismic. Before each shot, everyone in the area was asked to stay still, and the immediate surroundings were checked for cars. The geophones were extremely sensitive, enough to pick up a light foot tap 50m away. Wind and aircrafts also factored into the noise, especially on the West end of the student site where it can be seen in the data as an increase in white noise on some shots toward the end of the survey as the wind picked up in the afternoon. When the data was viewed, some shots were clearly errant, including some that looked like a double-strike resulting from a hammer or plate bounce, or appearing to have multiple sources, probably from an impulse like a footstep. These shots were removed, because these shots were re-taken.

The hammer seismic recorded on the east side of the student site line was offset to the north of the student line by about 100m to decrease noise from other groups working along the student site line. Unfortunately, neither DGPS nor handheld GPS points were fully taken along this line, leading to a lack of elevation information. Elevations cannot be approximated from the student site line because the survey was moved to a location with significantly different topography. Thus, Google Earth was used to approximate the elevations. If Google Earth is inaccurate, the velocity model will be inaccurate. On the three spots on the line where DGPS points were taken, the DPGS elevations varied from the Google Earth elevations by more than 20 meters, which suggests that the elevations from Google Earth are not accurate and therefore are a large source of error in the model.

Errors and Uncertainty from Processing

The sampling rate of the geophones in this survey is 2000Hz, or one sample every .5 ms. With a wave moving at 3500m/s, an arrival shifted by one time slice represents a shift in depth of almost two meters. Refraction analysis has an especially large degree of uncertainty, as it is largely qualitative. Based on the data it is reasonable to assume an accuracy of plus or minus 100m/s for determining velocity based on the slope of the head wave.

The data on the East side of the student line is particularly problematic. On the East side of the student side, V_2 was consistently higher to the West due to the increase in topography. Since the velocities are different looking East and West from a certain shot, it is difficult to determine the exact velocity. An attempt was made to correct the problem by averaging the velocities to the East and West. However, this leads to more uncertainty in the velocity models.

The reflection seen on the West end was identified 100-150 meters deep. This is a very deep reflection, especially for a shallow depth method such as hammer seismic. The reflector was riddled with noise and it is possible that this is a misinterpretation of noise and not a reflection.

6.5 Conclusion

Hammer seismic is a shallow geophysical method that is relatively simple and inexpensive to carry out in the field. Because this method requires minimal equipment, surveys can be conducted in remote locations where a deep seismic vibrator truck would have difficulty accessing. This year, the primary objectives were to image the dike located along the main line and to perform reconnaissance at the student site, a proposed location for the 2017 Geophysics Field Camp.

Hammer seismic is a near surface method with the resolution necessary to image a small subsurface structure such as a dike. The diffraction that the dike produces appears to be centered about 3 meters West of station 1673 along the main line seen on trace 28 (See Figure 6.14). The data from the dike survey matches a forward model

performed by the 2015 Field Camp (see Figure 6.1), implying that the perturbation seen in the seismic traces is a dike.

At the student site, both the West and East hammer seismic lines successfully imaged two layers in the subsurface. The uppermost layer is interpreted as a unconsolidated material based on the velocity found from refraction analysis. The second layer is higher velocity material and is interpreted as Mancos Shale. At the West end of the student line, the top layer is dipping gently to the West and at the East end, this top layer is relatively flat. However, more surveys need to be conducted in order to verify the orientation of these beds since the qualitative analysis of hammer seismic data contains some uncertainty. At the West end of the student line, a strong reflector was found approximately 100m below the surface. It is difficult to determine what the reflector represents without data from other methods, but based on geologic projections the Dakota Sandstone is a likely candidate.

6.5.1 Recommendations

The survey on the East side of the student line needed better GPS data for the elevation statics corrections. Having a specific near surface target is recommended as it allows for more processing than just the refraction analysis on the near surface soil. Dikes and near surface contact zones are good sites for a hammer seismic survey. The signal from hammer seismic has a shallow depth of penetration, so targets should be shallow, particularly in high velocity media like the Mancos Shale. In most of the survey areas, only the contact between loose alluvium and the underlying Mancos/Mesa Verde was visible and not the Dakota Sandstone underneath the Mancos, so hammer seismic should not be used to try to image thick, homogeneous layers.

The reflection seen on the West side of the student site was highly unusual and merits further investigation. The dip direction was opposite the expected dip of the geologic units in the area and the dip angle was shallow for a fault. Many different processing techniques were used to try to explain the reflector, and the results confirmed that the reflector is real and shallowly dipping to the West. There is not an accurate geologic interpretation for what the reflector could be, so the area on the East side of the student line warrants further investigation with another geophysical method, such as deep seismic, or another hammer seismic survey over the same region with a smaller station spacing.

References

[37] H. R. Burger, *Introduction to Applied Geophysics*. W.W. Norton and Company, 1992, pages 65–129 (cited on pages 67, 71, 74, 77).

[38] 2. C. G. F. Camp, “Geophysical investigation of geothermal systems in chromo, co”, 2015 (cited on pages 67, 68).

[39] Z. W. Edward Wooley Ting-Li Lin and B. Shi, “The role of local soil-induced amplification in the 27 july 1980 northeastern kentucky earthquake”, *Environmental and Engineering Geoscience*, volume 14, number 4, pages 267–280, 2008 (cited on page 69).

[40] F. Jones, “Ray paths in layered media”, 2007 (cited on page 68).

[41] M. Keynes, “Geode seismograph”, 2016 (cited on page 75).

[42] C. B. Park, “What is seismic survey”, 2015 (cited on page 74).

[43] P. Sava, “Gpgn305 lab 8 instructions”, 2015 (cited on page 69).

7. Gravity

Contents

7.1 Introduction

A relative gravity survey is a passive survey method that is sensitive to density contrasts in the subsurface. Differences in material density below and around a survey will produce a change in gravitational acceleration, of which the vertical component is measured by a sensitive instrument called a gravimeter, or gravity meter. A relative gravity survey can be conducted in nearly any terrestrial location, as this instrument is compact enough to

be carried by a single person. A standard relative gravity survey includes referencing a base station of known gravity (usually around 9.81 m/s^2) and determining the difference between this value and the value measured at any point along the survey line. Such a survey might prove valuable in mineral exploration, reservoir monitoring, and geologic mapping, which is the aim of this project.

The subsurface property exploited in a gravity survey is density, or more specifically, a density contrast. As a lithologic unit's local density changes due to mineralization, fluid presence, or a change in geology, the variation in density is measured at the surface by a gravimeter. Since the gravitational force due to any object decreases with distance but never truly reaches zero, a gravity survey has no definite depth of interpretation. Such a sensitive instrument as a gravimeter will incorporate the force due to far off mountains just as it will to a small object directly below the instrument.

7.1.1 Background

The regions specific to the main line and chosen student site in Pagosa Springs have not previously been the subject of a relative gravity survey. As a result, there is no supplemental material which can be directly referenced in this region, for this method. Previous field camps have found success using gravity surveys. In 2015, the geophysics field camp surveyed the Chromo area south of Pagosa Springs, and with the use of a gravity survey, successfully identified a previously unknown low density zone. This lithologic unit was not clearly established in the seismic data, and its depth prohibited smaller scale surveys from identifying it [31].

In the 2016 field camp survey, as aforementioned, the primary objective was to characterize local geology. In such a pursuit, the gravity survey might prove valuable in identifying any faults, as they can produce a significant density contrast.

7.1.2 Theory

Newton's Law of Universal Gravitation states that the force felt by one mass on another due to gravity is given by:

$$F = G\frac{m_1 m_2}{r^2} \tag{7.1}$$

where m_1 and m_2 represent the two masses in question, r represents the distance between the two masses, and G is the gravitational constant, $6.67X10^{-11}Nm^2/kg^2$. The force felt by the gravimeter is therefore proportional to the product of the two masses, which change according to their density, via the following relationship:

$$m = \rho V. \tag{7.2}$$

In Equation 7.2, V represents volume and ρ is density, which is inherent to the material. As a result, larger density values near or below the survey will yield a larger force acting on the gravimeter and smaller density values will do the opposite. This is the basic idea behind a geophysical gravity survey [47].

7.2 Objectives

1. Be able to collect data accurately and sufficiently with the Lacoste & Romberg gravity meter and the Scintrex CG-5 gravity meter.
2. Correct data for instrumental drift, elevation, isostatic compensation, free air gradient, and latitude.
3. Utilize data to create a model of the subsurface in conjunction with other methods, specifically processed seismic and borehole data.

7.3 Methods

7.3.1 Survey Location

Two relative gravity surveys were conducted in Pagosa Springs during the 2016 Field Camp session. The first survey was done along the main line, County Road 302, illustrated in Figure 7.1 by a red line, and a second

survey was done at the Student Site north of Pagosa Springs, illustrated in Figure 7.1 as a blue line.

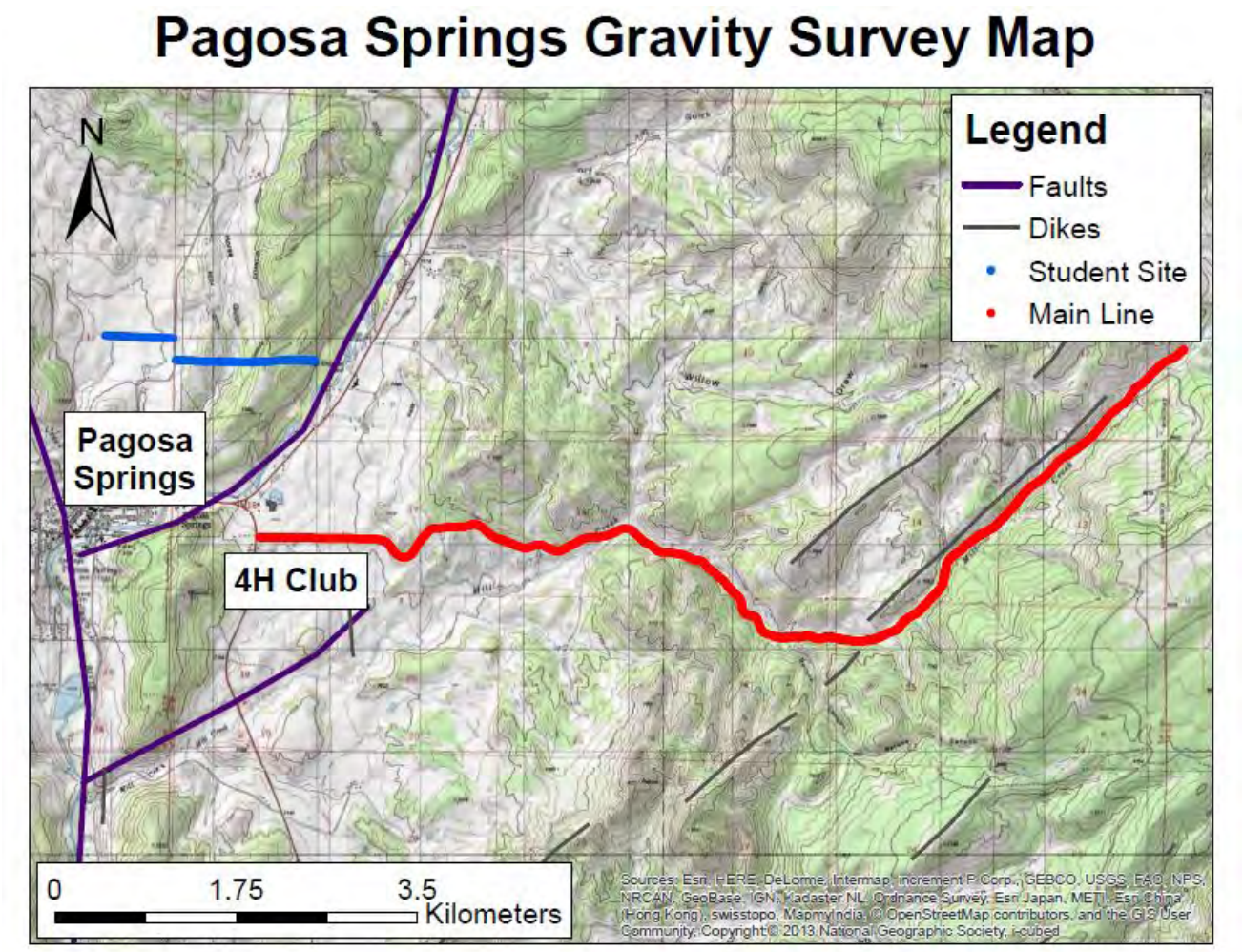

Figure 7.1: *Gravity surveys conducted along the main line (or CR302) in Pagosa Springs, Colorado (red) and at a student site line in northern Pagosa Springs (blue).*

7.3.2 Data Acquisition

We used relative gravimeters to acquire gravitational acceleration data along the main line and at the student site. Relative gravimeters, unlike absolute gravimeters, provide relative gravity measurements, meaning that the variations in acceleration due to gravity are measured between two or more points. Absolute gravimeters, in contrast, provide an absolute gravity value at the location of measurement.

Along the main line, we used two Scintrex CG-5 gravimeters. Base station gravity measurements were made at the beginning and end of each survey. Additional base station measurements were made every two-three hours. The base station was located near the southwest corner of the 4H center. Along the main line, gravity readings were taken every 40 m (four flags) for the majority of the survey. This was done in a leap frog fashion such that each individual gravimeter took a gravity reading every 80 m (eight flags). Three 20 second readings were taken at each flag. Some flags required more than three measurements due to standard deviations greater than 0.20 mGal, vehicles in close proximity, and/or high winds. Near the dike feature (approximately flag 1670), measurement spacing was decreased to 10 or 20 m in order to sample more finely over an area of interest. Additionally, gravity measurements were taken at a spacing of 80m in the interest of time. At the student site, one Lacoste & Romberg

(L&R) gravimeter was used to collect gravity data. Measurements were taken every 20 m (one flag) or 40 m (two flags). We recorded at least two measurements at each location with the L&R gravimeter.

The gravimeter field procedure consisted of carrying the gravimeter to the measurement site, placing the gravimeter on the leveling plate, and leveling the gravimeter. Once the instrument was leveled, the gravity readings were recorded. The CG-5 gravity values were displayed digitally after the sampling time, whereas the L&R values were read directly off the gravimeter [46].

7.3.3 Equipment List

- Scintrex CG-5 Autograv gravimeter (Figure 7.2a)
- CG-5 leveling plate (Figure 7.2b)
- Soft shell carrying case for CG-5
- Umbrella
- Lacoste and Romberg (L&R) gravimeter (Figure 7.3a)
- L&R leveling plates of two sizes (Figure 7.3b)
- L&R hard shell carrying case

(a) *(b)*

Figure 7.2: *Scintrex CG-5 Autograv gravimeter, (a) top view and (b) side view with leveling plate. We used the CG-5 gravimeter to collect data along the main line (CR302).[45]*

(a) *(b)*

Figure 7.3: *Lacoste and Romberg L&R gravimeter, (a) top view and (b) side view with leveling plate. We used the L&R gravimeter to collect gravity data at the student site north of Pagosa Springs.[45]*

7.3.4 Processing

The raw gravity data sets for the main line and student site were initially viewed in Microsoft Office *Excel*. The CG-5 gravimeter provided data files containing the station number, gravity value, standard deviation, measurement time, and date. The L&R gravimeter values were manually recorded and input into a spreadsheet. These data files contained the flag number, gravity reading, and time. Prior to any corrections, both data sets were condensed to only include the median gravity measurement for each station. The L&R gravity values required a unit conversion as the values were counter readings. We used the calibration table for CSM's Gravimeter G491 to complete this process (See Figure 7.4). The following equation was used:

$$G_R = (C_R - T_V) * I_F + V_M \tag{7.3}$$

where G_R is the gravity reading in mGal, C_R is the counter reading, T_V is the table value in mGal, I_F tabled interval factor, and V_M is the tabled mGal value.

MILLIGAL VALUES FOR LACOSTE & ROMBERG, INC. MODEL G GRAVITY METER #G- 491

COUNTER READING*	VALUE IN MILLIGALS	FACTOR FOR INTERVAL	COUNTER READING*	VALUE IN MILLIGALS	FACTOR FOR INTERVAL
000	000.00	1.02136			
100	102.14	1.02121	3600	3682.28	1.02563
200	204.26	1.02111	3700	3784.84	1.02579
300	306.37	1.02111	3800	3887.42	1.02593
400	408.48	1.02113	3900	3990.01	1.02607
500	510.59	1.02118	4000	4092.62	1.02620
600	612.71	1.02124	4100	4195.24	1.02631
700	714.83	1.02133	4200	4297.87	1.02640
800	816.97	1.02142	4300	4400.51	1.02648
900	919.11	1.02152	4400	4503.16	1.02657
1000	1021.26	1.02165	4500	4605.82	1.02665
1100	1123.43	1.02177	4600	4708.48	1.02673
1200	1225.60	1.02192	4700	4811.16	1.02680
1300	1327.80	1.02205	4800	4913.84	1.02688
1400	1430.00	1.02218	4900	5016.52	1.02696
1500	1532.22	1.02232	5000	5119.22	1.02701
1600	1634.45	1.02245	5100	5221.92	1.02706
1700	1736.70	1.02260	5200	5324.63	1.02709
1800	1838.96	1.02275	5300	5427.34	1.02712
1900	1941.23	1.02290	5400	5530.05	1.02712
2000	2043.52	1.02305	5500	5632.76	1.02712
2100	2145.83	1.02318	5600	5735.47	1.02706
2200	2248.14	1.02333	5700	5838.18	1.02698
2300	2350.48	1.02348	5800	5940.88	1.02688
2400	2452.82	1.02363	5900	6043.56	1.02676
2500	2555.19	1.02379	6000	6146.24	1.02663
2600	2657.57	1.02394	6100	6248.90	1.02649
2700	2759.96	1.02409	6200	6351.55	1.02633
2800	2862.37	1.02426	6300	6454.18	1.02616
2900	2964.80	1.02444	6400	6556.80	1.02597
3000	3067.24	1.02463	6500	6659.40	1.02576
3100	3169.70	1.02481	6600	6761.97	1.02557
3200	3272.18	1.02499	6700	6864.53	1.02537
3300	3374.68	1.02516	6800	6967.07	1.02515
3400	3477.20	1.02534	6900	7069.58	1.02495
3500	3579.73	1.02547	7000	7172.08	

* Note: Right-hand wheel on counter indicates approximately 0.1 milligal.

Figure 7.4: *Conversion Table of L&R gravimeter G491. We used this table to convert counter readings to mGal.*

Next, we used *Excel* and *MatLab* to perform instrument and tidal drift corrections. The instrument drift correction accounts for slow changes, or drift, in the gravimeter caused by temperature fluctuations, internal spring fatigue, and minor internal readjustments [49]. The tidal drift correction accounts for background variations due to changes in the relative positions of the Earth, Moon, and Sun [47]. Both the instrument and tidal drift are corrected for when the drift correction equation is applied. The drift correction equation varied depending on the loop setup, but the basic drift equation used was:

$$G_{DC} = G_n - \frac{g_2 - g_1}{t_2 - t_1} t_n + g_1 - \frac{g_2 - g_1}{t_2 - t_1} t_1 \tag{7.4}$$

where G_{DC} is the drift corrected gravity, G_n is the raw gravity value, g_2 and g_1 are the base station observations, t_2 and t_1 are the times of base station observations, and t_n is the time of the raw gravity measurement. The L&R gravimeter data required additional processing to remove a tear in the data. The data tear was likely caused by improper gravimeter handling. We then used the *GEOSOFT* program to perform latitude, free-air gradient,

complete Bouguer, and terrain corrections. The latitude correction accounts for latitude dependent distance to the center of the Earth. The free-air correction removes the effect of topography on gravity values (acceleration due to gravity reduces as location above sea level increases) [46]. The Bouguer correction compensates for the effect of rock layer thickness related to elevation. The effect of topography near the station site is removed using the terrain correction [49]. The terrain correction within *GEOSOFT* required a local digital elevation model (DEM).

Later, we used the *GEOSOFT*'s GM-SYS package to create models of the subsurface. The GM-SYS software allowed us to integrate seismic depth migrated images, well logs, and magnetic data into our modeling procedure. The goal of this modeling was to produce a geological model with a theoretical gravity response matching the field data. During this procedure, we removed the Bouguer correction from the gravity data. The Bouguer correction eliminates the rock thickness and composition information, which was the target of our gravity investigation. Thus, the Bouguer correction was not included during the modeling process.

We used a preliminary depth migrated seismic image, geologic cross sections, and borehole data to create our initial model. The reflections in the seismic images were used to determine approximate layer locations and geometries. The geologic cross sections and borehole data provided initial geologic geometry and density information, respectively. We improved our model with updated seismic images and data from other methods, specifically TDEM.

7.4 Discussion

7.4.1 Expectations

Along the main line we expected the gravity data to gently dip towards the east with a slope of approximately 5°. Near flag 1672 we hoped to see an increase in the gravity value indicating the presence of the dike, a higher density body. The dike may also redirect fluid flow, creating localized water storage. Varying gravity values might be present near these storage areas. Stark density contrasts in the data might also indicate faulting.

We expected the student site gravity data to gently slope to the east, similar to the main line. Additionally, we hoped to see an obvious density contrast indicating the location of the Victoire fault.

7.4.2 Results

The corrected gravity data along the main line shallowly dips towards the east (See Figure 7.5b). This correlates with the shallowly dipping beds suggested by the cross sections. We did not see a noticeable increase in the gravity values near the dike. The corrected gravity data at the student site is fairly noisy, but generally increases towards the east (Reference Figure 7.6b). The eastern portion of the line is especially noisy. No faults were indicated by the main line data, although the student site data set suggests the possibility of a fault.

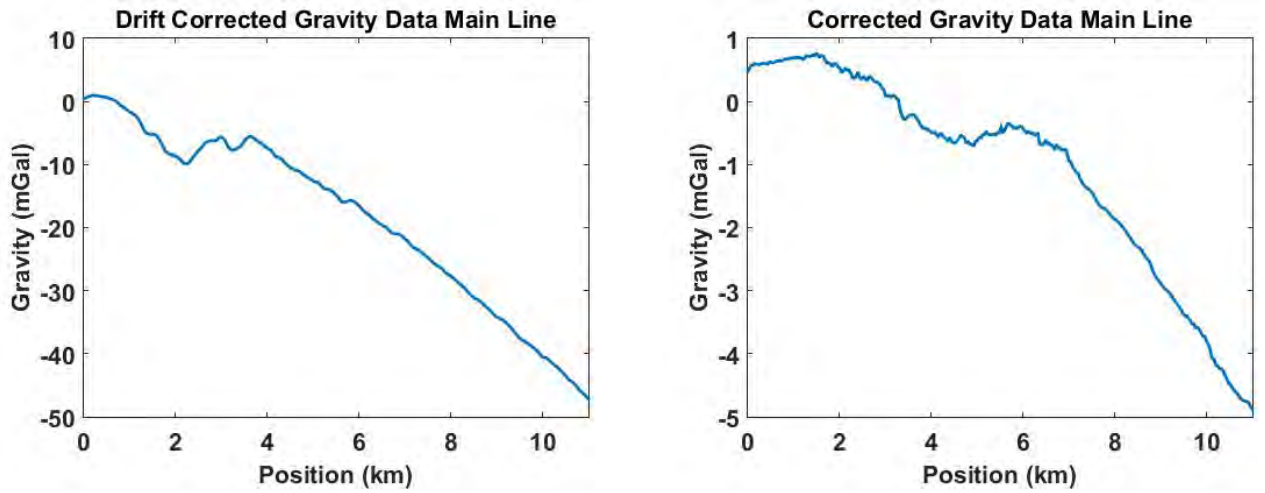

(a) *(b)*

Figure 7.5: *Raw gravity data along main line post drift correction (left) and final data along main line with Bouguer, free-air gradient, instrumental drift, latitude, terrain, and tidal corrections (right). The shallow dip towards the east in the final corrected gravity data is consistent with the geologic cross sections.*

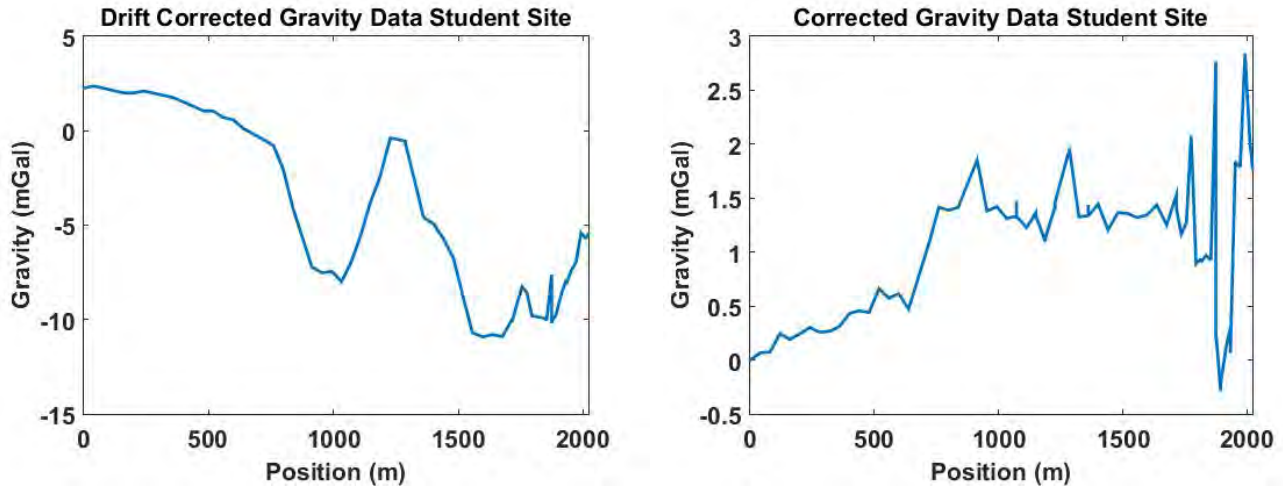

(a) *(b)*

Figure 7.6: *Raw gravity data along student line post drift correction (left) and final data along student line with Bouguer, free-air gradient, instrumental drift, latitude, terrain, and tidal corrections (right). Overall, the student site gravity data is quite noisy, especially near the east end of the survey line.*

Formation	Density (g/cm^3)	Thickness (m)
Lewis Shale	2.43	-
Mesa Verde	2.53	110
Mancos Shale	2.55	550
Dakota Sandstone	2.62	80
Morrison Formation	2.63	210
Wanakah Formation	2.68	30
Entrada Sandstone	2.50	48
Basement	2.80	-

Table 7.1: *Formation density and thickness values from cross sections, local geology, and borehole data. These values were used to create the forward models with GEOSOFT software.*

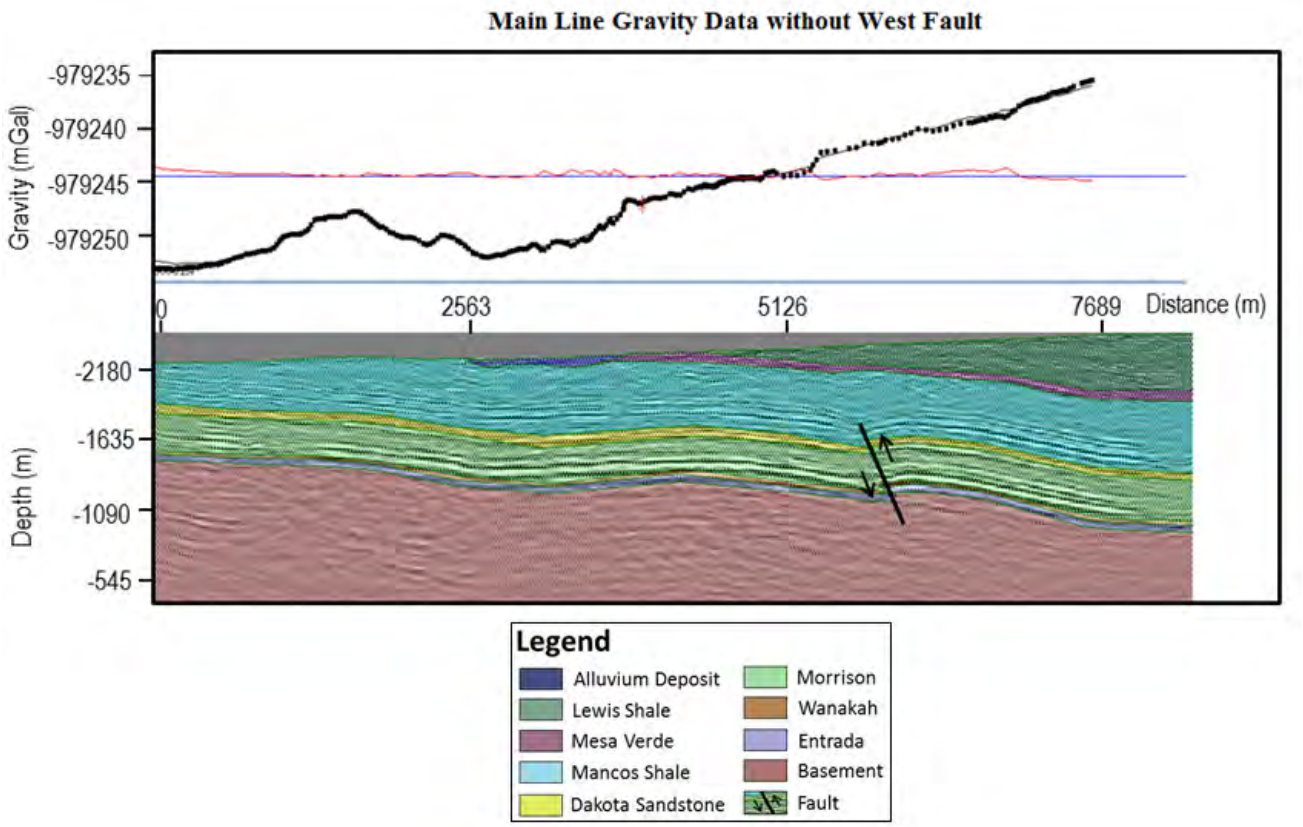

Figure 7.7: *Model of subsurface along main survey line created using GEOSOFT. Each color represents a different layer with specific density and thickness values taken from Table 7.1. Notice the correlation between this model and the depth migrated seismic image in the background. This model closely resembles the geologic cross sections.*

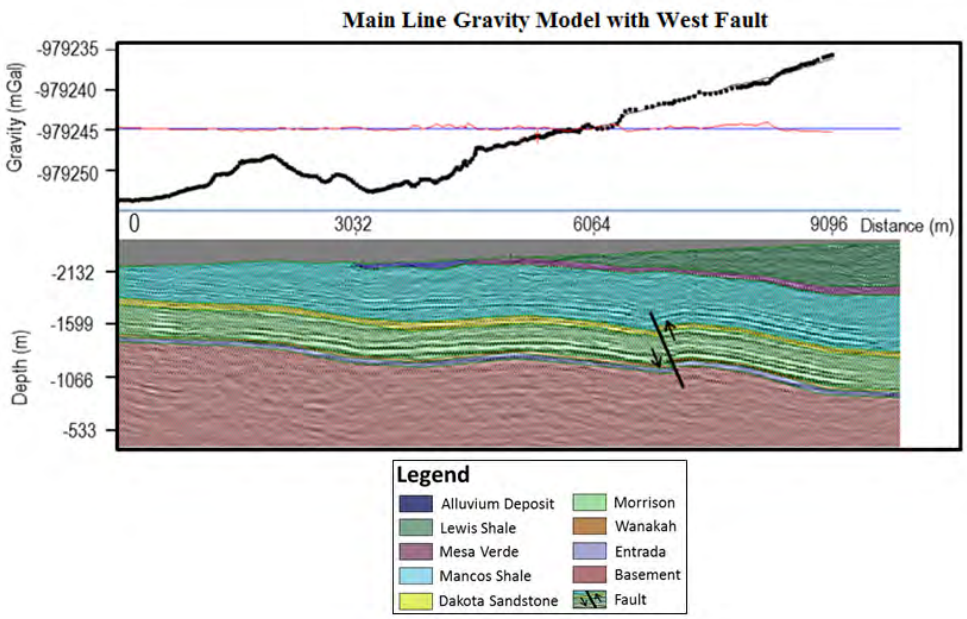

Figure 7.8: *Model of subsurface along main survey line created using GEOSOFT. A fault-like feature was placed West of the start of the survey line. Each color represents a different layer with specific density and thickness values taken from Table 7.1. Notice the correlation between this model and the depth migrated seismic image in the background. This model closely resembles the geologic cross sections and accounts for the decrease in gravity at the West end of the line.*

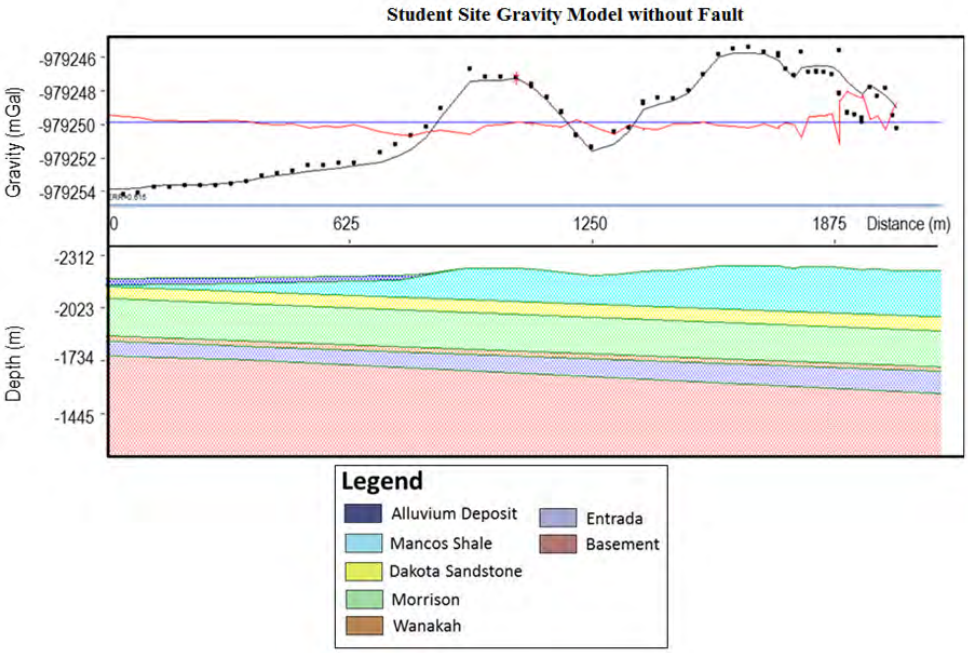

Figure 7.9: *Model of subsurface at student site created using GEOSOFT. Each color represents a different layer with specific density and thickness values taken from Table 7.1. This model closely resembles the geologic cross sections.*

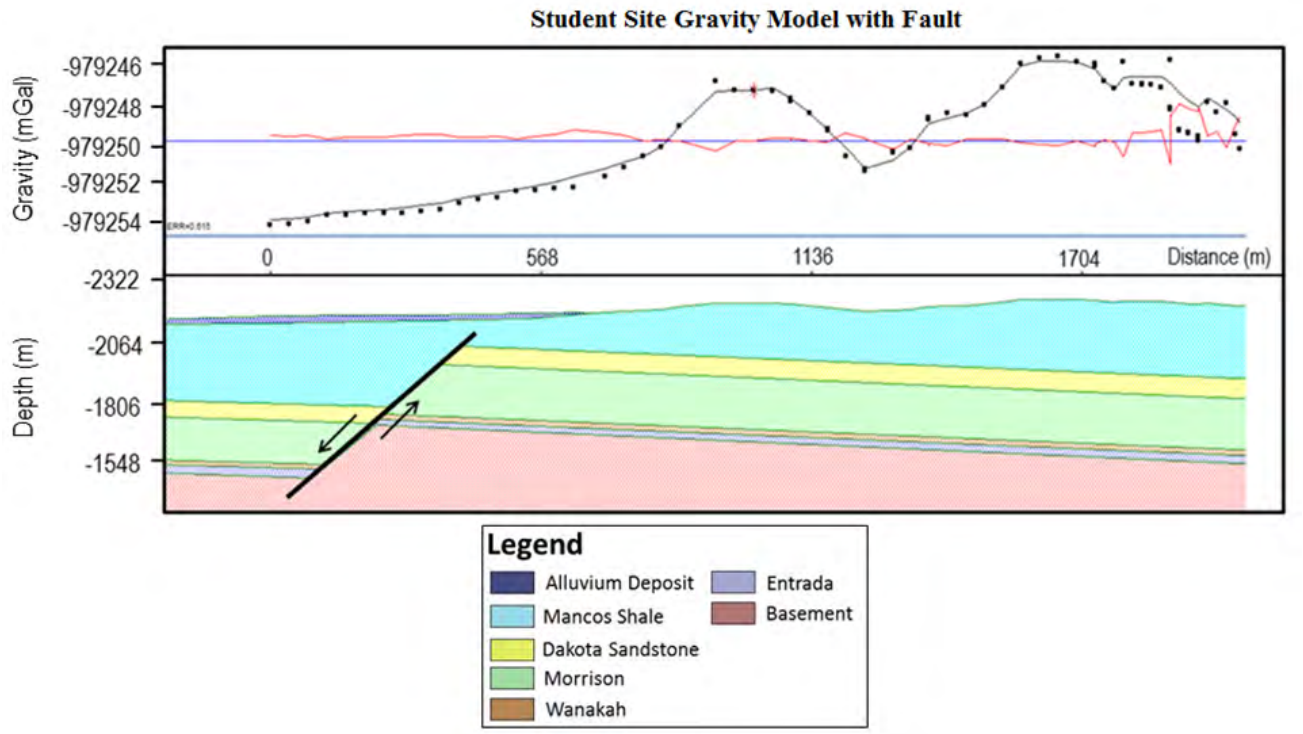

Figure 7.10: *Model of subsurface at student site created using GEOSOFT. Each color represents a different layer with specific density and thickness values taken from Table 7.1. This model closely resembles the geologic cross sections. The west dipping fault may represent Victoire splay fault.*

7.4.3 Interpretation

After applying the appropriate corrections via *GEOSOFT*, a model was created using a provided seismic profile and the density values given in Table 7.1. The gravity data reflects an early iteration of a subsurface model for the main line very closely, with only small variations. Based on the data collected, there is a high probability that the basement drops directly West of the mainline. This could be caused by a fault and is close to the predicted location of the Victoire Fault. As seen in Figure **??**, the theoretical gravity response fits more closely with the actual gravity response. In contrast, the absence of a fault-like feature, as seen in Figure **??**, causes a slight misfit between the theoretical and actual gravity response. Furthermore, a region of low density to the west of the dike is apparent, at between 4 and 5 km. This might be explained by a buildup of fluid to the west of the dike, or possibly an alluvial deposit. A reverse fault was proposed approximately 7 km from the start of the line. The fault has a fairly steep eastward dip and offset of about 50 m.

Alternatively, the data collected for the student site suggests that there may be a normal fault running beneath the west end of the student site at the 260 *m* mark, as measured from the far west end of the line. This fault is inconsistent with the previously discovered Victoire Fault as it dips in the opposite direction. This new fault could be a splay off of the Victoire Fault. The presence of this fault is not certain (See Figure 7.10). We were able to also build a similar model without the fault that provided a similar fit (See Figure 7.9). The large offset seen in the model with the fault seems unrealistic, but both models fit within 2 *mGal* of the actual data. Our interpretation of the gravity data from the student site follows the suggested geologic profiles with the exception of the fault.

7.4.4 Errors and Uncertainty

As the CG-5 is extremely sensitive to changes in vertical acceleration, it is very prone to errors due to personal, cultural, and meteorological sources which might move the instrument after it has been successfully leveled. Additionally, a large possible error caused by the operator in a gravity survey includes the improper leveling of the gravimeter. The CG-5 instrument allowed the user to level the unit with the help of an digital interface, and at each location a final tilt of less than $\pm 2 arcsec$ was attempted. The L&R allows for the user to level it using a set of bubble levels, and is therefore not as precise. As trigonometry dictates, any tilt in either instrument results in both a vertical and horizontal component, and since this method is specific to the vertical component, it is very important to minimize the possibility of any tilt.

In the case of the main line survey, passing vehicles posed a very large source of error as the moving mass near the unit causes both a change in measured gravitational acceleration, as well as a slight ground movement. In the case of a passing vehicle, the gravity survey was temporarily stopped until the user felt that the vehicle was far enough to be negligible. Furthermore, the Vibroseis truck was also problematic when in the vicinity of the gravimeter for the same reason. To mitigate these erroneous measurements the gravity team avoided the seismic crew whenever possible, and the CG-5's seismic filter was applied throughout the survey.

An additional cultural source of error apparent in both the main line and student site gravity surveys were nearby students and faculty. Similar to a moving vehicle, nearby people will produce variations in gravitational acceleration and might also move the instrument by walking near it. As aforementioned, since gravimeters are extremely sensitive and must remain perfectly vertical, it is extremely important for the operator to remain as still as possible while measuring. Great effort was taken by the operator in the attempt to remain still and to not shift weight while doing so. Other meteorological effects such as wind and heavy rain can also move the instrument slightly, so an umbrella was carried at all times.

Lastly, on the student site east survey line some gravity measurements may be subject to a vertical gradient error, and measurements along the main line are subject to 3D effects. Since the topography changes quickly with respect to the student survey line, some flagged locations required the operator to level the instrument on a hillside. The resulting gravitational acceleration vector may not be directly downward, as more mass (hillside) lies to one side of the measurement location. In the case of the main line, especially the second half, the gravity measurements incorporate the mass of the mountainous terrain surrounding the survey. This source of error was accounted for in the terrain correction applied within *Oasis-Montaj*.

Errors in processing are mainly a result of human error and include improper correction of raw data. Such an error may occur in drift or Bouguer corrections if the user defines an incorrect constant or references the wrong values when performing these corrections. In practice, tidal variations and spring sag results in a drift over time, and base station readings should be taken every two to three hours in order to account for a linear drift. To account for this, a base station reading was taken at least every two hours in the field.

Larger scale uncertainties in both gravimeters can result in irregular drift, resulting from improper handling of the unit such as dropping, bumping, not locking the spring (on the L&R), and temperature extremes. Small scale uncertainties in relative gravity readings are inherent to the respective instrument. The Standard Field Repeatability of the Scintrex CG-5 is given as $< 5 \mu Gal$ [44]. The main line survey may have encountered some degree of uncertainty, one of the CG-5 units proved to drift non-linearly; this drift was expected to be a result of a 'shock' or significant bump to the instrument. To mitigate this, the unit was left to settle for two days before using again. Alternatively, the L&R contains a larger magnitude of uncertainty. The bubble levels on the L&R are subject to thermal expansion, which can account for up to $40 \mu Gal$. Additionally, since the measurements are analog, the user may read a value which is very slightly incorrect. For the purpose of this field survey, mechanical and analog issues result in an uncertainty of approximately $20 \mu Gal$ [48].

7.5 Conclusion

Relative gravity surveys were completed over both the main and student site survey lines. Along the main line, County Road 302, two CG-5 gravimeters were used with two teams leap-frogging to collect more information in the interest of time. For the majority of the main line, a station spacing of 40 meters was used, although near the dyke, an infill survey of 10 meter spacing was used. For the student site, an L&R Model G was to collect relative gravity measurements at 20 or 40 meter spacing. Great effort was taken to prevent any noise and/or error in the measurements by minimizing tilt and stopping a measurement if it was exposed to any vibration from foot or vehicle traffic. As a result, the main line gravity data was processed and modeled, and fit the seismic model appropriately. The gravity model resembled the local geologic cross sections. The main line gravity data was very useful in the overall interpretation, and aided several complementary surveys.

Similarly, the student site survey data followed local geologic cross sections. The models indicated that a west dipping fault may be present 280 *m* from the far west end of the survey line. The final result includes a higher element of uncertainty compared to the main line due to improper gravimeter use.

7.5.1 Recommendations

As the main line gravity profile agreed well with data from complementary methods, this survey was successful. However, in the interest of time, a large portion of this survey was sampled coarsely at 80 meters, whereas around the dike, sampling was more fine at 10 meters. In future surveys it would prove beneficial to sample as finely as possible in all areas. In the case of the student site, where the data was deemed to be unreliable, it is very important to practice good instrument protocol to prevent a loss of data. Additional data along the east side of the student site would have been extremely useful.

References

[44] *CG-5 Autograv Gravity Meter | Land Gravity | Scintrex*. [Online]. Available: http://www.scintrexltd.com/documents/CG-5BrochureRev1.pdf (visited on 06/03/2016) (cited on page 99).

[45] G. Crookston, *Magnetic and Electromagnetic Survey*, Nov. 2015. (visited on 06/09/2016) (cited on pages 91, 92).

[46] *Exploration Technique: Ground Gravity Survey | Geothermal Energy*. [Online]. Available: http://en.openei.org/wiki/Ground_Gravity_Survey (visited on 06/02/2016) (cited on pages 91, 94).

[31] "Geophysical Investigation of the Geothermal System within the Chromo Anticline", English, Colorado School of Mines, Upper San Juan Basin, Archuleta County, CO, Tech. Rep., Jun. 2015. [Online]. Available: http://inside.mines.edu/UserFiles/File/geophysics/fieldcamp/GPGN468_FinalReport.pdf (cited on pages 40, 89).

[47] J. Milsom and A. Eriksen, *Field geophysics*, 4th ed, series The geological field guide series. Hoboken, NJ: Wiley, 2011, OCLC: ocn657270827, ISBN: 978-0-470-74984-5 (cited on pages 89, 93, 102).

[48] *Model G & D Gravity Meters | Instruction Manual | LaCoste & Romberg*, 2004. [Online]. Available: https://www.ifg.tu-clausthal.de/fileadmin/grav/gdmanual.pdf (visited on 06/03/2016) (cited on page 99).

[49] *Using and Understanding Gravity Data | University of Texas at El Paso*. [Online]. Available: https://research.utep.edu/Default.aspx?PageContentID=3948&tabid=38186 (visited on 06/02/2016) (cited on pages 93, 94).

8. Magnetics

Contents

8.1 Introduction

Magnetics is a passive geophysical method used to measure magnetic variations caused by susceptibility differences in rocks and minerals as well as materials with remnant magnetization. Earth's primary magnetic field is created by circulating electric currents in Earth's liquid outer core. This magnetic field envelopes the globe, and can be simplified to a dipole, or a magnet. Near the equator, the magnetic field has no dip on the Earth's surface

while at the poles has approximately a 90 degree dip. For this reason, the measured magnetic field is stronger near the poles and weaker near the equator.

If the primary magnetic field B_p interacts with any susceptible bodies in the subsurface, a secondary magnetic field B_s is produced and can be measured by a magnetometer. These instruments are used to measure any small magnetic variations and can be set to either continuous or discrete modes. The continuous mode is most commonly used and requires the surveyor to move at a constant pace between marks while the instrument continuously measures. Discrete mode takes measurements at the user's discretion and is primarily used when the user cannot move at a generally constant pace. In addition to the mobile unit, a second magnetometer is normally used as a base station and helps correct for diurnal variation due to changes in the ionosphere from solar activity [47].

Due to the highly susceptible nature of metallic and mafic material, the magnetics method is commonly used in locating ore bodies, mapping igneous intrusions and faults, locating unexploded ordinances, and mapping archaeological features [54].

8.1.1 Background

Previous field camps did not complete magnetic surveys that can be referenced with respect to this year's mainline and student site. The 2015 field camp used magnetics to locate dikes on their reconnaissance site by conducting four survey lines in an orientation perpendicular to the expected dike direction.

For the 2016 field camp, the primary objective was to characterize faults and dikes in the local area. Along the main line, a dike protrusion is observed and magnetics could potentially help determine whether the dike continues underneath the road. For the student site, magnetics should help identify whether the Victoire fault extends further North and if any other faults are in the area. Dikes and faults can influence water flow and possibly give information on where the hot springs water originates.

8.1.2 Theory

A body placed in a magnetic field H acquires a magnetization M that is proportional to the field:

$$M = kH \tag{8.1}$$

In Equation 3, k represents the susceptibility, which is the degree of magnetization of a material in response to an applied magnetic field that can be either negative (diamagnetism) or positive (paramagnetism) [55]. The susceptibility depends on the amount of magnetic mineral content such as magnetite.

Ferro-magnetic and ferri-magnetic materials can contain remanent magnetization, both permanent and induced magnetic fields, meaning their magnetizations might not be the same direction as the Earth's magnetic field. Ferro-magnetic materials, such as iron, have small magnetic fields that align with each other while ferri-magnetic materials have small magnetic fields that oppose each other [47] [51].

8.2 Objectives

1. Collect data with the Geometrics G-858 MagMapper cesium magnetometer and G-856 proton magnetometer base station.
2. Apply diurnal variation correction.
3. Make interpretation of subsurface from processed magnetic data and incorporate results with other methods.

8.3 Methods

8.3.1 Survey Location

Two walking magnetic surveys were completed in the same locations as gravity: along County Road 302 and along the student site survey line. Reference Figure 8.1 for a map of the survey locations.

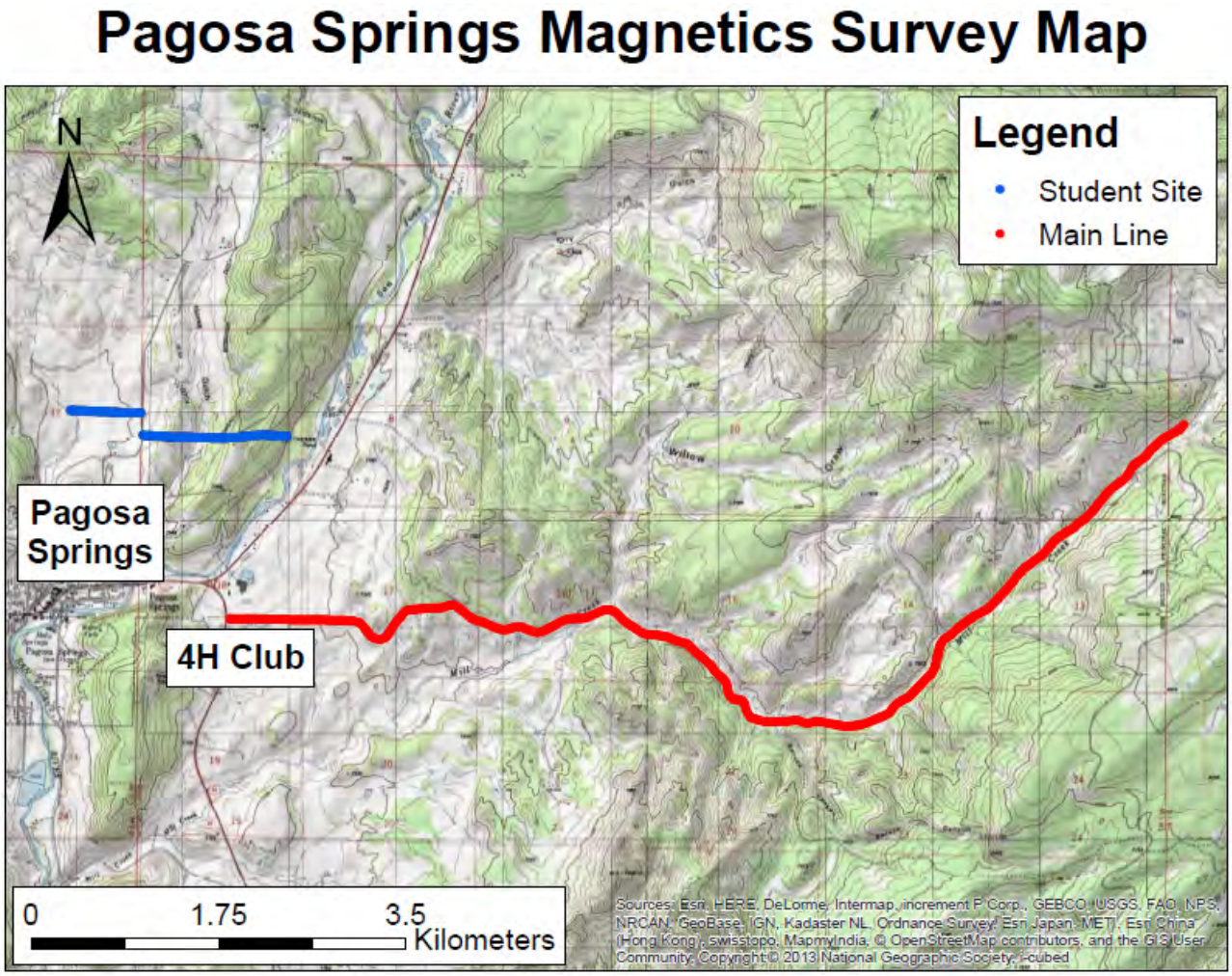

Figure 8.1: *The magnetics survey was conducted along the main line (CR302) (red) and at the student site in northern Pagosa Springs (blue).*

8.3.2 Data Acquisition

An important first step in executing a walking magnetometer survey is to ensure that the time stamps on both the mobile unit and base station are the same. This is crucial in correcting data for the diurnal variation.

To assemble the base proton procession magnetometer, the sensor needs to be connected to a metal rod, which should be vertically implanted into the ground. Next, the sensor cable and battery need to be attached to the data recording box. A base reading should be taken at this point and used to calibrate the magnetometer. To account for diurnal variations, the base unit should to be set to measure B_p every minute. For the Pagosa Springs region, reasonable total intensity values are around 50,000nT. [50].

To assemble the mobile cesium magnetometer, the counter weight must be attached to one end of the long metal rod, and the sensor rod needs to be attached to the opposite end in a perpendicular orientation. Next, attach the white sensors to each end of sensor rod, facing downwards towards the surface of the Earth. Connect the battery belt and data logger to the harness, and with the harness secured to the user, connect the battery and sensor cables to the data logger. To set up the data logger, create a new survey in continuous mode with a one-second measurement rate. To start the survey, begin a few meters before the first location to be measured, select the 'Mark' button on the data logger, and begin walking. Each time the sensors are aligned with a flagged location, hit

the 'Mark' button. Finally, when the end of the survey line is reached, continue walking a few meters past the last measured location before selecting the 'End Line' option.

In order to lower the amount of noise noise for the East end of the student site, the cesium magnetometer was attached to a backpack. The harness was still worn, but only one sensor was used and it attached to a metal rod that was firmly connected to the backpack. This allowed for measurements to be consistently taken at the same distance from the ground and at a constant pace in hilly terrain.

8.3.3 Equipment List

- Geometrics G-856 base proton procession magnetometer (Figure 8.2b)
- Metal rod
- Sensor cable
- Battery for base station magnetometer
- Data recording box for base station
- Geometrics G-858 MagMapper mobile cesium magnetometer, composed of 2 sensors (Figure 8.2a)
- Counterweight
- Metal rod to attach counterweight and cesium magnetometer
- Data logger for roving cesium magnetometer
- Battery for roving magnetometer
- Connection cables for the battery, data logger, and roving magnetometer
- Belt to carry battery and data logger for roving magnetometer

(a) *(b)*

Figure 8.2: *Mobile cesium magnetometer (left) and Base proton procession magnetometer (right).*

8.3.4 Processing

The raw magnetic data sets were viewed in MagMap 2000. This software was also used to perform the diurnal correction on the data. This was done by simply loading in the data from the G-858 MagMapper and the data collected by the base station. Then the data collected by the base station was subtracted from the data collected by

the MagMapper. This data was then exported as a `.dat` file and loaded into Matlab.

We used Matlab to "de-spike" the data. This involved first eliminating any major outlying data points that were several orders of magnitude above the rest of the data. Next, we applied a filter to the data that performed a moving average on the data using a rational transfer function. Applying this filter resulted in smoother data sets with the overall trends in the data left intact.

8.4 Discussion

8.4.1 Expectations

Along the main line, we expected to see an increased magnetic response near the dike located at Flag 1672. Dikes are made up of igneous rock and normally have a high magnetic susceptibility relative to the surrounding rock due to their high iron and magnesium content. Along the student line, we were hoping to better characterize the Victoire fault. Along with these focused expectations, we were hoping to pick up any other susceptibility anomalies in the subsurface of both sites.

8.4.2 Results

8.4.3 Interpretation

The results of the magnetic surveys tell little about the subsurface due to the low signal to noise ratio. As Figures 8.3, 8.4, 8.5 suggest, the data collected in each survey is too noisy for any specific features to be identified. Furthermore, the dike is not found on either of the mainline surveys. There is too much noise to determine if there are any peaks or troughs in the data, near where the dike was predicted to be, were actually indicative of a dike or just the result of processing noisy data.

8.4.4 Errors and Uncertainty

Prominent sources of error in a magnetics survey are largely due to cultural effects, such as power lines, metal fences, cattle grates, flags, electrodes, and vehicles. Each of these pose threats as they can be significantly conductive and therefore overwhelm true conductive and magnetic bodies in the subsurface. Examples of cultural effects can be seen at the west end of the student site as well as the first half of the main line. In both of these locations, metal fences run along the flags which results in noisy data that is difficult to interpret. Additionally, power lines run along these roads causing noisy data for a significant section of the survey. Furthermore, a cattle guard is located near where we expect the dike to intersect the road and might cause misinterpretations.

In addition to these cultural sources subject to the survey region, additional noise is expected from complementary survey methods. For example between Flags 1742-1868, the magnetic survey collided with the DC crew. In the same survey, the magnetics crew also surveyed near an EM47 survey around Flag 1788. In the process of pushing current through wires in these two methods, small magnetic fields are created and therefore directly affect magnetic measurements. Lastly, the presence of flags as well as seismic cables along the mainline stretch for a long distance which can cause a significant amount of error due to any small magnetic fields which they create.

Human errors inherent to a magnetics survey include taking measurements inconsistently on terrain, magnetically 'dirty' objects on the surveyor, and tuning the base magnetometer incorrectly. The east end of the student site is hilly and therefore it is essential to keep the magnetometer at a constant distance from ground surface and at a constant pace if in continuous mode. Additionally, since the magnetometer is sensitive to magnetic materials, the surveyor must not being carrying any metal objects such as radios or cell phones which might produce their own magnetic fields. Finally if the magnetometer base is incorrectly tuned, the mobile magnetometer data becomes useless as any diurnal variation cannot be accurately accounted for.

The cesium magnetometer has an innate uncertainty of approximately 1 nT, but is highly influenced by the errors previous mentioned [52][53].

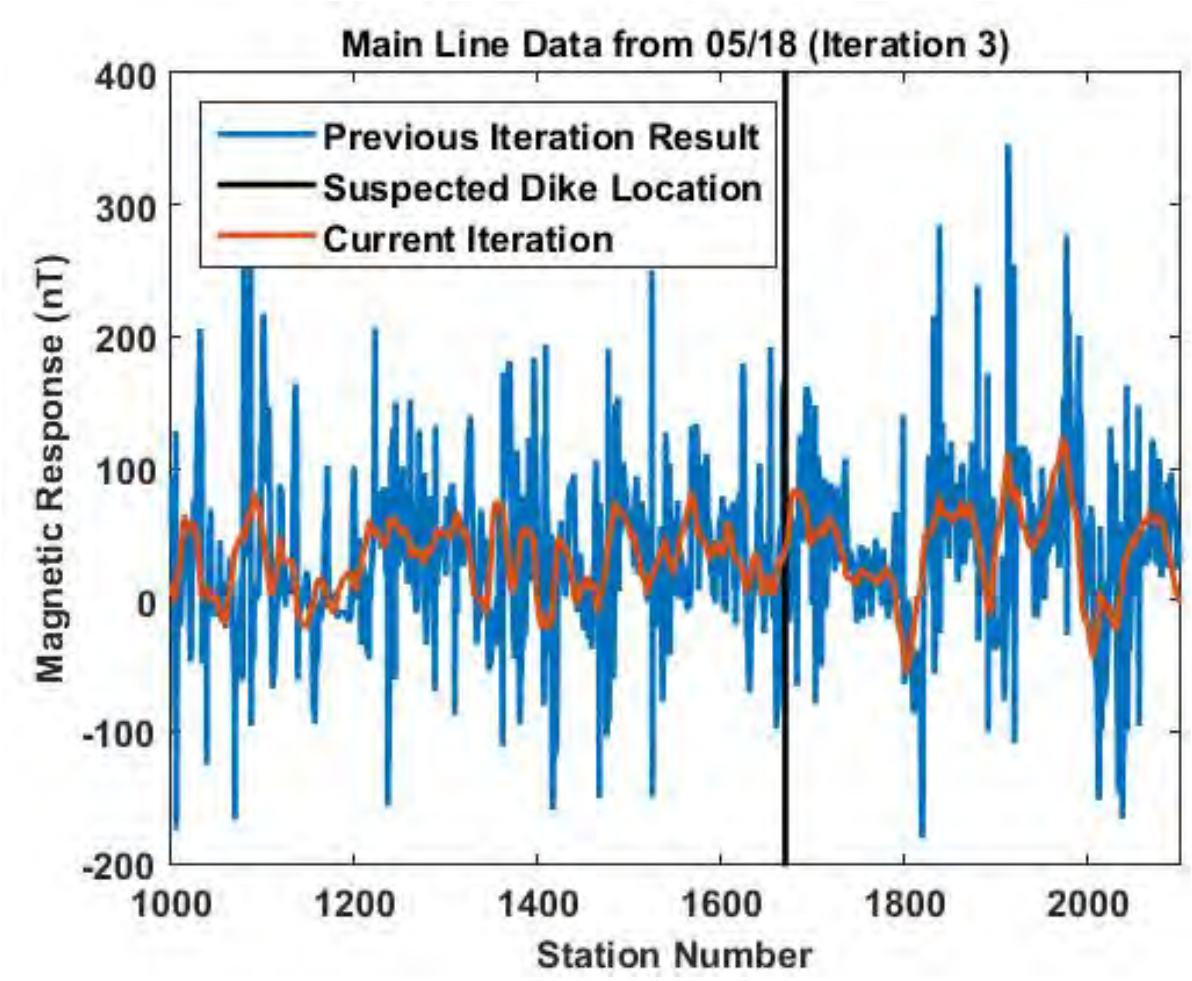

Figure 8.3: *The resulting smoothed magnetic response from the survey conducted walking east from the 4H club. The blue line represents the result of despiking the data. The orange line represents the result of applying a moving average to the despiked data. The red line is indicative of the suspected dike location.*

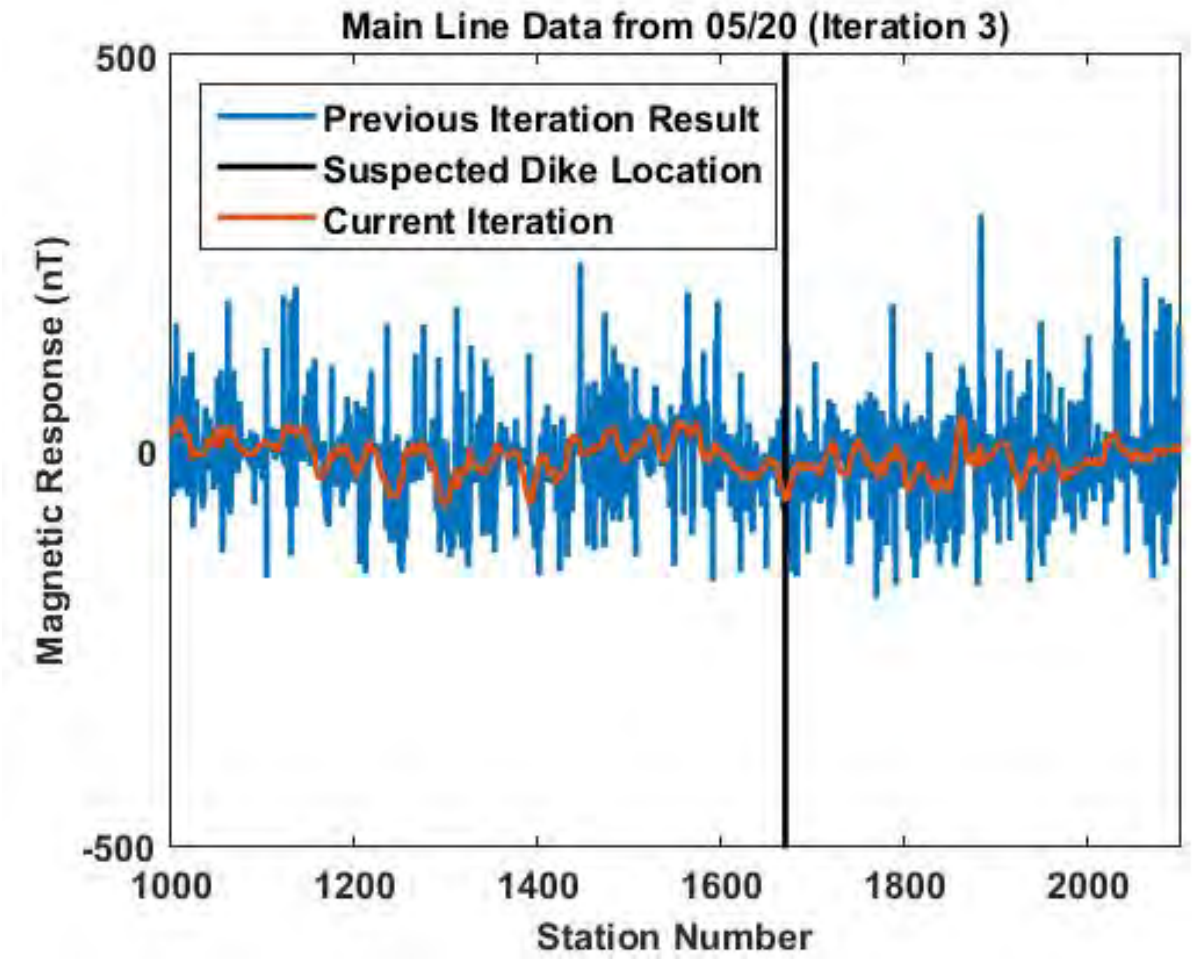

Figure 8.4: *The resulting smoothed magnetic response from the survey conducted walking from the east end of the main line back towards the 4H club. The blue line represents the result of despiking the data. The orange line represents the result of applying a moving average to the despiked data. The red line is indicative of the suspected dike location.*

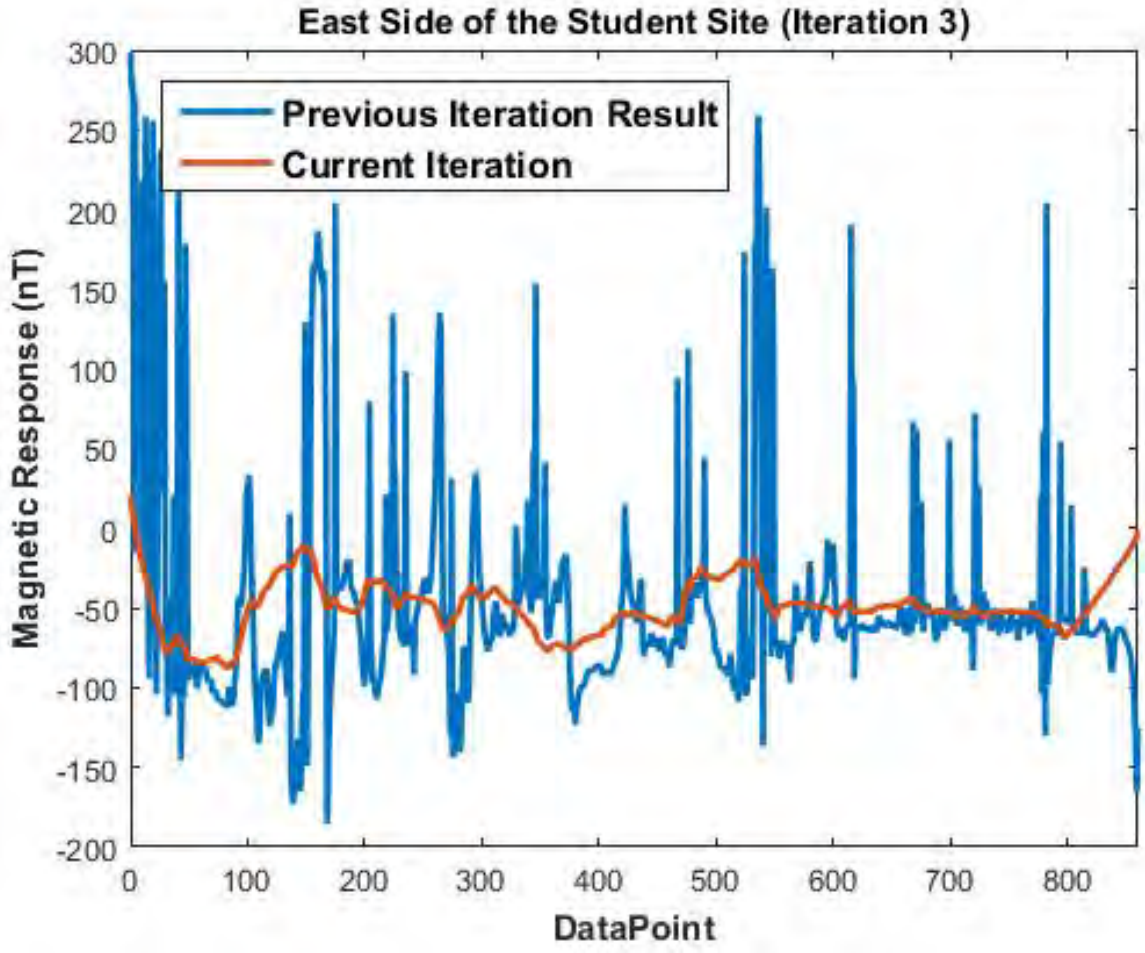

Figure 8.5: *The resulting smoothed magnetic response from the survey conducted at the east end of the student site. The survey was conducted walking west from the east end of the line towards CR200. The blue line represents the result of despiking the data. The orange line represents the result of applying a moving average to the despiked data.*

8.5 Conclusion

Magnetic surveys were completed for both the mainline (County Road 302) and the student site. A proton precession magnetometer was used as the base and a cesium mobile magnetometer was used to collect data along the survey line. Due to the conditions encountered along both survey lines, the resulting data for the mainline and student site are too noisy to interpret a trend that any anomalies might cause. As a result, the final magnetic models are inconclusive of any geologic features.

8.5.1 Recommendations

Due to the large amount of noise in and around Pagosa Springs, the magnetic surveys did not produce useful results. Taking this into account, we recommend that large scale magnetic surveys are not conducted in the future in Pagosa Springs. If, however, an opportunity arises in which the survey line is far from any cultural noise and complementary surveys, magnetics can be useful as demonstrated in previous field camp interpretations.

References

[50] N. G. D. Center, *NCEI Geomagnetic Calculators*, EN-US. [Online]. Available: `http://www.ngdc.noaa.gov/geomag-web/#igrfgrid` (visited on 06/02/2016) (cited on page 103).

[51] *Ferrimagnetism | physics | Britannica.com*. [Online]. Available: `http://www.britannica.com/science/ferrimagnetism` (visited on 06/02/2016) (cited on page 102).

[52] *G-856ax Memory-Mag Proton Precession Magnetometer | Operation Manual*, 2007. [Online]. Available: `ftp://geom.geometrics.com/pub/mag/Manuals/856Manual_E.pdf` (visited on 06/03/2016) (cited on page 105).

[53] *G-858 Magmapper | Operation Manual*, Jan. 2001. [Online]. Available: `ftp://geom.geometrics.com/pub/mag/Manuals/856Manual_E.pdf` (visited on 06/03/2016) (cited on page 105).

[54] *Magnetic method | survey fact file | Subsurface Geotechnical*. [Online]. Available: `http://www.geophysical.biz/magnetic.htm` (visited on 06/02/2016) (cited on page 102).

[55] *Magnetic Susceptibility | Geotek*. [Online]. Available: `http://www.geotek.co.uk/products/magsusc` (visited on 06/08/2016) (cited on page 102).

[47] J. Milsom and A. Eriksen, *Field geophysics*, 4th ed, series The geological field guide series. Hoboken, NJ: Wiley, 2011, OCLC: ocn657270827, ISBN: 978-0-470-74984-5 (cited on pages 89, 93, 102).

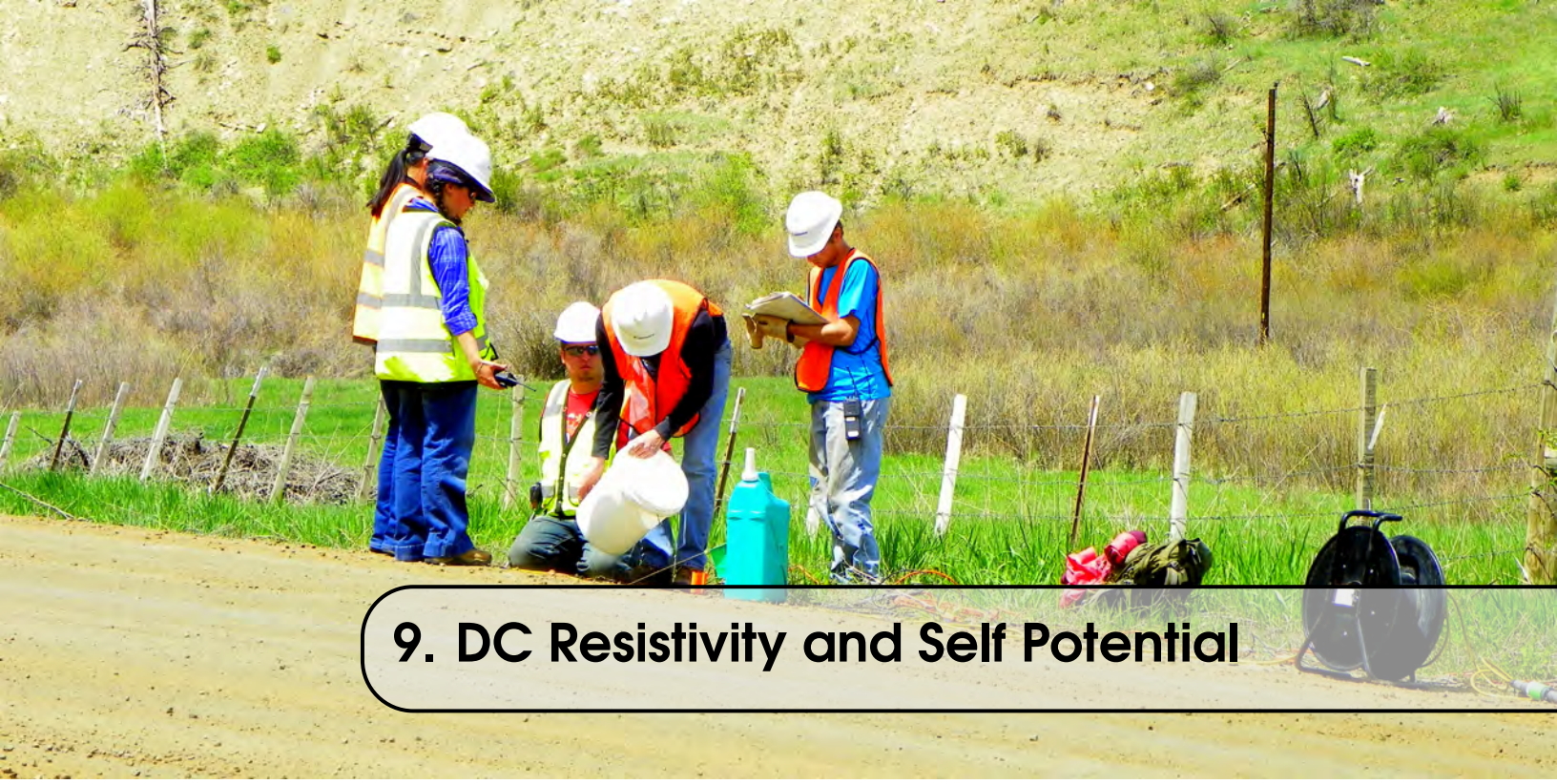

9. DC Resistivity and Self Potential

Contents

9.1 Introduction

DC resistivity and Self-potential (SP) are complementary electrical methods. SP is a passive method that measures telluric currents which create naturally occurring electrical fields in the subsurface. Telluric currents can potentially arise from water flow in the subsurface, making SP directly related to fluid flow. During the 2016 Geophysics Field Camp, SP was primarily used for detecting groundwater flow. SP can also be used for redox reactions, locating contaminant plumes, and temperature gradients in the subsurface. The data collected in SP surveys includes voltage differences between two non-polarizing electrodes along the desired survey line.

Sometimes in data interpretation, those voltage differences are not enough to analyze trends. In an SP survey, we are measuring a voltage, leaving two unknowns in Ohms law. This is why a DC resistivity survey is typically conducted alongside an SP survey. SP will provide a general outline of the effects on the surface due to the body of interest in the subsurface. A DC resistivity log will not give any information about telluric currents specifically, but can supply a conductivity/resistivity model that allows SP to be inverted. DC in coalition with SP will provide a more exact depiction of the location of this anomalous body, whether it be groundwater flow or contaminant plumes. Because of SP's analysis of the surface, the SP survey's depth of investigation is dependent on the complimentary data set that the respective DC resistivity log examines.

Based on total length of the survey and its station spacing, one can determine the general location of an area of interest. Other sets of data like seismic and DC resistivity will help locate the depth in the subsurface. However, SP data can be interpreted on its own and provide insight towards other method results and the fluid flow patterns in the subsurface.

DC resistivity is an active geophysical method which is also governed by Ohm's Law. Resistivity is determined from the acquisition of the other two parameters in Ohm's Law, current and voltage. In the case of DC resistivity, the current is controlled and sent through a pair of current electrodes. The voltage is also measured from a separate pair of voltage electrodes. These electrode arrangements are referred to as arrays. There are multiple array arrangements which are delineated by the order and spacing of the voltage and current electrodes. Examples of array types are Wenner, Dipole-Dipole, and Schlumberger. The depth of investigation varies based upon electrode spacing, total length of survey, and the type of array that is used on the survey. DC resistivity differs from SP in that it exploits subsurface conductivity, rather than telluric currents. DC can identify the location of conductive bodies in the subsurface, including water. SP provides information on the direction of the flow and the general area that the water is in, whereas DC pinpoints the location of said water. DC resistivity is also able to differentiate between contrasts in conductivity in the lithology and is useful for mapping the subsurface. Additionally, this method can identify conductive bodies that do not have flowing water, such as buried metals.

9.1.1 Background

Based on previous field work and investigations outlined by A. Revil, S. Cuttler, et al. 2015, several known faults are in Pagosa Springs that could give hints to the groundwater flow and what current DC surveys may show. In that particular study, researchers used DC resistivity, self-potential, and seismic to image faults in the area. Locations of different faults in the area are outlined in this study - the Victoire Fault, two North-Northeast trending faults (referred to as Fault A and Fault B), and the Eight Mile Mesa Fault [1]. Figure 9.1 shows the location of these faults. The location of the Victoire Fault is of particular interest to the current study, as the student site location was partially selected in hopes of imaging the northern extent of this fault. Locations of faults in this area are important for this study because they may serve as conduits for the flow of the Mother Spring water. DC and SP could both be used to show faulting. Since faults often provide pathways for fluid flow, SP can identify moving fluids through the generation of telluric currents carrying charged cations and anions with respect to faulted rock. Since faults provide offset of subsurface rock layers, DC Resistivity can image the change in conductivity across a fault as different layers are brought closer to the surface. No SP data was taken at the student site, but the DC data was conducted with the intention of showing an offset of conductivity layers if they were present and thus imaging the Victoire Fault as seen in figure 9.7. Results from the study showed that the Mother Spring and a warm spring 1.8km further South are in the middle of an intersection of the Victoire Fault and Fault A and Fault B. Additionally, this research suggested that a geothermal reservoir exists North of the Mother Spring [1]. The student site, parts of which are directly North of the Mother Spring, would be expected to show evidence of this reservoir by imaging it as a large pocket of conductive material.

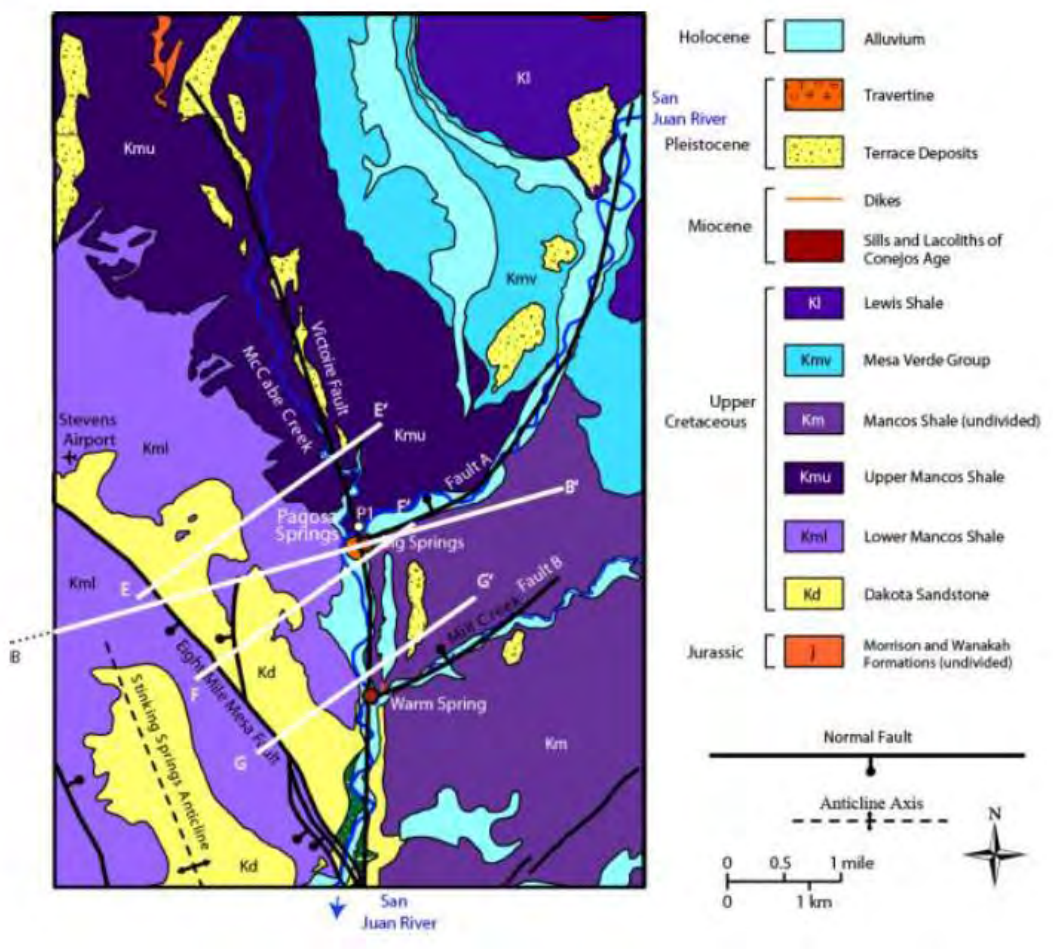

Figure 9.1: *This map was created by A. Revil et al. for the Pagosa Springs plumbing article (Figure 3) [1]. Included in this figure is the location of the faults mentioned above: Fault A, Fault B, the Victoire Fault, and the Eight Mile Mesa Fault. The Mother Spring and the Warm spring are also indicated, and they are located at the intersections of the Victoire Fault and Fault A and Fault B respectively. Lithology is also illustrated in this figure. The white lines are cross sections that were later described in the paper.*

9.1.2 Theory

DC Resistivity

DC Resistivity surveys work by injecting current into the subsurface and recording the electrical potential difference between two other points. The current pumped into the ground flows through conductive bodies in the subsurface and will create a voltage difference measured at the surface. The voltage difference depends on the distribution of resistivity of the bodies. The DC current alternates polarization in the form of a square wave in order to prevent charge build-up in the current electrodes. If the injected current does not alternate polarization, then charge buildup will occur and the apparent chargeability of the electrode will be recorded instead of the apparent resistivity. This type of survey is called induced polarization and was not performed at Field Camp. In the case of a DC survey, a small period of "off-time" is required to ensure all charge buildup has decayed. This is a consequence of instantaneously shutting off a current. Back EMF is a result of charge left over that quickly decays after the current is shut off and is not the desired voltage measurement. Examples of the DC waveform can be seen in Figures 9.2 and 9.3.

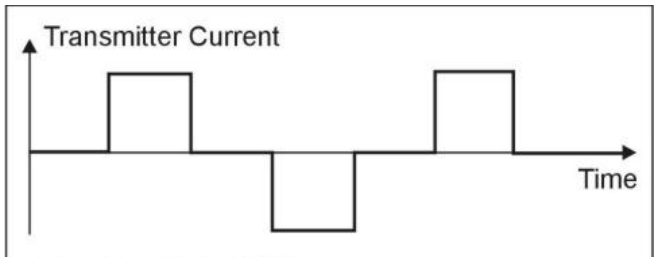

Figure 9.2: *Diagram of a square wave like that produced by a DC current. The positive areas are the on times, when current is being injected into the ground, the areas at zero are the off times, when no current is being injected, and the negative areas are on times with a switch in polarity. Polarity switches are done to prevent charge buildup in the electrode that would cause changes in the data of the measured apparent resistivity.*

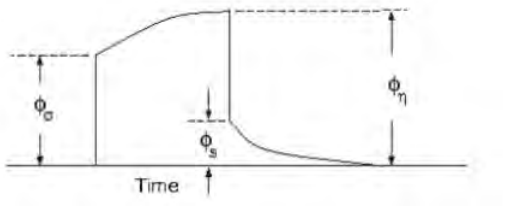

Figure 9.3: *Diagram of back EMF from a square wave DC current. Image from the DCIP2D Manual [56]. This image shows the three different DC potentials, the first being the potential measured without chargeability effects, the third being the limit value from charged material, and the second is a set of secondary potentials between the charged and uncharged material potentials.*

The apparent resistivity is a direct result of the measurement from a DC survey, while true resistivity is the desired property obtained from inversion through the use of Ohm's law:

$$V = IR \tag{9.1}$$

In the case of a DC survey, V is the measured voltage difference between two electrodes, I is the injected current, and R is the resistance of the ground. Determining the apparent resistivity is a simple calculation because a known current is injected and the potential difference is recorded, leaving resistance as the only unknown. Apparent resistivity at some pseudodepth can then be determined from resistance through a geometric factor. For a simple uniform resistor, resistivity (ρ, a material property) is related to resistance (R, an object property) by the following equation:

$$R = \rho \frac{L}{A} \tag{9.2}$$

where L is the object's length and A is the object's cross-sectional area (together, they comprise the geometric factor). In the case of a DC survey, the geometric factor, k, is similarly defined as a length divided by area. Because the current flows through a half space, the geometry is thought of as a half sphere. In terms of the electrode spacing, a, and a spacing multiplier, n, the geometric factor for our survey is given by:

$$k = \frac{1}{2\pi a} \tag{9.3}$$

Depending on the electrode setup used, the geometric factor changes. This geometric factor is for a Wenner array electrode setup. Multiplying the geometric factor by the resistivity yields resistance, seen in the following relation:

$$R = \frac{\rho_a}{2\pi n a} \tag{9.4}$$

where ρ_a is apparent resistivity. The apparent resistivity is the value that is desired whereas the resistance is what actually gets recorded. Apparent resistivity is a measure of the average resistivity of the half sphere current is flowing through. This means that while apparent resistivity is calculated, it is not an accurate representation of the subsurface. Through inversion, it is possible to recover a true resistivity model. True resistivity is a measure of the physical property at each point in the subsurface. While apparent resistivity is assigned a point in the subsurface so that it can be easily viewed, true resistivity is the real value of resistivity at a given point. True resistivity of the subsurface is the intended target of data recovery when inversion is run on DC resistivity data.

Self-Potential

Self Potential is the only geophysical method that can directly measure a response solely based on fluid flow in the subsurface [62]. In theory, this method could be used to identify water flow linked to the Mother Spring. Self Potential (SP) uses two non-polarizing electrodes to measure the potential difference produced by the naturally occurring electric fields associated with telluric currents. Non-polarizing electrodes are used in passive geophysical methods because they are sensitive to these small electric fields, since current is not injected into the ground. Copper-Copper Sulfate electrodes cause half-battery reactions. When two are placed in a conductive media (the ground), the voltage difference drives a battery reaction between the electrodes, causing current flow in the wire in one direction.

The non-polarizable electrodes work chemically through the half battery reactions between salts and associated metals, shown in Figure 9.4. A non-polarizable electrode consists of salts, such as copper sulfate, silver chloride, or lead chloride mixed in solution. A voltage difference sent through the electrode will disassociate the ions. In an example pertaining to the copper sulfate electrodes, copper disassociates from the sulfate and the remaining 2 electrons are stripped from the copper. The sulfate chemically bonds to hydrogen in the solution, the copper becomes solid, and the electrons travel through the wire to produce an electric signal that can be measured, shown in Figure 9.5 [60].

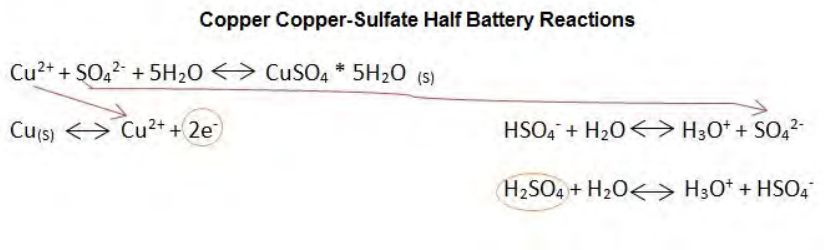

Figure 9.4: *The chemical reaction that occurs between the Copper-Sulfate solution and solid Copper in SP electrodes. This results in 2 spare electrons that can travel through the wire to the partner electrode, and the chemical bond of sulfate to hydrogen.*

A voltmeter is connected to both electrodes to measure the voltage difference (in mV). Changes across a linear separation indicate a change in the current flow in the subsurface. A larger current flow produces a higher voltage gradient between the two electrodes. This can be due to groundwater movement, redox reactions, coal seam fires, or man-made features. The major interest in this survey is subsurface fluid flow, which causes electric fields in the direction of flow. Dissolved ions moving in water act like electrons traveling through a wire. Upward travel of these ions, like in upwelling of a spring, can be measured as large positive voltage values.

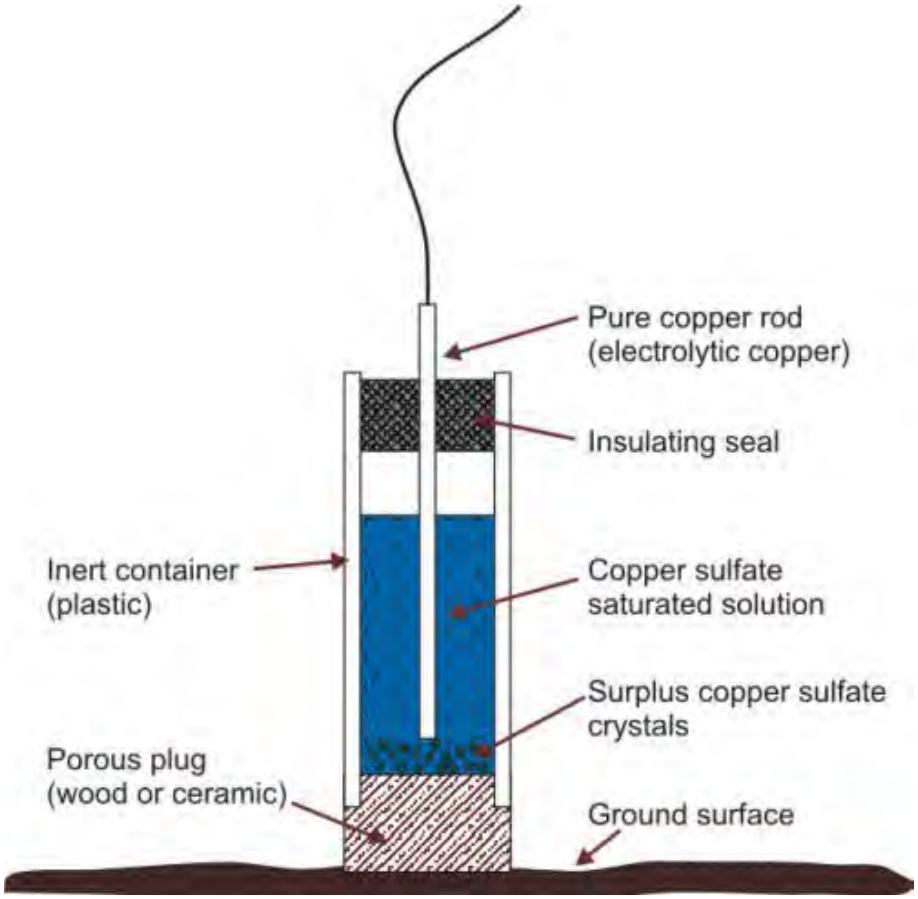

Figure 9.5: *Diagram of a copper sulfate non-polarizable electrode. Shows a cross section image of how the copper bar extends into the electrode, and sits in the copper sulfate solution. The porous plug enables the transfer of electrons from the ground into the solution, and is then sent through the attached wire at the top to produce an electric signal. This signal is interpreted by the voltmeter to express the voltage difference.*

Like DC resistivity, self-potential can be analyzed using Ohm's law. However, both I and R are unknowns in SP data, where V is measured. Self-Potential is sometimes coupled with DC resistivity data, which allows to solve for I spatially. However, self-potential is useful on its own as well.

9.2 Objectives

1. To gain helpful experience with DC Resistivity and Self-potential methods, in the field, and with processing the data.
2. Verify consistency of geological interpretations by comparing results from DC and SP data with results from other methods.
3. Invert DC data using the DCIP2D inversion code (UBC Geophysical) to create images of subsurface resistivities in order to identify possible geologic contacts, as well as to provide conductivity estimates to aid in the inversion of Electromagnetic methods.
4. Using SP to delineate regional water flow trends in an effort to identify faults or intrusive bodies that could divert water and lead to geothermal upwelling.

9.3 Methods

9.3.1 Survey Location

For DC resistivity, there is a continuous survey that spans along the main line and two closely related surveys taking place at the student site. On the main line, the survey spans from flag positions 1900-1582, traveling East to West. The DC survey on the student site covers the majority of the survey line. There are two separate survey lines for DC on the student site, seen in Figure 9.6. The Western line, from May 25th, is an extension of the student site main line. For our self-potential surveys, the main line is covered from Flags 1000-1900 as seen in figure 9.7. The line was completed in parts, in no particular order. However, no SP survey was performed at the student site.

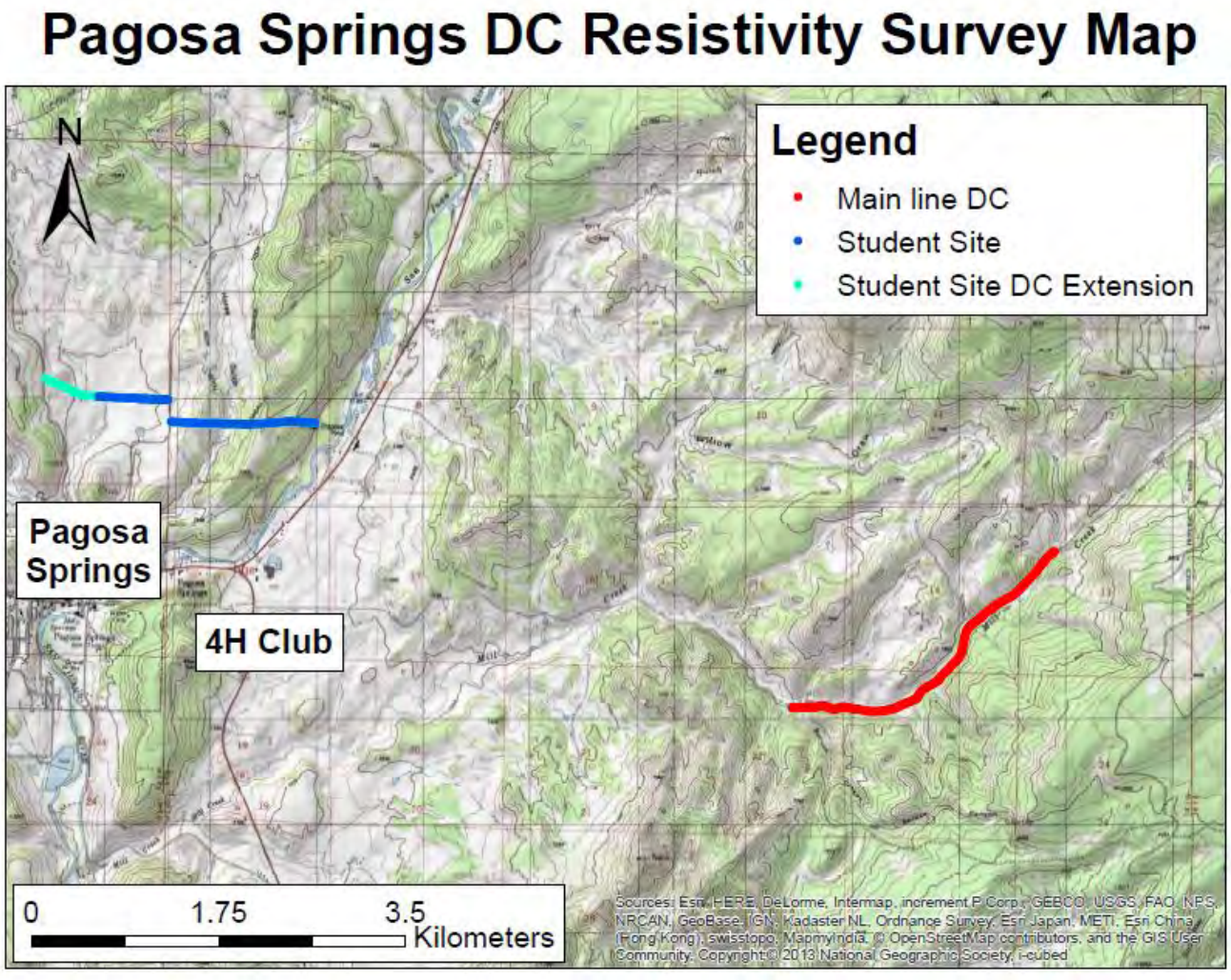

Figure 9.6: *An image of DC Resistivity surveys performed. The red line shows the extent of the main line that the DC resistivity survey covered. The survey spanned from Flags 1582 to 1900. The blue lines show the DC resistivity surveys performed at the student site.*

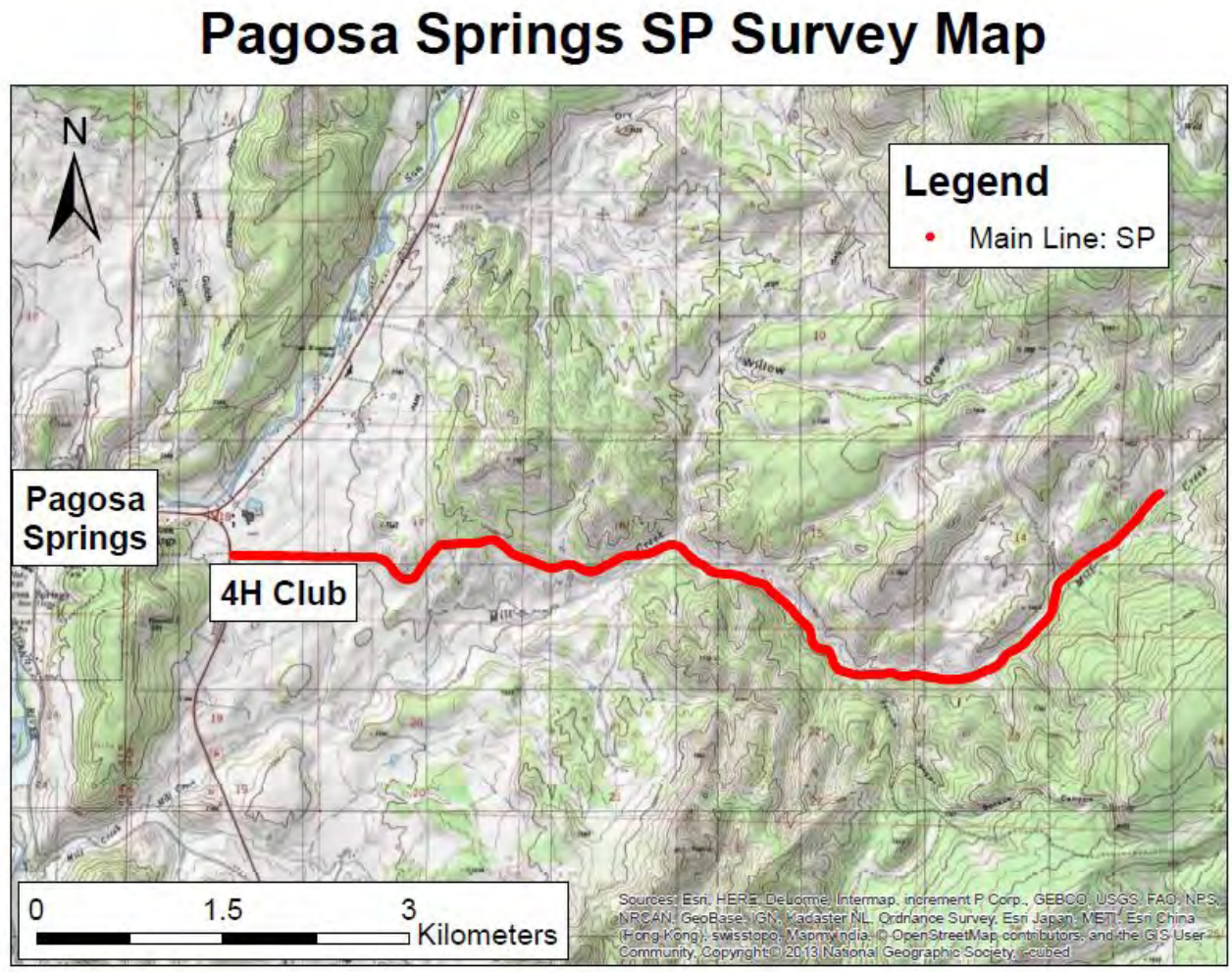

Figure 9.7: *Map illustration the SP survey conducted along the main line.*

9.3.2 Data Acquisition

DC Equipment List

Figure 9.8: *Students collecting DC resistivity data along the student line in Pagosa Springs. The ABEM is set up and connected to each of the electrodes through ABEM cables.*

1. ABEM (Shown in Figure 9.9)
2. 8 ABEM cables
3. 7 cable connectors
4. 64 electrodes
5. Switchbox and cable to connect to ABEM
6. 12V battery
7. Hammer
8. Saltwater
9. Road guards for wires
10. Jumpers to connect ABEM cables to electrodes
11. Notebook

Figure 9.9: *Photo of the ABEM unit used in the field [59].*

DC Resistivity

This study used a Wenner array set up for all surveys. This means that the spacing between the current and voltage electrodes are all the same distance, seen in Figure 9.10. To begin the survey, students chose the survey parameters (the same across all surveys): 64 electrodes with 20m spacing, a square wave current of 500mA, an error limit of five percent, and a minimum stack of two with a max stack of five. The stack represents how many times the ABEM (the data recorder) will take a measurement either before the max stack of five is reached or the measurements are within the error limit. Each electrode was put two thirds of its total length into the ground to establish good contact. The ABEM can handle a total of 64 electrodes and each cable can handle eight electrodes. The ABEM was in the middle with 32 electrodes on each side of it. The electrodes were then connected to the ABEM through the eight ABEM cables. The cables have pullout points which allow the electrodes to be connected via jumpers. The connectors between cables are directional, meaning that they must face a specified direction. This is important when laying out the cables.

Once the survey was laid out, the next step was to troubleshoot all the components from the ABEM. The ABEM checked the activity of all the electrode pairs from its two electrode tests shown on the prompt screen. The ABEM sent a current into electrode 1 and electrode 2 receives the signal. If the circuit was complete, the ABEM approved both electrodes and continued onto the next pair. If the current was not received, then the ABEM marked both those electrodes as failed. Then the ABEM selected the first electrode that was successful and used that to delineate which electrodes did not work out of the failed pairs. Failed electrodes had to be fixed in order to take measurements from them. Common fixes included: putting the electrode deeper into the ground, watering the area around the electrode with saline water, checking the cable connection to the failed electrodes, and checking cable-to-cable connectors [57]. The ABEM troubleshoot function was run again to show if the electrodes that originally failed are now fixed. If an electrode could not be fixed, it was ignored, which created missing data points in the respective psuedosection. After troubleshooting, the survey was run on the ABEM and the data was stored in the unit.

DC surveys can be extended by performing a roll along. In this case, the survey extends past electrode 64 rather than electrode 1. The ABEM was shut down and disconnected from the battery and switchbox. The roll along took place in 16 electrode increments. At the beginning of the survey, cables 1 and 2 were disconnected from respective cables and electrodes. The 16 electrodes were disconnected from the ground.The two cables and 16 electrodes were transferred to the end of the line and the ABEM was reconnected to the middle of the array. Cables 3 and 4 are then the new cables 1 and 2, and the disconnected cables are 7 and 8. The troubleshoot process was repeated and the survey continued. These surveys go faster because of the overlapping of some psuedosection data points are already stored in the ABEM. When processing the pseudosection the ABEM ignores the overlapped points and the new points are amended to the end of the pseudosection. By performing the roll along, the horizontal length of the psuedosection is then extended.

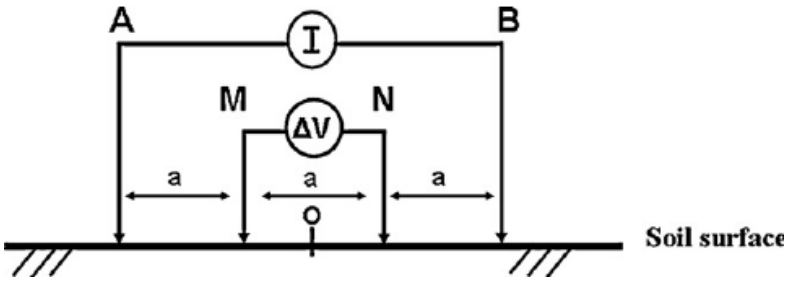

Figure 9.10: *Diagram of a Wenner array setup. A and B are electrodes that inject current into the ground. M and N are voltage electrode that measure the potential in between them. The spacing between all the electrodes in a Wenner array are the same.*

SP Equipment List

1. Two Non-Polarizable, Copper-Copper Sulfate electrodes (Figure 9.11)
2. 500m long cable
3. Connector wires and banana clips
4. Multimeter (Figure 9.11)
5. Pickax
6. Notebook

Figure 9.11: *Copper Copper-Sulfate electrodes and multimeter used in SP surveys.*

Self-Potential

The self-potential (SP) method is a fast, inexpensive, and relatively simple method that involves two non-polarizable electrodes, a cable, and a multimeter [61]. The electrodes need to be non-polarizable, meaning they are not affected by charge buildup when current flows through them. The copper sulfate electrodes have a porous bottom to allow electrons to flow freely into the electrode from the subsurface, causing a measurable voltage gradient.

First, plug an electrode into the reference port to establish a stationary electrode. Perform a tip to tip measurement between the two electrodes to account for instrumental drift. The voltage reading should be within $\pm 10mV$. Using a rock hammer, dig a hole and bury the reference electrode and connect it to one of the long cables with a banana clip. Each station has a spacing of 20m along the mainline, shown in Figure 9.6. This spacing was chosen to agree with the DC survey, and to get the largest spread of quality data in the available time. At each site, dig a hole until brown soil is shown and a good contact can be made. Plug the cable and roaming electrode into the voltmeter. Record the potential at that site, shown in Figure 9.12. Note that the number will never settle on a specific value in the voltmeter. Wait ten to fifteen seconds and choose a value within the oscillating range. Record the voltage and time by hand. The recorded time at each flag is used to apply drift corrections to the raw data. At occasional sites take a resistance measurement to help differentiate anomalies and identify instrument problems. At the end of the survey take another tip to tip measurement to account for instrumental drift. Complete the main survey line in sections, over the course of six days. Each completed section should overlap with a previous SP survey in order to tie different surveys together and account for changing reference points.

Figure 9.12: *Students collecting SP data along the main line in Pagosa Springs. A multimeter is used to measure voltage between the roving electrode (shown), and the reference electrode (not shown). Data is recorded in a notebook.*

9.3.3 Data Expectations

No forward modeling was used for these particular methods. However, appropriate expectations were drawn from cross sections and previous knowledge of the area. Because the main line does not cross over any known faults, the DC data from the main line will likely show only the different layers of geology. This is also expected for the Western side of the student site. As a rule of thumb, a Wenner Array can see to a depth of a/2, where a is the electrode spacing of the maximum arrangement of electrodes. In this survey, the maximum spread is 1280m. Because there are three 'a's in this spread (one between A and M, one between M and N, and one between N and B), the 'a' value is 426.6m (1280m/3). Therefore, the maximum expected depth of interpretation for this survey is 213m (426m/2). Based off of knowledge about the local geology, the top two geologic layers - Mancos Shale and Dakota Sandstone - will likely be seen in the DC data. The Morrison Formation, which is under the Dakota Sandstone, may also be seen depending on the actual thicknesses of the layers and the actual depth that the DC data can investigate.

Both the eastern and western sides of the student site may likely show the upper extension of the Victoire Fault. The location of the student site is directly North of this fault, which is a large reason why students selected this location. Assuming the offset of the Victoire Fault is large enough, the DC data may see a resistivity contrast.

No forward modeling was performed for the SP data as well. Since SP is not used to identify rock layers, the main outcome from the data will be to identify fluid flow features in the subsurface. The survey along the main line might discover a disruption in the groundwater flow due to the dike near the end of the line, or a previously unknown fault. It is also possible to discover the presence of water upwelling from the mother spring. If upwelling occurs, it will present itself with high positive voltage values in a region close to the beginning of the line. This could indicate the eastern extent of vertical movement of water contributing to the Mother Spring.

9.3.4 Processing

DC Resistivity

The DCIP2D inversion code, written by UBC Geophysical Inversion Facility, allows students to process the field DC data collected over portions of both the main and student site lines. DCIP2D utilizes a non-linear inversion to extract subsurface electrical conductivity from the measured DC potentials. A conversion code included with DCIP2D, intended to convert ABEM formatted data files to the format required by DCIP2D, converts acquired field data to the format required by DCIP2D. Note that a pre-processing step using the Terrameter software is required to convert data from the raw format on the ABEM device to a format usable with the DCIP2D conversion code. Following data conversion, a student identifies and removes anomalous data points which are assumed to be due to instrumental error (ie. only a single data point is anomalous). A plain text editor is used to create metadata files to accompany data files for inversion. These metadata files include a mesh file, which tells the inversion algorithm how many cells to use for discretizing the model, and a topography file. DCIP2D will iterate the inversion until the data misfit converges on the target misfit, and the model norm plateaus (becomes invariant with consecutive iterations).
DCIP2D allows the parameter controlling the target data misfit value to be set to a default or discrepancy mode. The default mode functions well enough for typical datasets, while the discrepancy mode can provide more robust inversion (ie. less overfitting/underfitting of the data) when uncertainty values for the dataset are known. The Terrameter software can convert raw data from the ABEM into a format which includes the recorded standard deviations. Additionally, DCIP2D allows for the inclusion of standard deviations in the required data format. Reiterating the inversion using files containing uncertainty values will aid in choosing an appropriate target data misfit value for the dataset, allowing for less over/under-fitting of the data.

DC inversion is non-linear due to the nature of the survey and determines the true resistivities of the subsurface [56]. It is non-linear because removing a single data point affects the response from other points. In other words, the response at a given location is in part dependent on the response from other locations. As a result, a linear inversion will not account for the inter-dependencies of DC data. The non-linear inversion problem is solved by linearizing the data equations, applying global misfit criterion, and including a general weighting matrix [56].

The DCIP2D inversion code requires a number of parameters to be set in order to perform inversion. Of note are the mesh size, topography, target data misfit value, and the presence of a reference model. Mesh size is always chosen to be larger and finer than the survey extent. This is to account for large degrees of complexity in Earth conductivity distributions; an infinite number arbitrary subsurface conductivity distributions are capable of reproducing the data. This ties into the presence of a reference model. When prior information on the subsurface geologic environment is available, creating a reference model to use as a starting point for inversion can aid in producing a model which is geologically sound. The use of a reference model can be particularly convenient for normalizing the magnitudes of calculated subsurface conductivities across different models. Due to a lack of detailed information on the subsurface geologic environment, inversions of the field DC data from both the main-line and student site were carried out using a single conductivity value for the starting reference model.

The students chose a conductivity value of 0.02 S/m (50 Ohm-m) as a starting point for the inversion, as the geologic environment around the survey locations along the main and student site lines is believed to be Mancos shale. Borehole resistivity log data collected by another student crew from wells in the Pagosa Springs area allowed this conductivity value for the Mancos shale to be chosen. The target data misfit value is chosen in one of two ways, either using default DCIP2D settings or by the discrepancy principle. DCIP2D's default setting is used when uncertainty of the data is not recorded; the program will set five percent of each measurement to be the uncertainty used in inversion. The discrepancy principle sets the target data misfit value based on the number of data points and the chi factor, as well as the uncertainties provided for the data.

The inversion parameters stated above are specific to the survey design and site location, and as such are set individually for each survey site. On the main line, a mesh of 10 meter (horizontal) by 5 meter (vertical) cells covers the main area of interest. Alternatively, on the student site, a mesh of 5 meter (horizontal) by 2.5 meter (vertical) cells is used. The finer mesh size at the student site is required due to the smaller extent of the surveys, in order to provide enough degrees of freedom in our model to reproduce complex subsurface conductivity distributions. For each site, topography is taken from differential GPS (DGPS) elevations. Note that topography has two effects on DC data - topography alters the horizontal distance between electrodes, and also changes the relative position of the air-ground interface.

For the purposes of this investigation, the primary effect to account for is the change in the position of the air-ground interface; horizontal distances between electrodes are already varied by the presence of curves in the line. The target data misfit value is chosen using the discrepancy principle for surveys over the main line and the East side of the student site. For the main line survey, the chi factor, which is the ratio between the target misfit value and the number of data [58], is changed to two because the data was being over-fit, while the East side of the student site converged well with a chi factor equal to one. DC data from the West side of the student site would not converge when using the discrepancy principle, likely due to inconsistencies in the uncertainties provided. Therefore, the default DCIP2D protocol is used to set the target data misfit value for this survey site.

Self-Potential

The raw self-potential data is recorded in notebooks during field collection. For processing, these values are entered into an Excel spreadsheet and organized by flag number. The tip to tip (T2T) measurements taken in the field are used to apply a linear drift correction to the data. This is done to each daily survey individually. The drift equation is based on the times at which each measurement is taken.

$$Drift = \left(\frac{FinalT2T - InitialT2T}{TotalSurveyTime} * MinutesSinceInitialT2T \right) - InitialT2T \tag{9.5}$$

The drift for each data point is subtracted from the measured value. Once each set of data is drift corrected, they must all be normalized to one point. All the SP data sets are normalized to the start flag (1000). Overlapping flag measurements from two surveys are used to relate two data sets together. The average difference between repeated data points from two surveys is subtracted from the entire data set. All daily surveys were normalized starting at flag 1000 and working towards flag 1900. Once all SP data is drift corrected and normalized, the voltage can be plotted as a line in Grapher, or as a colorbar over topography in ArcGIS.

9.4 Discussion

9.4.1 Results

DC Resistivity

Inversion of DC data was run both with erroneous data points as well as with these data points removed. Inversions with erroneous data points present generally result in an inversion model which is one small area of some kind of anomaly, with the rest of the model being relatively uniform. This is an indication that the inversion model is not suitable for use in interpretation, especially when the points in pseudo section are singular points of anomaly with little to no similar points in the vicinity. Inversions following the removal of the of erroneous points, show smoother models, there is still some overfitting at the near surface in the models, however. All data has displayed is done so after having been converted to a log scale.

Main line data was taken from flags 1582-1900, which represents a small section near the East side. Errors in the field system resulted in non completion of the line. The area of the main line which was completed using DC resistivity, was analyzed, and can be seen in Figure 9.16.

There is one main area of low resistivity in the subsurface of this section of the main line with values of around 1.2 Ohm m This layer seems to start at a depth of approximately 200m (note that 0m depth is above the line of elevation on the West side) and extends to the end of our depth of investigation (around 312m). Above, there is a thin layer of more resistive material, about 1.6Ohm-m. In places, this layer seems to be about 100m thick, but seems thinner in some areas, particularly at the East end of the line, where it may be less than 50m thick. The contact between this layer and the more conductive layer underneath, as well as the topography, show the layers shallowly dipping to the West. Within the more conductive layer, starting at a depth of about 210m at extending from a position of 1570m to 3000m, there is an area of slightly greater conductivity (a resistivity value of around 0.6Ohm-m). This layer is about 100m thick and seems to be dipping in the same direction as the other layers.

Two lines of data were collected at the student site. One was done on the East side of County Road 200, and the other was taken on the West side of the road. Each was completed after the ABEM was rendered inert, due to damage to its cables, and after a way to circumvent the damage was discovered. Each of the two lines were completed using sixty-four electrodes, with 20 meter spacing. The East side of the student site included a significant amount of terrain, this terrain had to be corrected for when inverting the data.

While the West side of the student size contained less topography than the East side, there was a bend in the line. This bend can be seen in Figure 9.6. The topography of the East side was taken into account, the bend in the West side, which breaks the 2D assumption, is not corrected for in the inversion process. In the inverted model of the West side, Figure 9.18, there is a distinct resistive layer which can be seen in the subsurface. This layer extends across the entire section, it also appears to extend the resistive section present on the East student site. The conductive layer seen in the West side of the student site has conductivities ranging from 2.7 Ohm-m to 2.1 Ohm-m. While this resistive layer is the bulk of response on the West side of the line, there is an area of low resistivity near the eastern side of the section. This feature is present at about 1.1 Ohm-m.

On the West end of the East side of the student site, there is a thin layer of less resistive material (thickness of about 50m, resistivity of about 1.5 Ohm-m) overlaying a layer of more resistive material. This second layer seems to extend from 100m depth to around 220m and has a resistivity of around 1.9Ohm-m. There also seems to be a layer underneath that is slightly less resistive, about 1.8Ohm-m. The East end of this line is interesting. There are two areas of low resistivity on the topographic high. The one on the far West is slightly bigger in thickness and extent, and has a less resistive value of around 1Ohm-m. The second has a resistivity value of 1.2Ohm-m. These two areas are separated by about 50m with a resistive layer of about 1.9Ohm-m in between. This also seems to be the resistivity of a thin layer on top of both the less resistive anomalies.

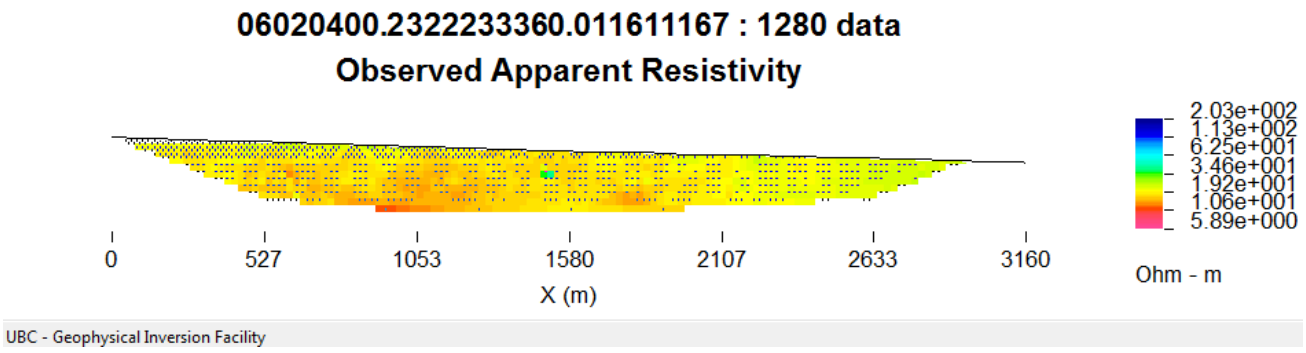

Figure 9.13: *DC Resistivity pseudosection of the mainline. Bad data points have been manually removed. Topography has been added*

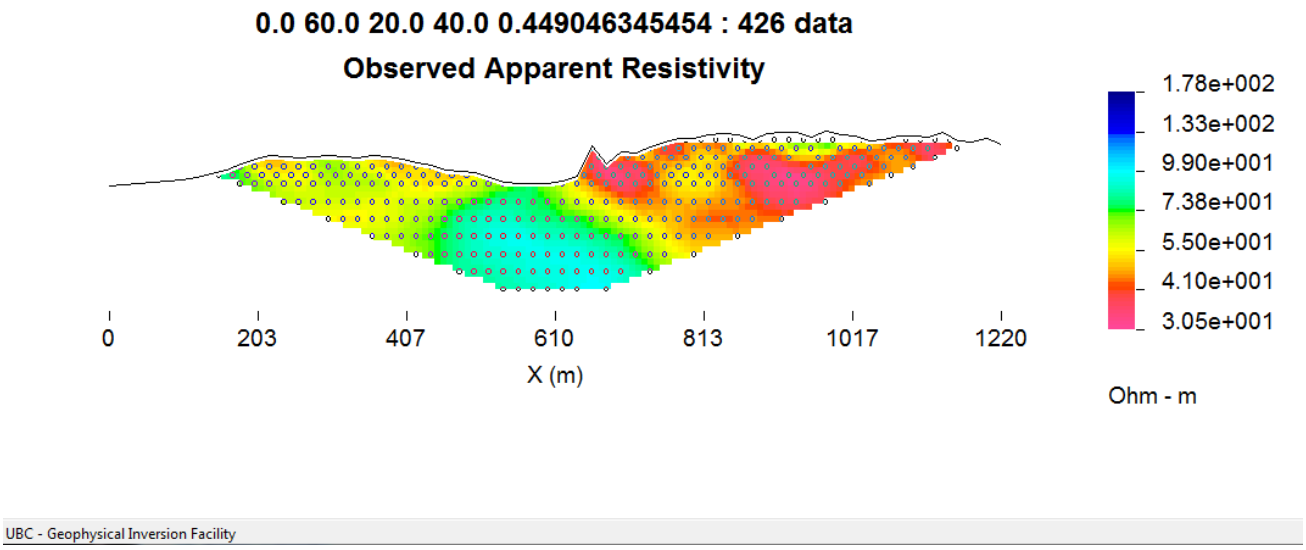

Figure 9.14: *DC Resistivity pseudosection of the East Side of the student site. Bad data points have been manually removed. Topography has been added*

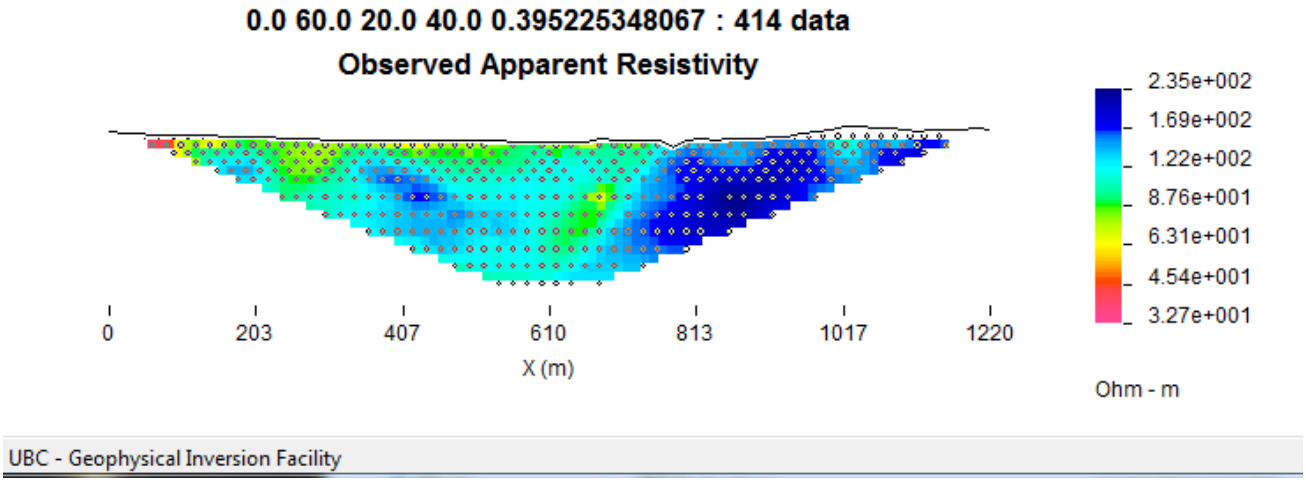

Figure 9.15: *DC Resistivity pseudosection of the West Side of the student site. Bad data points have been manually removed. Topography has been added*

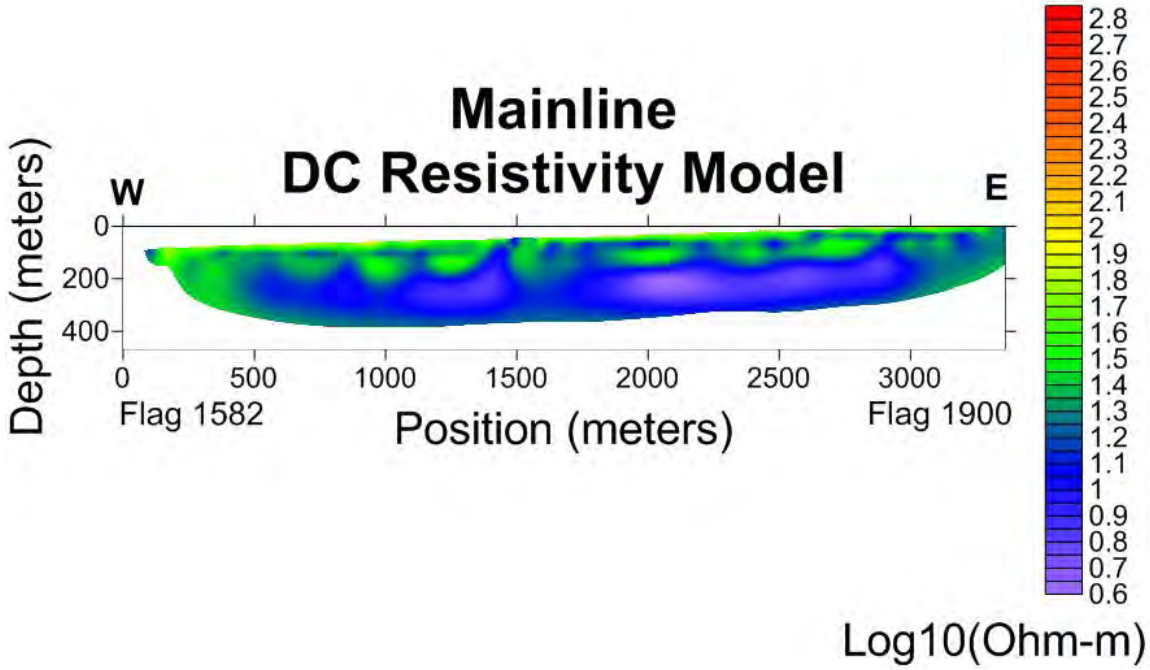

Figure 9.16: *DC Resistivity model as interpreted by Surfer. The black line represents approximately the depth of investigation, or the depth that the survey could image seen from the DCIP2D results (included in appendix). This survey covers the main line from flag 1582 to flag 1900.*

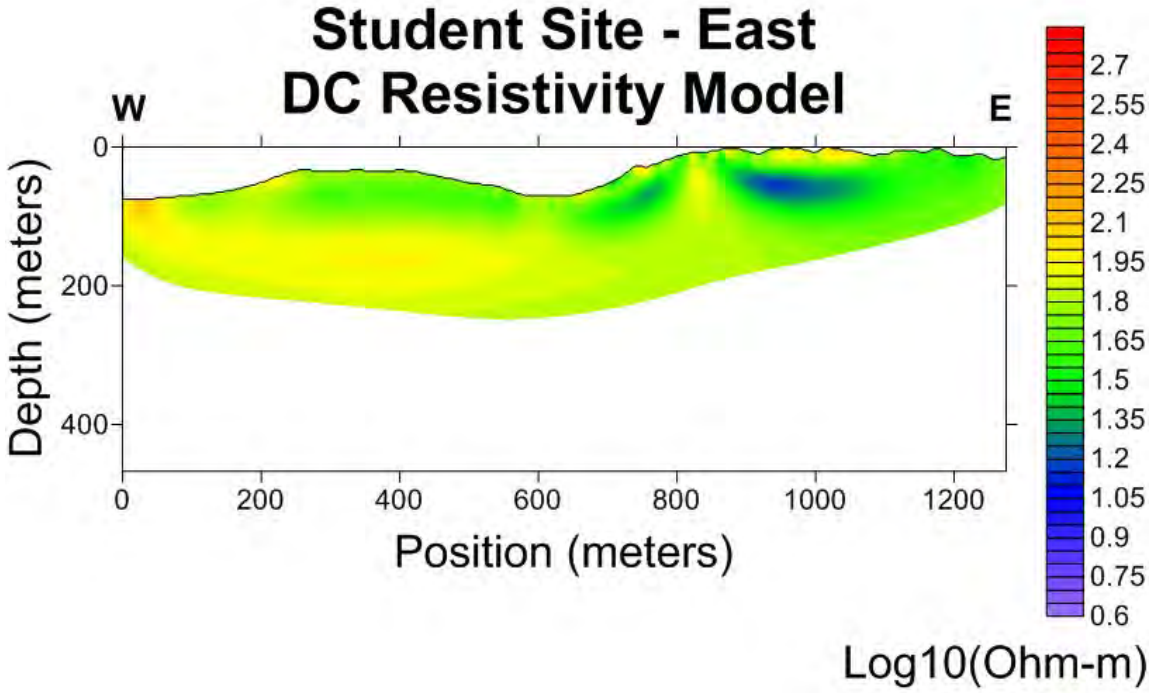

Figure 9.17: *Student Site East side DC Resistivity model as interpreted by Surfer. The black line indicates approximately the depth of investigation, or the depth that the survey could image, as seen from the DCIP2D inversion image.*

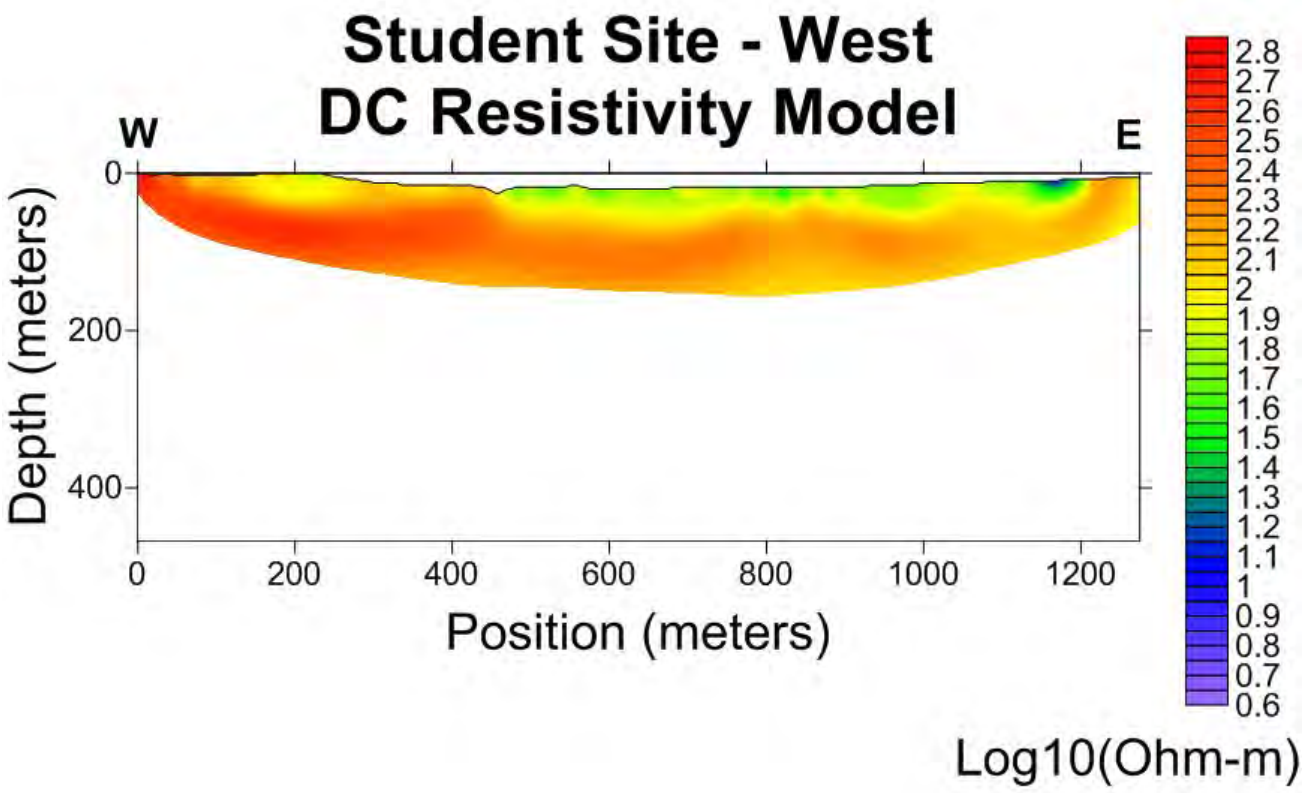

Figure 9.18: *Student Site West side DC Resistivity model as interpreted by Surfer. Again, the black line indicates approximately the depth that the survey could image, as seen from the DCIP2D inversion image.*

Self-Potential

The self-potential data collected along the main line in Pagosa Springs was drift corrected and normalized before it was analyzed for subsurface trends. Figure 9.19 shows both the raw data and the processed data. The raw data for each survey was adjusted for instrument drift, and the entire dataset was normalized to the first point. The corrected voltage values are plotted in Figures 9.21 and 9.20. The data is recorded in mV every 20m, and is plotted against distance from the first flag (1000). The results are generally noisy, because of survey conditions and the fluctuation in each voltage reading. SP is generally avoided among geophysicists because of effects of electrical noise and difficulties with interpretation [61]. However, the dominant trends can be analyzed confidently.

The data from flags 1100-1670 is dominantly linear, shown in Figure 9.20. This is expected, since there are no anomalous features to alter the current flow along the line in these areas. Mill Creek is following the main line in this region, so the signal is dominated by this constant flow. Around flag 1670 there is a noticeable dip in the SP data, indicating a block of fluid flow. This is near the location of a subsurface dike. The dike is visible in an outcrop North of the main line, but this data can help pinpoint the exact location where the subsurface feature passes beneath the survey.

The SP values have an upward trend toward the start of the line. These growing values indicate higher current in the region closest to the 4-H club. Shown in red in Figure 9.21, these high voltages could indicate upwelling as we move closer to the mother springs. It could also be a product of noisy conditions as the line enters a more urban setting. Even though power lines are present along this portion of the line, there is no indication of oscillation due to alternating current in the multimeter. Some 60-Hz filters in modern voltmeters eliminate most cultural noise [61].

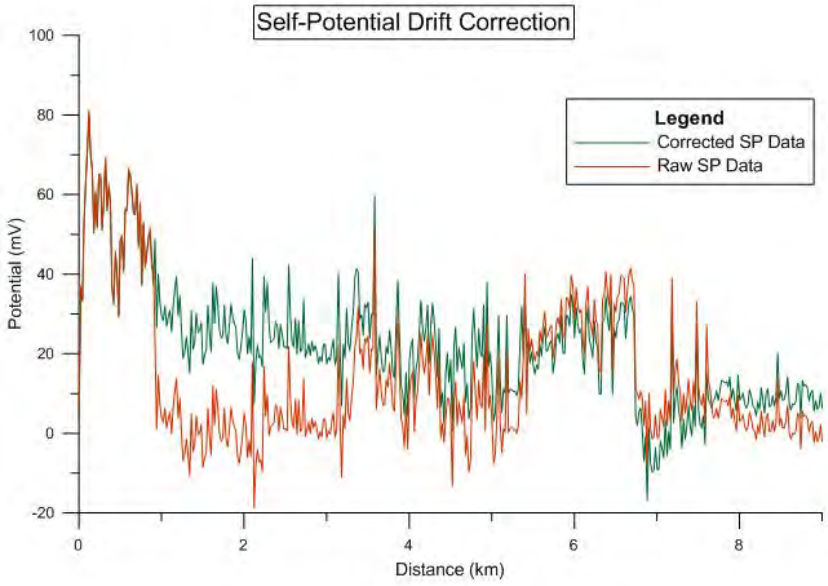

Figure 9.19: *Mill Creek Self-Potential Data: Pre and Post processing. The orange line shows the raw SP data collected in the field. The green line shows the data after electrode drift corrections from each survey's tip-to-tip measurements. The corrected data has also been normalized to the base station (Flag 1000).*

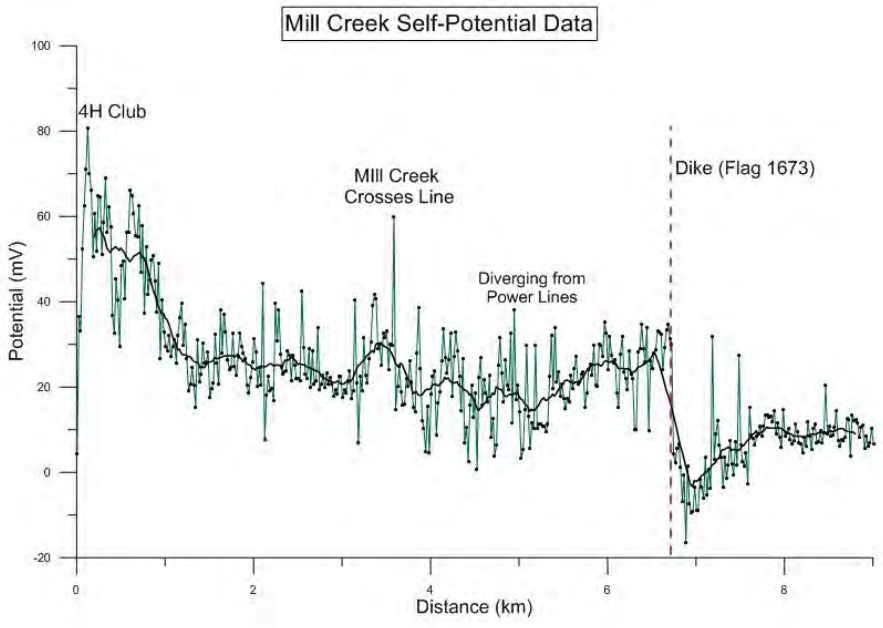

Figure 9.20: *Mill Creek SP data along the main line, from flag 1000 to 1900 (9km). The drop in the data around point 6.7 marks a dike crossing beneath the survey line (flag 1673), disrupting fluid flow on the East side. High voltages near the beginning of the line could indicate upwelling, or could be due to noisy conditions.*

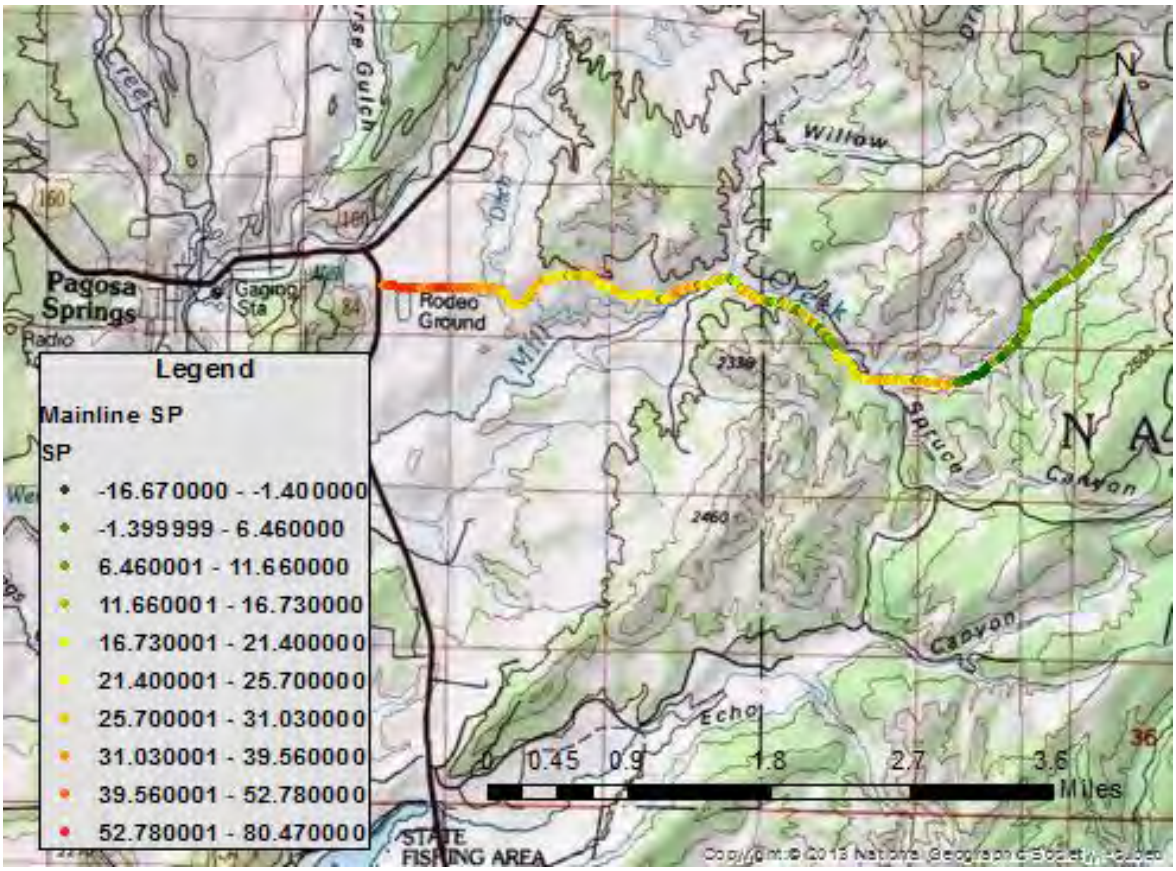

Figure 9.21: *Mill Creek SP data plotted on a plan view topographic map of the main line. The values are assigned a color value to emphasize large changes in voltage.*

9.4.2 Interpretation

DC Resistivity

Geologically, it is known that Lewis Shale outcrops along the area of the mainline where DC data was taken. It is also known that a dike is present at approximately 900 in Figure 9.16, although it is not seen in the inversion. Using these pieces of information, it is thought that the conductive layer being seen is Lewis Shale. As the resistivity values increase as you move toward the West, and it is known that the Lewis dips at approximately 10 degrees, the change in resistivity is a result of seeing a more resistive layer approaching the surface underneath. Mesa Verde is a more resistive layer, in comparison to the Lewis Shale, which approaches the surface near the West end of the DC line. Additionally, there are a number of artifacts that can be seen in the inverted data, these are a result of the topographic effect on the sides of the main line. This topographic effect from the surrounding mountains increases the conductivity of the model created, as it includes the shale in the nearby hills, which are not directly in the theoretical half-space.

Observations of the West student site, show a resistive layer, in between two layers of relatively conductive units. Both the upper and lower units show very similar levels of conductivity, with values that correspond to that of Mancos Shale. With a resistive middle layer, Niobrara is the logical unit to be present. This is consistent with geologic interpretations, which show an outcrop of Niobrara in this area, as well as showing the Niobrara being located within the Mancos. The small conductive are toward the east of the section is the result of noise in the system, not contributing meaningfully to the model.

The east section of the student site, shows a resistive layer extending from the West end. This is a continuation of the Niobrara that was seen on the West side of the student site. Mancos once again overlays the Niobrara, as

well as is present below. The conductive layer seen at approximately 700m, on the east site, is again Mancos, but with the Niobrara having dipped down into the Earth, the Mancos is being imaged alone, instead of being influenced by the more resistive body.

Self-Potential

The key features in the Self-Potential data include the high voltage trends at the beginning of the survey and the drop in voltage 6.74km into the survey. The large drop in voltage is consistent with the location of a subsurface dike. Based on the outcrop of the dike North of the main line, it was predicted to cross at flag 1671. The data shows that the dike has disrupted fluid flow in the subsurface. Based on the data, the true location of the dike is at flag 1673, just before the voltage drop. The groundwater flow is dramatically changed at the location of the dike, causing the entire eastern portion of the line after the dike to have significantly lower potentials.

The high voltage trend at the start of the survey line could be the product of cultural noise. The beginning of the line is complicated by power lines, fences, a cement plant, and the 4H building. There are probably more buried cables and other manmade anomalies. However, even with the presence of power lines along the main line, there was no evidence of oscillations due to alternating current on the multimeter. Another possible explanation for the increased voltage values is fluid upwelling. The West end of the main line is the closest location to the Mother Spring. This is the most likely location for evidence of fluids traveling towards the surface. It would be exciting to use the SP survey to identify the start location of spring upwelling, but cultural noise at this end of the line discourages the confidence in this interpretation.

9.4.3 Errors and Uncertainty

Environmental Errors

Self-Potential and DC Resistivity are affected by similar noise contributers. Cultural noise along the West end of the main line include power lines, metal fences, buried cables, the cement plant and 4H club. Houses along the main line can mean buried cables affecting current in the ground. Additionally, along the main line there are culverts, guard rails, ponds, and flowing water in Mill Creek at different locations contributing to the noise and spikes in the data.

Human Errors

When recording Self-Potential voltages off the multimeter, there is a certain amount of instrument and human error when choosing a value. The multimeter will never settle on one true voltage value. Instead, the readings will constantly change within a certain range and the recorder must choose the most fitting voltage. This provides human error in the data, as no two people will choose the same values throughout an entire survey.

Field Errors/Issues

Self Potential

Self Potential is a passive geophysical method meaning it is more sensitive to noise from other active methods. If SP is in proximity to any method that injects current into the ground, the results can be catastrophically altered. The voltage signal registered on the multimeter will be dominated by the active current injected in the ground, rather than the passive current flow caused by fluid movement. To avoid this source of error, SP is performed away from TDEM and DC Resistivity. To be safe, it is also kept away from FDEM and Magnetics. SP was also kept away from seismic processes, as a safety precaution.

DC Resistivity

Damage to the ABEM system occurred. It is thought damage is the result of a car running over the system. A number of electrodes had been bent, and cables displayed a number of marks matching tire tread. Initially, the damage was thought to only have effected electrodes, as a number were bent, as can be seen in Figure 9.22. Damage was discovered on May 21st. On May 22nd, the ABEM system was used by students to run one survey, with minor problems, a small number of electrodes failing, then the system was then rolled over, forty electrodes

fail, evidence of a major issue in the system.

Figure 9.22: *Some damaged electrodes, from unidentified persons tampering with the main line.*

Following damage, and failure of the ABEM to function in the field, the ABEM was returned to the 4H club to be assessed. Firstly, the ABEM's switch box was examined to ensure the issue didn't result from direct damage. The top of the switch box was removed, and examined, and no damage was found within.

Cables are the next step in finding the errors in the ABEM. Eight cables were investigated, as they were the cables used when the errors occurred. Each of the cables has ports for eight electrodes, at spacing of twenty meters apart. This results in a cable being one hundred sixty meters long, with additional cable on the ends to be used to connect to the ABEM, as well as to other cables. Within each cable, thirty-two channels are present. To test each of the channels in a cable, a multimeter was used, with pins connected to the in and out channels. These were then used, by those investigating, to confirm connectivity of each individual channel. In the process of checking the connections, students created a key illustrating connection combinations.

In addition to errors with the ABEM machine, other errors occurred from not inserting the electrodes deep enough into the ground to obtain good conductivity. On every survey conducted, when running the pre-survey tests with the ABEM (that would check to see if each electrode is working properly), several electrodes would need to be skipped because they were reported as malfunctioning. This could have been a result of the electrode not being deep enough into the ground. It could also have been a result of the ground itself at those locations not being conductive enough or too dry. As fix to the ground being too resistive, salt water can be poured onto the ground near the electrode. This will fix the problem if it is related to the conductivity of the ground, however, if the issue is a result of some other error, there will still be errors created.

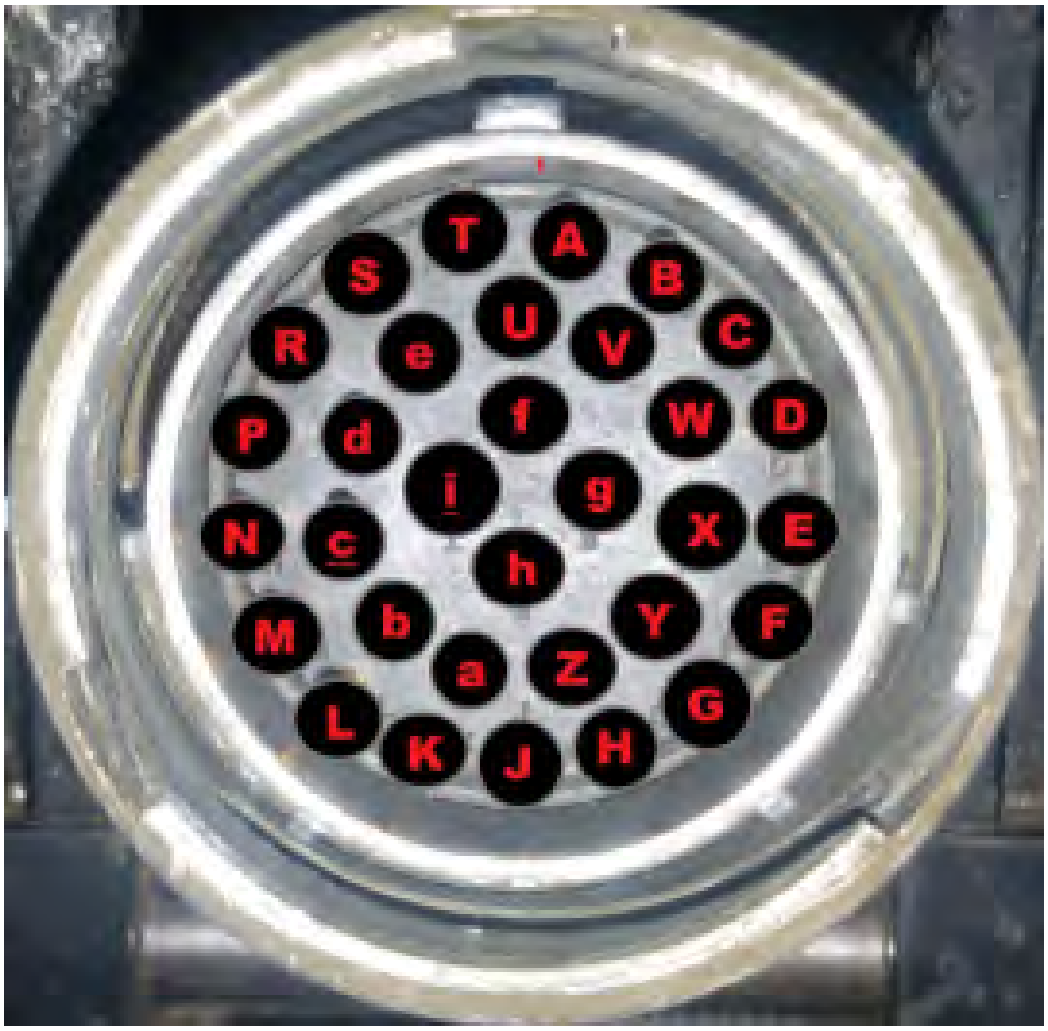

Figure 9.23: *Display of the naming convention used to determine the location of pins within each cable.*

A-H	F-C	L-L	S-S	X-X	c-c	h-h
B-G	G-B	M-M	T-T	Y-Y	d-d	i-i
C-F	H-A	N-N	U-U	Z-Z	e-e	-
D-E	J-J	P-P	V-V	a-a	f-f	-
E-D	K-K	R-R	W-W	b-b	g-g	-

Table 9.1: *Map displaying connection from one end of the cable to the pins, of the same configuration, on the other.*

Using the mapping scheme seen in Table 9.1, it is possible to efficiently move through each of the cables. Students discovered, while there are thirty-two channels in each cable, only eight are associated with the electrodes directly attached to the cable, while the other channels act as through conduits for electrodes further down the line. This means that should a cable be the first attached to the switch box, in a full array, all thirty-two channels are used, as all thirty-two electrodes worth of information has to pass through the cable. However, as a cable is further from the switch box, eight less channels are used for each position it moves. The end of the line, either electrodes 1-8 or 57-64, use only eight of the channels in a cable. Through the process of pinning out each of the

connections, the investigation found five cables had no errors in any connections. Cable 6 contained one broken connection, cable 4 had three broken connections, and cable 8 had fifteen broken connections.

No investigation of the ABEM control unit itself was done, the conclusion drawn as a result of the investigation was that all errors created are a result of the broken connections in the cables. As a rolling array was being facilitated when the electrodes all failed, the hypothesis was that the damaged cables had been located on the end of the array, but with the rollover, were moved to an inner position, making all of the channels in the cables necessary for operation, as opposed to only those channels associated with electrodes directly attached to the cables.

Knowing the amount of damage to each cable, students developed a cable layout which mitigates the impact of the damaged cables. The set up of the ABEM system, taking into account there are no replacement cables, was tested in the back of the 4H club. No data was collected by the system, the test was conducted purely to see if data can be retrieved from each electrode. Having set up the system, and running the electrode test, it was found that all sixty-four electrodes worked again. The configuration discovered to work for the ABEM can be seen in Table 9.2.

Cable Number	Electrode Number
Cable 6	1-8
Cable 2	9-16
Cable 3	17-24
Cable 1	25-32
Cable 7	33-40
Cable 5	41-48
Cable 4	49-56
Cable 8	57-64

Table 9.2: *Layout of ABEM cables for a working 64 electrode Wenner array*

The results of the of trouble shooting the ABEM, was a working 64 electrode array. However, one of the results of damage to the cables, was that a rolling array could no longer be used in data collection. Due to the fact that too many of the channels in a number of cables have been broken, it is not possible to move cables to inner positions within the array.

Processing and Interpretation Errors

Discrepancies occur between different interpolation programs. For example, the Surfer images and the DCIP2D images did not match up exactly because the programs interpolate with different algorithms. There is much more near surface variations in the DCIP2D image compared to the Surfer image due to this algorithmic difference.

Additionally, students added five percent to the standard deviation values from raw data for using the inversion code. When using the original standard deviation values, the images produced were very monochromatic and over-fitted. Five percent is added on to give a larger error bar for the code to fit models to fit to. This is necessary because when the standard deviation values are too small, the inversion code will try to over-fit the data by creating models that near-perfectly reproduce the data. This results in noise and uncertainties present in the data to be reproduced in the model. An ideal model reproduces the data within a degree justified by the uncertainty of the data provided. An interesting note is that the default DCIP2D protocol uses five percent of each measurement as uncertainty for inversion. The process in which students added five percent to the output standard deviation values from the ABEM device is remarkably similar to the default DCIP2D protocol.

Another processing error could come from the cell sizes selected for the mesh file. When creating a mesh file, the cell size affects the inversion algorithm. Larger cells will include more data points within it. For every

line, the cells have the same width but the height varies with depth. Cell sizes were adjusted to accommodate over-fitting or under-fitting the data. These values were chosen to have greater density near surface because this is the main area of interest. Padding cells were included around the main area of interest to remove unwanted effects on our calculated model due to boundary conditions.

A notable source of processing error comes from running inversions using DCIP2D without a suitable reference model. This has two primary effects. First, it causes the magnitudes of conductivities used for models in different inversions to be chosen arbitrarily. This makes it particularly difficult to determine rock formations based on typical conductivity values, as well as to make inferences on locations of formations from different surveys. Additionally, a reference model aids in creating a geologically sound model. When no reference model is used, it is more difficult to identify geological contacts. In the processing performed during this investigation, the most simple reference model for inversion is used - a half-space conductivity value. While this starting point for inversion allows the modeled conductivity values to be more consistent, it does not accurately recreate the subsurface geology and as such does not aid in better resolving geologic contacts and stratigraphy.

Some errors are also associated with interpreting the data. There are limitations in the extent of the data acquired. Only a portion of the main line was covered by DC (flag 1584 to flag 1900), SP does not cover any of the student site. This report attempts to correlate the SP and DC data together, however it is important to note these data gaps. In addition, this makes it difficult to cross correlate with other methods. Furthermore, the SP data is not inverted because students lack the programs available and the time to write an inversion code. While inverted data would be better for analysis and correlating datasets, the uninverted SP data is still useful because it shows the general trends in voltages. These trends can be used to infer flow directions.

Adjusting the number of interval contours in Surfer greatly affects the appearance of the model and how it is interpreted. The number of interval contours were chosen in an attempt to match plots created by DCIP2D. However, because the number of contours does seem to change the image significantly, and the number was chosen based off of only one other plot, this is likely a source of error.

Another source of error that may be present is the inversion of 2D data over a 3D space. Present along the lines are curves, as well as topography. This issue can be mitigated using topography files during the inversion process. A topography file will create the landscape when data is displayed, but it also changes the way in which geometric factors are calculated. In areas where hills are present, it is likely that high apparent resistivity is recorded, due to the fact that there is a section of air included in the half sphere, topography files allow the inversion to take this into account. Topography changes are present in all three of the lines which were measured. While the student site was largely linear, the main line had a significant amount of curvature, as a result of following the road.

Topography can play another role in creating error in the field DC data. DCIP2D is an inversion code intended for processing of 2D subsurface conductivity distributions. Therefore, DCIP2D can not account for conductivity contrasts perpendicular to the survey spread. While the survey lines used for DC surveying at the student site and the main line are roughly oriented perpendicular to geologic strike, topographic rises or drops can create apparent conductivity contrasts perpendicular to the line. At the main line, the topography perpendicular to the line consisted of hills to the North, and a stream valley to the South. This manifests as a conductive body to the North, and a resistive body (air) to the South, creating a conductivity contrast perpendicular to the survey line which cannot be accounted for using the DCIP2D code. Contrarily, at the student site, the topography is in-line with the survey line. Instead of following a stream valley with mountains on the other side, the line is oriented perpendicular to ridges and stream valleys in the area. As such, at every point on the survey line the topography in both directions perpendicular to the survey line is identical, eliminating potential conductivity contrasts in the orthogonal direction and allowing the subsurface environment to be more accurately approximated with a 2D conductivity distribution in DCIP2D.

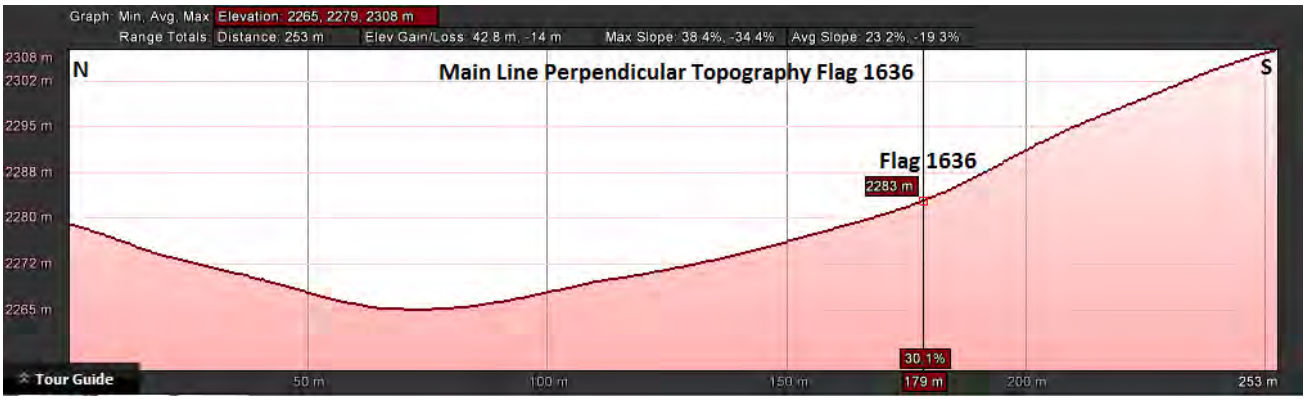

Figure 9.24: *Topography running perpendicular to the main line at flag 1636. Used to show error in inversion resulting from topography not on the inverted line. Significant topography changes can be seen to both the North, and the South of the line. This will affect the conductivity of the inverted data by a large amount.*

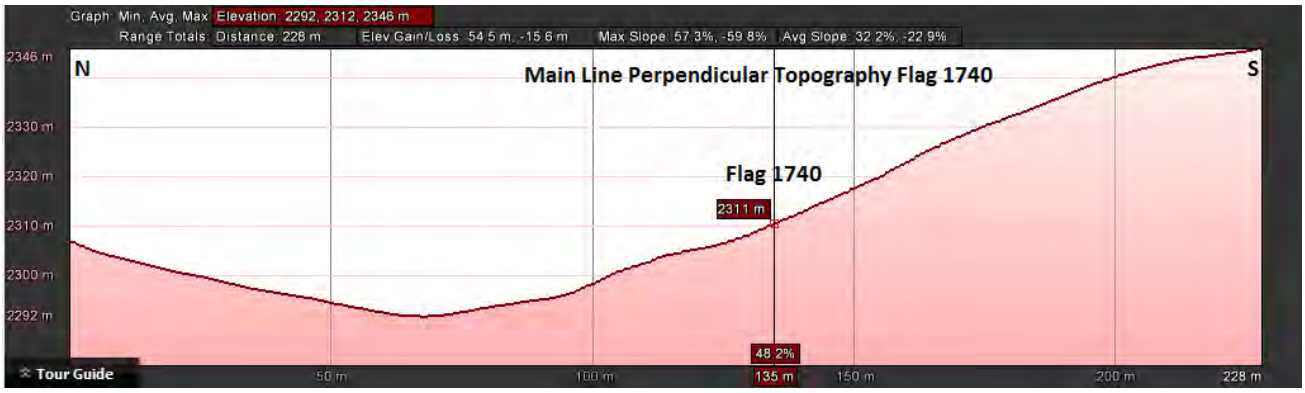

Figure 9.25: *Topography running perpendicular to the main line at flag 1740Used to show error in inversion resulting from topography not on the inverted line. Similar to the topography changes seen on the previous main line topography. It can be seen that to each side of the main line, there are significant changes in elevation.*

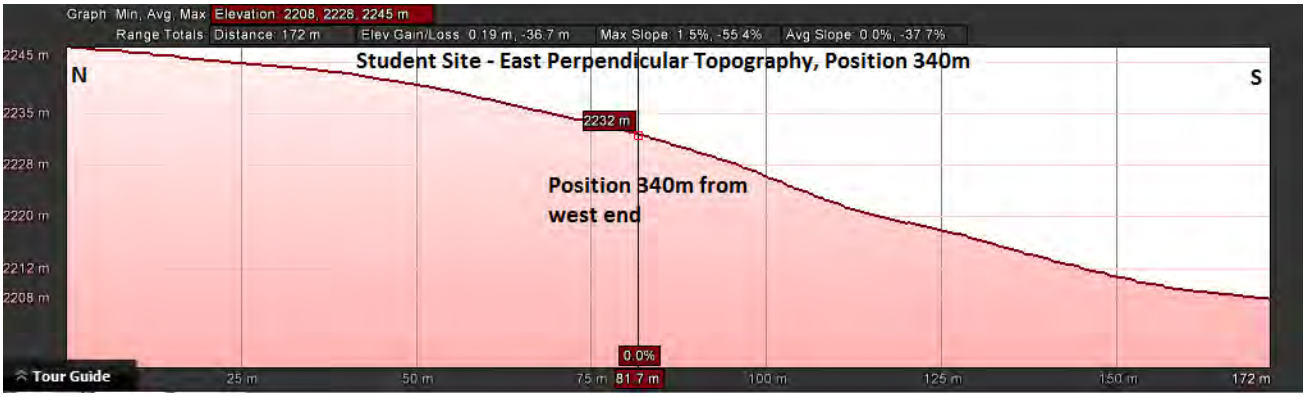

Figure 9.26: *Topography running perpendicular to the main line 340m in from the West end of the survey. Used to show error in inversion resulting from topography not on the inverted line. A large drop in elevation is present to the South of the line. While not as extreme as the changes in the main line, it causes error in the data.*

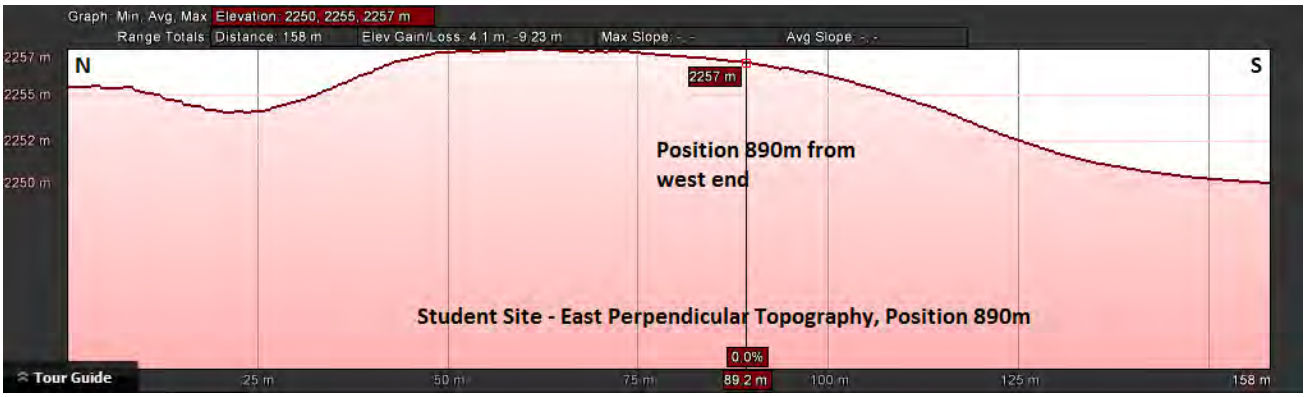

Figure 9.27: *Topography running perpendicular to the main line 890m in from the West end of the survey. Used to show error in inversion resulting from topography not on the inverted line. There is a slight change in elevation to the South, little to the North. Overall change in Elevation is not overly dramatic.*

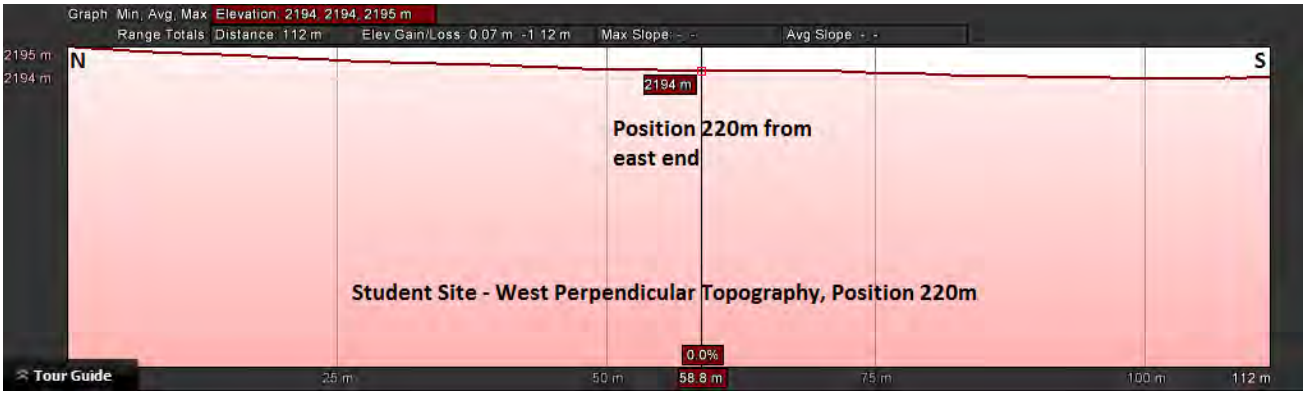

Figure 9.28: *Topography running perpendicular to the main line 220m in from the East end of the survey. Used to show error in inversion resulting from topography not on the inverted line. Little change in elevation is present.*

9.5 Conclusion

The DC Resistivity and Self-Potential data collected at the 2016 Geophysics Field Camp provided several insights into the subsurface geology of Pagosa Springs, CO. The SP effort was focused on 9km of the main survey line, along Mill Creek Road. After drift corrections, the data confidently identified the location of a subsurface dike on the eastern end of the line. It also showed the possibility of spring upwelling at the western end (towards the town center), but this section is complicated by cultural noise.

DC was interpreted over the main line, as well as at the student site. On the main line, data was collected using a rolling Wenner array. Following inversion of the data, as well as applying topographic effects along the line, the main line is seen to be largely conductive. The large area of conductivity observed, corresponds to Lewis Shale, as data moves toward the West, Mesa Verde Group becomes visible to the DC system. There is no direct indication of the dike in any of the DC data. Local topography, not located directly along the line, has a very strong effect on the data. Due to the fact that the line was done in an approximate valley, the presence of hills on the side of the line, violate the halfsphere assumption, under which data is inverted.

At the student site, the West line imaged the Niobrara lodged within the Mancos. This is characterized by a very resistive band present within a fairly uniform body, which is more conductive. This band approaches the surface on the West side of the line. Similarly, on the East side of the student site, a conductive band is present.

This conductive band appears to dip upward toward the West side. There is also a set of conductive bodies near the surface at high topography. At this point the Niobrara is deep enough to not be imaged, resulting in more conductive half spheres.

9.5.1 Recommendations

Overall the DC surveys at the Student Site proved to be more successful and produced better results. The mainline ran into multiple problems in the field, such as the demolition of the survey line and electrodes. The DC resistivity survey only spanned about 3.5km of the 11km main line. The survey did not span far enough West to gain good insight on possible water presence past the dike, or upwelling that may be occurring closer to the mother spring. The ABEM was down for half of the day May 22nd, 2016 and down for the full day of May 23rd, 2016. The lack of DC data on the West side of the mainline also inhibits the interpretation of the SP data. Without sufficient evidence from a resistivity data set the SP data is limited to just the interpenetration of the voltage differences. Due to time constraints there was no collection of SP data on the student site to compliment the DC data collected.

Further investigation can take place over the missed areas where SP and DC resistivity failed to collect data. Some complimentary data sets from SP over the student site would provide more insight on the subsurface. More information along the mainline spanning farther past the dike (located at flag 1673) could help confirm or disprove the hypothesis of water flow in a Westward direction from the dike. More analysis of the area surrounding our student site can be further investigated to try and locate a possible extension of the Victoire fault (discovered by Geophysics Field Camp 2013) into the subsurface.

The SP anomaly at the beginning of the main survey line indicating the possibility of upwelling could be more confidently analyzed with more detailed notes about cultural noise in the region. With more information about the location of buried cables, grounded power lines, and irrigation, the affects of this noise could be separated from the natural telluric response. The upwelling of the Mother Spring could be positively discovered with better data.

References

[1] S. C. A. Revil, J. Z. M. Karaoulis, and M. B. B. Raynolds, "The plumbing system of the Pagosa thermal Springs, Colorado: Application of image-guided geophysical inversion and data fusion", English, *Journal of Volcanology and Geothermal Research*, volume 299, pages 1–18, Jun. 2015. DOI: 10.1016/j.jvolgeores.2015.04.005. [Online]. Available: http://dx.doi.org/10.1016/j.jvolgeores.2015.04.005 (cited on pages 3, 111, 112).

[56] U. of British Columbia, *DCIP2d: A Program Library for Forward Modelling and Inversion of DC/IP Data over 2d Structure*, English, Jul. 2013 (cited on pages 113, 122).

[57] S. Cuttler, *ABEM Instructions*, 2016 (cited on page 119).

[58] N. P. F. Jones, *Glossary*, English, Jun. 2007. [Online]. Available: https://www.eoas.ubc.ca/ubcgif/iag/tutorials/glossary.htm (cited on page 123).

[59] M. Geoscience, *ABEM Terrameter SAS 1000/4000*, 2014. [Online]. Available: http://www.abem.se/resistivity/sas1000.htm (cited on page 118).

[60] D. R. S. Heather A.G. Stern and J. W. Tester, "Copper sulfate reference electrode", English, *Journal of Electroanalytical Chemistry*, volume 659, pages 143–150, Jul. 2011. DOI: 10.1016/j.jelechem.2011.05.014 (cited on page 114).

[61] C. E. C. Jonathan E. Nyquist, "Self-potential: The ugly duckling of environmental geophysics", *The Leading Edge*, number May 2002, pages 446–451, May 2002. DOI: 10.1190/1.1481251. [Online]. Available: http://library.seg.org/doi/pdf/10.1190/1.1481251 (cited on pages 120, 127).

[62] M. R. Sheffer, *Forward modelling and inversion of streaming potential for the interpretation of hydraulic conditions from self-potential data*, English, Dec. 2007. [Online]. Available: https://www.eoas.ubc.ca/ubcgif/pubs/theses/sheffer_phd_thesis.pdf (cited on page 114).

10. Magnetotellurics

Contents

10.1 Introduction

Magnetotellurics (MT) is a passive geophysical method that can measure resistive properties of the earth's subsurface at great depths, simply observing how the primary electromagnetic field affects them. When Earth's naturally occurring magnetic field reaches the surface, part of the energy is reflected and part is transmitted into the earth. Once the magnetic field has entered the earth, electric currents are generated, creating telluric currents. Induced eddy currents, in turn, create a measurable secondary field. Simultaneously, MT measures the time-varying components of the magnetic field in both the horizontal directions (H_x and H_y), and the vertical

direction (H_z), in addition to the electric field in the horizontal directions (E_x and E_y), induced by Earth's primary field [67]. A ratio of these components can be used to calculate the electrical resistivity of the subsurface, which varies with depth. MT can investigate depths of 300 to 10,000 m depending on the sampling frequency and length of the survey. The method is used for many applications including hydrocarbon, mineral, and groundwater exploration, and has been recently applied in deep crustal research [65]. The method was applied in the 2016 Field Camp survey for the investigation of a geothermal source and the characterization of subsurface geology in the area.

10.1.1 Background

Past field sessions have investigated the anomaly that is Pagosa Springs Hot spring, and the unexplained geothermal activity that lies beneath the surface. For many years, Colorado School of Mines has traveled to Pagosa Springs with the intention to explore and eventually explain what is happening within the subsurface of Pagosa Springs, including the source of the hot springs and the geologic features that may exist. The 2014 and 2015 camps surveyed similar areas near Chromo, Colorado, while earlier years have worked on areas closer to the Mother Spring. Unfortunately, MT surveys were not performed during these earlier years. Several wells have been drilled in the Pagosa Springs area, many of which have been used for important information such as resistivity and gamma logs. These help determine the physical properties and identities of the rock layers in the area and are useful for comparison and interpretation once the data is inverted.

10.1.2 Theory

The electrical properties of materials are characterized by electric field and magnetic field variations that occur in the subsurface. Magnetic fields have a source of moving charges (solar or lightning storms); thus, the changes within an electric field create a magnetic field, as displayed in equation 10.1 [67]. Electromagnetic (EM) energy that penetrates the earth can come from solar wind interaction with the Earth's field that creates low-frequency EM energy typically less than 1 Hz or from equator lightning storms that generates high-frequency EM energy typically greater than 1 Hz. High frequencies are effective at representing the near surface areas whereas the lower frequencies allow for seeing deeper into the subsurface. The frequency range between the high frequencies of lightning storms and the low frequencies from solar wind is called the dead band, as it is often difficult to record the frequencies within this range without measuring for multiple days or greater [63].

Electromagnetic fields are developed and described by Maxwell's Equations under the assumption that the Earth itself does not generate electromagnetic energy, thus the following equations in their differential form hold true:

Faraday's Law

$$\nabla \times \mathbf{E} = -\frac{\delta \mathbf{B}}{\delta t} \tag{10.1}$$

where **E** is the electric field (V/m) and **B** is the magnetic field (Tesla), thus as the electric field changes, because of moving charges, the magnetic field will change in time, or be induced.

Ampere's Law

$$\nabla \times \mathbf{H} = \mathbf{J} + \frac{\delta \mathbf{D}}{\delta t} \tag{10.2}$$

where **H** is the free magnetic field (A/m), **D** is the free electric field (C/m^2), and **J** is the current density (A/m^2)

Electric Gauss' Law

$$\nabla \cdot \mathbf{D} = \rho \tag{10.3}$$

where ρ is the electric charge density (C/m^3)

Magnetic Gauss' Law

$$\nabla \cdot \mathbf{B} = 0 \tag{10.4}$$

These equations in their constitutive demonstrate relationships between intrinsic properties such as conductivity (mS/s) σ, dielectric permittivity (F/m) ε, and magnetic permeability (H/m) μ that describe Ohm's Law.

Ohm's Law

$$\mathrm{J} = \sigma \mathrm{E} \tag{10.5}$$

$$\mathrm{D} = \varepsilon \mathrm{E} \tag{10.6}$$

$$\mathrm{B} = \mu \mathrm{H} \tag{10.7}$$

Mathematical relationships between measured electric and magnetic fields give an impedance $Z(\omega)$ that reflects the ratio of the acquired electric and magnetic field measurements, and can be calculated at the top of the half space through the following equation:

$$\mathrm{Z}_N\ (\omega) = (\alpha_N/\sigma_N) \text{ where } \alpha_i = \sqrt{i\omega\mu_o\sigma_i} \tag{10.8}$$

Here, μ_o is the magnetic permeability constant $4\pi * 10^{-}7$ H/m and σ_N is the conductivity at the Nth layer. In this scenario the half space has an infinite thickness, and assumes that there is no variation in the EM field, making the electric and magnetic components orthogonal to one another. These assumptions differentiate it from the remaining layers at the Earth's surface whose impedance is calculated by:

$$\mathrm{Z}_i(\omega) = \frac{\alpha_i}{\sigma_i}\ [\frac{\tanh \alpha_i d_i + \frac{\sigma_i}{\alpha_i} Z_{i+1}(\omega)}{1 + \frac{\alpha_i}{d_i} Z_{i+1}(\omega) \tanh \alpha_i d_i}] \tag{10.9}$$

Here, ω is the frequency, σ_i is the conductivity at the ith layer, and d_i is the thickness at that layer. For further investigation such as identifying important features or separating layers the impedance can be related to phase and apparent resistivity by solving for $\rho_a(\omega)$ and $\phi(\omega)$.

$$\rho_a(\omega) = \frac{1}{\omega\mu_o} |Z(\omega)|^2 \tag{10.10}$$

$$\phi(\omega) = \tan^{-1} \frac{ImZ(\omega)}{ReZ(\omega)} \tag{10.11}$$

In uniform scenarios such as the half space, $\rho(\omega)$ represents the true resistivity and in non-uniform spaces the above calculation will yield an apparent resistivity $\rho_a(\omega)$, the same applies for the phase of the scenario [67].

10.2 Objectives

1. Obtain impedance values from the collected electric and magnetic fields.
2. Convert impedance values to apparent resistivity.
3. Invert based on the apparent resistivity to recover what the subsurface looks like.
4. Support the interpretation of other geophysical methods and connect the data to surveys from field camps in previous years.
5. To find the heat source for the mother spring, by searching for a deep conductive body.

10.3 Methods

10.3.1 Survey Location

There were seven specific sites chosen in the area at which data was collected. At one of these sites, two surveys were performed in the exact same location to produce two separate data sets. Since a large amount of error occurs due to cultural noise, the surveys could not operate directly on or near the main line. In order to reduce the amount of noise in the data, the MT sites were located hundreds of meters to a few kilometers away from power lines, buildings, or evidence of piping or tunneling underground that would effect the survey. Figure 10.1 shows the survey sites in relation to the main line and the town of Pagosa Springs, where the Mother Spring is located. Each site covered a 100-meter by 100-meter area and was mostly symmetrical in regards to topography going North-South and East-West. The center of the survey is ideally flat and clear. Sites in close proximity were chosen for comparison, and the outer sites MT 6 and MT 7 had the purpose of investigating at different places in the area. Due to limited equipment, sites were set-up at locations then moved once the surveys were completed. The data from site MT4 was not used due to lack of quality.

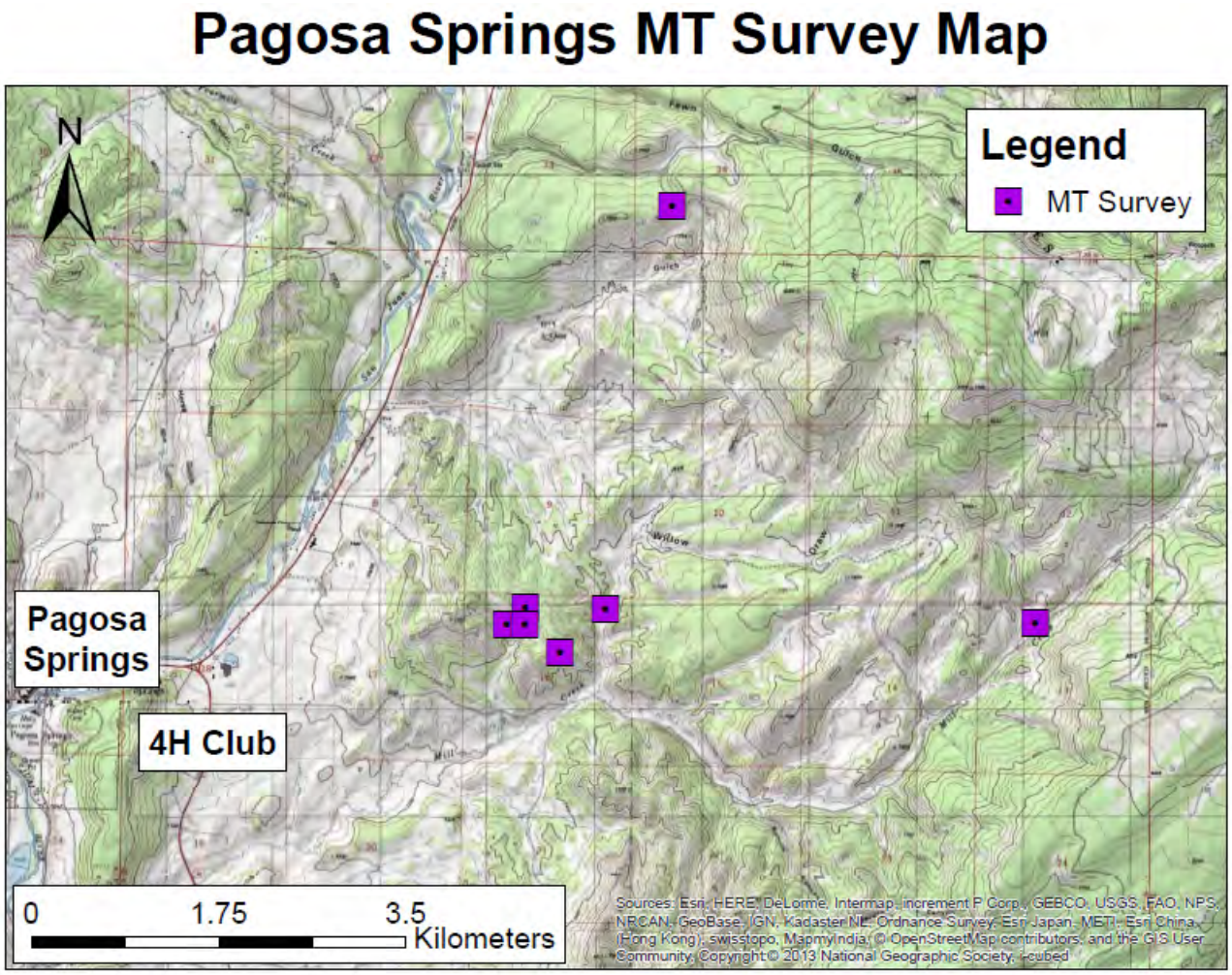

Figure 10.1: *The locations of the seven MT survey sites. These site, shown in purple, were chosen due to their accessibility and the distance away from cultural noise. Sites close to one another were chosen for comparison and the outlying sites were for the purpose of imaging different areas near the main line for a full interpretation of the area.*

10.3.2 Data Acquisition

The center point of a proposed site was chosen in order to maintain consistency with spacing and orientation. From a wooden stake placed in the center of the survey, four 50-meter lines were measured out directly with a compass for either true or magnetic North, South, East and West. Whether or not true or magnetic North was used does not affect the data, so long as the horizontal components are perpendicular. Wires were placed along these lines with buried electrodes connected at the ends. The three induction coils were buried roughly one foot deep and about 15-meters away from the center of the survey, and were oriented East-West, North-South and vertically for the z-component (if possible at the given site). The coils were connected with cables to the ADU box that lies in the center of the survey along with a laptop, GPS unit, and smaller wires that connected the electrodes to the system. Once all pieces of equipment were properly placed, the survey was set up using a laptop that controlled the ADU-07e box. A battery powered the system and a GPS was connected to the ADU-07e box prior to beginning the survey for a GPS time-based synchronization. The surveys were left to run for about 12 hours

and either picked up or continued the next day. The batteries had to be changed at least every 24 hours to ensure full performance and prevent survey error. Figure 10.2 shows the basic survey set-up. Any variation in set-up was due to equipment failure and topographic limitations, but few significant changes were made.

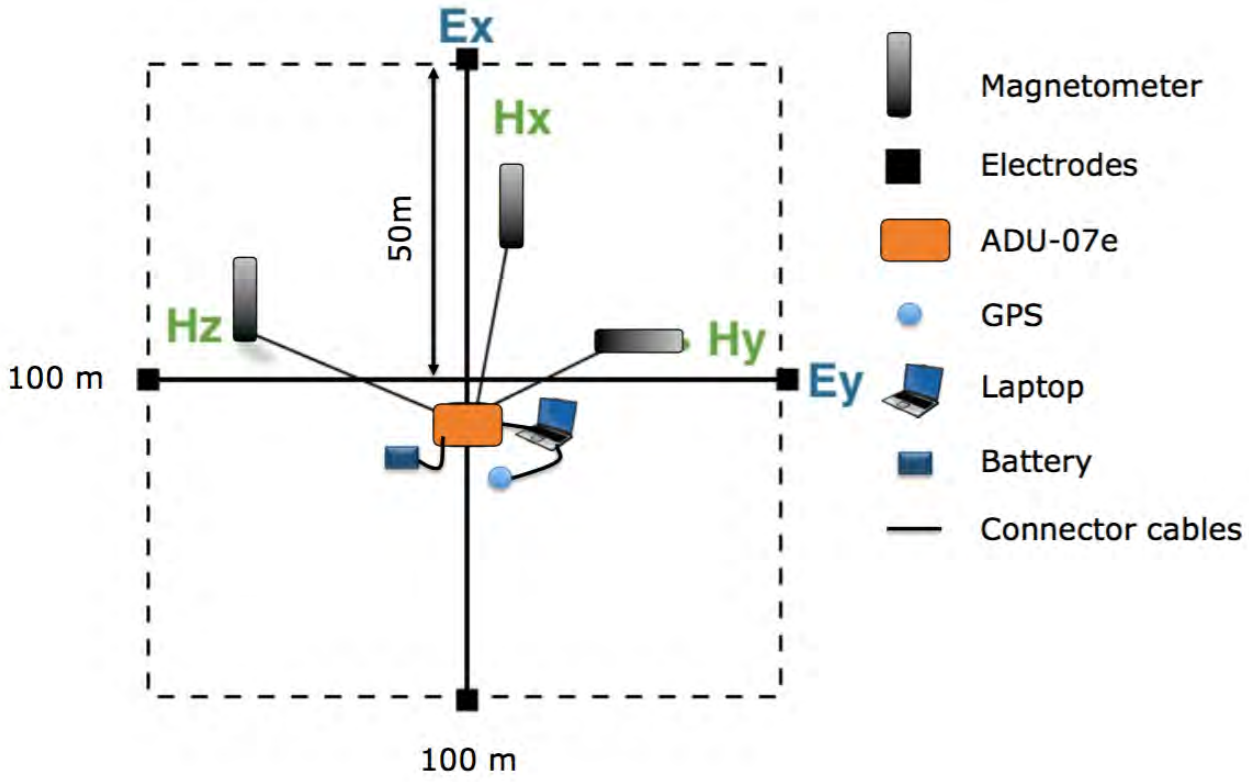

Figure 10.2: *Layout of an MT survey in the field. This setup is used for every MT survey no matter the location. Minor changes may include choosing to not set up one of the three magnetometers that would correspond to the H_z component. The H_x magnetometer is oriented North-South, the H_y magnetometer is oriented East-West, and the H_z magnetometer would be vertical and perpendicular to the ground.*

Equipment List

- **ADU-07e 24-bit Geophysical EM System**: Analog-to-Digital Unit that will be recording signal in the center of the survey
- **(3) Metronix MFS-07e Induction Coil Magnetometer**: read the telluric currents in the subsurface
- **4 non-polarizable copper sulfate electrodes**: are to be buried in each compass direction, may need bentonite to increase electrical contact with the ground
- **4 50m cables**: these will connect the ADU unit to the electrodes
- **3 10m cables**: these will connect the magnetometer to the ADU-07e
- **Mobile GPS**: allows the ADU-07 to correct for time drift during data collection.
- **Laptop**: interface to the ADU-07e, using the program AUD258 Setup LAN to navigate, initiate, and close out MT surveys
- **12V car battery**: to keep the laptop alive and power the ADU-07e

Smaller Essential

- **Wooden stake**: to be placed in the center of the survey for ease of reeling out cables
- **100m measuring tapes**

- **Shovel**: to bury the magnetometers
- **Compass + level**: to correctly orient and level the survey due North and for the placement of each magnetometer

10.3.3 Processing

In the field the data was downloaded from the ADU-07 onto the MT field laptop in .ats format. The data was then opened in *Mapros* for processing the recorded signals. This program allows for the data to be viewed as a time series where it can be filtered digitally from the original 512Hz to 2Hz or further. Our group ran frequencies of 512Hz, 128Hz, 32Hz, 8Hz, and 2Hz. The program also allows for editing of the data to find noise which should be removed to allow for a final smooth data set. Filtering the data was based around a consistency of signal across the related B and E components: H_x and E_y, or H_y and E_x. In addition to uncorrelated spikes, times of increased frequency of signal or times consisting of irregularly sinusoidal frequencies were targets for removal as these suggest artificial signals. After each iteration of editing, a (/4) digital filter was applied which uses selected stacking to reduce to the next frequency. Selective stacking takes data that does not have a remote reference (a nearby site for comparison) and correlates the x and y components for magnetic and electric field to one another, filtering the data accordingly [64]. It is essentially the same processing of manually filtering the data; however, it is unsure to what extent this operation works. Although we do have nearby sites, remote referencing is not used due to a lack of available coordinates. Instead, sites in close proximity are compared and analyzed after processing. The success of modifying the data can be seen in Figure 10.3 where it is desirable that the data return to a coherency of 1 after an expected dip in the dead band. This coherency plot updated after each frequency was run so that the progress was visible. In *Mapros*, upon smoothing and filtering the data a Fast Fourier Transform was applied by choosing 'Start Processing', switching the data set from time domain to frequency domain, which is necessary for finding the apparent resistivities. It is important to ensure that after selecting 'Start Processing,' the 'Don't use marked parts' box is checked under the 'Advanced' tab within the Processing options [64].

The edited data was exported from *Mapros* as a text file. This is done by choosing 'Export ASCII' and specifying the bands that were filtered. The exported file required modifying the 27 columns of information that were included. Refer to Table 10.1 for a list of what values these columns represent. This file was reformatted in order to be readable into the program *ipi2win* through the use of Excel Workbook. This file included the square root of the period, apparent resistivity, and phase. The value used to represent the square root of the period was $1/f$, as this gave an approximate representation for our purposes. Due to repetition of apparent resistivities and phase in *Mapros* with the different frequencies, it was necessary to average each of these values if repeated for certain frequencies. Two files with this information were made for each site 1-7, one with xy data and one with yx. The difference in this data is due to the orientation (xy represents the E_x and H_y and yx represents E_y and H_x). The goal was to create a generally smooth curve for each orientation to represent the data and to have no repeating values. The files were downloaded as a **.mt** file and that could then both opened and overlain in *ipi2win*. This program was selected due to its inherent ability to produce consistently pulchritudinous apparent resistivity curves. It is important to note that two sets of data were processed for MT 3, however one was ignored due to obvious equipment failure during the survey.

Once opened, the displayed graphs represent the apparent resistivity and phase curves for each site. The graphs were assigned a best-fit line and a model that represented the subsurface layers, which could be done by manually inputting the number of layers and adjusting their resistivities or letting the program invert the data [66]. Due to large amounts of noise still existing within the data, the error bars often became too large to be effective before the model reached a depth greater than 5 kilometers. Figures were created with error bars included; however, many of the error bars were too large and did not even appear in the model. Since the error bars did not appear, there was no range of resistivities to try to match to, and therefore, were removed.

Column	Information
1	MT Site
2	Band
3	Frequency (Hz)
4	$Z_{xx,real}$
5	$Z_{xx,imaginary}$
6	Z_{xx} variance
7	$Z_{xy,real}$
8	$Z_{xy,imaginary}$
9	Z_{xy} variance
10	$Z_{yx,real}$
11	$Z_{yx,imaginary}$
12	Z_{yx} variance
13	$Z_{yy,real}$
14	$Z_{yy,imaginary}$
15	Z_{yy} variance
16	$Tx, real$
17	$TX, imaginary$
18	$Ty, real$
19	$Ty, imaginary$
20	ρ_{xy}
21	ϕ_{xy}
22	ρ_{xy} variance
23	ϕ_{xy} variance
24	ρ_{yx}
25	ϕ_{yx}
26	ρ_{yx} variance
27	ϕ_{yx} variance

Table 10.1: *Column identifications for the ASCII export from Mapros. Z refers to the impedance tensor, T refers to the 'Tipper' or vertical magnetic field H_Z, ρ refers to resistivity and ϕ is the phase. Columns 3, 20, 21, 24 and 25 were used.*

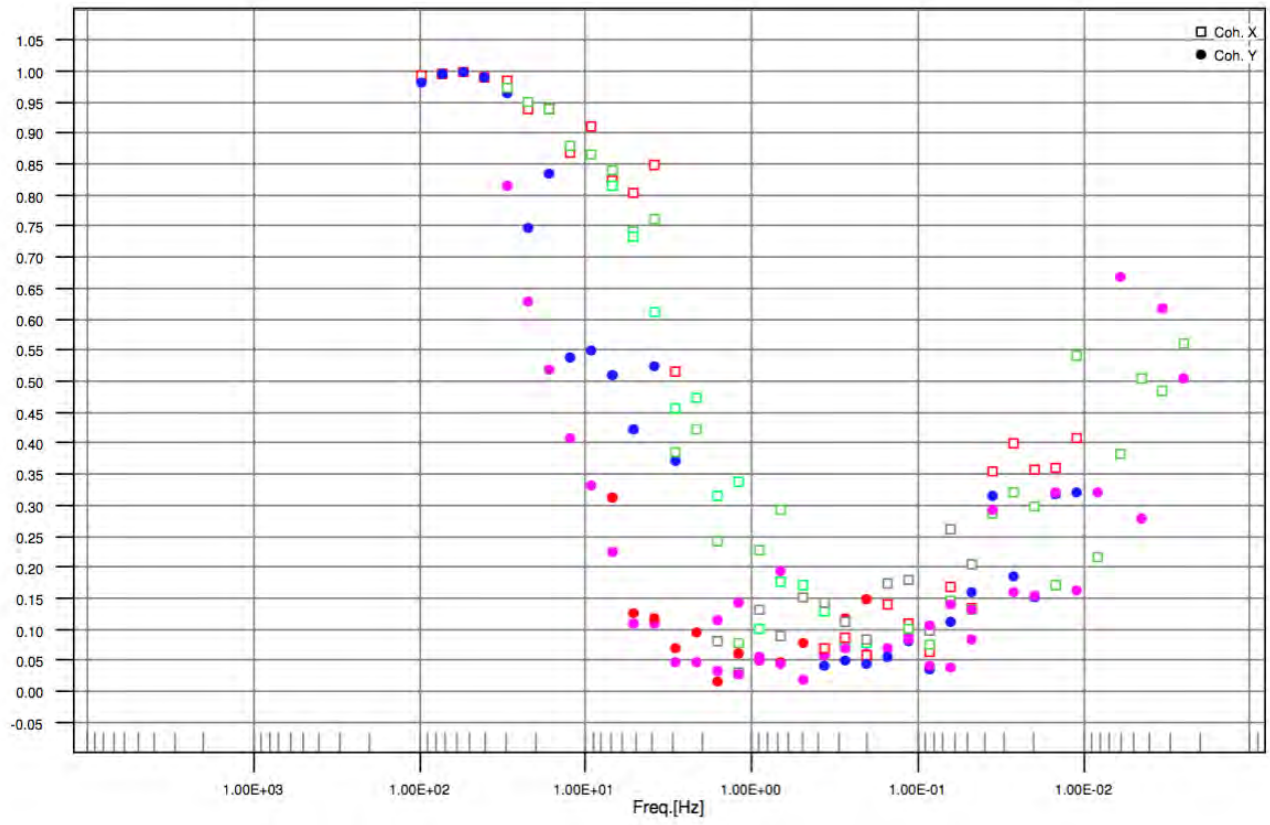

Figure 10.3: *Graph of coherency. The "U" shape is an expected result due to the dead band of frequencies that occur. In a best case scenario the coherency would return back to one, but a limited amount of run time for the MT survey restricted this ability. The closer the points are to a value of 1.0, the more confidence we can have in our data.*

10.4 Discussion

10.4.1 Expectations

Forward modeling was not used as a preliminary step for processing this data; however, there were initial expectations that allowed the assessment of data quality. It was expected that depths of 300-2000 meters would be seen due to the comparison of survey lengths and results from the 2015 field camps, which would allow basement material to be identified in many cases. Another expectation was that sites MT 1, MT 2 and MT 3 would show similar results, considering that they were all in the range of a couple hundred meters and were placed at similar elevations. Due to the presence of the Mother Spring and several other smaller hot springs nearby, it was predicted that geothermal activity may be identified through the inversion of the apparent resistivity and phase curves.

10.4.2 Results

Since MT is a method that can observe properties at great depths and we know that basement rock is going to be rather resistive as seen in Figure 10.4, we can use MT to help confirm actual depth to basement. Other geophysical methods that are capable of having a depth of investigation as low as the basement rock in Pagosa Springs only get a vague idea of its depth, while MT can help pinpoint its location.

The few sites that were not bunched together (MT 5, MT 6, and MT 7) contained a considerable amount of noise within the data sets. Even after removing the irregularities, there was a poor signal-to-noise-ratio (SNR). To account for this, we averaged the resistivity and phase values from the remaining site: MT 1, MT 2, MT 3, and MT 4. The averaging of these sites resulted in an inversion model that seemed more realistic due to where we could place the basement rock. Although these models were not run long enough to attain a reliable signal at lower frequencies, we collected enough reliable signal to have relatively precise depths for up to around 10 kilometers. Furthermore, any depths deeper than 10 kilometers are not easily observed.

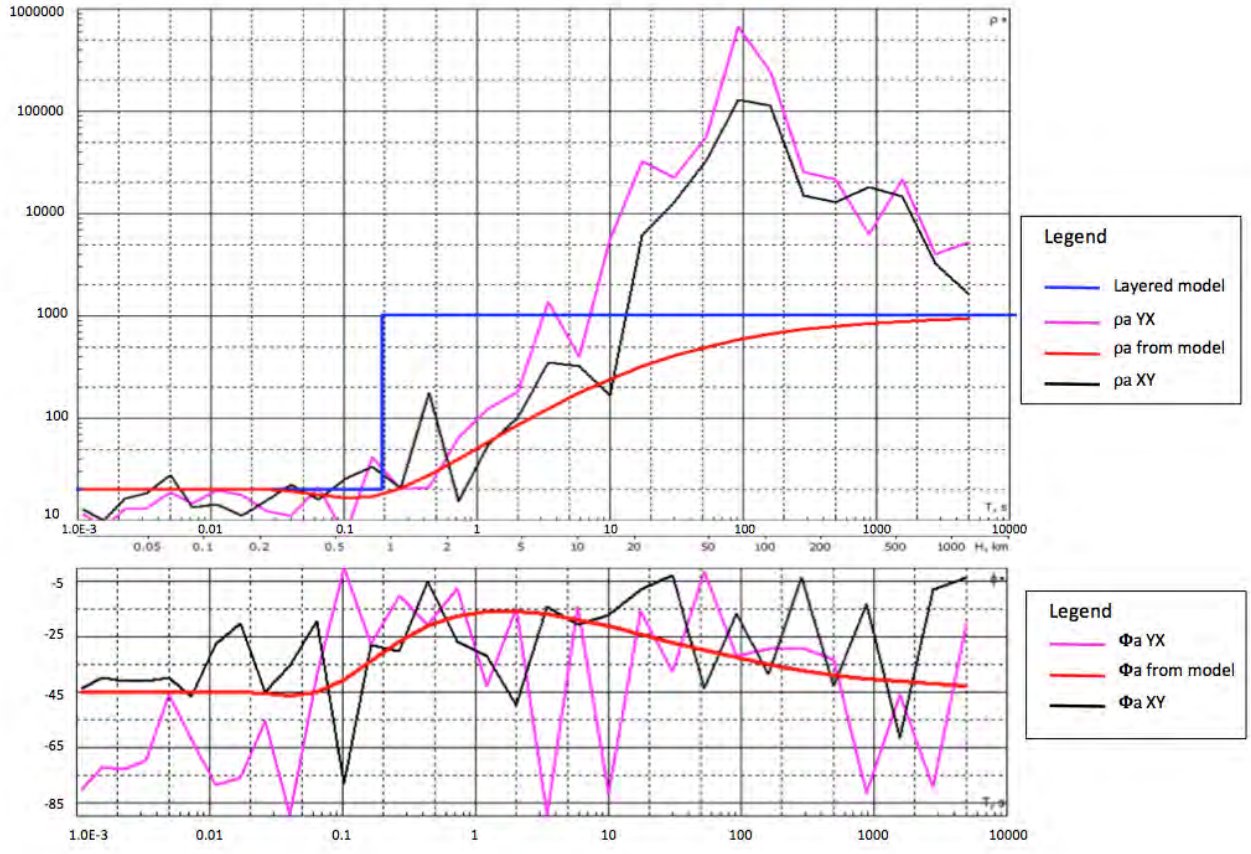

Figure 10.4: *Inversion model. This model was created in the ipi2win.MT program by averaging the resistivity and phase values from sites MT 1-4. It was expected that the layers closer to the surface would be relatively more conductive, and we should see a rise in resistivity due to Precambrian basement rock. The averaged sites were from points north of the line and was projected with geology to flag 1360. Due to the length of time the surveys were performed, the confidence in the data and accuracy is only accurate to roughly 10 km. This model shows the apparent resistivity of the model (red line) diverging from the inverted resistivity (black line) just past 10km of depth. A large jump from a low to a high resistivity can be seen around 900 meters depth.*

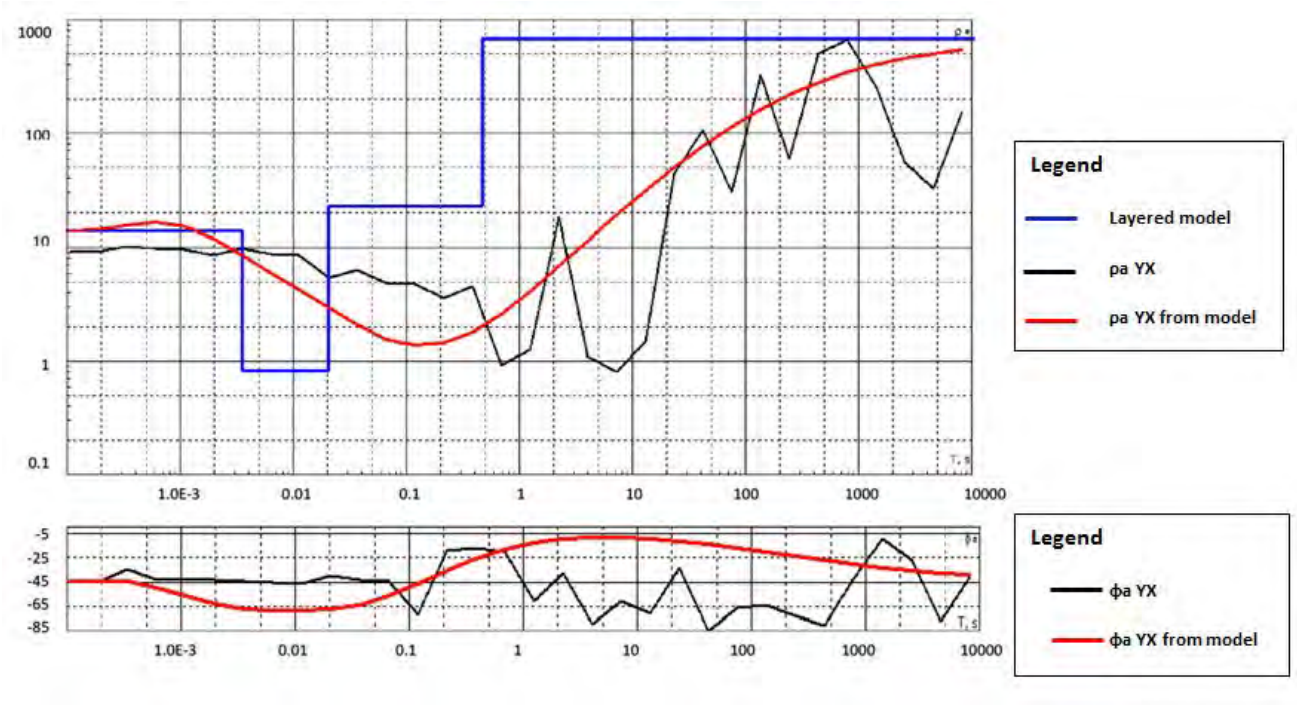

Figure 10.5: *Inversion model. This model was created in the ipi2win.MT program with the data collected at MT site 6. It was expected that the layers closer to the surface would be relatively more conductive, and we should see a rise in resistivity due to Precambrian basement rock. The data was collected far north of the line but projected back to the line using a geologic map. Due to the length of time the surveys were performed, the confidence in the data and accuracy is only accurate to roughly 10 km. This model shows the apparent resistivity of the model (red line) diverging from the inverted resistivity (black line) just past 10km of depth. An increase in conductivity can be seen in the upper 200 meters before leveling off until around 1300 meters where a large jump in resistivity occurs.*

10.4.3 Interpretation

The results of our MT data processing produced an apparent resistivity plot with respect to depth on both the west and the east side of the dike. Figure 10.4 shows results from the west side, at Flag 1360. One can see an upper resistivity of around 20 $\Omega * m$, which is to be expected for the general behavior of the sedimentary geologic layers of the area that range from roughly 10-30 $\Omega * m$. At a depth of approximately 900 meters from the surface, there is a jump in conductivity to 495 $\Omega * m$, which is representative of a relatively resistive layer that can be interpreted as the basement contact. The curve was not fit to further depths as the survey times stretched from about 12-24 hours at most, resulting in a limited depth of investigation.

Figure 10.5, shows a site east of the dike around Flag 1900. Here, one can observe a more variant resistivity plot. In the upper 50 to 150 meters an increase in conductivity can be seen, which may confirm the existence of the Lewis Shale with existing water saturation. Below this, resistivity of around 22.7 $\Omega * m$ is seen, which was interpreted as an average representation of the sedimentary geologic layers of the area. A large decrease in conductivity is seen below this, representing basement material. Only one orientation of electrodes and induction coils (YX) was used in the image because the data in the other orientation did not show results consistent with the local geology, potentially due to data processing issues. Another site projected to approximately the same location provided similar results, but was more noisy and therefore not included.

Between Figure 10.4 and Figure 10.5, a basement depth of 900 meters from the location can be observed, projected from Flag 1360 to a basement depth of around 1300 meters down from surface at Flag 1900. This represents a basement elevation of 1390 meters above sea level right at Flag 1360 and a basement elevation of 1070 meters above sea level at Flag 1900. This interpretation of the drop in basement elevation across the line from West to East is expected because the direction of dip.

10.4.4 Errors and Uncertainty

MT surveys are sensitive to the smallest of changes in electric fields or magnetic fields occurring within a kilometer of the survey site. Any electric currents occurring in the area would induce a magnetic field and would both be detected by the MT survey. This means power lines, electric fences, or proximity to houses would cause a great deal of noise because of the resulting telluric currents in the subsurface that are not easily seen; turning on/off at all hours of the day. Ideally, an MT site should be set up on a large flat area to minimize errors with topography or differences in detection of electromagnetic fields in any specific direction. Houses were not always visible from the survey locations; however, survey locations were kept to an optimal distance from the roads, any nearby houses and somewhere relatively flat. Although the surveys were run overnight in order to reduce the amount of human activity near the sites, it is possible that humans or even wildlife could have approached and tampered with the equipment. This is unlikely, however, because there are no major errors in the data sets. Overall, lighting storms were avoided during the time the surveys were running. However, it is noted that there was most likely a storm during one of the nights that the MT 7 site was running. This may have created false signals that will affect the interpretation of the data.

During processing, we attempted to digitally filter out errors and artificial noise. As stated in Section 10.3.3, the data was analyzed at six different frequencies and unwanted data was marked and filtered from the data. Spikes and periods of anomalous data were cut from the time series because they were indicators of artificial noise. Large jumps and abrupt changes in the data were representative of this, as naturally occurring signals show a more gradual trend. In certain data sets, the coherency decreased throughout the filtering process, leading to the unfiltered data being used as the input for the inversion codes. This subjective aspect to filtering data could result in missing important signals by removal or including misleading noise in the data, if not removed.The lack of an established method of filtering data leads to different interpretations of similar data.

Error was quantified with error bars used in the inversion program. For almost all of the data sets, the error bars quickly increased in size as depth increased, and would sometimes not even appear on the image. This means the confidence in the data is decreasing as depth increases, so error bars were excluded from the inverted images. The unconstrained resistivities were used instead, which could lead to some degree of error.

10.5 Conclusion

The goal of magnetotelluric surveys on the main line was to confirm the basic geologic structure that was concluded by other geophysical methods; in addition to potentially identify geothermal activity in the area. After digitally filtering and smoothing the raw data from the 7 MT sites, it was inverted from the generated apparent resistivity and phase curves. The inversions exemplified a model of the subsurface, showing changes in resistivity with depth. Due to the availability of data in close proximity, an average was calculated that allowed a more accurate interpretation of the geologic structure in the area. The results identified the depth of the basement rock and suggested the existence of a conductive layer in the upper 200 meters on the east side of the dike. This information coupled with results from other geophysical methods helped to confirm the overall thicknesses of the overlying beds and the location of the basement.

10.5.1 Recommendations

The main recommendation would be to run more surveys at sites in closer proximity to locations investigated this year. Doing this will allow a more in-depth comparison to ensure that the surveys are consistent. Having TEM data at similar locations would also be useful, since it would allow the comparison of 1D features to incorporate into a 2D prediction. Although it is difficult, choosing survey sites that are more remote may improve data as well. It is important that MT surveys are performed at least 1 kilometer away from any cultural noise, which was difficult to accomplish with the time and terrain constraints of the field schedule. Having access to additional private properties and roads, with the goal of accessing remote locations, may make this easier. As explained in Section 10.1, the depth of investigation varies with sampling frequency and time. Longer surveys may be performed in order to see at greater depths and obtain data regarding the subsurface. Further investigation for geothermal activity using a combination of geophysical methods in the Pagosa Springs area is recommended for future field camps.

References

[63] K. R. Christopherson, *Mt gauges earth's electric fields*, 1.0, AAPG, AAPG Explorer, Jan. 1999, pages 22–31 (cited on page 140).

[64] B. Friedrichs, *Mapros*, 0.87b, Used for information on exporting, Metronix, Metronix, Jan. 2007 (cited on page 145).

[65] Geometrics, *Geophysical methods-magnetotellurics*, Geometrics, Jan. 2015 (cited on page 140).

[66] D. o. G. Moscow State University, *Ipi2win user's manual*, 2.0, Used for inversion, Moscow State University, Geoscan-M Ltd., 2002 (cited on page 145).

[67] G. D. Naidu, *Deep crustal structure of the son-narmada-tapti lineament, central india*, 1.0, Berlin, Germany: Springer-Verlag, Jan. 2012, pages 13–28 (cited on pages 140, 142).

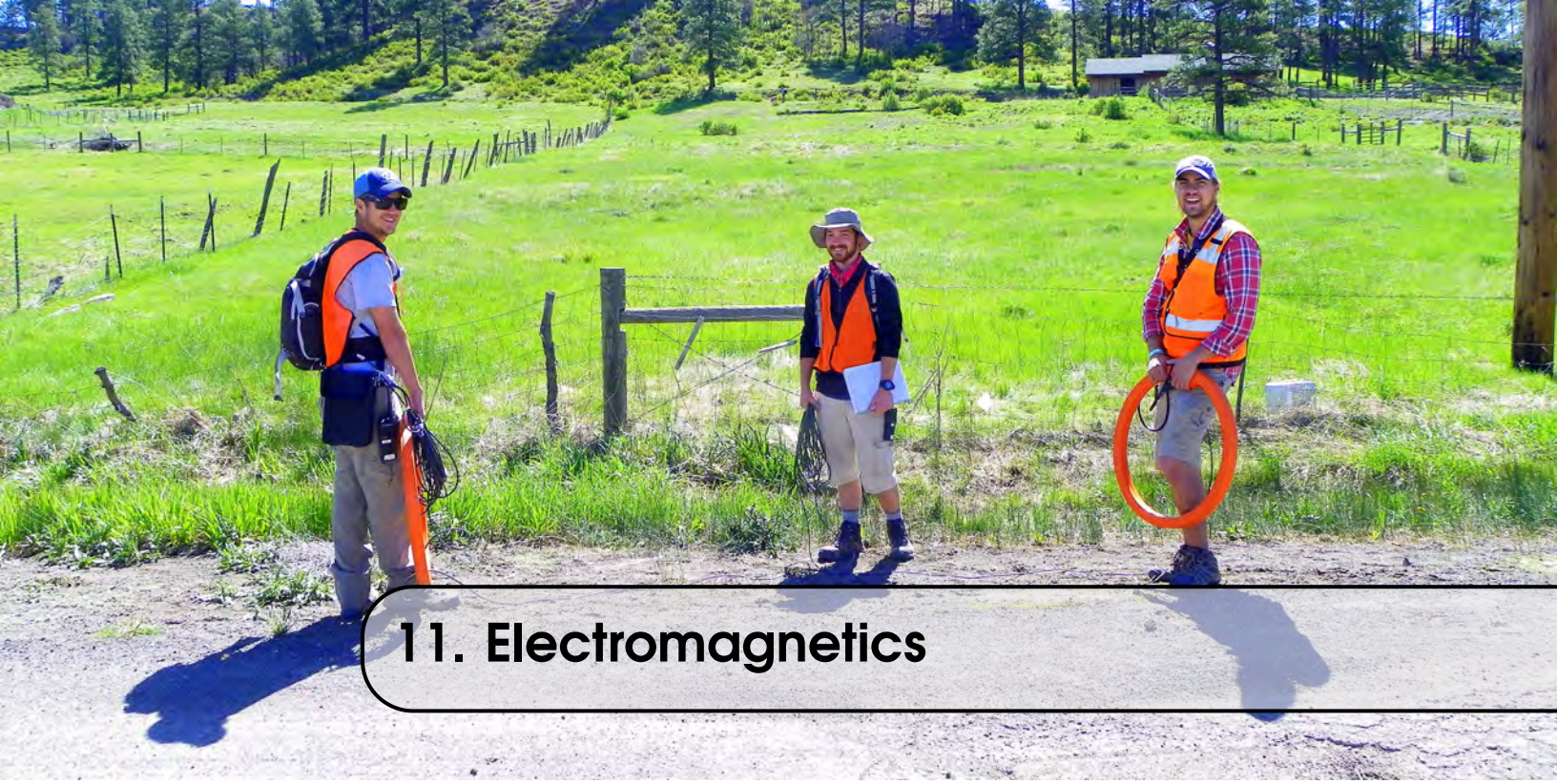

11. Electromagnetics

Contents

11.1 Introduction

There are two main types of active source of geophysical electromagnetic methods: time domain EM (TDEM) and frequency domain EM (FDEM). Time domain electromagnetic (TDEM) methods, occasionally referred to as TEM or transient electromagnetics, are used to obtain a one dimensional vertical profile of the electrical conductivity of the subsurface. This is used to characterize the rock type. For example, shales have a higher conductivity than dry quartz rich sandstones. This allows us to identify the approximate depth of the contacts between formations. TDEM is used to obtain conductivity profiles extending to depths of several hundred meters, depending on the subsurface characteristics, the transmitter frequency, loop size and the amount of noise in the

data [77]. By conducting multiple soundings in an area, we can develop an idea of the regional behavior of the subsurface, including any heterogeneity, which could be indicative of a fault, or of a significant change in the fracture/joint patterns.

Frequency domain electromagnetic (FDEM) methods are similar to TDEM and are used to map conductivity values of the subsurface. The conductivity values correspond to depths depending on the frequency at which the current oscillates, as well as the distance of separation and size of transmitter and receiver coils.

TDEM is more deeply penetrating than FDEM and is often used to generate a vertical conductivity sounding that can be used to constrain other methods, or to identify the contacts between different geologic units or zones of differing fluid content and composition. As a result TDEM surveys are often used for mineral and groundwater exploration, and for environmental mapping and monitoring of things like contaminant plumes. TDEM methods also can be used for unexploded ordinance detection and location [77].

FDEM surveys can be used for many of the same applications as TDEM, although these are generally limited to a much shallower depth (typically tens of meters). However, because FDEM methods typically record values corresponding to the conductivity at a relatively consistent depth, they can be used to quickly generate a map of how conductivities vary laterally near the surface. This is particularly useful for identifying changes in water saturation, pipes, buried cables, structures, metallic objects (like unexploded ordinance), disturbed areas (like a hole that was filled in), and vertically oriented, near surface features (like a dike hidden by a thin layer of overburden). Both FDEM and TDEM methods are often used for large scale surveys or initial exploration surveys because they don't need to be in contact with the ground so they can be mounted on aircraft or towed behind ships, enabling more rapid data collection. This is also advantageous in situations where we wouldn't want to disturb the ground, like at an archaeological site where placing electrodes may damage artifacts, or in a minefield where a person on the ground is at risk of accidentally triggering an explosion.

There have not been extensive investigations of the geology to the east of Pagosa Springs where we conducted our main survey. This meant existing information was limited to geologic outcrops, and a few boreholes. The outcrops were infrequent because of vegetation and weathering of the shale at the surface. The few boreholes in the area provided limited data, particularly at the near-surface (most of the wells were cased near the top, and thus were not logged at near surface) [71] [79] [69]. Previous field sessions have conducted extensive investigations in nearby areas, and have identified several previously unknown faults, some of which may have a significant impact on groundwater flow. Several previous surveys have also concluded that the Dakota Formation is highly fractured throughout the region, and may be facilitating significant groundwater flow. The main survey line has relatively well known surface geology; however, because of the limited number of well logs we have access to, we do not know the depths or thicknesses of the subsurface formations with a high degree of certainty along this line. Using TDEM soundings in several locations along the main line, we can identify the depths of the formations which are distinguishable by changes in their conductivity. This allows us to create a control point for other methods like gravity or seismic imaging.

The student survey site is located to the northeast of Pagosa Springs. Students chose this site with the intention of determining if the Victoire fault, discovered immediately east of the main Mother Spring by the 2012 Colorado School of Mines Geophysical Field Session, extends to the north of it's known position, possibly connecting to the Northline faults also identified by the 2012 field session near the west end of the Student Site [79]. Because we don't have any borehole logs for this particular area, and we were unable to locate any outcrops or exposed surface contacts between formations, we have very little information on the subsurface. We expect to see some sort of conductivity contrast in the subsurface representing the top of the Dakota Formation (sandstone) which should be below the overlying shale. This would give us information to use when interpreting and processing the other methods used on the site, like gravimetry and hammer seismic.

11.1.1 Theory

The physics behind FDEM and TDEM are very similar. In both cases, a transmitter puts current into a loop of wire. This generates a toroidal magnetic field surrounding the transmitting loop as described by Ampère's law,

shown in equation 11.1. With a transmitter loop oriented horizontally on the ground surface, a portion of this magnetic field penetrates through the subsurface, and induces a current flow in the subsurface. Ampère's law is as follows:

$$\vec{\nabla} \times \vec{B} = \mu_0 \vec{J} \tag{11.1}$$

where $\vec{B}$ is the magnetic field, μ_0 is the magnetic constant (equal to $4\pi \times 10^{-7} N/A^2$), and J is the current density in the transmitter loop.

For TDEM, we abruptly shut off the transmitter current which leads to a back-EMF effect that generates a ring of current flow immediately below the transmitter wire in the subsurface. This ring of current generates another toroidal magnetic field, as described by Faraday's law, shown in equation 11.2. The result is a series of 'smoke rings' of induced current that move downward and expand outward over time as dissipation occurs [80]. A graphical representation of this concept is shown in figure 11.1. The rate of movement and dissipation is affected by the conductivity of the material the smoke ring travels through. Using receiver coils, we can record the way the current ring decays and moves through the subsurface by measuring the magnetic field it generates. This allows us to calculate the apparent resistivity of the subsurface using the formula shown in equation 11.3. A trio of receiver coils, oriented in orthogonal x, y, and z planes, are used with the TEM-47 system which allows 3D interpretation of the subsurface. With the TEM-57 system, only one receiver coil is used, meaning only a 1D sounding is recorded.

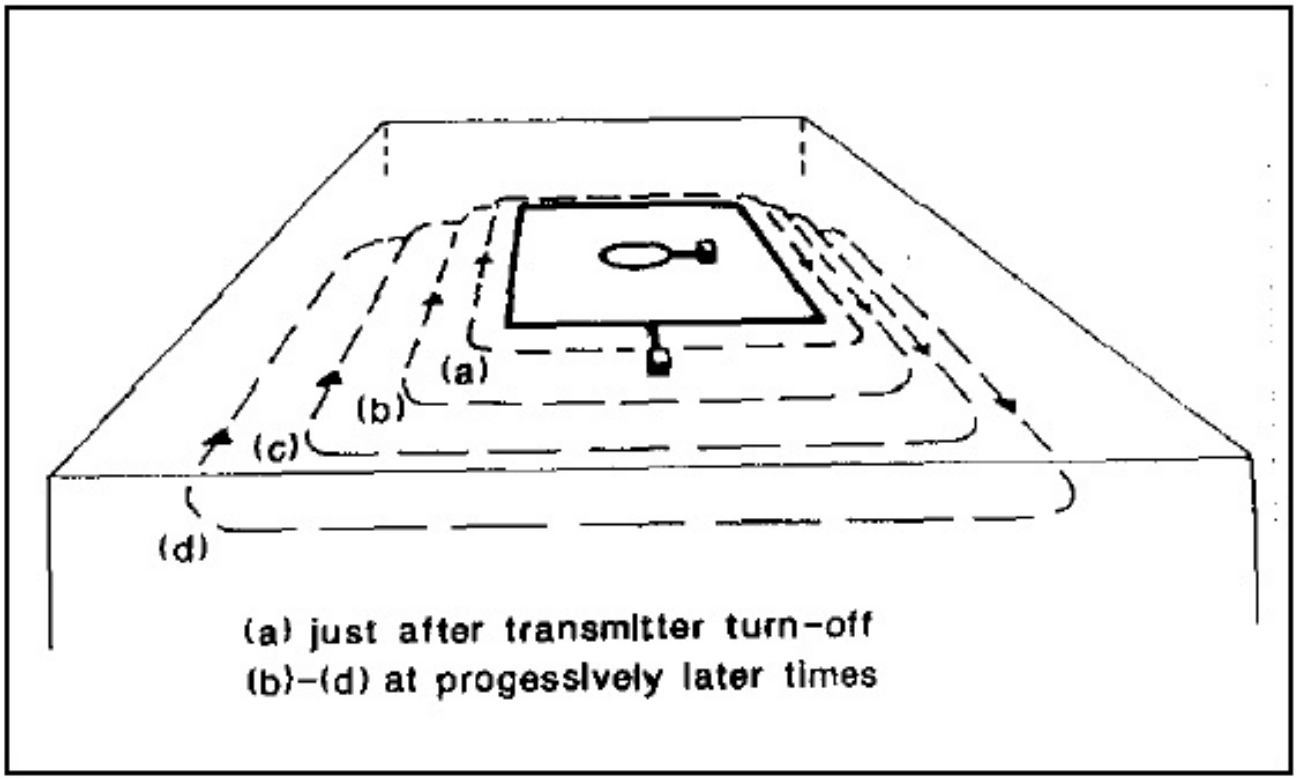

Figure 11.1: *Diagram showing the way the 'smoke rings' form and propagate downward and outward [82].*

Faraday's law is:

$$\vec{\nabla} \times \vec{E} = -\frac{d\vec{B}}{dt} \tag{11.2}$$

where $\vec{B}$ is the magnetic field and $\vec{E}$ is the electric field. Below is the relationship between the observed magnetic field and apparent resistivity of the subsurface.

$$\frac{\delta B_z}{\delta t} = \frac{I\sigma^{\frac{3}{2}}\mu_0^{\frac{5}{2}}a^2}{20\pi^{\frac{1}{2}}}t^{\frac{-5}{2}} \tag{11.3}$$

where B_z is the z component of the magnetic field, σ is the conductivity, μ_0 is the magnetic constant, t is time, and a is the receiver coil area.

The concept of skin depth is very important for time domain electromagnetics, as it limits the maximum depth of penetration that we can achieve. Skin depth is the depth in a particular medium at which the amplitude of the signal decreases by a factor of $\frac{1}{e}$. The equation for skin depth is shown in equation 11.4. With this relationship you can see that as the frequency of the alternating current and as the conductivity of the medium increases, the skin depth decreases, limiting the depth we can observe as the source signal decays faster. We used the following skin depth equation:

$$\delta = \sqrt{\frac{2}{\omega\sigma\mu}} \tag{11.4}$$

where ω is angular frequency (1/s), σ is conductivity (S/m), μ is the permeability of free space, ($4\pi \times 10^{-7} N/A^2$), and δ is skin depth.

FDEM operates on the same physical concepts as TDEM, except FDEM uses a sinusoidal alternating current, as opposed to the square-wave based current shutoff sequence used by TDEM. This difference in transmitter current dictates the different ways in which TDEM and FDEM are used and recorded. Since TDEM uses abrupt current shutoffs, the voltage induced in the receiver must be carefully recorded as a decay of voltage with respect to time. Since FDEM features a current alternating at constant rate with respect to time (typical AC), the voltage induced in the receiver is a constant value at each measurement station. It depends only on the frequency used, which, because of the skin depth effect, can be used to set the maximum depth we want to observe based on the conductivity of the subsurface.

The relationship between the magnetic field and conductivity/resistivity can be described by rewriting Faraday's law into equation 11.5 using Ohms law. Since for FDEM the magnetic field changes in a constant fashion with respect to time, a constant electric field will be produced. If a specific frequency is used, the current density (J) induced in the medium depends directly on the conductivity of the medium, where they have an inverse relationship (the greater the conductivity, the smaller the current density). Faraday's law can be rewritten as:

$$\vec{\nabla} \times \frac{\vec{J}}{\sigma} = -\frac{d\vec{B}}{dt} \tag{11.5}$$

where $\vec{J}$ is current density, σ is conductivity, and B is the magnetic field.

11.2 Objectives

1. To identify depths to formations of interest with sudden resistivity changes which can be used in processing other methods.
2. To locate potentially saturated zones, which may be potential geothermal flow paths.
3. To identify vertical offsets in geologic formations that may indicate a feature like a fault or fold that could be influencing geothermal fluid flow.
4. To image a possible northern extension of the Victoire fault beneath the student side.
5. To identify sudden lateral conductivity variations that may be the result of a fault (FDEM only).

11.3 Methods

11.3.1 Survey Location

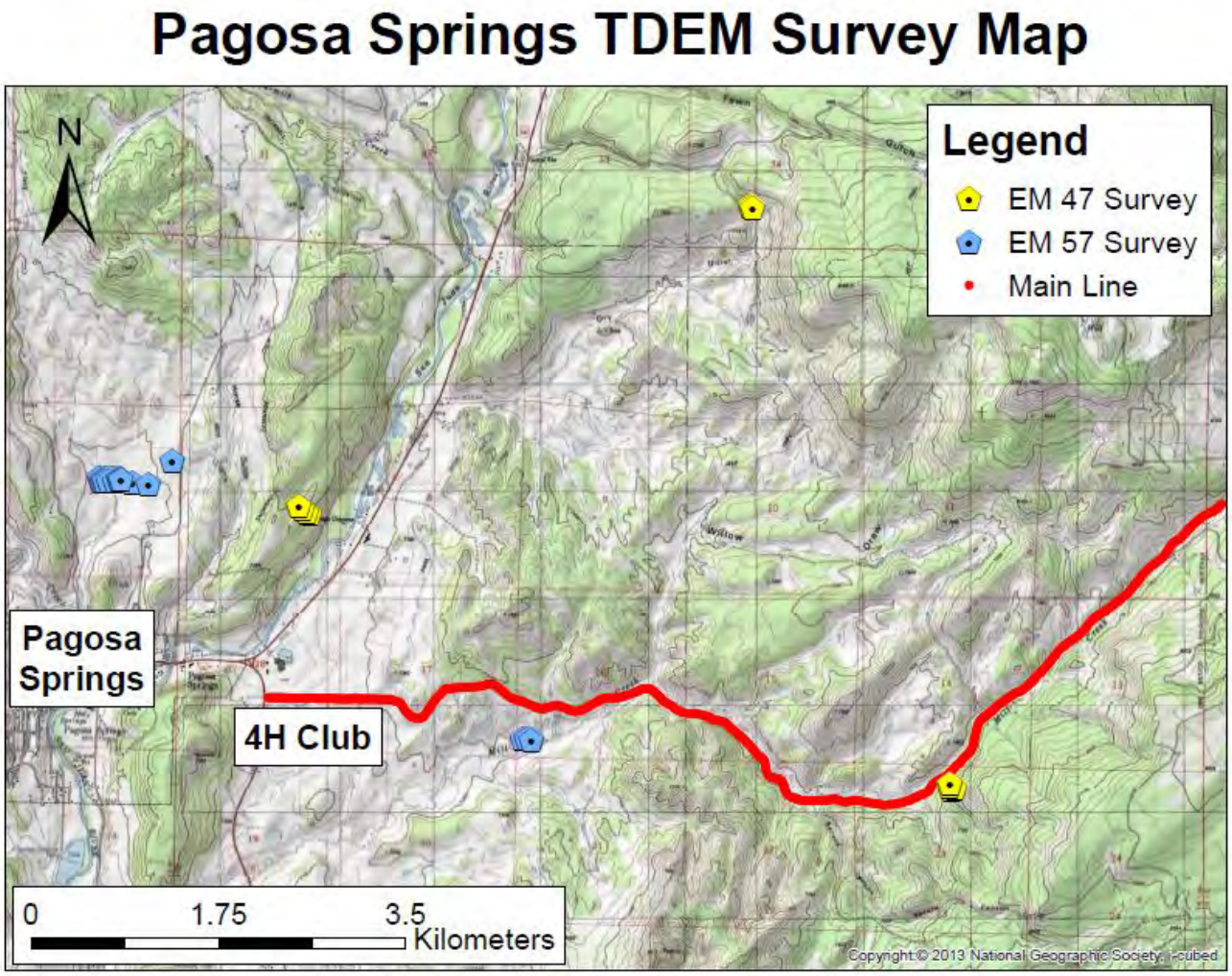

Figure 11.2: *Map of all electromagnetic survey sites (EM34,TEM47 and TEM57) along the Main Line and Student Site survey lines. Each point is the location of an center, in-loop receiver sounding. Each color represents a different piece of equipment, blue shows locations with the TEM57, yellow are the TEM47 survey locations.*

A total of nine TDEM surveys were conducted, six closer to the student site line and three near the main line

as seen in Figure 11.2). The criteria used for choosing each location was that each site must have/be: 200m from underground/overhead power lines, permission to be on the property, easy access, flat terrain, and relatively close to the area of interest. All except for one of the nine TDEM surveys are within 250 meters of either the student site or main line. The TEM-47 survey on May 19, 2016 is approximately 5km away from the main line. Although it is a large distance from our main survey location, the information acquired from it might prove useful as it provides a reference point. Unfortunately, because of the constraints mentioned above, we were unable to collect a regularly spaced set of soundings in most areas, and were unable to collect readings along significant stretches of the main survey line.

11.3.2 Data Acquisition

FDEM (EM34)

Two EM34 surveys were completed along the Student Site survey line, Figure **??**. Students used 20m reference cable spacing traversing from West to East and 40m reference cable spacing traversing from East to West. Each survey required a minimum of two operators, one to position and orient the transmitter coil and the other to position and record the readings from the receiver coil. A third person was helpful to adjust the reference cable to the correct position of the two coil operators, as well as to hand write each reading in a notebook. The preparation portion of the survey required to appoint a reference cable spacing, set the coil orientation and to properly connect the equipment. Three different sized reference cables were available, allowing us to choose from three different survey sizes: 10m, 20m and 40m reference cables. Based on our objectives for the student site, to find indications of a fault, we decided to select the reference cables that would provide the greatest depth analysis, those being the 20m and 40m reference cables. The coil orientation chosen was vertical co-planar (Horizontal Dipole) since the orientation provides the greatest depth analysis as well as being better suited for the constant alternating terrain. In order to connect the EM34 equipment properly we followed the EM34 manual: connect the transmitter coil to the transmitter box, connect one end of the reference table to the transmitter coil and the other end to the receiver box, and lastly connect the receiver coil to the receiver box with a three foot cord [81]. Once everything was connected we took into account the background noise by nulling the receiver coil. This was done by disconnecting the receiver coil from the receiver box and adjusting the sensitivity and conductivity null screws until both values read zero. Once the null process is complete the receiver coil is connected back to the receiver box. The null process was repeated every hour to minimize noise and instrumental drift.

For both reference-cable-spacings, a reading was taken every 20m at the Student Site survey line. The two operators would spread out evenly until the center of the reference cable between the two would lie directly above the point of interest. Both operators would then position the coils vertically with the marking on the coils facing the same direction. Next, the receiver operator would adjust the sensitivity to the proper range while informing the transmitter operator to adjust the transmitter coil to the desired orientation. Once the sensitivity value reached to its lowest value possible for that location, the receiver operator would relay the measured conductivity value to the third student who recorded it in a notebook. The process was repeated across the Student Site survey line for a total of 103 readings.

TDEM (TEM47)

All of the TEM47 survey sites were located in a reasonably flat (slope of no more than 10 degrees), clear place to simplify the process of laying out large wire antennae and orienting the receiver coils. The transmitter wire was laid out in a large square (the size being limited by the amount of space available at the site, but we tried to get a square of at least 40m per side), with the corners fixed in place using plastic stakes. At the point where the two ends of the wire met, we placed the transmitter control box (with battery), and connected the transmitter loop ends to it. It does not matter how the transmitter loop is oriented relative to north. In the center of the transmitter loop, which we marked with another stake, we placed the receiver coil assembly, which was unfolded into it's 3d form (it's normally folded flat for storage and carrying). The coil was oriented using the compass mounted on the base so that the coil designated as "y" was coplanar with respect to geographic north. We then leveled the coil by

Figure 11.3: *Students using the EM34 at site in Pagosa Springs. Photo credit goes to Dawn Umpleby.*

adjusting the leg heights, and checked using the spirit level mounted on the base. At this point, we connected the amplifier box, ProTEM recorder, and receiver coils using the connecting cables, and taking care that each of the coils is connected to the appropriate cable (the "z" coil is connected to the cable labeled "z"). The ProTEM was then relocated to a position approximately 5m away from the receiver (the cable connecting the two was about 5m long) to minimize the effects that the operators, or the electronics in the ProTEM, might have on the receiver coils. Finally, we ran a reference cable between the transmitter controller and ProTEM. This ensures that both are properly synchronized so the ProTEM starts recording when the transmitter turns off. This general setup is shown in figure 11.4. For some surveys, we also conducted variations on this, where the receiver was located outside of the transmitter loop, or at some point in the loop other than the center. We also conducted some surveys with an additional identical transmitter loop immediately adjacent to the first, but with the current flowing in the opposite direction. This forms a quadrapole magnetic field instead of the dipole formed by a single loop. For all of the surveys we recorded GPS coordinates for each corner of the transmitter loops, and for each receiver location.

After the transmitter and receiver are fully assembled and connected, we turn on both the transmitter and the ProTEM. After the ProTEM has booted, and after all system tests have been passed, we can enter the survey parameters. For all of our TEM47 surveys, the parameters listed in table 11.1 were kept the same. We also set the integration time for the next sounding, as determined by the frequency we are using, so a 285Hz sounding would have a 4 second integration time, 75Hz would have a 8 second integration time, and 30Hz would have a 15 second integration time. By changing the integration time we are changing the amount of time that the ProTEM is measuring for each record in the sounding (lower frequency cycles decay slower, and can be measured for a longer period of time). The operator also enters the station and line number to identify the sounding, and selects the number of records (typically between 8 and 20) and number of time gates (either 20 or 30). The number

of records determines the number of measurement cycles that the ProTEM records for each component for the current sounding, and has a significant impact on the time each sounding takes, and on the signal to noise ratio of the data, with more records increasing the time and decreasing the signal to noise ratio. The time gates are the intervals that the ProTEM divides the integration time into to discretize the measurements, and with 30 gates giving a higher resolution. The reason why we switched between the two was because different crews had been told different things about whether the analysis software could handle 30 time gates.

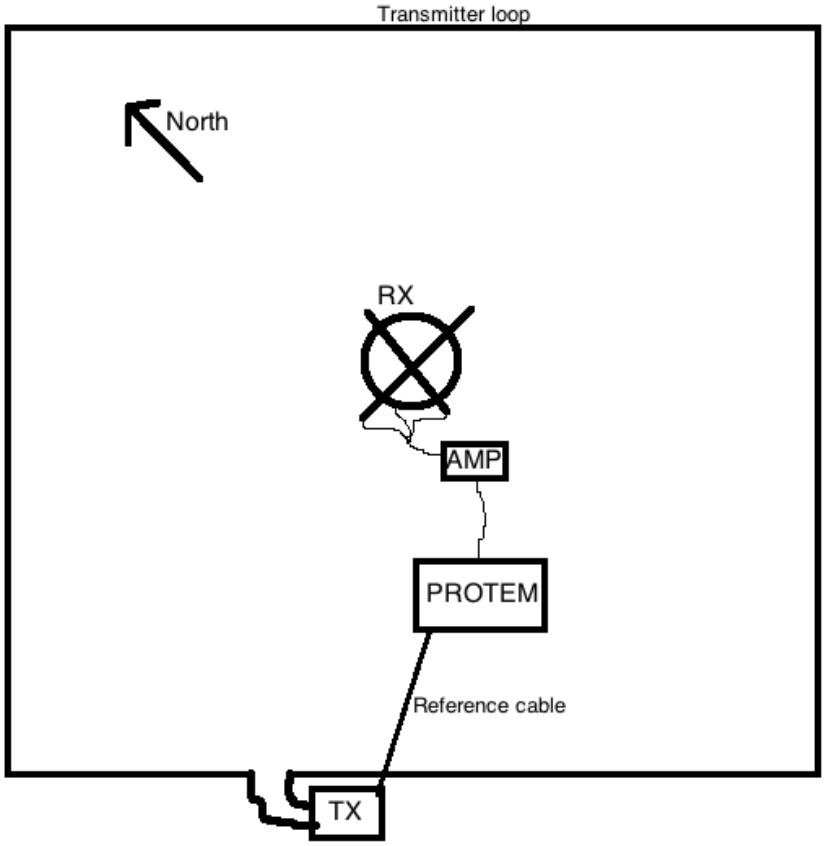

Figure 11.4: *General setup/layout of a TEM47 survey. The large square is the transmitter loop, the box labeled "TX" is the transmitter controller, the box labeled "AMP" is the amplifier, and the crossed circle labeled "RX" is the receiver coil assembly. Note that this is only a schematic representation, and is not to scale.*

After the operating parameters have been entered, the transmitter controller is turned on and the current adjusted to just below 3 amps (the maximum the transmitter can output safely), and the battery voltage is checked and recorded (checking it before each sounding makes it easier to check if it is dying). After the transmitter is turned on and adjusted, the ProTEM operator allows the system to set the gain (which ranges from 1 to 7), and starts the sounding. After the sounding is complete, the operator changes the frequency to the next in the series (we typically do three soundings in each receiver location, one for 30Hz, 75Hz, and 285Hz), the station number (or line number, depending on the operator), and adjusts the integration time to the new frequency. The transmitter is then readjusted to 3 Amps, and the current and battery voltage are recorded. We then allow the ProTEM to adjust the gain again and start the next sounding. This is repeated for all 3 frequencies at this receiver location,

Parameter	Value	Description
turn off time	3μs	time required for transmitter to turn off current
synch mode	ref	using reference cable to synchronize ProTEM and transmitter
coil type	3d1	using 3-component coil, measuring 1 component at a time
display noise	z	display noise for 'z' component on built-in screen
gain change	auto	automatically adjust gain value for each reading
rx delay time	0	begin recording as soon as transmitter turns off
on-time measurement	no	don't measure while transmitter is on
rx coil area	31.4m^2	effective receiver area

Table 11.1: *Parameters set in the ProTEM interface which are the same for all of our TEM47 surveys.*

after which the receiver is relocated to a new position. When set up, the TEM47 surveys appear similar to the TEM57 survey shown in figure 11.5.

TDEM (TEM57)

The general set up and operation of the TEM57 is similar to that of the TEM47 described above. The primary differences are the frequency at which current is set to alternate at, the size of the transmitter loop system, and the use of a one component receiver coil instead of a 3-component coil assembly. The TEM57, like the TEM47, uses a large square transmitter loop, although it is typically much larger for the TEM57 (often 100 or more meters on a side). Like the TEM47, we connect a transmitter where the loop wires meet, but instead of the battery powered unit used for TEM47 soundings, we use a larger, higher voltage transmitter, the TEM57-MK2A, powered with a portable gasoline generator. Since more power is needed for the TEM57, a generator is used as a power source instead of a 12 volt battery. Because of the higher voltages and currents used, and the generator used to provide this power, additional safety precautions are taken, including positioning a fire extinguisher nearby.

The 1D TEM57 receiver coil is placed at a carefully measured position within or outside of this loop. Unlike the EM47 receiver coil, the 1D EM57 receiver coil is only designed to accurately measure changing magnetic field across a plane perpendicular to the Z direction. In contrast, the 3D EM47 receiver coil is built to accurately measure magnetic fields changing across planes perpendicular to the X, Y and Z directions (hence the 3D). Connected to the EM57 1D receiver coil, is the ProTEM receiver, with which one specifies all the parameters and commands necessary to conduct the survey. The ProTEM 57-MK2 transmitter and ProTEM receiver allow current shut off sequences to alternate at frequencies of 3, 7.5 or 30 Hz (given 60Hz power line frequency), which gives us a penetration depth of up to 500m, significantly deeper than the TEM47 system's penetration of around 150m [68] [76]. Given this difference in scope, the TEM57 requires much more current, typically 15 amps or more, while the TEM47 cannot output more then 3 amps through its current loop. Besides the differences described, the TEM57 and the TEM47 systems acquire data in the same manner.

Equipment List

FDEM (EM34)

- Geonics EM34-3 transmitter
- Geonics EM34-3 receiver
- Geonics EM34-3 receiver and transmitter coil antenna set
- 20m and 40m reference cables
- spare batteries for receiver and transmitter

TDEM (TEM47 and TEM57)

- Geonics ProTEM receiver, with battery, using 60Hz powerline frequency setting
- Geonics HF-3D-1 receiver/amplifier (for TEM47 surveys only)
- Geonics EM47 3D1 receiver coil (for TEM47 surveys only)

Figure 11.5: *Photo of a TEM57 survey in progress on the Student Site. This was taken on May 23rd at Loop C, near the West end of the line. The transmitter controller and the generator power supply is in the center foreground, and the ProTEM and receiver loop are visible further back on the left. The transmitter loop extends almost to the fence in the background, about 50m beyond the receiver. Photo courtesy of Dawn Umpleby.*

- Geonics TEM47 transmitter (for TEM47 surveys only)
- spare TEM47 battery packs (for TEM47 survey only)
- Geonics TEM57-MK2A transmitter (for TEM57 surveys only)
- Geonics EM57 1d receiver coil (for TEM57 surveys only)
- gasoline generator (TEM57 surveys only)
- fire extinguisher (TEM57 surveys only)
- 2-conductor reference cable
- single conductor transmitter wire (up to 600m, in 100m and 200m reels)
- nonmetallic stakes (to hold transmitter wire in place)
- single jack hammer to place stakes
- minimum of 2 50m tape measures
- handheld gps, set to use wgs84 datum and UTM coordinates
- multimeter (very helpful in troubleshooting)
- handheld radios (1 per person on survey crew)

Figure 11.6: *Geonics EM34 system similar to what we used (this shows an optional digital logger that our system doesn't support). The orange rings are the transmitter and receiver coils, the box leaning on the left ring is the receiver, and the smaller box on the right ring is the transmitter. [72]*

11.3.3 Processing

FDEM (EM34)

We manually recorded the location, sensitivity, and conductivity readings for each station in field notebooks which were then typed into a spreadsheet on a field laptop. Once the data was recorded in the spread sheet we imported it to MATLAB and plotted the conductivity against the line position.

TDEM (TEM47 and TEM57)

The TEM47 and TEM57 have a ProTEM digital recorder from which we were able to download the data in the form of a .Gx7 file. The data from each day is downloaded as one file with all the soundings recorded as a single long list using the Protem program. The data was presented as one big file requiring us to open the .Gx7 's in a text editor to be able to separate the data file into different soundings. We separated the soundings by looking through the notes from students present during that set of data collection. In the end we sorted out the center loop sounding for the z component with each frequency for each transmitter location.

Additionally, each day recorded the location of the transmitter corners and receiver locations using various coordinate systems. We spent a good portion of a day creating a map with all the UTM coordinates for every sounding and its subsequent transmitters. This helped us to understand which site locations would provide the

(a) ProTEM

(b) TEM47 transmitter

(c) TEM57MK2A transmitter

(d) EM57 receiver

(e) EM47 receiver and HF-3D-1 amplifier

Figure 11.7: *Some of the equipment used for the TEM47 and TEM57 TDEM surveys. [73] [74] [75] [78]*

best insight when paired with the other methods. We selected three specific locations as the highest priority to try to process. The first is directly off the mainline recorded May 20th using the TEM47 transmitter/receiver pair. The second is on the east end of the student site also using the TEM47 from May 25th. The third and final location we deemed the highest priority, is located on the west side of the student site and was taken with the TEM57 on May 21st.

To view the data we used two different sets of software. The TEM47 data is processed with the SPIA software package and the TEM57 data is processed first by running through a code written by Joe Capriotti and then put into the IX1D software program. For both the TEM47 and TEM57 the edited and sorted data files are needed. After sorting the data files, how we processed the data differs.

Processing the TEM47 data was done with SPIA. It took a full day of working with the SPIA software and help from Joe Capriotti, Ben Bloss, and Michael Sleevi to learn to convert the .Gx7 data files into the correct database file type and open the project in SPIA. To be able to import the data, we need the data files but also the geometry file (Protem47Digital.pff). The converter is important because it takes the .Gx7 files and turns them into a database with the file extension .gdb. The importer is unable to work with the TEM57 data files. We made the decision to return to Joe's code that would allow for the use of the IX1D software program and guarantee some processing of the TEM57 data.

Once we were able to upload the TEM47 data to SPIA the noisy parts of the data were manually filtered out. shows the display window that we used to work with SPIA. Before downloading the data the ProTEM receiver was instructed to filter out the 60 Hz background cultural noise that is present in almost every TDEM survey conducted in the United States. No other corrections were made to the data. With the noise and 60 Hz filtered out, we ran a simple inversion through SPIA and received a very preliminary inversion model. We were then able to modify the model until it fit the ground truth that was provided by the geology group.

With the TEM57 data, we had to first run it through code provided by teaching assistant Joe Capriotti before it could then be imported into the IX1D software [70]. The code took the data from the TEM57 and reformatted data until it was in a style that IX1D was able to read and interpret. We opened the IX1D program and set it up for a center, in-loop TEM sounding. Once we had the software set-up the TEM57 data is copy and pasted into IX1D. We hand filtered out noisy points and ran it through the inversion process.

We chose to exclusively interpret center, in-loop soundings for both the TEM47 and TEM57 because of limitations in the software. In the time that we had to learn SPIA and apply it to the data we were unable to determine how to change the receiver location with respect to the transmitter, or how to use the x or y components from the TEM47 soundings. It may be possible but requires further study. For the sake of consistency we applied this restriction to both data sets for practical cross comparisons later on.

11.4 Discussion

11.4.1 Expectations

Our expectations for our data is mostly based on knowledge we have gleaned from two separate well logs, the PV-TG1 well drilled on December 6th, 2014 near Pagosa Springs to the southwest of the main survey line, and the Brown Federal well, drilled on August 25th, 1988 several kilometers to the east of the main survey line. The results of the two well logs differ significantly in their portrayal of the subsurface, so we have developed different expectations for each survey site based on their proximity to each well. The Brown Federal well portrays a fairly stable and constant apparent resistivity ranging from 6 to 12 Ohm-meters from 900 to 3196 feet (274 to 974 meters), with a weak but thick resistor existing from 1000 to 1120 meters. The PV-TG1 well on the other hand portrays a subsurface with a fairly constant, conductive subsurface throughout, except for a moderate increase in resistivity visible from 110 to 160 meters of depth, and highly resistive Precambrian rock at 400 meters of depth. It is important to keep in mind that the maximum depth of investigation for the TEM47 is about 200 meters, while the TEM57 has a maximum depth of investigation of 500 meters. So for survey sites located to the east of the main line we are only expecting to see small variation in our apparent resistivities, without any significant resistivity values except with significant depth (at least 300 meters). The survey sites on the eastern portion of the survey, especially those close to the student site, are expected to possibly pick up the same increase in resistivity detected at 110 meters in the PV-TG1 well (moderate increase of resisitivity described earlier). In short, the survey sites west relative to the main line are expected to show only small contrasts in conductivity without the presence of any significant resistors, while the survey sites east of the main line are expected to have a greater chance of sensing a resistive formation in the subsurface (or rather sense the absence of significant conductivity, since these methods are only sensitive to conductive media).

Most of these features might be impossible to detect given the limited scope of the TEM47 and TEM57, so the only anomalies we might be concerned with could be contrasts in conductivity caused by different levels of water saturation, or anomalous surface deposits (e.g. conductive alluvial deposits). This will be especially true in the case of the TEM47 with its more limited depth of investigation.

11.4.2 Results

FDEM (EM34)

The EM34 frequency domain electromagnetic survey results visible in figure 11.8 describe the conductivity values found given a 40 meter and 20 meter interval of coil separation. Since the conductivity values collected

using a 40 meter coil separation finds conductivity values corresponding to media at greater depths then those taken using a 20 meter coil separation, whenever the 20 meter coil separation conductivity values exceed the 40 meter coil separation conductivity value, the near surface is more conductive then the deeper subsurface. When the 40 meter coil separation conductivity values exceed the 20 meter coil separation conductivity values, you know that the surface is less conductive then the deeper subsurface. One is able to observe how the conductivity values gathered using 20 meter coil separation are consistently larger then the corresponding values using 40 meter separation throughout the student line, except for parts of the eastern student site survey line. This suggests that for much of the student site, there exists a conductive body in the near surface overlying a resistive body. These finding do not contradict the findings found from TDEM data from student site, where a large resistor was found to override a conductor. Given the limited depth of investigation for the EM34, even with a 40 meter coil separation, the fact that near surface media are more conductive then lower media merely suggests that some thin conductive layer exists near the surface (possibly alluvial deposits).

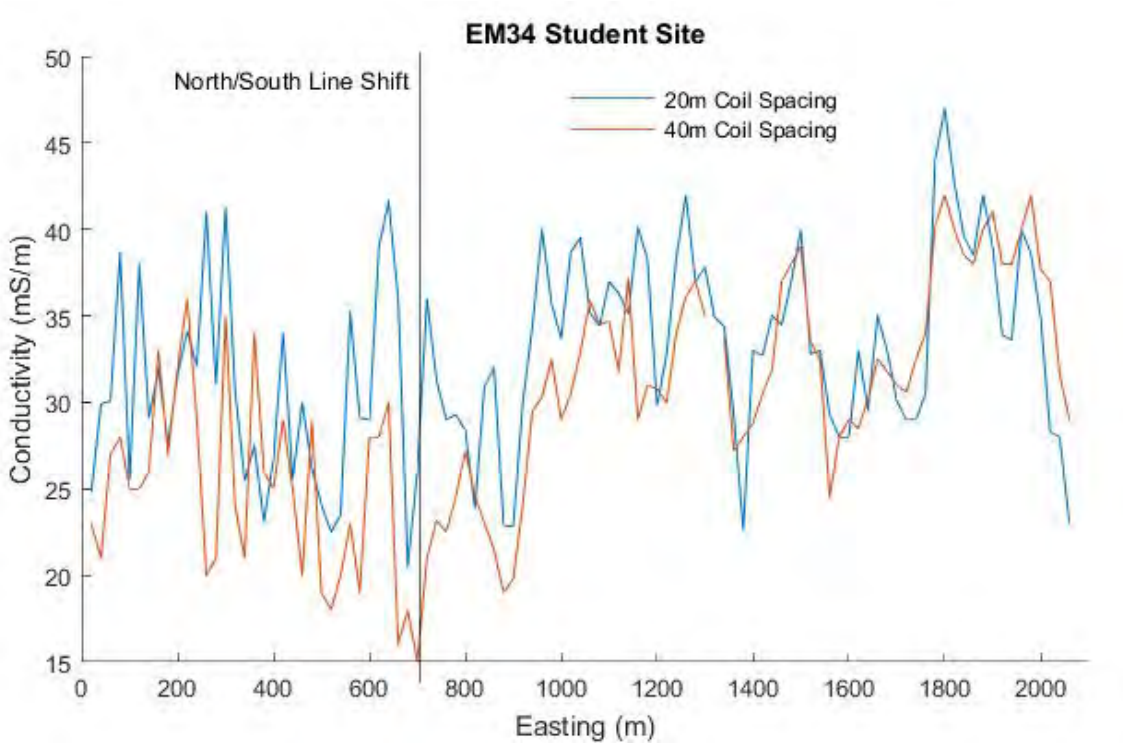

Figure 11.8: *Student Site EM34 data. Two surveys were completed running from West to East and from East to West. The blue line is the first survey completed using a 20 meter spacing between the EM34 coils (see figure 11.3 for visual of equipment in the field). The second survey is shown in red and was conducted using a 40 meter coil spacing. The black line dividing the page around 700m shows the switch in location from the west line to the east line. The both surveys on the west line eys show a large amount of noise but the east side it is possible to see the same trend in both independent sets of data.*

TDEM (TEM47 and TEM57)

If one were to take note of the resistivity models displayed in Figures 11.11, 11.12, 11.13, 11.14, 11.15, and represented in table 11.3 and 11.2, clues towards the apparent lithology of the subsurface become more clear. Firstly, all four locations of data acquisition collected on May 21st and May 23rd (Figures, 11.11, 11.12, 11.13, and 11.14) depict a strong resistor overlying a comparatively conductive medium. The interface between this resistor and conductor also appears to increase in depth as one travels from east to west along the survey line. On the far east end of the student survey line we conducted a TEM47 survey on May 25th, the results of this

survey, visible in figure 11.15, indicate that a strong conductor overrides a resistor of approximately the same resistivity as the resistor shown to override a conductor in data collected on May 21st and 23rd (Figures 11.11, 11.12, 11.13, and 11.14). It is probably a fair assumption that the resistor overriding a conductor in the TEM57 data shown in (figures 11.11, 11.12, 11.13, and 11.14) is the same resistor being overridden by a conductor in the May 25th TEM47 data portrayed in figure 11.15. All that is known about this resistor is that on the eastern portion of the student site its upper interface is approximately 130 meters deep, on the western portion of the student site its bottom interface has an average depth of approximately 330 meters, and the resistivity of this resistor is approximately 320 Ohm meters. Unfortunately we have far fewer TEM surveys placed along the main seismic line then we have along the student site survey line. We have conducted two surveys along the main line: a TEM47 survey conducted on the middle-eastern portion of the main seismic line collected on May 20th, and a TEM57 survey conducted on the western portion of the main seismic line collected on May 24th. The TEM57 data collected on the western portion of the main seismic line produces a subsurface model figure 11.9 which displays a model equivalence (green dashed lines which display the other possible models which might also fit the data) which appears quite consistent and relatively well fitting for this model. The resistivity values and depths represented in the inverse model created from western main line, May 24th data is inconsistent with all other information known about the site and gathered throughout the main line. The lack of any in the inversion solutions of the TEM57 data collected by the western seismic line data renders its models too unreliable for conclusive results to be concluded from it. The TEM47 survey conducted on the eastern portion of the main seismic line produced a more reliable model, shown in figure 11.10.

It appears that there are not any obvious or easily apparent bodies or formations with anomalous resistivities in the near subsurface (upper 200 meters) of the main seismic line. These findings are consistent with values recorded from the Brown Federal well log, which found the lack of any significant contrasts in resistivity down to depth of 974 meters.

Main Line

Survey	**Top Layer**		**Second Layer**		**Third Layer**		**Fourth Layer**		**Fifth Layer**
	Depth (m)	Resistivity (Ω-m)	Depth (m)	Resistivity (Ω-m)	Depth (m)	Resistivity (Ω-m)	Depth (m)	Resistivity (Ω-m)	Resistivity (Ω-m)
TEM47 May 20th	5.71	77.8	7.38	1.29	17.5	9.51	70.1	6.36	5.29
TEM57 May 24th	191.91	1182.8	214.95	17.831	-	48.784	-	-	-

Table 11.2: *Resulting parameters for the mainline inversions in order from West to East. TEM57 available frequencies: L=3Hz, M=7.5Hz, H=30Hz. TEM47 available frequencies: H=30Hz, V=75Hz, U=285Hz. Depth is the depth from the surface to the bottom of that layer. Note that the first layer extends from the surface, and that no bottom depth is listed for the deepest observed layer.*

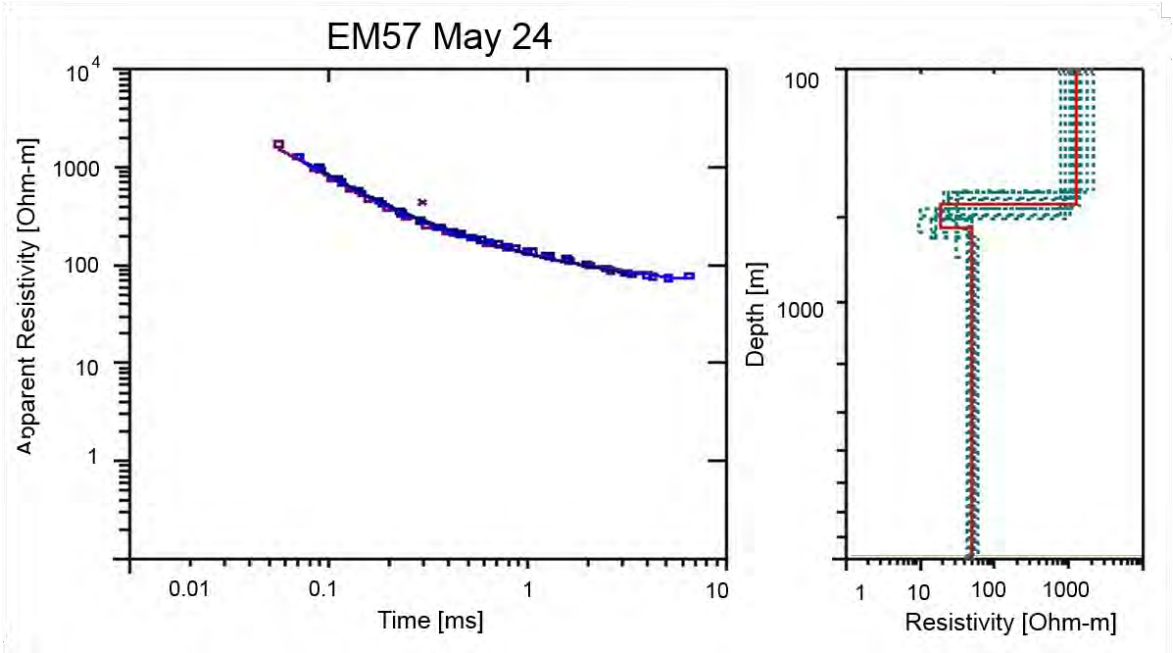

Figure 11.9: *Mainline, May 24th: Left: Apparent resistivity and time elapsed after primary current turn off on a log scale. Right:Depth below land surface and subsurface resistivity from inversion on a log scale. Notice the small degree of variation in the model equivalence (green dashed lines). Data misfit (RMS) of 6.72%*

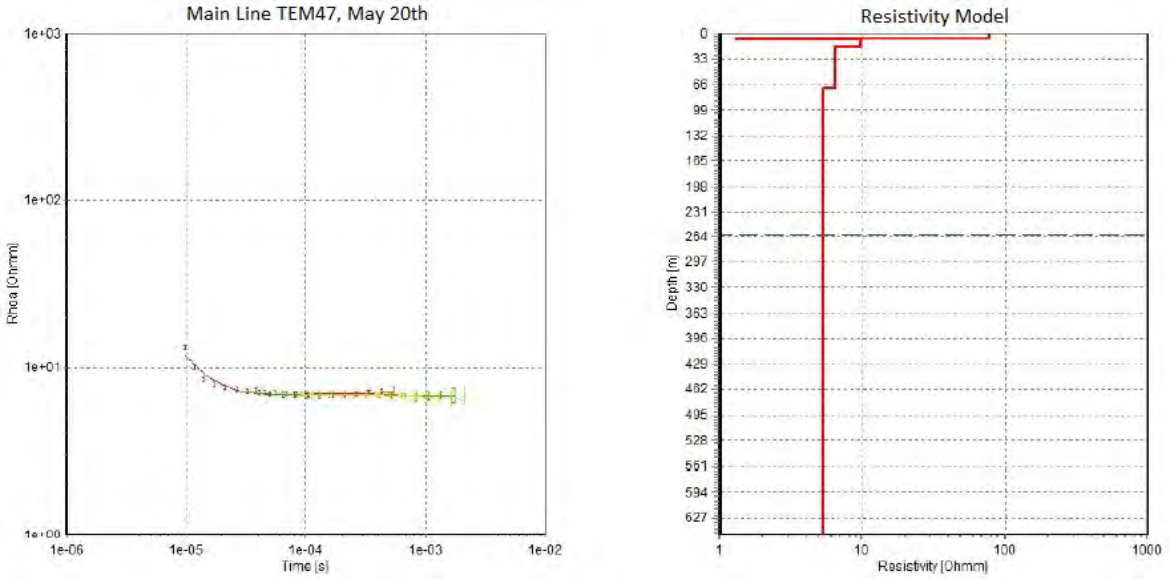

Figure 11.10: *Mainline, May 20th. Left: Apparent resistivity and time elapsed after primary current turn off on a log scale. Right: Depth below land surface and subsurface resistivity from inversion on a log scale.*

Student Site

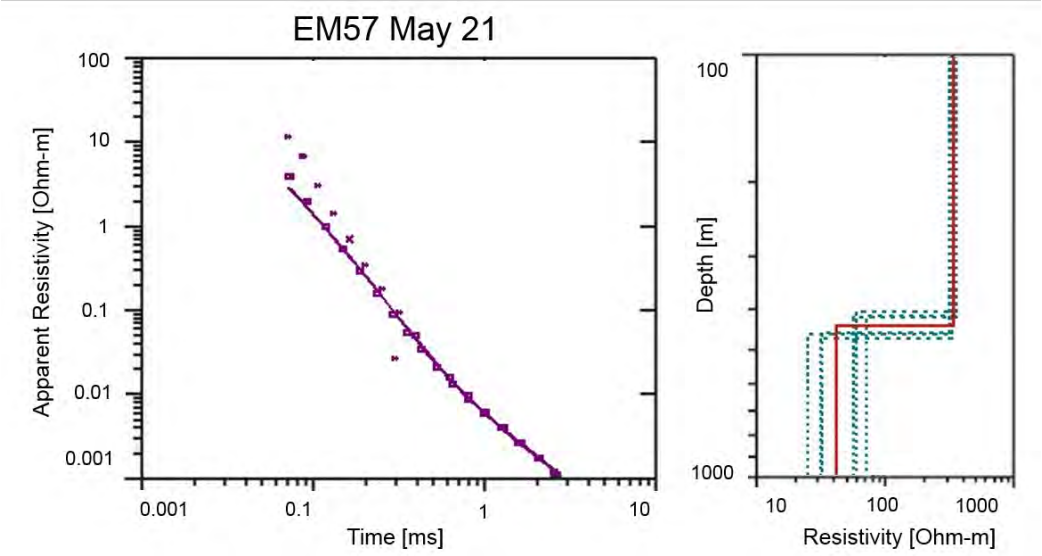

Figure 11.11: *West side of student site, May 21st. Left: Apparent resistivity and time elapsed after primary current turn off on a log scale. Right: Depth below land surface and subsurface resistivity from inversion on a log scale Notice strong resistor (335 Ohm meters). Notice moderate variation in model equivalence possible (green dashed lines). Data misfit (RMS) of 9.32%*

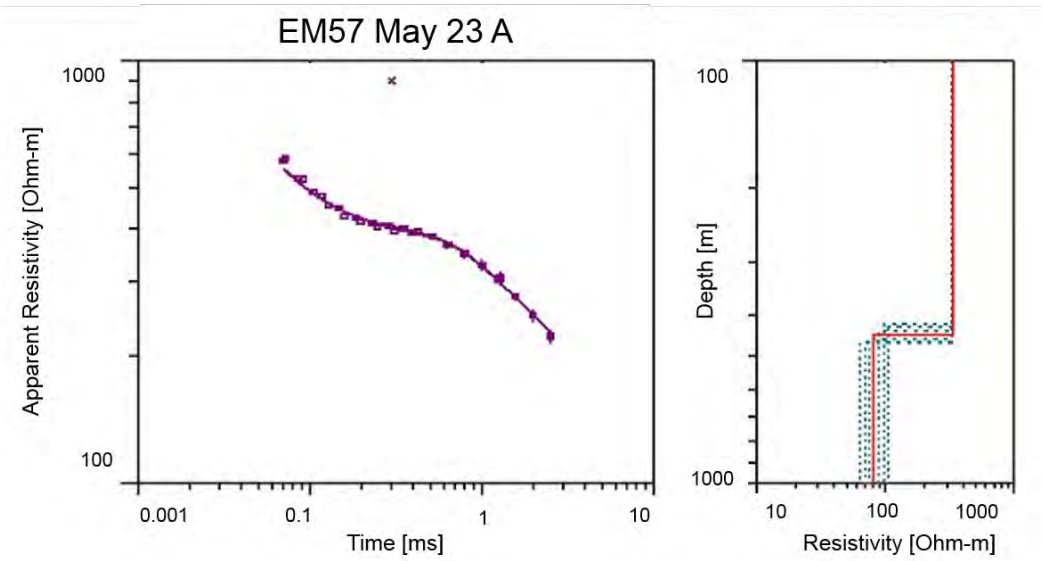

Figure 11.12: *West side of student site, May 23rd site A (furthest west). Left: Apparent resistivity and time elapsed after primary current turn off on a log scale. Right: Depth below land surface and subsurface resistivity from inversion on a log scale Notice presence of resistor (330 Ohm meter) above conductor. Variation of model equivalence (green dashed line) is relatively small. Data misfit (RMS) of 3.02%*

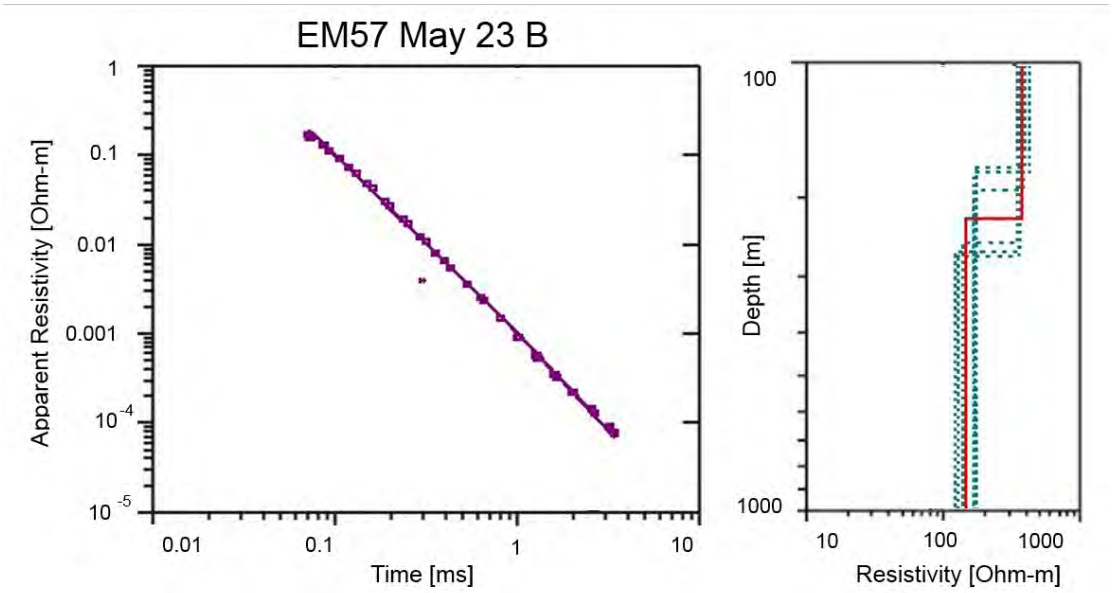

Figure 11.13: *West side of student site, May 23rd site B. Left: Apparent resistivity and time elapsed after primary current turn off on a log scale. Right: Depth below land surface and subsurface resistivity from inversion on a log scale. Notice how variation of model equivalence (green dashed line denoting equivalent models possible) is relatively large for this dataset. Data misfit (RMS) of 7.61%*

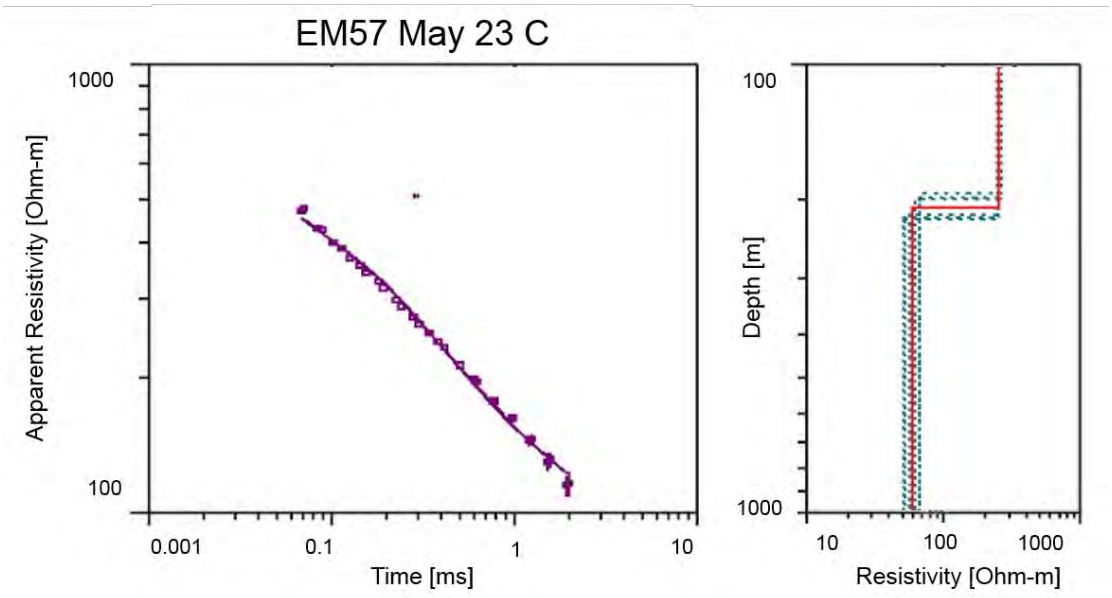

Figure 11.14: *West side of student site, May 23rd loop site C. Left: Apparent resistivity and time elapsed after primary current turn off on a log scale. Right: Depth below land surface and subsurface resistivity from inversion on a log scale. Notice, once again, the strong resistor (258 Ohm-meters) located above the conductor. One can see variation of model equivalence (green dashed line) is relatively small. Data misfit (RMS) of 4.12%*

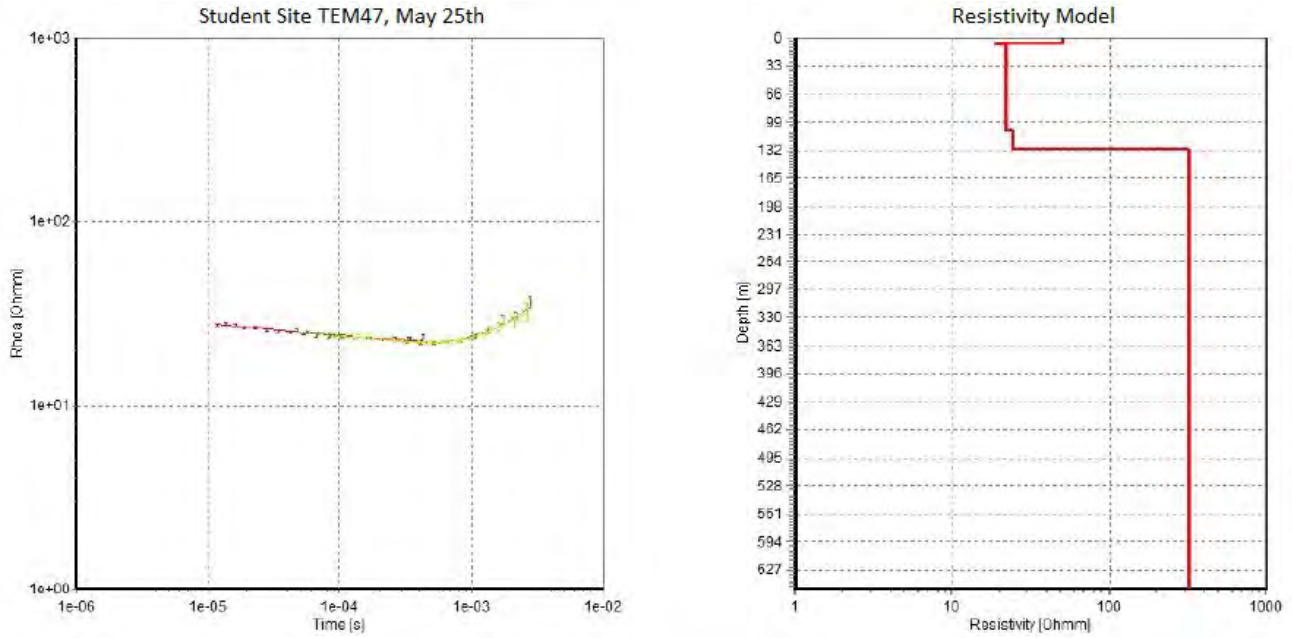

Figure 11.15: *East side of the Student Site, May 25th. Left: Apparent resistivity and time elapsed after primary current turn off on a log scale. Right: Depth below land surface and subsurface resistivity from inversion on a log scale. Unfortunately, a data misfit value was not available with modeling software used.*

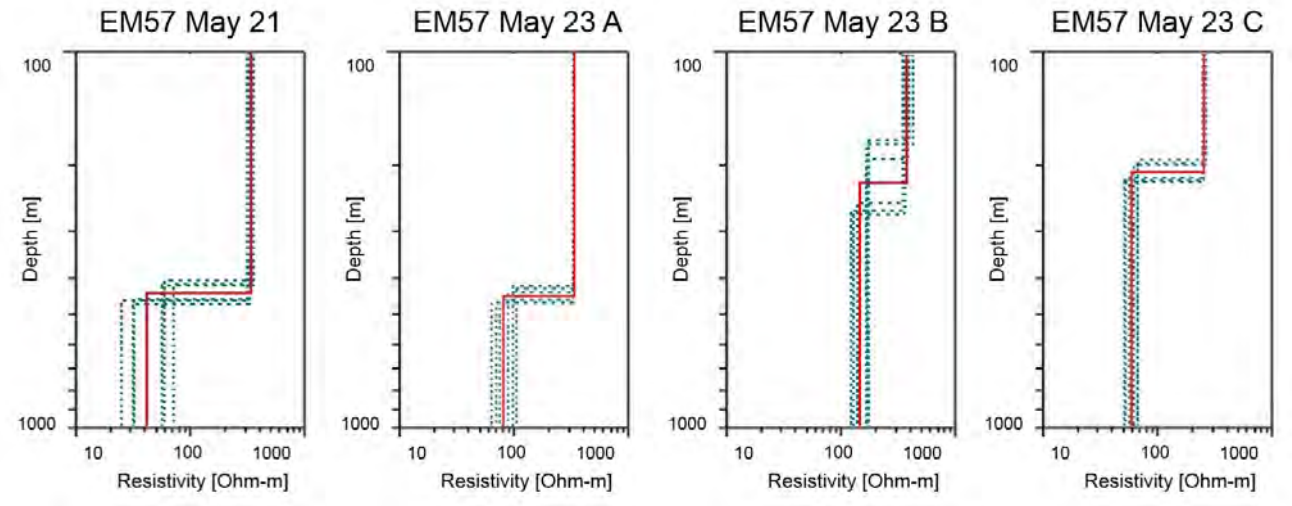

Figure 11.16: *Resistivity models from inversion of apparent resistivity values. West end of student site from west to east. Notice the top layer depth shift between sites May 23 A and May 23 B.*

11.4.3 Interpretation

Mainline

Along the main line, we found little sign of any significant resistivity contrast in the upper subsurface (down to about 150 meters). The only conclusive information we have on the lithology existing beneath the main seismic line is from the TEM47 survey which was conducted on the eastern portion of the main seismic line on May 20th. This survey was conducted on a moderate slope, so because the survey was not conducted on a flat, horizontal

Survey	Top Layer		Second Layer		Third Layer	Freq.
	Depth (m)	Resistivity (Ω-m)	Depth (m)	Resistivity (Ω-m)	Resistivity (Ω-m)	
TEM57 May 21	435	335	-	42	-	M,H
TEM57 May 23 Site A	448	330	-	80	-	M,H
TEM57 May 23 Site B	227	372	-	142	-	M,H
TEM57 May 23 Site C	208	258	-	60	-	M,H
TEM47 May 25	5.56	47.6	12	21	142	H,V,U

Table 11.3: *Resulting parameters for the student site inversions in order from West to East. TEM57 available frequencies: L=3Hz, M=7.5Hz, H=30Hz. TEM47 available frequencies: H=30Hz, V=75Hz, U=285Hz. Depth is the depth from the surface to the bottom of that layer. Note that the first layer extends from the surface, and that no bottom depth is listed for the deepest observed layer.*

surface, the slightly resistive layers apparent in the first 70 meters of the subsurface is likely due to the topography of the site (non-horizontal transmitter loop). The inverted model from this survey, visible in figure 11.10, shows some weak resistors present in the near surface (down to about 70 meters) but otherwise, there is little to no obvious apparent contrast in resistivity. Judging from this model, throughout the relatively limited depth of investigation for this TEM47 system the resistivity of the subsurface is essentially homogeneous. All we can thus determine is that no significant changes in resistivity are apparent in the middle-eastern section of the main seismic line down to the depth of investigation of the TEM47 unit (about 200- 150 meters).

Student Site

The four TEM57 central loop soundings at the west end of the student site all shared a similar result within the 600m range of sensitivity. That being a two layered subsurface model with a resistive layer at the surface and a second more conductive layer at a greater depth. The top layer has a resistivity ranging from 330Ωm to 370Ωm with the exception of site (TEM57 survey on western student site) which shows a resistivity of 258Ωm. This more conductive top layer observed at site May 23 C (figure 11.16) is likely due to a pond, approximately 10m X 10m, inside the TX loop at the time of recording. The second layer for each site along the west side of the student site shows to be more conductive with a range of resistivities of 40Ωm to 80Ωm, except for the May 23 B survey which shows, in figure 11.16, to be more resistive with a resistivity of 145 Ωm. Sites May 21 and May 23 A-C are all overlaying over Mancos Shale, however instead of seeing a conductor we are seeing a resistor. This is likely due to the Colorado group (layered beds of Mancos Shale and resistive formations: Greenhorn Limestone, Niobrara shale) near the bottom interface of the Mancos Shale followed by a similar resistive Dakota sandstone layer. The second layer is the top of the Morrison formation which is a more conductive layer which follows after the Dakota Sandstone. The depths of the top layer in the TEM57 surveys are inconsistent as we travel from West to East as shown in figure 11.16. For TEM57 sites conducted on May 21st and site A of May 23rd (all on western section of student site) the depths of the top layer ranges from 208m to 230m and changes to a depth of 430-450 at sites May 23 B and May 23 C. Since the top layer resistivities remain consistent, meaning the same rock unit at the top layer, there is a possibility of a fault (or fold) between sites May 23 A and May 23 B. The fault would also explain the high second layer resistivity for the site May 23 B. Since the TEM57 induced voltage readings are the sum of the surroundings at the location, the resistivity reading might be a combination of the resistive top layer measured at site May 23 A and the 40-80 Ωm resistivity of the second layer. At the East end of the student site, survey May 24, the TEM47 central loop sounding showed a Four layered model. The geology at the surface of site TEM47 May 25 is Quaternary alluvial deposits which shows as the first layer in the resistivity inversion figure 11.15 to a depth of 5.56 meters. A conductor shows as the second and third layer, which is the expected Mancos shale, changing resistivity sligthly. The fourth layer resistivity 320 Ωm is about the same resistivity value we see at the west end of the survey line, therefore we can assume that they are the same layer, a combination of

the Colorado group followed by the Dakota Sandstone.

In conclusion based upon the results of our TEM47 and TEM57 survey data from the student site we concluded that a resistor possessing a large resistivity contrast relative to its neighboring formations exists from essentially the surface to approximately 208 meters with a possible fault changing the depth of this resistivity contrast to a depth of 448 meters to the west on the western section of the student site survey line. This resistor exists from approximately 131 meters to some unknown depth on the eastern section of the student site. The resistor appears to have an approximate apparent resistivity of 320 Ohm meters. Below this resistor exists a conductive formation of unknown thickness, which has an approximate resistivity of 80 Ohm-meters. On the far eastern portion of the student site there exists a conductor with an approximate resistivity of 21.6 Ohm-meters which overrides the same resistor described earlier.

11.4.4 Errors and Uncertainty

There are many different potential sources of error or noise that could have a measurable effect on the data and inversions. There are errors associated with the survey design and equipment or processing. Noise can be introduced by both natural and man-made sources.

Survey Design and Equipment Errors

- Incorrectly oriented or leveled receiver coils may record data not representative of the expected component.
- When the receiver is not in same placed in the same plane the as transmitter, it records the field at an offset, and doesn't measure the full amplitude expected.
- If the battery voltage fluctuates during a sounding, the transmitter current will change, changing the amplitude of the recorded signals.
- The ProTEM assumes a preset turn off time. If this is too short, it will record parts of the primary field. If this is too long, it won't record the earlier signals.
- Any sort of poor connection, short circuit, or faulty cabling in the system can distort the signals, or change the apparent resistivity in unpredictable ways.
- Thermal variations created in the equipment from sun or weather conditions that can cause changes in resistance within the equipment, potentially changing the behavior of the receiver ant transmitter coils.
- If the transmitter is not in a perfect rectangle it becomes difficult to calculate the exact area of the loop.
- Equipment malfunctions like delays in the reference cable or incorrectly set up or drifting crystal syncs can cause the ProTEM to record at the wrong times, potentially overlapping the transmission phase.

Processing Errors

- Incorrect data processing assumptions may have been made when processing the data.
- The inverted models are under-constrained and there may be multiple models that fit the observed data.

- **Data (mis)management**
  - The data files from the TEM47 and TEM57 contain an entire days worth of soundings in a single file. If an error is made when splitting these into separate soundings and components, the data may become corrupted or invalidated.
  - The soundings are not labeled and are broken up based on the field notes of students. If the notes are unclear or incorrect, the wrong data for a particular sounding could be used and, therefore, becomes invalid.
  - In some files incorrect survey parameters were discovered. In some of the TEM47 data an incorrectly recorded transmitter current was discovered, and some files from both systems recorded incorrect transmitter loop sizes.
  - It was discovered that the SPIA TEM software was unable to handle TEM57 data, and the software provide was unable to provide us with a solution, forcing us to use IX1D for the TEM57 soundings.

  - TEM57 and TEM47 inversion results are reported in a slightly different form in each program, and with different depths of investigation and sensitivities, making comparisons between the two more difficult.
  - Multiple days worth of data (including both TEM57 and TEM47 soundings with 20 and 30 time gates) were downloaded into the same file when one group forgot to download their data. This was not initially reported to the processors, and required significant time to correct.
  - Some survey crews recorded data with 20 time gates, and others recorded for 30, and didn't always include this in their notes.

Man-made Background Noise

- Some things, like transmission lines, pipes, and grounded metal fences can induce subsurface currents that interfere with our measurements.
- External electromagnetic emitters like cars, generators, and radio transmitters can induce currents in the subsurface and in our receiver, potentially distorting or masking our desired signal.
- Large metallic items like automobiles can interact with our magnetic fields with unpredictable results.
- Some surveys were conducted in agricultural areas, and groundwater from recently irrigated fields may introduce significant near surface lateral conductivity variations.

Natural Background Noise

- Solar storms, solar wind, and atmospheric activity can induce magnetotelluric currents that can be recorded by our receivers. These have a significantly more severe impact on the horizontal components of the magnetic field, potentially masking any heterogeneities we might observe.
- Strongly magnetic rocks in the investigation area can distort the magnetic field.

11.5 Conclusion

The student site consisted of five TDEM surveys and one FDEM survey. Out of the five TDEM surveys four of them were conducted at the west end of the student site using the TEM57. The resistivity model from the resistivity curve inversions remained consistent in showing a two layered model. These two layers are represented as the resistive Colorado group with the Dakota Sandstone and the conductive top layer of the Morrison Formation. Due to the Colorado group having a similar resistivity as the Dakota Sandstone we were unable to accurately locate the interface of the two layers, therefore they were combined into one layer. Between sites May 21 A and May 23 B the resistivity models show a large change between the layer depth of the Dakota Sandstone from 448m to 227m, which indicates the possibility of a fault/fold between the two sites. The fifth TDEM survey conducted at the student site was an TEM47 survey at site May 25. This site was located at the east end of the student site and modeled three layers. A top thin Quaternary alluvial deposits layer, the top conductive layer of the Mancos shale and the resistive Colorado group. The third resistive layer matched the resistivity range(320-350) of the top layer of the west side of the student site therefore we can accurately conclude that they are the same layer. The TDEM survey consisted of using the EM34 along the student site survey line with a spacing of 20 m with two coil separations, 20m and 40m. The two coil separations provided a similar trend in conductivity with respect to distance. The visible trend shown depicts the conductivity decreasing as we travel from west to east. There is one exception at 700m in Figure 11.8 which is due to the offset of the student site survey line. We also observe that the near surface conductivity values (20m coil separation) are more conductive than the deep surface conductivity values (40m coil separation) throughout the student site survey line.

The main seismic line features two TDEM surveys, one TEM47 survey on the eastern main seismic line, and one TEM57 survey on the western main seismic line. Only the eastern TEM47 survey yields plausible results. We have found that the near surface of the eastern main seismic line features a homogeneous resistivity. Using the one reliable data set we collected along the main seismic line (whole model is illustrated in Figure 11), we have

concluded that there is little substantial variation in resistivity within the upper 150-200 meters of the eastern main seismic lines subsurface.

11.5.1 Recommendations

Prior to conducting another TDEM survey, we would strongly encourage the survey crew to spend some time familiarizing themselves with the processing software, and in particular, it's limitations, such as the inability to process quadrupole readings or x and y components. We would also recommend creating a more comprehensive plan, including a list of sites where a TDEM survey would be most helpful, and where there is enough space to set up a survey. It would also be helpful to include a guideline in this plan outlining how each survey or sounding is recorded.

In addition, we would recommend conducting TEM47 and TEM57 surveys centered on the same receiver position, so we can synthesize a conductivity sounding from the surface to a point several hundred meters deep, instead of a shallow sounding extending 150m deep, and a separate, unrelated sounding in another location beginning around 150m, and extending several hundred meters below that point. In order to do this, it may be necessary to obtain a second ProTEM recorder so that TEM57 and TEM47 surveys can be conducted simultaneously, and at different locations to avoid interference.

For any future FDEM survey crews, we would recommend a thorough discussion about the utility of a survey like the EM34, especially in areas where there is likely to be significant noise and error introduced from power lines and fences along the planned survey line. Because tools like the EM34 are relatively shallow, it may not be appropriate to conduct a full survey, and the time saved may be better spent on other methods, like on a second TDEM crew. However, the FDEM method and it's shallow penetration depth may be useful to collect additional information about selected areas of the main survey lines where the initial processing attempts by other methods show some feature of interest, like an anomalous DC resistivity reading suggesting a dike where we were not expecting anything.

References

[68] Aegis Instruments Limited, *Tem 57 mid-range transmitter*. [Online]. Available: `http://www.aegis-instruments.com/products/brochures/tem-57.html` (cited on page 160).

[69] Albeesh Deema, AlGhamdi Rami, AlManaa Mohammed, Alselemi Ghadeer, Barnier Guillaume, Blitz Thomas, Brush Jennifer, Bui Thu Thao, Duan Yuting, Dunham Michael, Dutcher Elena, Eppeheimer Jarred, Geimer Paul, Haich Spencer, Huebner Mickolas, Huffington David, Jennings Joseph, Kohnke Colton, Kosmicki Max, Kreeprasertkul Kritti, Lozier Alyson, Luo Simon, Malcolm Brennan, Meer Ibrahim, Mueller Staci, Newbill Stevie, Pacher Chris, Patrikeeva Natalya, Pettinger Elizabeth, Plescia Steven, Sebelin Linus, Stanley Karyn, Stone Ian, Thomas Elijah, Yanke Andrew, Zhang Junwei, Abdelgawad Aly, Ayaa O'Biale Anthony, Coe Samuel, Colle Caroline, Feuilleaubois Laurent Oliver, Haji Ashari Nur Azimah, Kazyyeva and Dinara, Kurniawan Baskoro, Lai Jiayun, Chen Ning Ivan Lim, Yalin Luan, Mangeon Stephane, Mearns Leanne Connie, Metcalfe Richard, Nurmaanov Nurlan, Pacharakittiwich Rapapasra, Sprague Daniel, Wang Xi, Xu Zuo, and Yermukhan Aidar, *Geophysical investigation of the pagosa springs geothermal system -upper san juan basin, archuleta county, colorado*, digital, Jun. 2013 (cited on page 153).

[70] J. Capriotti, "Untitled", python program wriiten to convert TEM57 .Gx7 datafiles from 30 time gates to 20 time gates, 2016 (cited on page 164).

[71] M. J. Galloway, *Hydrogeologic and geothermal investigation of pagosa springs, colorado*, work performed under contract DE-AS07-77-ET28365, 1980. [Online]. Available: `http://www.osti.gov/scitech/servlets/purl/6623866` (cited on page 153).

[72] Geomatrix Earth Science Ltd, *Em34-3 - electromagnetic geophysical land products*. [Online]. Available: `http://www.geomatrix.co.uk/land-products/electromagnetic/em34-3/` (cited on page 162).

[73] ——, *Protem - electromagnetic geophysical land products*. [Online]. Available: http://www.geomatrix.co.uk/land-products/electromagnetic/protem/ (cited on page 163).

[74] ——, *Tem47 - electromagnetic geophysical land products*. [Online]. Available: http://www.geomatrix.co.uk/land-products/electromagnetic/tem47/ (cited on page 163).

[75] ——, *Tem57mk2a - electromagnetic geophysical land products*. [Online]. Available: http://www.geomatrix.co.uk/land-products/electromagnetic/tem57a-mk2/ (cited on page 163).

[76] Geonics Limited, *Tem47 transmitter*. [Online]. Available: http://www.geonics.com/html/tem47.html (cited on page 160).

[77] John Milsom and Asger Eriksen, *Field Geophysics*, 4th. West Sussex, UK and Daryagani, New Delhi, India: Wiley Blackwell and Shri Adhya Educational Books Pvt. Ltd., 2011, part of the Geological Field Guide Series (cited on page 153).

[78] C. Kohnke, "2016-05-20_10_56_32", Photo taken on 20160520 during field session., May 2016 (cited on page 163).

[79] Mohamed Abdulla, Norah Aldossary, Hamid Almumtin, Hala Alqatari, Elias Arias, Ihmad Atshan, Stephen Cuttler, Johannes Douma, Matt Doyle, Matt Emmet, Clement Fleury, Arantxa Gallastegui, James Geyer, Chris Graziano, Allie Grazulis, Dettchai Ittharat, Heather Johnson, Alison Knaak, Jasmine Lambert, Liz Maag, Russell Mah, Gabe Martinez, Paul Meier, Karen Moll, Lindsay Patterson, Cai Pengfei, Francesco Perrone, Thomas Rapstine, Dan Shannon, Loralee Wheeler, Georgie Zelenak, Jieyi Zhou, Khalil Al Hooti, Astrid Caratge, Uygar Ceyhan, Karin Maria Eres Guardia, Camila Franca, Phansakorn Kaewprain, Saniya Kanafina, Petros Karalis, Junhee Kim, Elena Kokoshina, Nanxin Li, Jia Long Loh, Iskandar Masri, Aminayanasa Ngeri, John Northall, Eleanor Oakley, Veronica Omofoma, Jack Phillips, Gustav Polisano, Siobhan Prise, Litty Rajesh Kumar, Haroon Rasheed, Noble Tamunobereton-ari, Angus Watson, Liang Zhang, and Terence Kratzer, *Geothermal characterisation of the geothermal system in pagosa springs area, upper san juan basin, archuleta county, colorado, geophysics field camp 2012*, digital, Jun. 2012. [Online]. Available: http://geophysics.mines.edu/UserFiles/File/geophysics/fieldcamp/Pagosa_Springs_Field_Camp_2012_Final_Report%202.pdf (cited on page 153).

[80] M. N. Nabighian, "Quasi-static transient response of a conducting half-space – an approximate representation", *Geophysics*, volume 44, number 10, pages 1700–1705, Oct. 1979. DOI: 10.1190/1.1440931. [Online]. Available: http://library.seg.org/doi/abs/10.1190/1.1440931?journalCode=gpysa7 (cited on page 154).

[81] *Operating instructions: em34-3 data logging system for field computer allegro cx field pc*, 1.0, Geonics Limited, Mississauga, Ontario, Canada, Jul. 2005. [Online]. Available: http://www/geonics.com/pdfs/documentation/eM34_manuals/em34-3_cx.pdf (cited on page 157).

[82] United States Army Corps of Engineers, *Em 1110-1-1802: geophysical exploration for engineering and environmental investigations*, figure 4-27, United States Armed Forces, Washington DC, Aug. 1995, [Online]. Available: http://www.publications.usace.army.mil/Portals/76/Publications/EngineerManuals/EM_1110-1-1802.pdf (cited on page 154).

12. Joint Interpretation

Contents

12.1 Introduction

Each method for the acquisition of geophysical data can reveal and highlight certain properties of the subsurface; however, for a reliable model, multiple methods must be integrated to collect and combine as much information as possible. When attempting to answer a specific question, it is best to consider as many methods as economically feasible. Each method provides insights to different properties, depths-of-investigation, and signal-to-noise ratios. Method integration utilizes all method results to create one encompassing interpretation. Overlapping results from different methods allows for the identification of inconsistencies within data collection or processing. If inconsistencies are small enough, they can be resolved. If inconsistencies are too large and do not correlate with other methods, the reliability of the model is questionable. For this field camp, we present figures that combine all relateable data sets from the main line and student site into complementary images.

12.2 Objectives

1. Consolidate all methods to better interpret the subsurface beneath the Main Line and the student line.
2. Determine if there is a correlation between anomalies found in the data from different methods.
3. Better constrain where the Mother Spring water is coming from.

12.3 Interpretation

12.3.1 Main Line

Overview

Joint interpretation on the Main Line began with a cross-section created from well-logs and basic geologic knowledge of the Pagosa Springs area (Figure 12.1). The 2016 Field Camp collected different sets of geophysical data that overlapped on the Main Line. These data sets were combined and interpreted to provide insight and modify the initial cross-section.

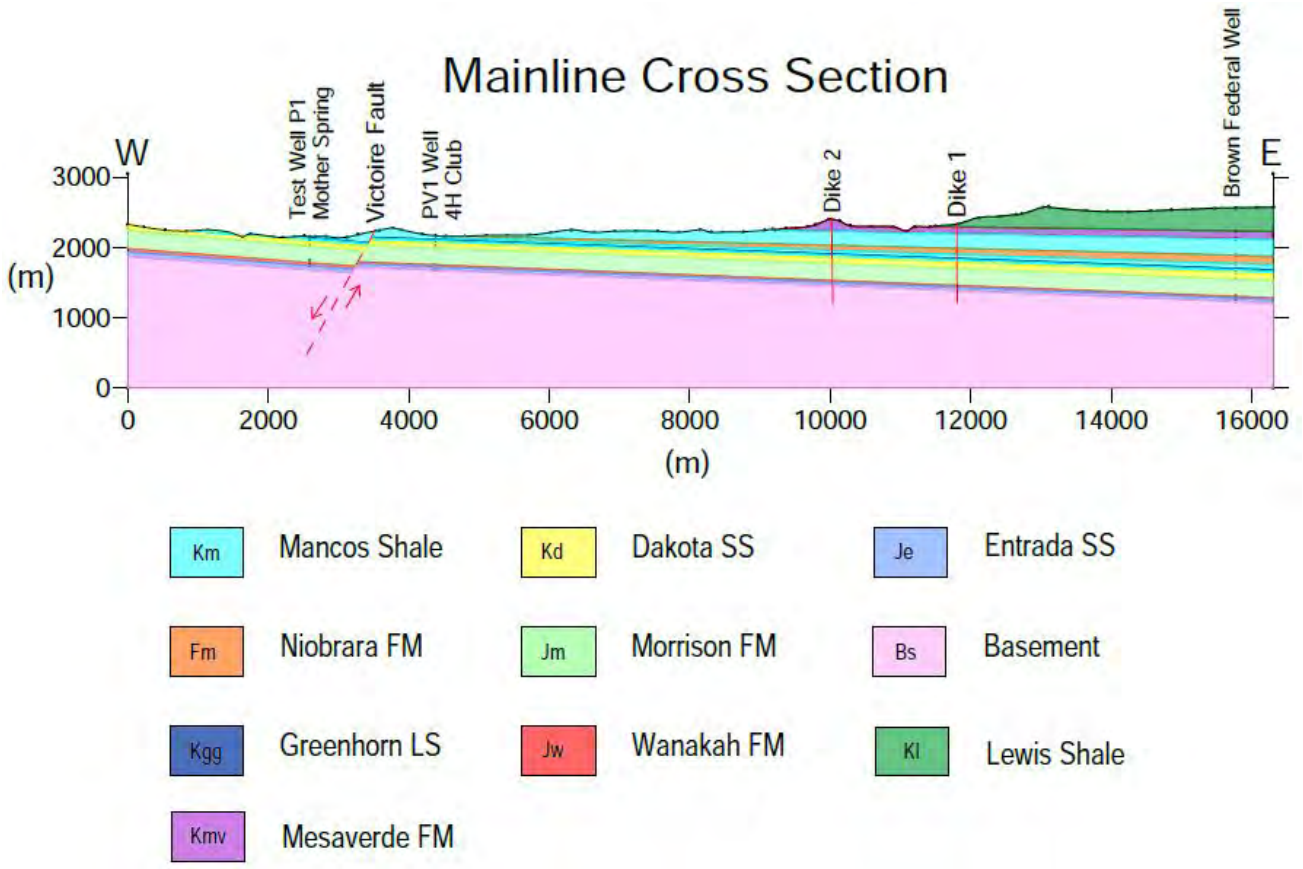

Figure 12.1: *Initial geological cross-section created from well-logs and surface outcrops.*

Deep seismic and gravity methods were the two largest surveys performed and therefore provided a strong foundation for other methods. MT complemented both deep seismic and gravity surveys because of its great depth Of investigation (DOI).

Other complementary data sets performed along the Main Line included SP, DC resistivity, and TDEM. These electrical and electromagnetic surveys are compared because they measure similar physical properties of the subsurface. SP and hammer seismic data were used to identify a dike along the mainline. These joint interpretations are discussed in the following sections and culminate in a final geological cross-section.

MT and Seismic

The first step in understanding the geology of the mainline is identifying the basement depth. A known basement depth creates a foundation where stratigraphic layers can be defined for further development of reliable subsurface geology. MT is an effective method for achieving this, due to its great depth of investigation. In Figure 12.2 there are two MT soundings which are used to identify basement depth. The Pre-Cambrian basement was

found at 900 *m* deep at 3.6 km along the survey line, and 1,300 *m* deep at 9 km along the survey line. Next, in Figure 12.3, the MT soundings are overlaid on the seismic image. Together they can be used to constrain the location of the basement contact with confidence. This image shows a general dip of the basement contact across the length of the main line.

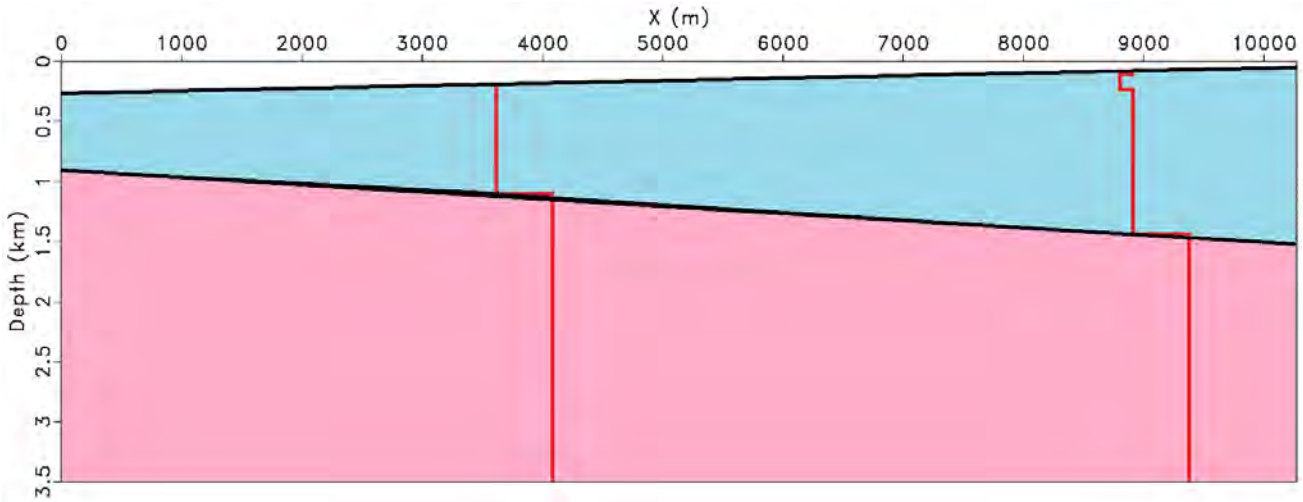

Figure 12.2: *Two MT soundings, seen in red, at different points on the Main Line, used to locate basement. In the figure the blue color represents the sedimentary geology of the area. The pink layer represents basement. The black line is the basement contact line inferred between the two locations of basement.*

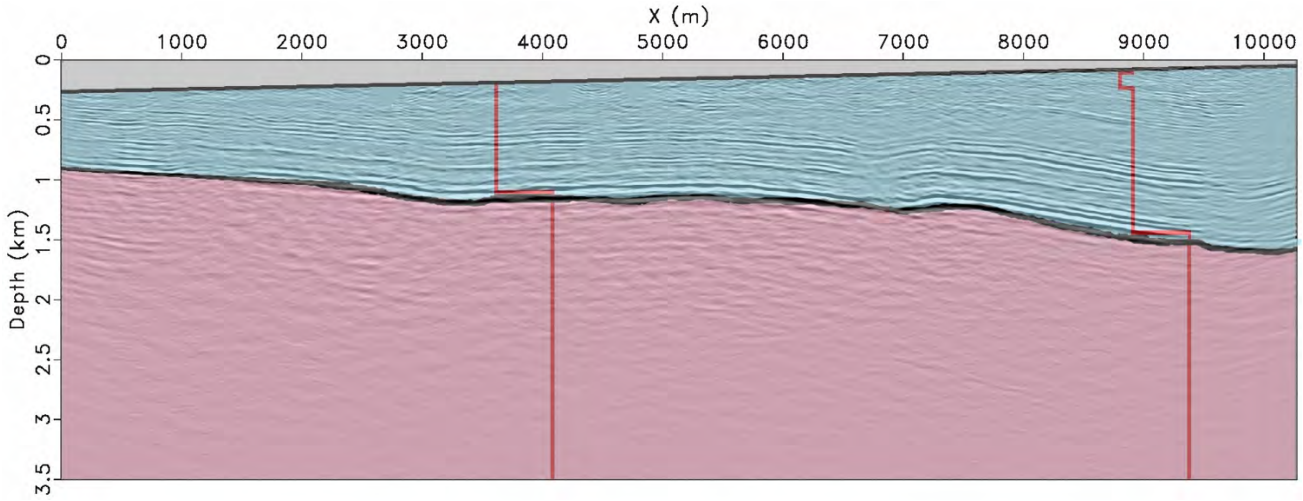

Figure 12.3: *The MT soundings overlaid on the produced seismic image. The blue is the sedimentary geology of the area and the pink is the basement. The MT locations of basement can be seen to align with the location of basement identified by MT. The black line representing the basement contact had been adjusted based on the seismic image.*

DC Resistivity and Geology

The Main Line DC Model displayed in figure 12.4 supports the stratigraphy of the initial geologic cross section. The blue areas are more conductive and are a result of the Mesa Verde. The East side of the model is more resistive because the Mesa Verde is at greater depth and does not influence the model as much. It should be

noted that the shallow areas of conductivity are not areas of Mesa Verde and are instead a result of surrounding topographic effects on the inversion code.

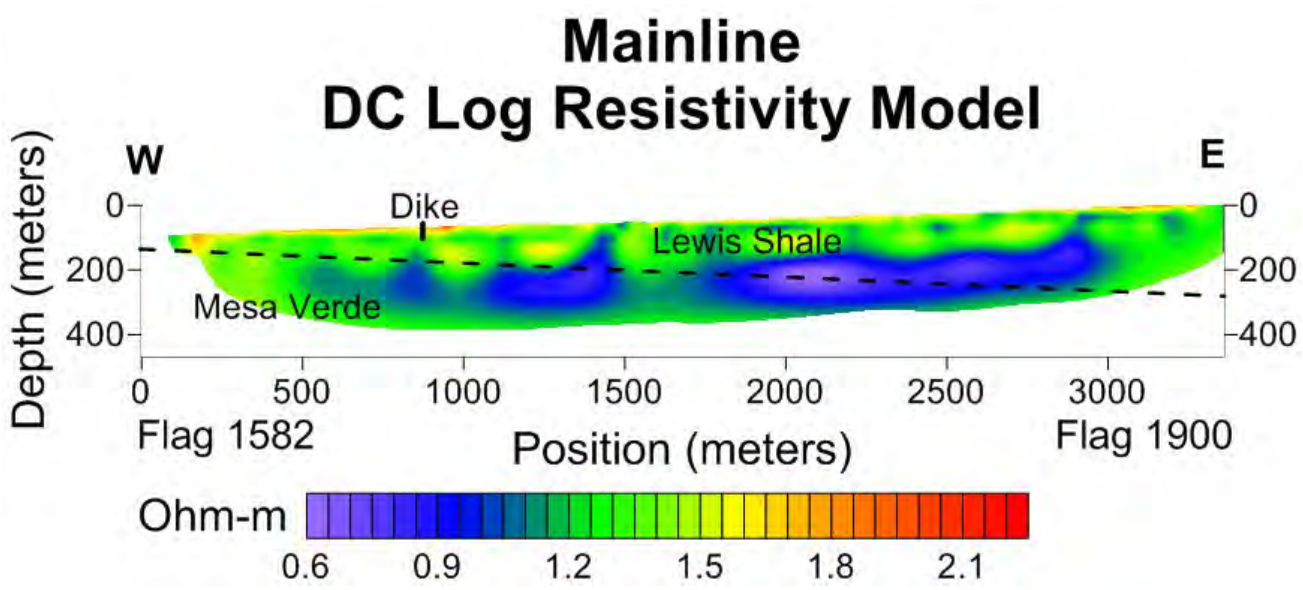

Figure 12.4: *DC Resistivity model displaying log base 10 values of actual resistivity from flag 1582 to flag 1900. The model is overlaid with approximate locations of the dike and contact between Mesa Verde and Lewis Shale.*

Accounting for this lack of topography in the final model, the model in figure 12.4 should have a linear contact dipping to the East, supporting the geology in the initial cross-section (figure 12.1).

Gravity, Seismic and MT

We overlaid the gravity model onto the joint MT and deep seismic image shown in Figure 12.5 to validate of the data. All three methods determined the basement depth within a 50m range. The correlation of these three methods validated the steps taken and assumptions made when processing data.

This combined model reinforces the interpretation of a fault around the 7000m mark of the Main Line. The gravity data fits well with the fault that was first interpreted from the seismic data. The layers created in the gravity model also fit well with the location of the reflectors found during seismic processing. Deep seismic interpreted a second fault East of the fault displayed in Figure 12.5 (see Chapter 5); however, the gravity data did not find any evidence of said fault. The lack of correlation between the data eliminated the fault from the final interpretation.

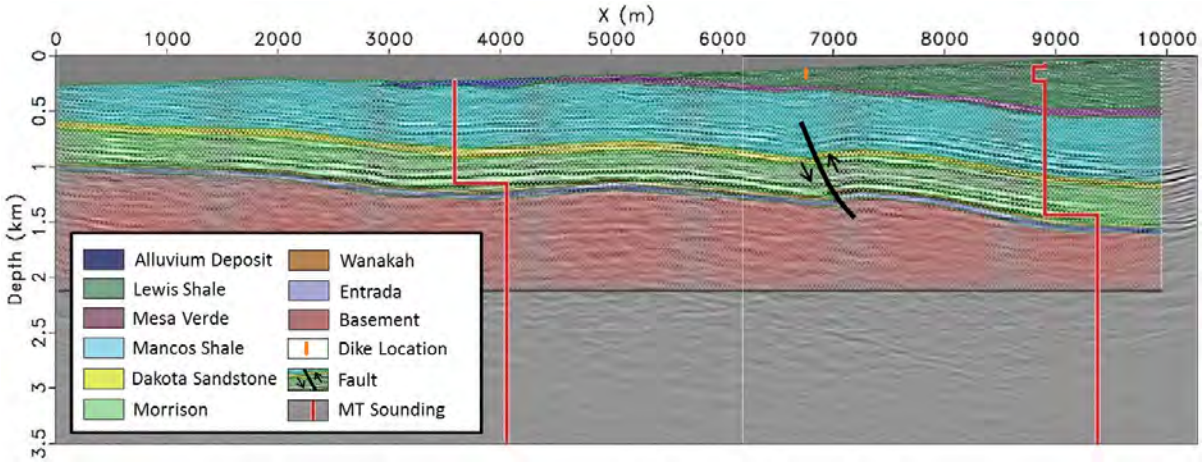

Figure 12.5: *Final interpretation of subsurface with deep seismic, MT, and gravity data. The fault found using deep seismic was further reinforced as it fits well with the gravity data. The MT soundings, gravity model, and seismic data all confirm the location of the basement within* 50 *m of each other. The reflectors that show up in the seismic data match the location of the layers used in the gravity model.*

SP with Hammer Seismic

Before any surveys were conducted, the location of the dike was known due to an outcropping near the Main Line. This is useful because it provides a specific area of interest on the Main Line. By examining the slopes of the first arrival and the head wave, refraction analysis can determine the seismic velocity of the subsurface. Through this analysis, a near surface velocity model was created from hammer seismic data. In addition, the dike was identified as a small perturbation in the head wave, as shown in figure 12.6.

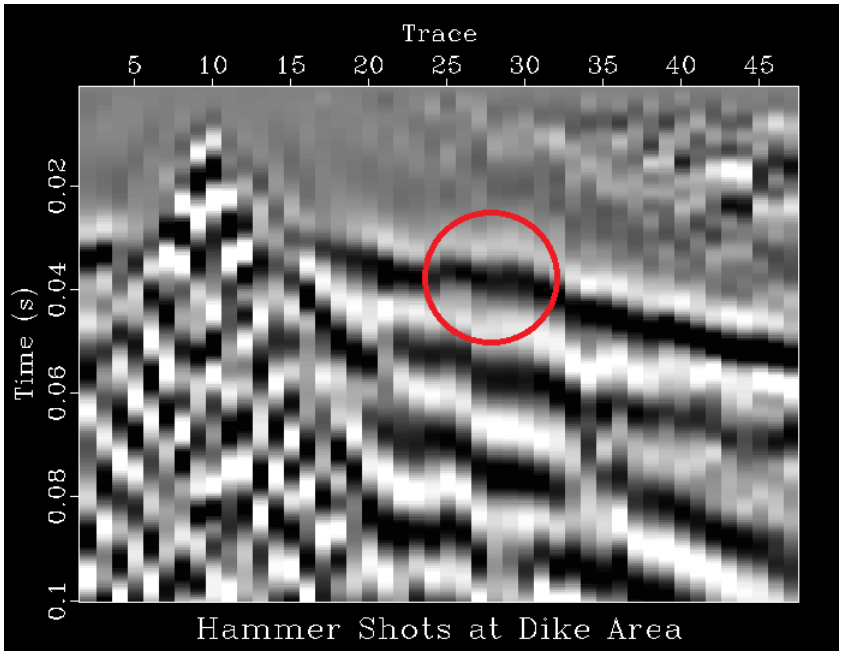

Figure 12.6: *Hammer seismic stack displaying the dike as a perturbation on Main Line. The perturbation has an earlier arrival time meaning it is associated with a higher velocity material. This material is believed to be the dike.*

The dike was observed approximately 3m West of flag 1673 by the hammer seismic survey and buried under 2-3m of unconsolidated material. Figure 12.7 displays a decrease of 30-40 mV in SP data from the West side of the dike to the East side. This decrease in voltage to the East is a result of the dike blocking fluid flow. The fact that the dike causes an SP response in subsurface flow meri ts more investigation in the context of the spring system.

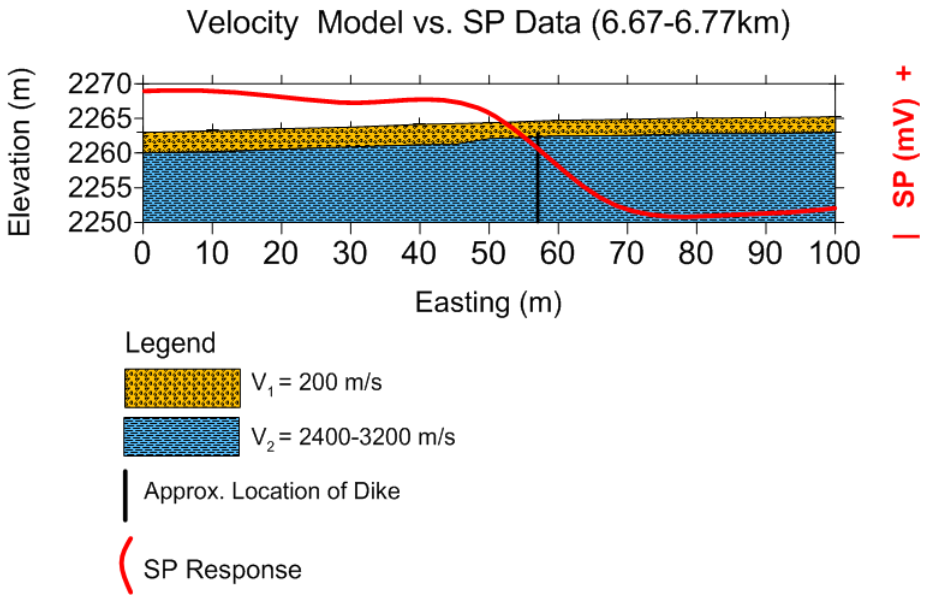

Figure 12.7: *Near surface velocity model created by refraction analysis of hammer seismic data overlaid with SP data collected near the dike.*

12.3.2 Gravity, Seismic, MT, and SP

Gravity, seismic, and MT have revealed discrete sediment layers, fault, and folds in the subsurface. Self-potential helps to tie all the geologic interpretations into subsurface fluid flow trends. Figure 12.8 displays the SP response for the main survey line over the final interpreted cross section generated by previous methods. The SP data has two areas of interest, a drop in voltage approximately 6.73km into the main line and an upward trend on the western end of the line. The dike has been imaged by SP and hammer seismic, seen in Figure 12.7. The interpreted cross section (Figure 12.8) shows a fault at nearly the same location. It is possible that the dike followed the fault path during formation. Low potential readings indicate that either the dike, fault, or both have blocked fluid flow on the eastern end of the survey line. Telluric currents east of the fault and dike are extremely low, indicating little movement in groundwater flow. The current increases west of the dike, and stays approximately linear until 1km from the beginning of the survey line. The western end of the line does not have geologic anomalies; however, the SP data shows a rise in potential readings. This region is the closest area to the Mother Spring, so the upward trend could be an indication of spring upwelling. However, due to relatively high noise in the area, this trend can not be explained confidently. With more information about local cultural noise like irrigation and buried cables, this could be interpreted as quality data.

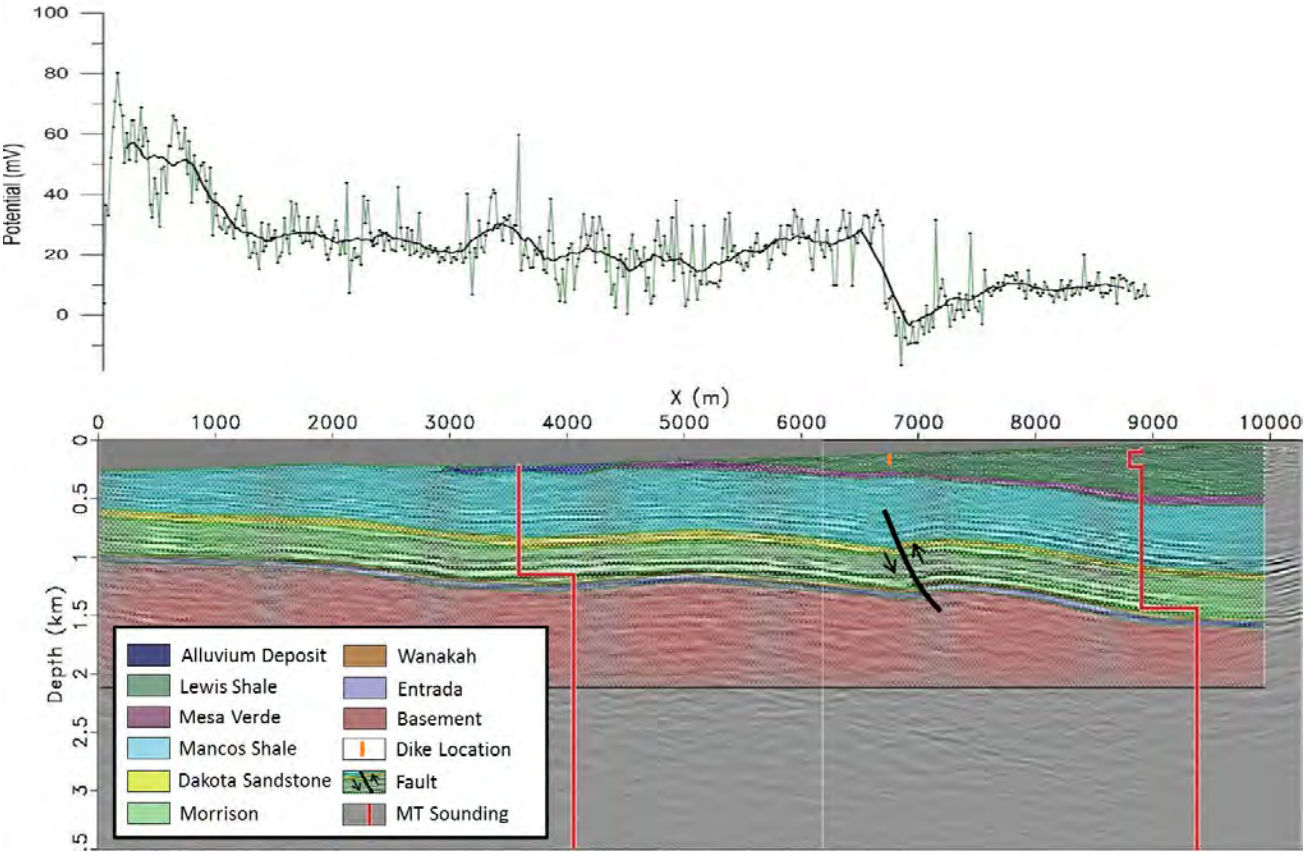

Figure 12.8: *SP data graphed above the interpreted cross section from gravity, seismic, and MT (Figure 12.5) along the main line. The drop SP data marks the location of the dike, also seen in the interpreted cross section as the near location of a fault.*

12.3.3 Final Geologic Cross Section

The final cross section shown in Figure 12.9 was compiled using the cross interpretations. The results of seismic, gravity, and MT identified clearly the locations of all the layers, dikes, and the suspected fault. The results found from hammer seismic and SP helped to characterize Dike 1 shown in Figure 12.9. DC was able help further prove the location of the Mesa Verde formation.

All of the results used to determine the subsurface characterization for the final cross section were free of major inconsistencies. This allows for the cross section shown in Figure 12.9 to have a high confidence level in terms of accuracy. It is still possible; however, that this cross section could be further refined in the future with more information about the subsurface.

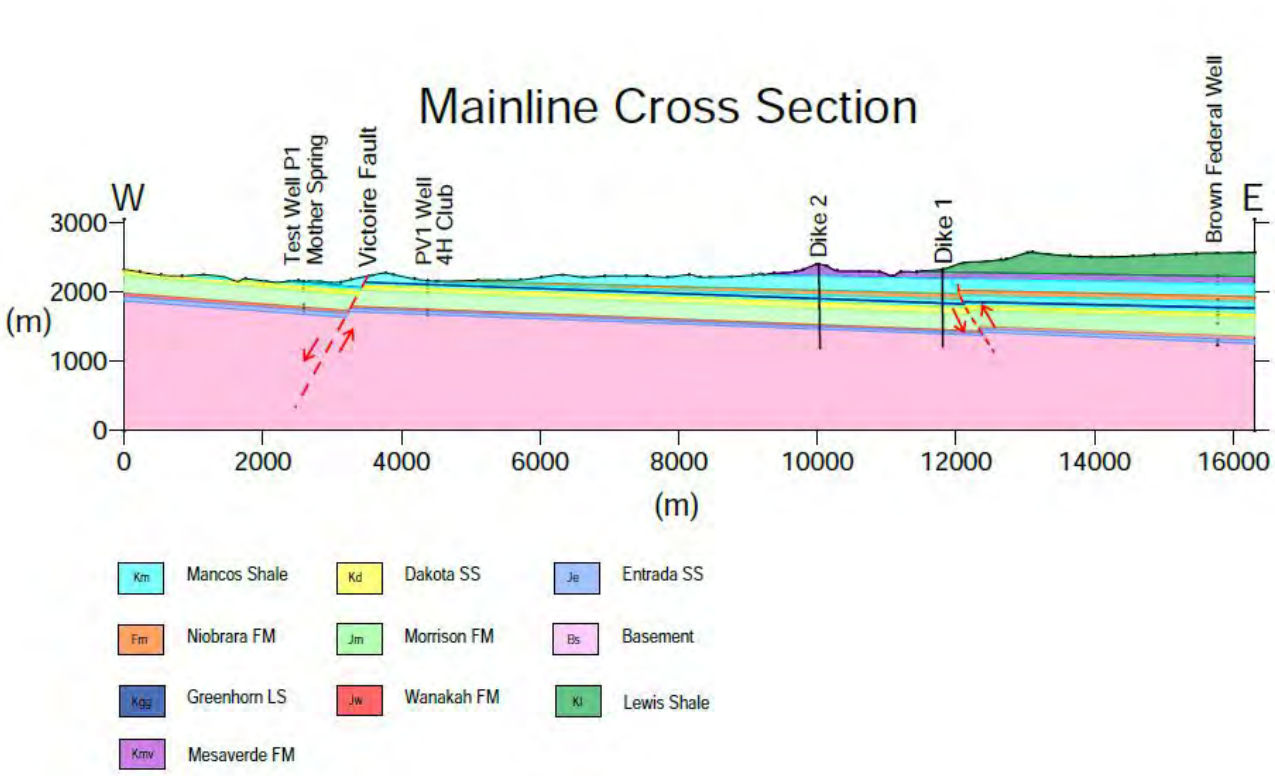

Figure 12.9: *Final geologic cross section of the mainline, updated with the fault found by seismic.*

12.3.4 Student Site

Overview

Similar to the Main Line, a joint interpretation model was completed for the Student Site, starting with gravity, which provided a good basis for subsurface interpretation. Combining the TDEM surveys with gravity was essential for mapping the subsurface of the student site line in its entirety. TDEM data was also useful to integrate to Hammer Seismic and DC, since both of these methods have shallow depths of investigations and can use TDEM resistivity curves to find geologic layers and features at depth. Figure 12.10 displays the initial cross section for the student site.

Hammer Seismic with TDEM

An anomaly was found at approximately 200 m from the West end of the student line by both the hammer and TDEM surveys. The EM57 crew found a conductive layer 150m from the West end at a depth of 448 m. An adjacent survey conducted at 300 m from the West end found the same conductive layer at a depth of 227 m. Along this same section of the line, the hammer seismic crew located a strong reflector dipping West at a 100 m depth. The reflector is possibly a fault because it is at a shallower depth than where geologic layers can be found (Depths of 100+ m according to the DC resistivity survey and geologic maps). The dip of the fault observed in the seismic traces is the apparent dip rather than the true dip. Therefore a static correction was applied to the seismic reflection to account for the apparent dip, resulting in a final true dip of 51 degrees. The true dip of the fault is shown with the EM57 data in Figure 12.11. The strike was interpreted to be 45 degrees in a Northeast direction. The strike orientation of the fault is observed in Figure 12.12. The fault potentially extends to and intersects the Victoire Fault (found by the 2012 Field Camp students). This potential fault could therefore be following a similar pattern to the first splay of the major Victoire Fault, as observed in Figure 12.12.

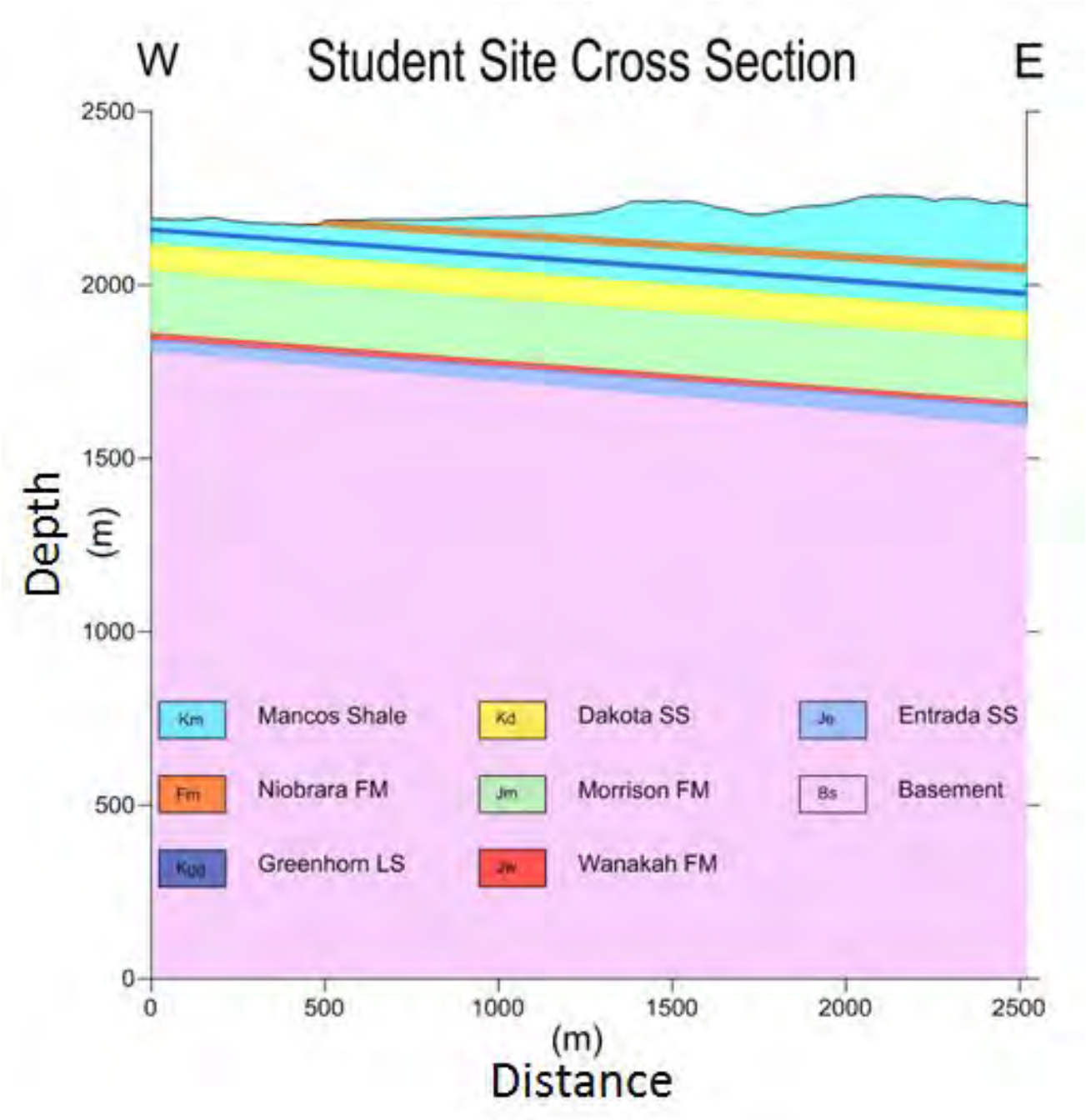

Figure 12.10: *Geologic cross section of the student site located North of Pagosa Springs. We use borehole data to constrain formation thickness.*

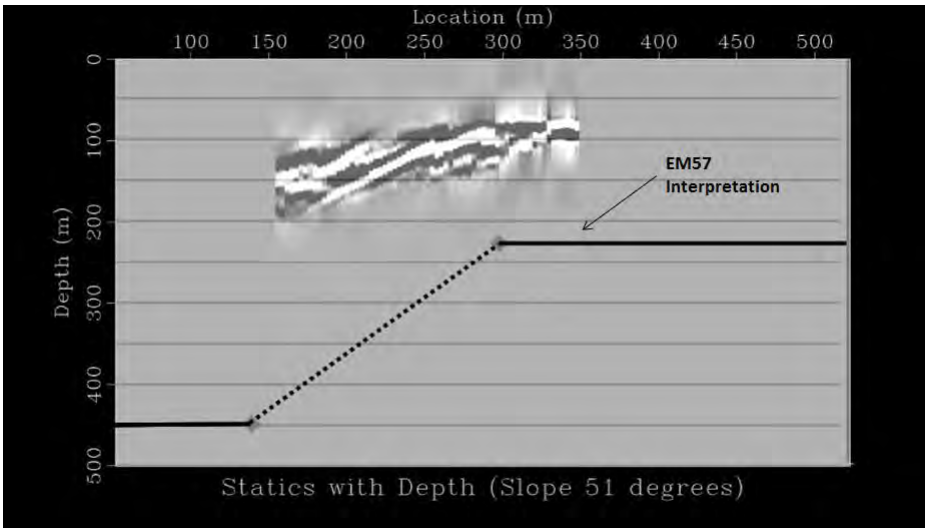

Figure 12.11: *A joint interpretation of EM57 data and hammer seismic is shown. The figure shows a reflection with a dip of 51 degrees.*

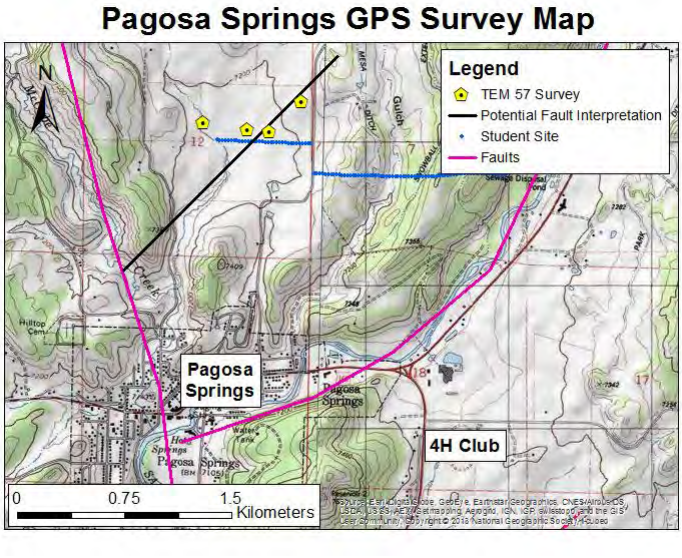

Figure 12.12: *A fault interpretation of the data shown in figure 12.11. The imaged fault could be branching off the main fault line, potentially following a similar pattern to the first splay fault of the major Victoire Fault.*

Gravity Model With Fault

TDEM soundings on the West end of the student line show an upward shift of a conductive layer from West to East, which appears to be a potential fault at approximately the same location as the fault interpreted by hammer seismic. This conductive layer is interpreted to be the Morrison Formation. Based on these results, a gravity model was created to match recorded gravity measurements and also include a normal fault on the West side. As seen in Figure 12.13, the gravity model that best matched the data contains a thin layer of low density alluvium on the surface and a normal fault which offsets the beds by approximately 200 m. The inclusion of this alluvium layer is justified because similar alluvium units have been mapped and observed on the surface, and this section of the survey line is located at the bottom of a valley where alluvium is deposited.

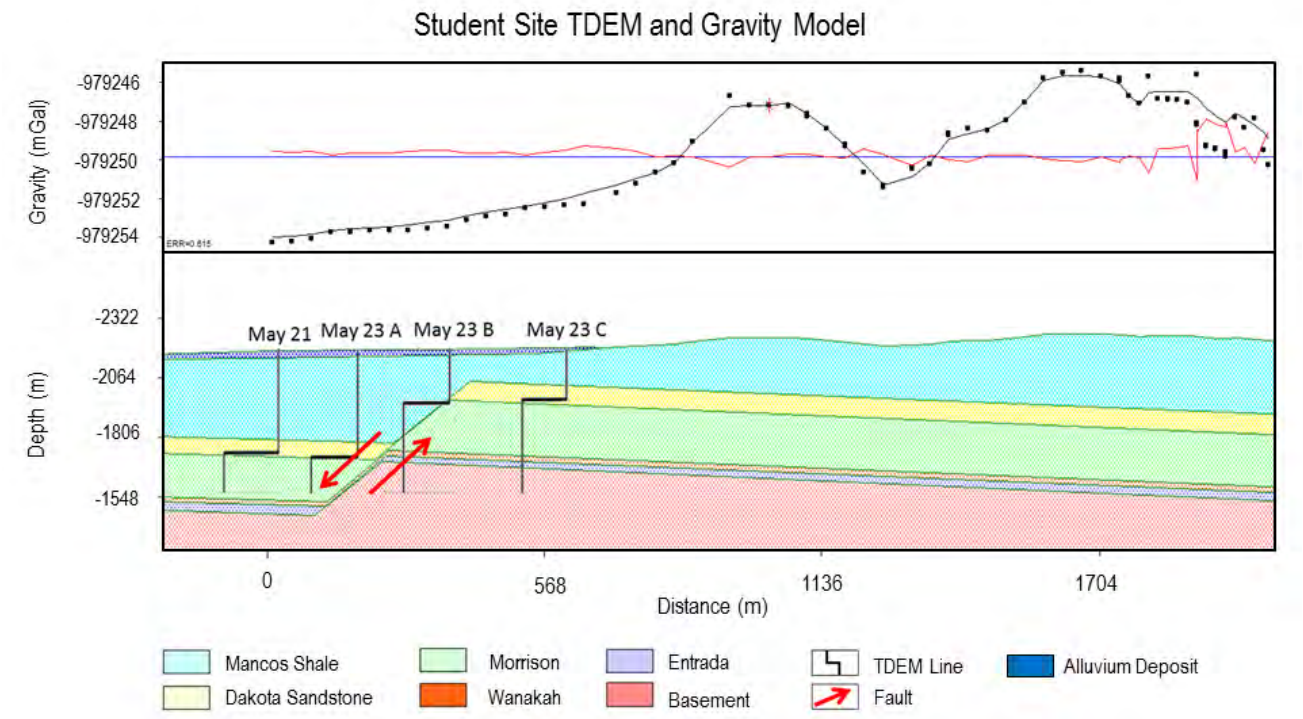

Figure 12.13: *Four of the TDEM soundings on the West end of the Student Site line overlaid with the geologic model derived from the gravity measurements. Note how the gravity model with the fault fits well with the TDEM sounding in the area. Faulting geometry appears inconsistent with local geology.*

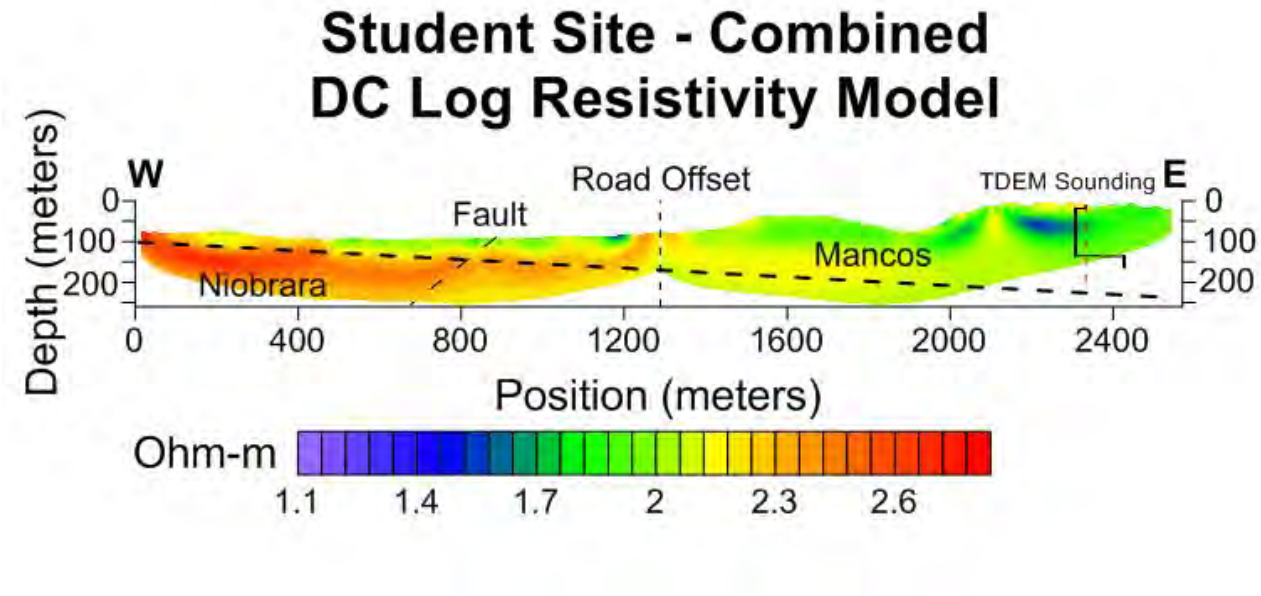

Figure 12.14: *Combined DC line at the student site. Displays the fault observed by hammer seismic, but was not strongly seen on DC. TDEM sounding from the East end of the Student Site line, images a thin resistive area on top of a less resistive unit.*

DC

The time domain electromagnetic soundings on the West end of the student site line (shown in Figure 12.13) show a clear offset in the lower, more conductive layer. The resistive layer that was detected in these soundings is interpreted as the Morrison formation. Since the resistive layer is below the depth of investigation for DC, the offset is too small, and there was not enough resistivity contrast, so the fault was unable to be seen by DC method. The gravity model included the fault with a 200m offset, which provided a better fit than the original model, and only required a thin layer of low density alluvium on the surface. The inclusion of this alluvium layer is reasonable because similar alluvium units have been mapped and observed by the side of a nearby ravine. This portion of the line is also at the bottom of a valley, where alluvium is likely to be deposited.

Gravity Model Without Fault

Based on the DC resistivity results, a gravity model was created to match recorded gravity data without including a fault on the West side. As seen in Figure 12.15, the gravity model that best matched the data still contains a thin layer of alluvium and fits the data just as well as the model with a fault.

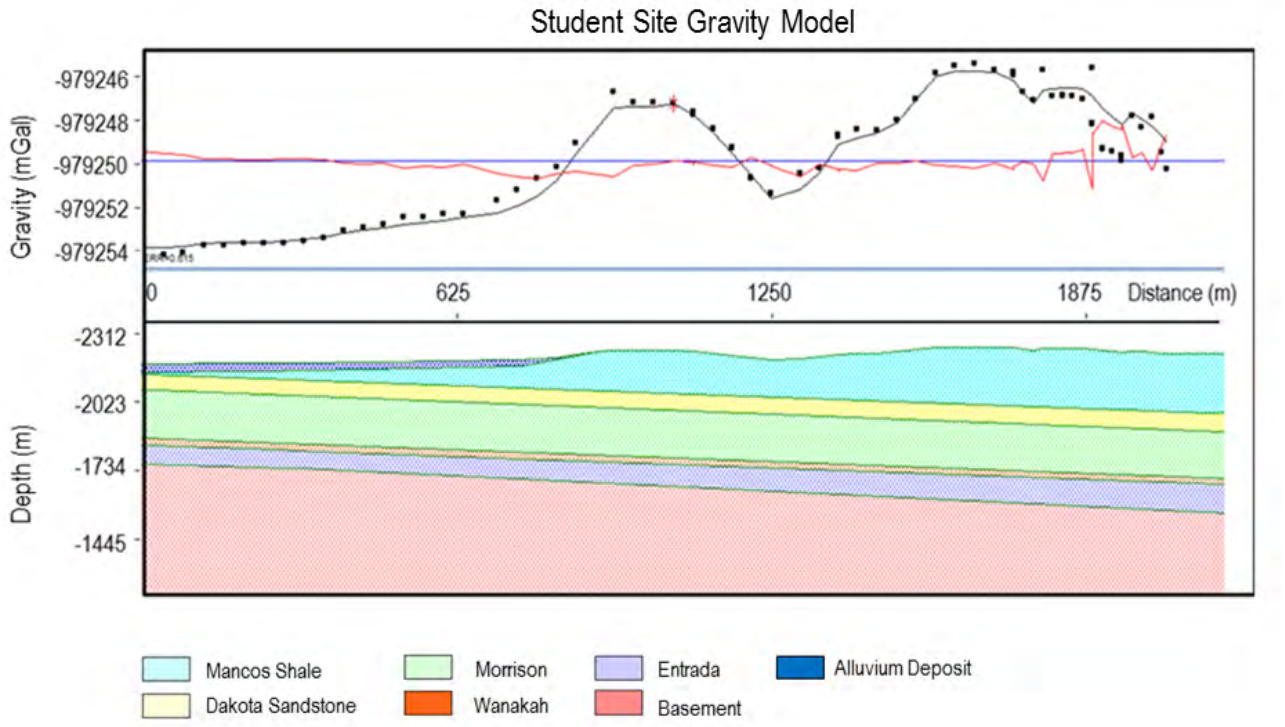

Figure 12.15: *Student site gravity model is consistent with local geologic cross sections and fits gravity response curve.*

Student Site Conclusion

Hammer seismic data located 200 m from the West end of the line seems to suggest the presence of a second splay fault extending from the Victoire Fault and intersecting the student line. The TDEM soundings correlate with these results since an offset of a conductive layer is observed at the same location. On the other hand, no evidence of a possible fault can be observed in the DC data at the same location. Gravity models were created for the two possible scenarios, however, both models matched the data very well leading to two non-unique solutions. Since the fault offset is approximately 200 m, and faulting of this magnitude is unrealistic, further investigation is necessary to corroborate the fault model.

Recommendations

Along the West line of the student site, a possible fault was located. To further investigate this feature, additional geophysical methods should be employed in this area. If a fault is present, it could potentially alter fluid flow through the subsurface; this phenomenon can be measured with SP as an offset in data. If possible, deep seismic data would provide valuable insight into subsurface trends that may show the presence of a fault. However, due to the location, the use of deep seismic is unlikely and as a result, other geophysical methods are recommended. If at least two reasonably electromagnetically quiet locations can be acquired, potential deep subsurface offsets may become visible. Additionally, further TDEM surveys can be completed either by repeating measurements at the original locations with both the TEM57 and TEM47, or at surrounding locations due to the flat nature of the area. These surveys would provide a more complete subsurface image as well as demonstrate repeatability. Finally, by moving or reorienting the survey line, a different picture of the potential fault might be seen. Since the possible fault seems to be a second splay fault of the major Victoire Fault, expanding the survey could provide more information about the potential fault system.

13. Recommendations

Contents

13.1 Future Student Sites

A potential location for a student site is to the West of this year's main line. There is evidence of several faults splitting off from the Victoire Fault to the North of Pagosa Springs, including a fault discovered during a previous field session that intersects with the western part of the Student Site line. It may be of interest to conduct a survey running roughly North-South parallel to the Victoire Fault, but one to two kilometers further East. This could provide additional information about several of the known splayed faults, including their displacement and their effects on the local hydrologic system. This area may also be an area of high heat flow because of its proximity to the Mother Spring.

Next, the Self-Potential data located an area of high telluric currents on the west side of the main line, near the 4H club. In future years, it would be helpful to continue this line towards Reservoir Hill, closer to the Mother Spring, to further investigate if this response is due to spring water upwelling. Lines perpendicular to the main line in this section could also provide more information about fluid flow closer to the Mother Spring.

Both of these proposed sites are in populated areas with power lines, creating an abundance of cultural noise. This is problematic for electrical and electromagnetic methods . It would be useful to scout out the area beforehand to locate all of the buried cables and power lines along the road. If a city power grid map could be acquired, it would be helpful in finding sites that are more remote and less noisy.

13.2 Future Main Lines

Past field camps have focused their energy to the South and West areas of Pagosa Springs and have been inconclusive with any geologic activity relating to the Mother Spring in those regions. This year, we focused our attention to the East of the Mother Spring. Future field sessions should focus on the area North of Pagosa Springs because little geophysical exploration has been performed in that region. There is also a geothermal gradient that

runs from the Mother Spring to the North. We would like to image the area where the gradient is present to see if there are subsurface structures influencing the thermal gradient. Figure 13.1 shows a map of the thermal gradient around Pagosa Springs.

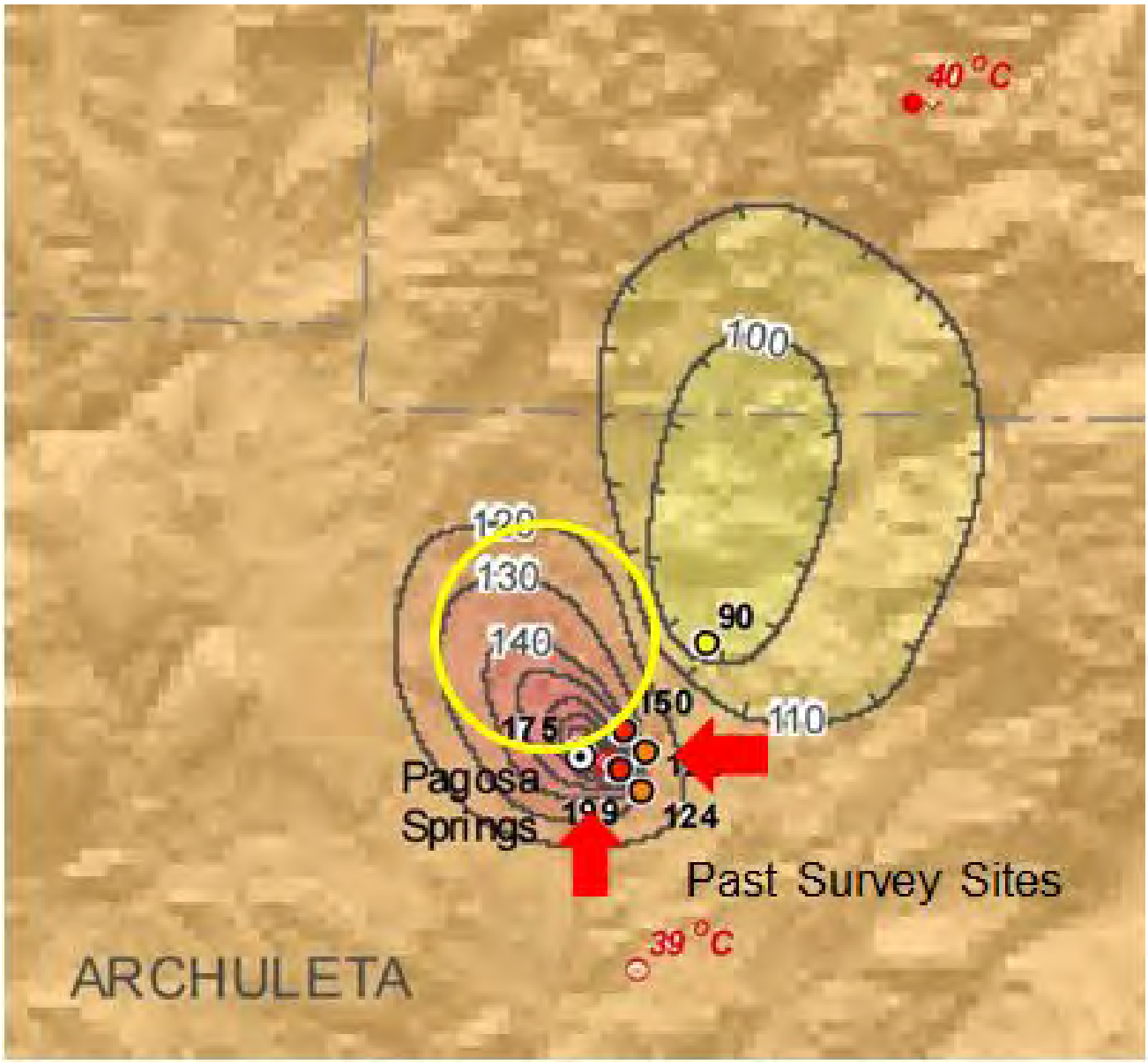

Figure 13.1: *A map of the thermal gradient near Pagosa Springs. Areas of past investigation are shown by red arrows and the yellow circle indicates areas for future investigation. Source: Colorado Geological Survey [5].*

Ideally, two lines would be performed to the North of the Mother Spring. One line would run North to South along the thermal gradient and have DC and SP surveys performed on it, to image fluid flow. The other line would intersect the North South Line and run East to West. This line would have gravity and seismic surveys performed on it to image faults potentially running North-South like the Victoire Fault. This would provide each method with useful targets that could provide valuable information about the geology around Pagosa Springs.

The student site this year provides a small snapshot of the area to the North. There are several small roads directly to the North that have potential to be a main line. The yellow line shown in Figure 13.2 is a long road that

runs North South. This road does run parallel to the strike of the sedimentary bedding, which is not ideal, but the fault trends in the area would intersect this line at an angle which may be obvious in future surveys.

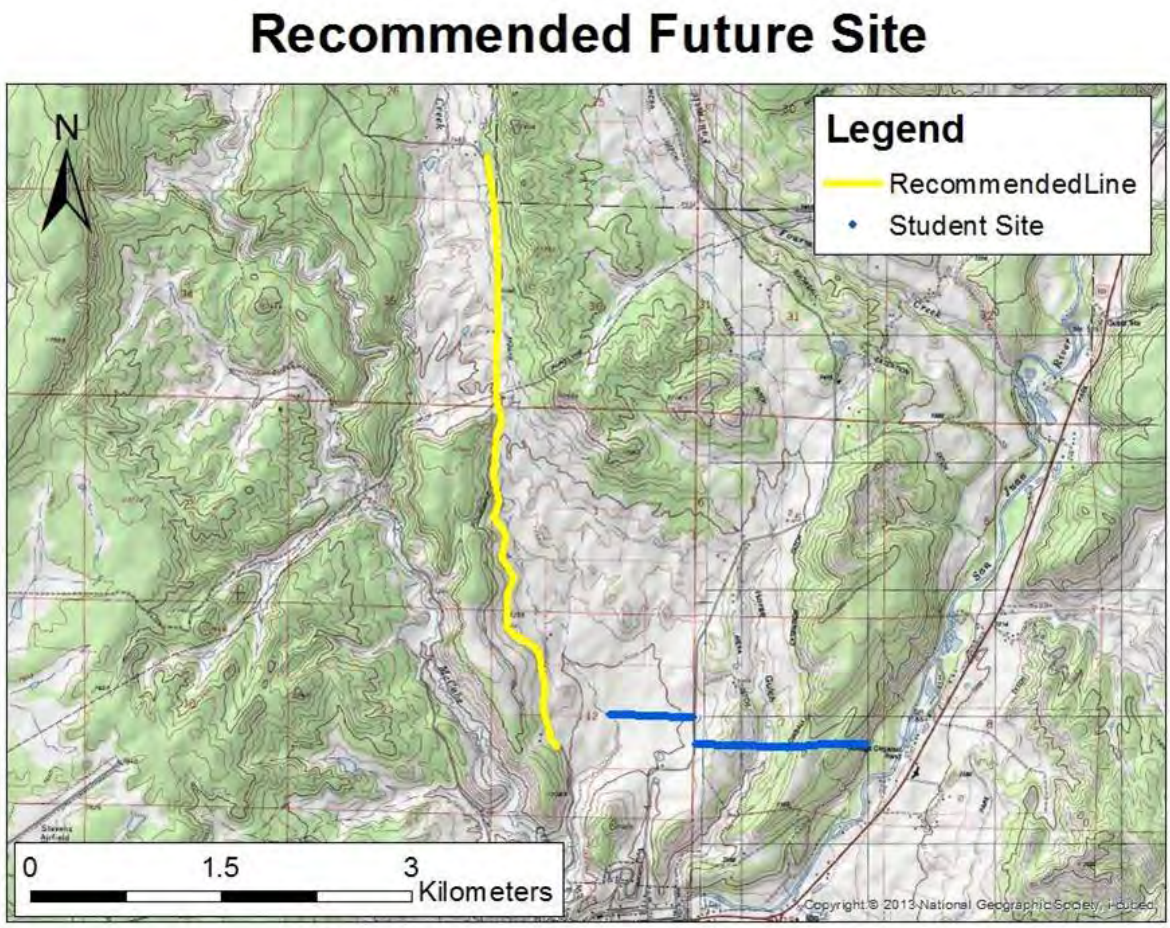

Figure 13.2: *Recommended site for future main line. This line runs from North to South and is located near this year's students site.*

References

[5] F. E. Berkman and C. J. Carroll, *Interpretive Geothermal Gradient of Colorado*, Geothermal Heat Flow Map, Oct. 2007. [Online]. Available: `http://coloradogeologicalsurvey.org/wp-content/uploads/2013/08/LoRes_Plate1_Interpretitive_Geothermal_Heat_Flow_Map.pdf` (cited on pages 15, 190).

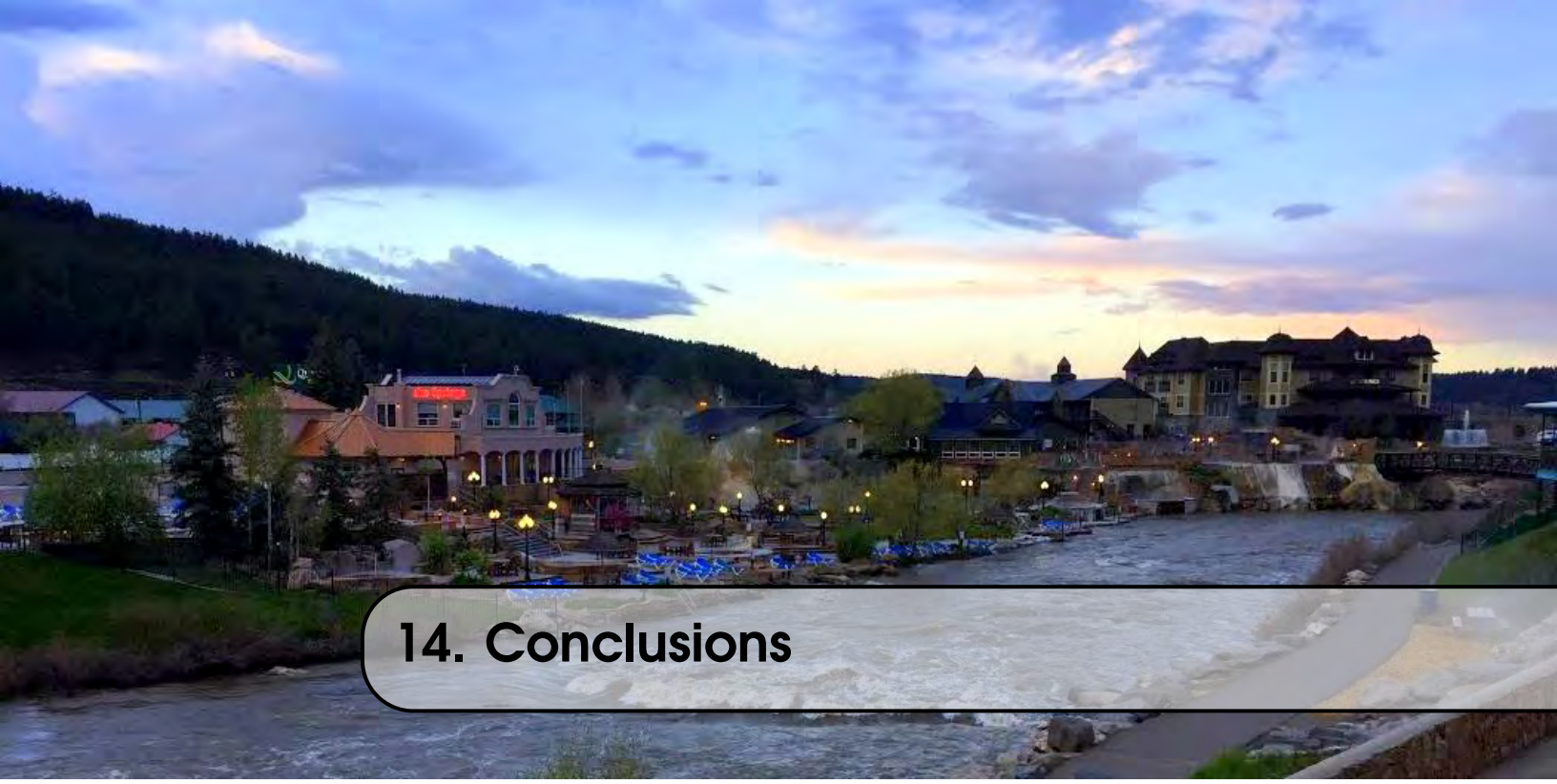

14. Conclusions

The 2016 Colorado School of Mines geophysics field camp conducted a series of passive and active source methods along two profiles in Pagosa Springs, from May 15th to June 10th, 2016. This field session was meant to expose students to the hands-on application of the theory learned over the past several semesters. With the assistance of academic and industry professionals, the data collected was processed and interpreted, and made available to the public. This report, as well as the accompanying presentation represent the students' efforts to produce a model characterizing Pagosa Springs' geology as well as an interpretation for the origin of the town's geothermal system.

To produce reliable interpretations, two survey locations were chosen such that they captured the subsurface geology of previously unexplored areas. The main line survey involved data acquisition along Mill Creek Road to the east of Pagosa Springs. It ran west to east along the road perpendicular to the strike of the geologic layers. This line utilized most of the methods available at field camp in order to investigate the area and characterize the groundwater flow. In addition to the main line, the student site was located to the north of Pagosa Springs crossing County Road 200. This site was chosen due to a possible fault in the area based on projections of known faults. This survey line also ran west to east and included many geophysical methods. No surveys had previously been conducted in the area, so the goal was to conduct an initial survey to set the groundwork for future investigation.

The analyses of the results showed a lot of potential in explaining the fluid flow properties of the area, including those in the direction of the Mother Spring in Pagosa. During the initial inspections of the main line, an intrusive dike outcrop was observed on the side of the road. Multiple methods focused on this anomaly during the data acquisition, including gravity, SP, and DC resistivity. The gravity survey looked for the dike, but came up inconclusive. SP found evidence to suggest the dike disrupted fluid flow on the East side. Hammer seismic also closely analyzed the area near the dike and determined there was faulting in the same region. It is possible that the dike formed by intruding along the fault plane. The dike could be blocking fluid flow along Mill Creek Road. SP found evidence for possible upwelling on the Western side of the main line, but noisy conditions discouraged any firm conclusions. The DC survey was unable to cover the entire line due to equipment failure, so it could not support SP data, or identify any conductive bodies further West along the survey.

Analysis of data collected on the Student Site provided evidence that supports the dipping beds seen along the mainline. Additionally, some methods indicate the possibility of a previously unknown fault located on the West line while other methods did not support this conclusion. The issue of a non-unique solution poses an inherent degree of uncertainty in the student site interpretation. Time domain electromagnetics provided evidence of a fault along the West line; although, it shows a possible offset of over 200m. Due to the low likelihood of this

geologic feature, the quality of the collected TDEM data is questionable. However, data collected across five separate sites provide similar measurements. The hammer seismic line along the West end identified a reflector at a depth of about 100m that could be the surface of a fault plane; however, the signal-to-noise-ratio decreases at such depths, so the reflector could be misinterpreted noise. The final gravity model for the Student Site also suggests that there may be a fault about 200m from the West end of the line. This fault was interpreted with the help of TDEM data. Accounting for the fault in our data allowed for the gravity response of our model to fit the collected data with a deviation of less than a mGal. This is a non-unique solution; however, the gravity response from a model without a fault fit the data with a similar deviation (also less than one mGal). Both of our gravity models included alluvium deposits on the West end of the line. This is consistent with similar units that have been previously observed within the area. The final method explored at the Student Site, DC resistivity, does not dispute these interpretations; however, it makes no clear interpretations of its own. DC resistivity data at the Student Site identifies the stratigraphy, but no faults are visible. Due to the inconsistency in possible interpretations, several non-unique solutions fit the majority of the data.

Further studies of the Pagosa Springs geothermal system should be located north of the town. The area north of Pagosa Springs is the one direction that has not been studied in depth. A possible fault was found on the West side of the Student Site which could be of interest concerning fluid flow.